PSL
UNIVERSITÉ PARIS

THÈSE DE DOCTORAT

DE L'UNIVERSITÉ PSL

Préparée à l'École Normale Supérieure
Dans le cadre d'une cotutelle avec l'Université Paris Cité

Coupling complex systems: from ecological meta-communities to non-reciprocal interactions

Soutenue par

Giulia Garcia Lorenzana

Le 17 Juin 2024

École doctorale n°564

EDPIF

Spécialité

Physique

Préparée au

LPENS

Composition du jury :

Leticia CUGLIANDOLO Sorbonne Université	*Présidente du jury*
Irene GIARDINA Sapienza University	*Rapporteuse*
Tobias GALLA IFISC	*Rapporteur*
Marc MÉZARD Bocconi University	*Examinateur*
Andrea GAMBASSI SISSA	*Examinateur*
Giulio BIROLI École Normale Supérieure	*Directeur de thèse*
Ada ALTIERI Université Paris Cité	*Co-encadrante*

ENS | PSL

Université Paris Cité

Acknowledgements

This thesis wouldn't exist without my brilliant supervisors, Giulio Biroli and Ada Altieri. With them I discovered the excitement of research, the value of scientific rigor and the joys of life in academia; learning what it means to do science under their guidance has been an incredible privilege. Feeling that they always believed in me gave me the confidence to broaden my scientific horizon, getting in touch with many amazing scientists throughout the world. Thanks for showing me the path, and for making me want to follow it. And of course, thanks for Beg Rohu and everything else.

During these years I have been immersed in an incredibly lively scientific environment, both in Paris and in the many conferences and summer schools that I had the chance to attend. I would like to thank in particular the members of the MSC theory group and my scientific tutors, Jorge Kurchan and Jean-Philippe Bouchaud, for their advice and support. Thanks to the members of the jury for taking the time to read and evaluate this thesis. I have also immensely benefited from the collaboration with Vincenzo Vitelli, who showed me yet another style of doing science, and a direction to follow for the next three years. Thanks to Silvia De Monte and Matthieu Barbier, for always being a source of inspiration. Spending some time at INTP has really reshaped my view of ecology and of research.

My journey through physics started nine years ago in Rome, and it would not have been the same without the amazing group of people with whom I shared the joys and hardships of the bachelor. Thanks to Venus, Gabriele, Lorenzo, Luca, Davide and Virginia for all these years of challenges and mutual support that always motivated me to give my best, from Aula Amaldi to the Dolomites.

If I have really come to feel at home in Paris, it is thanks to the wonderful people that have become my family here. Thanks to Margherita and Chiara for the best coloc I could have ever dreamed of; Rue Bob will be one of the dearest memories of these years. Thanks to Camilla, Chiara, Alex, Masha and Antonin for always being there in both beautiful times and difficult ones, and for making my years in Paris unforgettable.

It is not always easy to stay motivated during November's rainy days, but having the warm environment of the lab to look forward to definitely helps. Thanks to Lila, Nino, Rushi, Cory, Nirbhay, Luis, Sofia, Joseph and Jules for making me want to come to the office every morning, and to leave it early to go grab a beer.

Gianmarco, Alberto and Federico have been the best PhD companions I could have asked for. I feel so lucky to have shared such intense years with you, and I look forward to sharing more travels and science all over the world. A special thanks to Federico for always finding a way to be there, from the beginning to the end of this adventure.

Finally, thanks to my parents for transmitting me the passion for physics and complexity, and to my grandma for showing me the beauty of Paris. I couldn't have made it through all these years away from home without the love and support of my family.

Résumé en français

Les *systèmes complexes*, qu'il s'agisse de communautés écologiques, de réseaux de neurones, ou de l'économie mondiale, sont composés de nombreux éléments simples interagissant de manière hétérogène. Ces systèmes peuvent manifester des phénomènes inattendus et des comportements émergents. La *physique statistique*, qui étudie les propriétés des systèmes composés d'un grand nombre d'entités en interaction, fournit les clefs pour en comprendre l'origine. Plusieurs outils ont été développés pour étudier les systèmes dans lesquels les interactions hétérogènes jouent un rôle essentiel [7]. Pourtant, on en sait encore peu sur ce qui se produit lorsque deux ou plus de ces systèmes complexes sont *couplés*. Cette situation apparaît dès qu'il existe plusieurs niveaux d'organisation [8,9] : par exemple, des communautés écologiques locales reliées par la migration (Figure 1), des réseaux de neurones avec des objectifs opposés, ou encore des entreprises complexes formant une économie. C'est précisément cette problématique qui constitue le cœur de cette thése.

Les systèmes que j'ai étudiés sont également caractérisés par des processus *irréversibles*, où la dynamique du système se distingue nettement de celle observée si elle était jouée à rebours dans le temps. De nombreux exemples se rencontrent en écologie. L'extinction d'une espèce est un événement irréversible, tout comme l'évolution des abondances d'un prédateur et de sa proie. Dans une dynamique prédateur-proie, une augmentation des proies entraîne toujours une augmentation des prédateurs, tandis qu'une augmentation des prédateurs conduit inévitablement à une diminution des proies. Cette asymétrie est une conséquence des leurs *interactions non réciproques*. Ainsi, l'ordre des événements impose une direction temporelle bien définie.

Cette irréversibilité place ces systèmes hors d'équilibre, ce qui élargit considérablement la gamme des phénomènes possibles. Elle permet notamment l'émergence de dynamiques chaotiques, d'ondes d'activité ou encore de phases d'oscillation. Si ces comportements ont été largement étudiés dans le cas de peu de degrés de liberté couplés, leur généralisation aux systèmes complexes nécessite le développement de nouveaux cadres théoriques.

Cette thèse est divisée en deux parties : dans la Partie I, je décris des métacommunautés écologiques complexes (introduites au Chapitre 2); dans la Partie II, j'étudie des paires de systèmes complexes couplés par des interactions non réciproques (introduites au Chapitre 5). L'un des liens entre les deux parties est méthodologique : le principal outil théorique utilisé tout au long de la thèse est la théorie du champ moyen dynamique (ou Dynamical Mean Field Theory, DMFT), qui est introduite au Chapitre 3. Elle permet de donner une description d'un système composé de nombreux éléments en interaction à travers une dynamique effective d'un seul de ses éléments, couplé à une source de flutuations supplémentaire. Appliquée aux systèmes écologiques, elle nous permet de faire le lien entre les modèles écologiques complexes et les descriptions stochastiques d'une seule espèce, ce qui permet de comprendre pourquoi ces deux perspectives donnent souvent des résultats similaires.

Communautés écologiques

L'un des systèmes complexes auxquels je m'intéresse est celui des *communautés écologiques*, dont les composantes de base – souvent en très grand nombre – sont les espèces. Leurs interactions peuvent être extrêmement variées, allant de la compétition pour les ressources au mutualisme, en passant par la prédation. Leur dynamique n'est pas soumise aux mêmes contraintes que celles des systèmes physiques classiques, mais peut néanmoins être analysée à l'aide de techniques similaires [1, 5, 10–12].

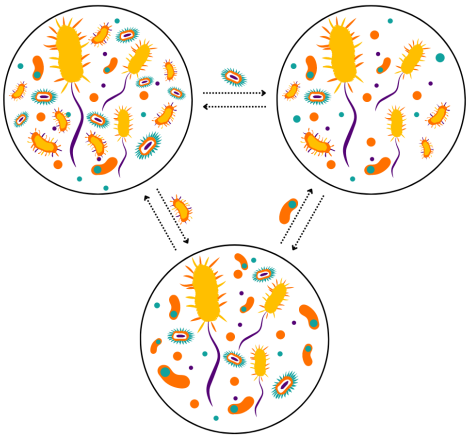

Figure 1: Schéma d'une méta-communauté écologique, qui sera étudié dans la partie I de la thèse.

Dans le Chapitre 4, j'étudie des systèmes écologiques à extension spatiale (ou méta-communautés) soumis à des fluctuations. Les écosystèmes naturels sont soumis à diverses *fluctuations*, dues à des perturbations externes, à la dynamique écologique (qui peut être chaotique) ou à la stochasticité de la naissance et de la mort des individus. Ces fluctuations provoquent des extinctions qui, dans une communauté isolée, entraînent une perte irréversible de la diversité. Cela est évité si l'on considère un *réseau spatial* de communautés interconnectées par la migration (Figure 1). Dans ce cas, une extinction locale peut être compensée par une recolonisation à partir d'individus provenant d'un site où l'espèce est abondante. En combinant des outils analytiques sophistiqués (comme la théorie du champ moyen dynamique, la méthode des répliques ou la théorie statistique des champs) et des simulations numériques, j'ai montré que la présence d'interactions hétérogènes permet de stabiliser le système bien au-delà de ce qui serait possible pour une espèce isolée [1]. Cela se produit grâce à l'émergence spontanée d'*interactions mutuellement bénéfiques*: seules les espèces qui collaborent survivent. Dans le même temps, ces interactions mutualistes génèrent un *point de bascule*, où l'écosystème peut soudainement s'effondrer, passant d'un état de grande diversité à un état d'extinction totale. Cette transition peut être déclenchée par une diminution du taux de migration qui, dans les écosystèmes naturels, pourrait être due à la fragmentation des habitats causée par l'homme. Après la transition, le système reste dans l'état dégradé, même si le taux de migration est à nouveau augmenté : il y a un effet d'hystérésis. Il est donc crucial de prévoir l'approche du point de bascule avant qu'il ne soit atteint. J'ai montré que cela peut être fait en étudiant la réponse du système aux perturbations, qui diverge avant le point de transition.

Interactions non réciproques

Dans le Chapitre 6, j'étudie le couplage macroscopique *non réciproque* d'agents dotés d'une dynamique interne complexe (Figure 2), comme des paires de réseaux de neurones avec des objectifs opposés. Ces systèmes présentent un intérêt majeur, tant sur le plan théorique que pour leurs applications pratiques, notamment dans le cadre des réseaux antagonistes génératifs. Toutefois, ils restent mal compris en raison des défis posés par l'étude simultanée des interactions hétérogènes et de la dynamique hors équilibre.

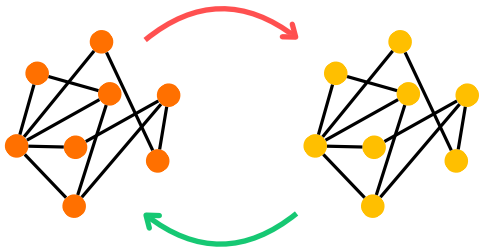

Figure 2: Schéma d'une paire de systèmes complexes couplés de manière non réciproque, qui seront étudiés dans la partie II de la thèse.

Certains systèmes complexes peuvent subir une transition de phase, après laquelle ils présentent un phénomène appelé *vieillissement* : plus le système est ancien, plus il évolue lentement. Il avait été suggéré que toute non-réciprocité détruirait ce phénomène, menant à la place à une dynamique chaotique [13]. Dans le Chapitre 6, je montre au contraire que le sort de cette phase ralentie dépend de la manière dont cette non-réciprocité est introduite [2]. J'ai découvert une transition d'une phase désordonnée statique à une phase amorphe oscillante, caractérisée par un vieillissement non réciproque avec une dynamique lente et des oscillations. Je travaille actuellement sur la généralisation de ces résultats à d'autres systèmes désordonnés. Quelques résultats préliminaires sont présentés au Chapitre 7.

Dans le Chapitre 8, j'étudie l'effet des interactions non réciproques sur le comportement critique de paires de systèmes subissant une transition de phase. J'ai développé des critères sur les propriétés des systèmes avant le couplage qui permettent de prédire si le comportement critique serait modifié par différents types de perturbations infinitésimales non réciproques.

Les outils pour l'étude des systèmes complexes couplés à l'échelle macroscopique que j'ai développés au cours de ma thèse pourraient avoir de nombreuses applications dans beaucoup d'autres systèmes biologiques où plusieurs niveaux d'organisation coexistent.

Contents

Chapter 1

Introduction

1.1 Complex systems

Statistical physics studies systems composed of many simple units. The central idea is to renounce to predicting the dynamics of each of the components, and giving instead a statistical description of the macroscopic properties of the whole system. Let us for example consider a glass of water, which is composed by an enormous number of molecules. While a single water molecule is not too strongly affected by moderate changes in temperature, cooling the entire glass of water can cause it to freeze, dramatically altering its physical properties. This is what we call a *phase transition*. Phase transitions cannot be understood extrapolating the behavior of just a few particles: they are a *collective phenomenon*. The observation that radically new properties emerge when going from a few to many components is well synthesized by the famous quote by P. W. Anderson "more is different" [14]. We will say that a system is *complex* if it exhibits such emergent properties.

The units that make up our system do not need to be particles or molecules: we can think of many neurons composing a brain, many birds flying together in a flock, or many species forming an ecosystem. The study of such diverse ecosystems will be a central focus of this thesis. A neuron, a bird, or a species may not be simple objects, but the emergent behavior of the systems they compose does not depend too strongly on their properties. We can therefore try to understand it studying simplified models with the tools of statistical physics. While the single unit's features are not too important, a crucial role will be played by their *interactions*.

The properties of complex systems are in general very robust: a flock can continue its flight even if one of its birds is attacked by a predator. This is the opposite of what happens in *complicated* systems, such as a clock, which also consist of many components but rely on each playing a precise role. In such a system, removing even a single element can immediately disrupt the collective behavior. This robustness is one of the reasons why complexity is so widespread in biological systems.

The interactions between components can be heterogeneous. In an ecosystem, the interaction between a wolf and a rabbit is very different to the one between a flower and a bee. This heterogeneity in the interaction network is itself the origin of distinctive phenomena, and we call systems that exhibit it *disordered systems*. An approach that has been very successful in a range of fields, from nuclear physics to machine learning, consists in replacing heterogeneity with *randomness*. For example, we will study models of ecosystems in which the interaction between any two species is randomly selected. Some of the properties of the system, such as the behavior of any individual species, will also turn out to be random. Crucially, however, some of the large scale phenomenology will be the same across typical realizations of the interaction network. As a result, predictions made on the random system will be relevant to the original

heterogeneous one.

1.2 Equilibrium and non-equilibrium

Many of the tools of statistical physics have been developed assuming that the system we want to study is at *equilibrium*. To be at equilibrium, a system needs to be stationary: any macroscopic property we might want to measure must be constant in time. This is nevertheless not sufficient. A classical system is at equilibrium if it is invariant under *time reversal*: this means that if we record a video of the evolution of the system and we play it backwards in time, the forward and backwards movies must be statistically indistinguishable. In other words, the forward and backward trajectories should have the same probability.

Classical physical systems are described by Newton's laws, which are reversible in time. In this case, if the system is isolated and we reach a stationary state, it will be an equilibrium one. We can then think of two reasons why a system could be out of equilibrium: either its dynamics is irreversible (and thus violates Newton's laws), or the system has not reached stationarity (yet, but maybe it never will). We will see examples of both cases in this thesis.

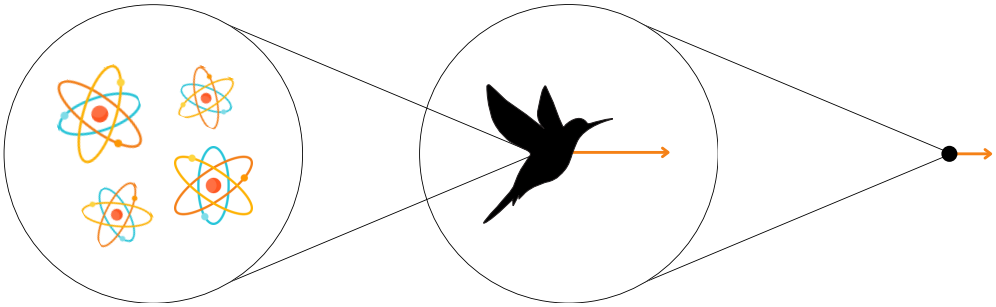

Figure 1.1: Irreversibility depends on the description scale: the dynamics of the atoms inside a bird are reversible, the flight of a bird is not. If we only observe the position of the bird, the dynamics could become reversible again.

An example of irreversible dynamics is the flight of a bird: watching the inverted movie it would be clear that the bird cannot possibly be flying backwards. Of course, all the microscopical dynamics of the atoms that compose the bird are perfectly reversible (albeit out of equilibrium). However, we can give a coarse-grained description of the system as a stylized shape of a bird and its position (Figure 1.1), and this would evolve according to an effective irreversible dynamics. Note that if we coarse grain the system even more, and we only consider the position, the dynamics might become reversible again, since the bird could be flying in either direction. Irreversibility can thus crucially depend on the *scale* at which we observe our system.

The dynamics of ecosystems is also often irreversible. The extinction of a species is for example an irreversible event. Another case that will be discussed in great detail in this thesis is *non-reciprocal interactions*, such as the ones between a predator and its prey (Figure 1.2). The two species have opposite effects on each other: an increase in the number of predators leads to a decrease in the prey, whereas an increase in the prey leads to an increase of the predators. This asymmetry allows us to easily distinguish the forward and backwards processes, highlighting the irreversibility of the dynamics.

An example of a system with a reversible microscopic dynamics that is out of equilibrium is glass. When a glass-forming material is rapidly cooled, its dynamics slows down dramatically. The time it would require to relax to equilibrium increases so much that it remains out of equilibrium on every reasonable timescale. Glasses therefore never reach a steady state. Instead,

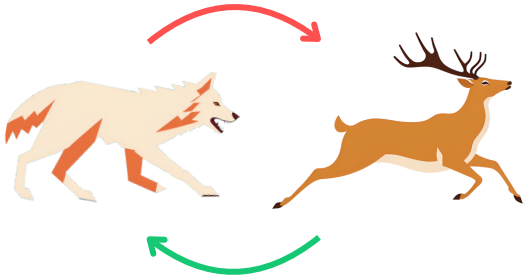

Figure 1.2: A predator and its prey interact in a non-reciprocal way.

they perform *aging*: as time goes on, their dynamics becomes slower and slower, explicitly depending on the age of the system. Their molecules don't have time to arrange in a crystalline structure, and remain stuck in an amorphous one, which is very similar to that of a liquid. Why liquid and glasses have such different physical properties despite having very similar structures is still an open question. Because of the disorder in their structure, glasses can exhibit similar behaviors to systems with random interactions. Many of the results on aging dynamics have been obtained studying *spin-glasses*, simplified models with random frustrated interactions that display a transition to an aging – or glassy – phase at low temperature.

Since much of statistical physics relies on equilibrium, studying dynamics that violate it leads to significant technical challenges. For this reason, these kinds of systems are still poorly understood. At the same time, being out of equilibrium allows for an incredible variety of complex phenomena, the most interesting of which might be life itself.

1.3 Coupled complex systems

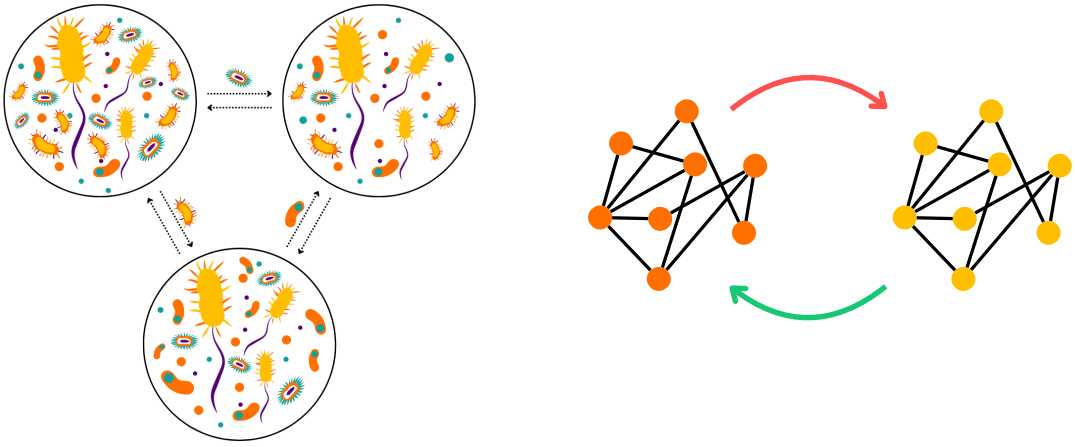

(a) Ecological meta-community (b) Non-reciprocally coupled complex systems

Figure 1.3: Sketches of (a) an ecological meta-community, which will be studied in Part I of the thesis, and (b) a pair of non reciprocally coupled complex systems, which will be studied in Part II.

Besides being complex and out of equilibrium, living systems often also display multiple levels of organization [8, 15]. For example, many cells can form an organism, many organisms form a population, and many populations form an ecosystem. At each of this organizational

levels complexity can play an important role. Modeling such hierarchical structures requires understanding what happens if we couple two — or many — complex systems. This question will be central throughout this thesis.

I will study two concrete examples of coupled complex systems. In Part I of the thesis, I will describe spatially-extended diverse ecosystems (Figure 1.3a), in which local ecological communities – each composed of many species – are coupled in space by migration of individuals from site to site. In Part II of the thesis, I will study what happens when two complex systems are non-reciprocally coupled at the macroscopic level (Figure 1.3b). I will in particular investigate how this affects aging dynamics and phase transitions. Because these two subjects belong to quite different fields, I have decided to introduce them separately, respectively in Chapter 2 and Chapter 5.

There are nevertheless several points of contact between the two parts. In both cases we will deal with systems in which heterogeneity plays an important role, and we will model it via random interactions. The non-equilibrium nature of both systems will restrict our choice of analytical techniques. A central tool throughout the thesis will be Dynamical Mean Field Theory (DMFT), which is presented in Chapter 3. It allow us to give an effective description of a many-body system in terms of the dynamics of a single representative degree of freedom, which is subjected to some additional noise and memory terms. Because of the hierarchical structure of the systems I studied, I had to generalize this method to consider *multiple* coupled representative degrees of freedom: one for each local community in the case of spatially extended ecosystems, and one for each agent in the case of the non-reciprocally coupled complex systems.

The rest of the thesis is organized as follows. In Chapter 4, based on reference [1], I study a model for spatially extended ecosystems composed of many heterogeneously interacting species subject to fluctuations. In Chapter 6, drawing on references [2] and [3] (both currently under review), I explore the dynamics arising from the non-reciprocal coupling of two simple aging systems. In Chapter 7, I present ongoing work extending the results of the previous chapter to more complex models. In Chapter 8, I investigate the conditions under which the introduction of a small degree of non-reciprocity can dramatically alter a phase transition. These results will be the subject of a forthcoming publication [4]. Finally, Chapter 9 offers concluding remarks and future perspectives. Two of my publications, references [5] and [6], will not be treated in this thesis.

Part I

Diverse ecological systems

Chapter 2

Community Ecology and Disordered Systems

Ecology studies how different living organisms interact with each other and with their environment. It encompasses multiple scales both in the system size, going from bacteria interacting in the gut of a fly [16] to a tropical forest [17], and in the organizational level, studying how individuals behave and interact with each other, but also the dynamics of a species' population, the way many species form a community, and how this community is embedded in an ecosystem. While many of the relevant processes are specific to the ecosystem we are considering, at each of these organizational levels common phenomena and patterns emerge [18]. This suggests that some of the mechanisms at play may be general and robust enough to be captured by highly simplified mathematical models.

The first common observation is the mere number of species that can be found in a given environment, called *species richness* or *diversity*. Why don't a handful of species out-compete all the others, driving them to extinction? This is one of the central questions of *community ecology*, which studies the patterns in the abundance and distribution of the species that live and interact in a given environment [19–21].

A very simple ecological experiment consists in walking through a forest and counting the number of individuals, or *abundance*, of each species encountered. As it was already noted by Darwin [22], we would find that species can strongly differ in frequency, with a few being very common and others quite rare. This is quantified by the Species Abundance Distribution (SAD), which describes how many species fall in a given range of abundances [18]. SADs have similar shapes in very different ecosystems, and this is one of the patterns that community ecology tries to explain.

Counting individuals and species is at the basis of the quantitative approach to ecology. In the last decades these tasks have been radically streamlined – especially for microbial communities – by the advent of high-throughput sequencing and metabarcoding [23–25]. These techniques allow to quickly determine which species are present and their relative abundance by analyzing the genetic material found in a sample. The increasing availability of spatio-temporal resolved data [26] has led to a renewed interest in the modeling of the time evolution of the species abundance in diverse ecological communities.

Besides the theoretical interest of uncovering the principles that determine how different life forms assemble and interact, ecology is rich in practical applications. Ecosystems benefit humans in a variety of ways, called *ecosystems services*: just to name a few examples, they provide food and resources, regulate hydrological and oxygen cycles, help mitigate the effects of extreme weather, and ensure crop pollination [27]. Understanding how the resilience and functioning of ecosystems might be affected by changing environmental conditions is a pressing question

in the light of climate change and human-induced habitat fragmentation [18, 28]. Because of the key role of the microbiome in regulating human health, predicting and possibly controlling behavioral shifts in complex ecosystems can also have important medical applications [29–31].

2.1 Niche versus neutral paradigm

Most ecological theories that try to make sense of the incredible diversity observed in natural ecosystems can be organized between two opposite paradigms: the *niche* and *neutral* theories.

The ecological niche of a species, first introduced by Joseph Grinnel in 1924 [32], was defined by Charles Elton as "its place in the abiotic environment, its relations to food and enemies" [33]. According to niche theory, species are able to coexist because each of them exploits the environment and the rest of the ecosystem in a different way. For example, birds with different beaks shapes have different feeding behaviors, allowing them to avoid competition [34]. The other side of the medal is the "competitive exclusion principle" [35, 36], which states that two species that occupy the same niche cannot coexist at constant population values. The concept of niche was later formalized by George Evelyn Hutchinson as the hyper-volume in the space of environmental variables (for example temperature, humidity, or a resource availability) in which a species is able to survive [37]. Because of competition with other species, each species does not occupy entirely this *fundamental niche*, but only its *realized* one. The interaction strength between two species can thus be linked to their *niche overlap*. On evolutionary time-scales, competing species will decrease their niche overlap, undergoing *niche differentiation*.

One of the main limitations of the niche framework is its lack of predictive power: it allow us to rationalize the coexistence of two species by contrasting their needs and preferences, but it is very hard to predict how many niches are present in a given environment without counting the species that actually occupy them. An attempt to address this issue was made by MacArthur with his consumer-resource model [38, 39], which describes the dynamics of the abundances of S species that rely on R resources. From the MacArthur model, it is possible to show that the ecosystem can only reach a stable equilibrium if $S \leq R$, meaning that the number of species cannot exceed the number of available resources. This bound is violated in many natural ecosystems, and most notably in planktonic communities: thousands of different species are found in a single sample of sea-water [40, 41], all relying on a handful of resources. This is sometimes called the "plankton paradox" [42].

While niche theory starts from the assumption that species are so different that they barely interact, neutral theory assumes that species are essentially indistinguishable, or *functionally equivalent*, and differences in species abundances derive from random fluctuations, called in this context *ecological drift* [43, 44]. This equivalence is usually assumed at the individual level, meaning that the birth and death rates of each individual do not depend on its species identity. Neutral theory can either be considered an approximation of real ecosystems, in which species are presumably not identical, or a null model, that allow us to assess the impact of other relevant ecological processes. Despite its shockingly simple assumptions, the theory is able to correctly reproduce several static macroecological patterns, such as the species abundance distribution or the species-area relationship [43, 45, 46]. If regarded as a null model, neutral theory suggests that many of such static patterns can be explained without much complex ecological modeling. This raises the question of which observables are affected by all the ecological processes that are not included in neutral theory, and would therefore allow to discriminate between alternative hypothesis. One promising candidate is temporal patterns [47], such as times to extinction, which neutral theory fails to reproduce accurately [48, 49]. This offers further motivation to the development of models that describe the dynamics of diversity-rich ecosystems.

2.2 Deterministic growth of a single species

In the following we will study mathematical models for the dynamics of the abundance, i.e. the number of individuals, of one or more species. This is a discrete (integer) variable, but we will rescale it by some typical size of the population N_{typ}, so that the abundance N will be of order 1. Since populations are often composed by a very large number of individuals, after the rescaling the discrete values that N can assume will be very closely spaced, and we will approximate it to be a continuous variable. This allows us to write differential equations for its evolution.

The simplest hypothesis we can make on a populations growth is that each individual reproduces and dies with the same rate. This implies that the growth of the population is at all times proportional to its abundance. Representing the abundance as a continuous variable N, we can write the general ecological differential equation:

$$\dot{N} = Nr(N, E) \ . \tag{2.1}$$

We have indicated with E all biotic and abiotic factors on which the growth rate r may depend, such as temperature, resource availability, or abundances of other species. The growth rate is the difference between the birth and the death rate, and as such it can also be negative. Despite its simplicity and generality, this equation has a first important property, that indeed is a crucial feature of ecological systems: $N = 0$ is a fixed point, meaning that if a species goes extinct, it will remain so indefinitely. In this sense, extinction is an *absorbing state*.

Assuming the growth rate to be simply a constant, we obtain the *Malthusian growth model*:

$$\dot{N} = r_0 N \ . \tag{2.2}$$

Starting from a finite population, the solution of this differential equation is exponential growth if $r_0 > 0$ (Fig. 2.1), and exponential decay if $r_0 < 0$.

Note that under the approximation of continuous N, even in the case of exponential decay the abundance remains strictly positive at all times. This means that the species never goes extinct, and if the growth rate suddenly changes sign it can grow back to finite abundances. Nevertheless the approximation of continuous N breaks down for $N \sim O(1/N_{typ})$, when the unrescaled number of individuals would approach 1. One way to reintroduce species extinctions is to impose an *extinction threshold*: if N crosses $1/N_{typ}$ we declare that the species is extinct and we set $N = 0$ at all later times.

While this could be a good approximation when a species is first introduced in a new environment [50], exponential growth cannot persist indefinitely: in any realistic system there is a finite concentration of resources (water, nutrients or even just space), which will eventually lead to competition between individuals and a slowdown of reproduction. To model this limitation effect, we can hypothesize that the growth rate is not constant, but depends on the abundance. In the *logistic growth model*, this dependence is assumed to be linear: $r = r_0 \left(1 - \frac{N}{k}\right)$, where k is the *carrying capacity* of the species. The dynamical equation then becomes:

$$\dot{N} = r_0 N \left(1 - \frac{N}{k}\right) \ , \tag{2.3}$$

whose solution is

$$N(t) = \frac{k}{1 + \left(\frac{k}{N(0)} - 1\right) e^{-r_0 t}} \ . \tag{2.4}$$

$N(t)$ converges to k for all initial conditions $N(0) > 0$ (Fig. 2.1): the carrying capacity is a stable fixed point of the dynamics. Indeed it represents the abundance at which the birth and death

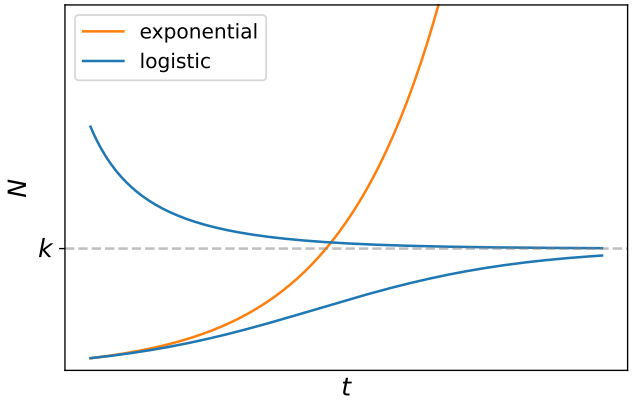

Figure 2.1: Exponential and logistic dynamics. For the latter, we considered two different initial conditions, showing that the abundance converges to the carrying capacity both from higher and lower initial conditions.

rates of the population are perfectly balanced, so that the growth rate is zero. By appropriately choosing the rescaling factor of N (which we called N_{typ}), we can always set $k = 1$.

In the following we will absorb a $1/k$ factor in the constant r_0, so that the dynamical equation becomes:

$$\dot{N} = r_0 N \left(k - N\right) \ . \tag{2.5}$$

The logistic equation can give a good quantitative description of the growth of an isolated species, but, being a phenomenological model, it has no guarantee to hold in every situation. Indeed, a plethora of other growth models have been proposed over the years. The limitation of growth could for example be non-linear, as in the θ-logistic model [51]:

$$\dot{N} = r_0 N \left(1 - \left(\frac{N}{k}\right)^{\theta}\right) \ . \tag{2.6}$$

Another popular approach consists in assuming that the growth of the population is limited by the availability of a resource R. In the Monod model [52] this is described by

$$\dot{N} = r_{max} \frac{R}{R + K_R} N \ , \tag{2.7}$$

where K_R is the concentration of the resource that allows growth at half the maximum rate. As the species grows, it consumes the resource according to:

$$\dot{R} = -\beta \dot{N} \ . \tag{2.8}$$

This model also leads to a saturation of growth, but this is more strongly nonlinear than in the logistic case, especially if the resource is initially widely available.

As we will argue in Section 2.6, the collective properties of complex ecosystems are often not too sensitive to the details of the dynamics. In the following, we will therefore focus on the logistic model because of its simplicity.

2.3 Stochastic dynamics

In a natural ecosystem, environmental conditions are not fixed: temperature, humidity or resources availability might fluctuate in time. Since we are not interested in building a model that would predict their behavior, we will assume that they undergo some stochastic dynamics. Moreover, since we do not know all the complex biological details that govern the life of each individual, we will also treat births and deaths as being random events.

We will distinguish two kinds of stochasticity: if it affects all individuals in the same way, we will call it *environmental*, if it acts on each individual independently, we will call it *demographic*.

2.3.1 Environmental noise

The probability of each individual to die or reproduce will generically depend on the environmental conditions. We will incorporate environmental fluctuations in the dynamical equation for the abundance of the population by adding a noise term to the carrying capacity [53–58]:

$$k(t) = k_0 + \xi(t) \ . \tag{2.9}$$

The statistics of the noise $\xi(t)$ depends on the process that generates the fluctuations: it could jump between two values depending on some binary condition (e.g. sun or rain), it could have an oscillating mean describing seasonal trends, or it could have a power law distribution. In the following, we will focus on the case in which the distribution of ξ is stationary and Gaussian. Thanks to the law of large numbers, this is a good approximation whenever the fluctuations are generated by the combination of many independent stochastic processes. We will absorb any deterministic component in the carrying capacity, so that the noise has zero mean. Thanks to Gaussianity, to fully determine its distribution we only need to specify its correlations:

$$\langle \xi(t)\xi(t') \rangle = C_\xi(t - t') \ . \tag{2.10}$$

We will indicate with angular brackets $\langle \cdot \rangle$ the average over noise. The correlation function $C_\xi(t-t')$ only depends on the difference between the two times because we are assuming the environment to be time translationally invariant. It will generically be a monotonically decreasing function that decays to zero at long times. We can for example consider exponentially correlated noise:

$$\langle \xi(t)\xi(t') \rangle = \frac{2T_\xi}{\tau} e^{-\frac{|t-t'|}{\tau}} \ . \tag{2.11}$$

T_ξ is the amplitude of the noise, whereas τ is its correlation time.

When $\tau \to 0$, i.e. when the intrinsic timescale of the fluctuations is much smaller than the ecological timescales, the noise becomes delta correlated in time:

$$\langle \xi(t)\xi(t') \rangle = 2T_\xi \delta(t - t') \ . \tag{2.12}$$

We will refer to this case as *white noise*, and to the finite τ one as *colored noise*.

Since this noise is added to the carrying capacity, in the dynamical equation it will multiply the abundance[1]:

$$\dot{N} = r_0 N \left(k + \xi(t) - N\right) \ . \tag{2.13}$$

[1] Since the noise is multiplicative, it is important to state which discretization we are using. Because even in the white noise case we imagine these fluctuations to be the limit of some finite correlation noise, we will use in this case Stratonovich discretization.

This means that when the species is at low abundances the noise term will be small. We will show in Chapter 3 that in the continuous N approximation these fluctuations cannot lead a species to extinction [53–57]. This is instead possible if we again consider an extinction threshold, or the combined effect of demographic and environmental stochasticity.

Typical realizations of the time evolution of N under white and colored environmental noise are shown in Figure 2.2a and 2.2b.

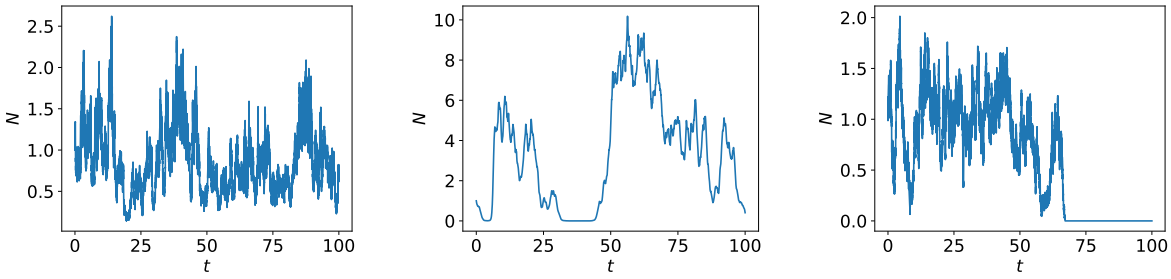

(a) Environmental noise, $\tau = 0$ (b) Environmental noise, $\tau = 10$ (c) Demographic noise

Figure 2.2: Time evolution of the abundance under environmental (Eq. (2.13), $T_\xi = 0.3$) or demographic (Eq. (2.14), $T = 0.1$) noise.

2.3.2 Demographic noise

Stochasticity also occurs at the individual level: the death or reproduction of each individual depends on random encounters with predators or resources and on many biological details that we do not aim to model here[2]. We will therefore assume that each individual has a certain probability rate of dying (decreasing by 1 the number of individuals) or reproducing (increasing by 1 the number of individuals). The combination of these independent stochastic processes leads to demographic fluctuations of the abundance N. Thanks to the law of large numbers, when the number of individuals is large these fluctuations are Gaussian, and their variance is proportional to N. This can be rigorously shown starting from an agent-based description of the population [59, 60].

We will model these fluctuations as a Gaussian white noise[3], with amplitude proportional to $\sqrt{N}$:

$$\dot{N} = r_0 N \left(k - N + \xi(t)\right) + \eta(t)\sqrt{N} \ , \tag{2.14}$$

where

$$\langle \eta(t)\eta(t')\rangle = 2T\delta(t-t') \ . \tag{2.15}$$

We will see that T plays the role of an effective temperature. Changing the rescaling factor N_{typ} modifies the effective temperature as $T \propto 1/N_{typ}$ [5, 59, 60]. Demographic noise is therefore only relevant if the characteristic size of the population is not too large. Its relative effect is maximal at small abundances, i.e. when the species is close to extinction.

[2] It could also be relevant to consider stochasticity sources that are correlated over some fraction of the individuals, possibly leading to some intermediate scaling. We will not consider this possibility.

[3] The amplitude of the fluctuations at time $t+dt$ depends on the number of individuals that can die or reproduce at time t, it is therefore natural to use Ito discretization. This correctly leads to the fact that if a species is extinct its abundance will stop fluctuating, and it will remain extinct at all later times. With Stratonovich discretization it is instead possible for the fluctuations to bring a species back from extinction. In the following it will be useful to transform the equation in Stratonovich discretization, which is always possible by adding some extra term.

We will show in Chapter 3 that, contrarily to environmental noise, demographic noise *can* lead a species to extinction even in the absence of an extinction threshold, as shown in Figure 2.2. The average *persistence time* (the time after which a species goes extinct), or, equivalently, the extinction rate, is of direct ecological relevance, since it is both experimentally accessible and crucial for ecosystems management and biodiversity conservation [61,62]. Numerous studies have addressed its calculation in the presence of both demographic and environmental stochasticity [54–58]. When only demographic noise is considered, extinction times are unrealistically long; conversely, environmental stochasticity alone leads to strong abundance fluctuations, but species never go extinct. The interplay of these two types of fluctuations leads to more realistic extinction rates.

Since in the presence of demographic noise there is a finite probability rate for the species to go extinct, sooner or later this will happen. Since extinction is an irreversible event, the species will then remain at zero abundance at all later times. The only possible steady state is therefore the one in which the species is extinct. We will see in the next section that in order to prevent irreversible extinctions and obtain a non-trivial steady state we can allow individuals to reinvade the community from other spatial locations.

2.4 Migration and metacommunities

We have so far considered a single well mixed ecological community, in which each individual can interact with all the others. While this could be a good approximation for microorganisms in a test tube [63], natural ecosystems are generally characterized by multiple spatial scales: individuals interact and reproduce locally, and can then migrate to different locations.

The simplest way to introduce migration is the island-mainland model [64]: we assume that the ecosystem that we want to model is an island close to a mainland, from which individuals can reinvade the community at a constant (but usually small) rate. This results in a constant term in the growth of the abundance:

$$\dot{N} = r_0 N \left(k - N + \xi(t)\right) + \eta(t)\sqrt{N} + \lambda \ , \tag{2.16}$$

$\lambda \geq 0$ is the immigration rate. Note that $N = 0$ is not a fixed point anymore: if individuals are continuously added to the community, the population can never go extinct. This allow us to obtain a finite-abundance steady state in the presence of demographic noise.

This island–mainland framework has been highly influential, as it provides the minimal setting to study the assembly of ecological communities from a regional species pool [5, 10–12, 43, 65–67]. By balancing extinction and colonization rates, it helps explain patterns of species richness in insular systems as a function of island size and degree of isolation. Assuming that the extinction rate decreases with the island size, whereas the colonization rate decreases with distance from the mainland, the theory predicts that islands that are larger and closer to the mainland should have a higher equilibrium diversity, as it can be indeed verified experimentally [64, 68].

However, assuming a constant immigration flow is only justified if the mainland is an infinite reservoir of individuals, undergoing no ecological dynamics. To rephrase the issue, we have solved the problem of extinctions in our island thanks to immigration, but why shouldn't the species go extinct in the mainland?

To avoid relaying on the existence of a static and infinite reservoir of individuals, we can consider a *network* of islands coupled by migration [1, 20, 69–82], as shown in Figure 2.3. Each circle represents a local population; we will call their collection a *metapopulation*, or *metacommunity* if multiple species are present at each site. The presence of multiple locations provides an "insurance" (or "storage") effect [73–79], because if a species goes locally extinct in one of

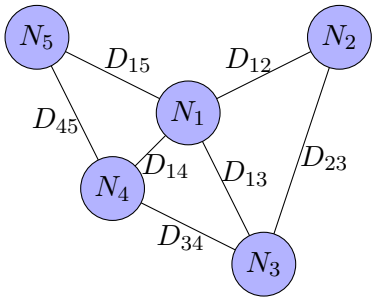

Figure 2.3: Sketch of a metapopulation: circles represents local populations, lines the possible migration paths.

the communities, immigrants from the neighboring ones can re-colonize it. If the environmental conditions differ across sites, this can further enhance diversity: each species can find some sites in which the conditions are favorable to its growth, and spread individuals to the rest of the system [1,70–72,82–84]. This is known as *source-sink* effect, and it is often found to be maximal at intermediate dispersal rates [70,72,81,84].

The abundance in each population, now carrying a space index u, undergoes the same ecological dynamics as described by Equation 2.14. Individuals can then migrate from one site to one of its neighbors by passive diffusion. The resulting stochastic process reads:

$$\dot{N}_u = r_0 N_u \left(k_u - N_u + \xi(t)\right) + \eta(t)\sqrt{N_u} + \sum_{v \in \partial u} D_{uv}(N_v - N_u). \tag{2.17}$$

D_{uv} is the migration rate between site v and one of its neighbors u, the graph of sites and migration paths defines the spatial network. It could make sense to consider asymmetric migration rates, for example when currents or seasonal migrations are important, but in the following we will assume $D_{uv} = D_{vu}$. In general the carrying capacity could also depend on the site, we have therefore labeled it k_μ. While the system is well defined for any spatial network, we will mostly consider systems that are invariant under translation, as it is the case for regular lattices or fully connected networks.

In a fully connected network, each site is connected to all the others. We will consider uniform migration rates. To ensure that the total contribution from migration remains finite in the limit where the number of sites L goes to infinity, it is convenient to rescale the migration rate with L:

$$\dot{N}_u = r_0 N_u \left(k - N_u + \xi(t)\right) + \eta(t)\sqrt{N_u} + \frac{D}{L}\sum_{v=1}^{L}(N_v - N_u). \tag{2.18}$$

The discrete metapopulation framework is relevant whenever the species can only survive in specific locations: the typical example is a network of islands, but the discrete sites could also be water sources, or hosts for their microbiome [85]. A metacommunity structure has also been recently proposed to model metastatic growth in tumors [86]. In other cases, it could be more relevant to consider a continuous spatial structure. This can be done by promoting N to be a function of space, and replacing the migration term with a diffusion one [87,88]:

$$\dot{N}(x,t) = r_0 N(x,t)\left(k - N(x,t) + \xi(x,t)\right) + \eta(x,t)\sqrt{N(x,t)} + D\nabla^2 N(x,t). \tag{2.19}$$

This continuous limit can be obtained from a discrete lattice by appropriately rescaling the lattice spacing and migration rates [89]. In the following, we will mostly focus on discrete spatial structures.

We will see that in the limit of an infinite number of sites the introduction of a spatial structure indeed allow us to prevent extinctions if the migration rate is sufficiently strong. Lowering the migration rate, the system undergoes a phase transition to extinction that falls in the *Directed Percolation* (DP) universality class, which we present in the next section.

2.4.1 Directed Percolation

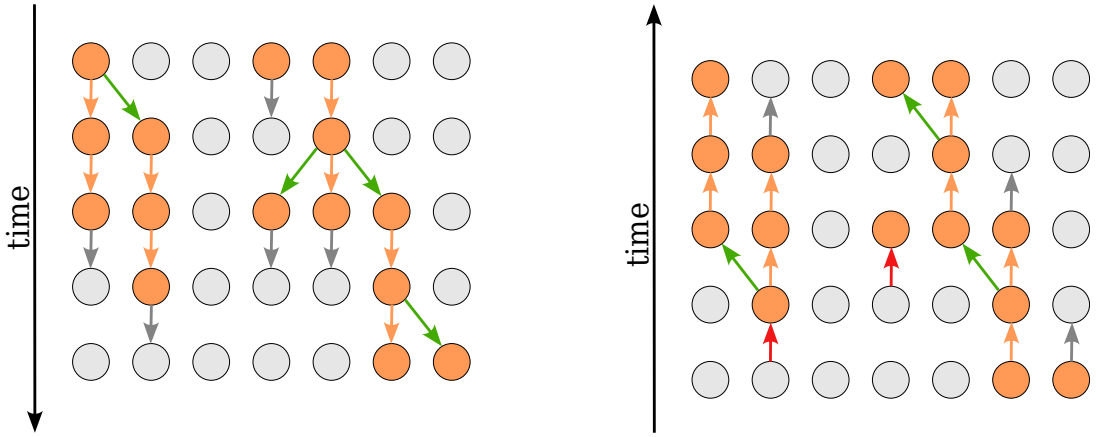

(a) Directed percolation (b) Time reversed process

Figure 2.4: (a) Directed percolation on an array of 7 sites. Each row represents a different time step, green arrows indicate birth, gray arrows death, and orange arrows survival. (b) Time reversed process. Red arrows indicate impossible events.

Directed Percolation is a paradigmatic model studied in out-of-equilibrium physics and statistical field theory [89–91], which was originally introduced to describe spreading phenomena, from forest fires to epidemics. It models particles that hop on a network and are subjected to reproduction and death. A graphical illustration of the process can be found in Figure 2.4a for a one-dimensional network of 7 sites. In our case, the sites of the network represent the spatial location on which (and from which) the species can migrate; the particles indicate which sites are colonized by the species, or "active". With some given probability rate, the particles can produce an offspring in a neighboring site or die. In our case, this corresponds to colonization or extinction. Depending on the competition between death and birth rates, the activity can spread to the entire system and lead to a finite density of particles (active, self-sustaining state) or die out (absorbing, inactive state). Between these two phases, there is a continuous phase transition, characterized by universal critical behavior [89, 91]. The phase diagram for Directed Percolation in the mean-field approximation (Figure 4.2) will be derived in Section 4.2.1. A direct link between DP and our metapopulation model can be obtained by coarse-graining [89, 91–93]. Upon coarse-graining, the discrete DP occupation variable becomes a continuous quantity that represents the mean occupation, the competition between birth and death rates gives rise to a logistic growth, hopping is replaced by diffusion and the stochastic fluctuations generate the demographic noise.

Note that the active phase can only persist indefinitely in an infinite system: if the number of sites is finite, sooner or later an unfortunate fluctuation will lead to a global extinction. Nevertheless the probability of this event is exponentially small in the number of sites, which means that in a sufficiently large system this would only happen on extremely long timescales.

Directed percolation is a non-equilibrium system because of the microscopic irreversibility of deaths: if a particle without any neighbors self-annihilates, the time-reversed event is simply

impossible. Such events are indicated by red arrows in the time-reversed process in Figure 2.4b. For this reason DP cannot be studied with the standard equilibrium tools, but requires a dynamical treatment. The sole exception is the case of an infinite fully-connected network, in which every particle always has a neighbor (except for in the absorbing state).

2.5 Two species: Lotka-Volterra interactions

Going back to the model without fluctuations nor spatial structure, we will now consider *two* species, indexed by $i = 1, 2$. Assuming that the presence of one species linearly modifies the growth rate of the other leads to the Lotka-Volterra model:

$$\begin{aligned} \dot{N}_1 &= r_1 N_1 \left(k_1 - N_1 - \alpha_{12} N_2\right) \\ \dot{N}_2 &= r_2 N_2 \left(k_2 - N_2 - \alpha_{21} N_1\right) \end{aligned} \tag{2.20}$$

α_{12} and α_{21} are the interaction coefficients. Note that, because of the sign convention used, a positive α_{ij} means that the presence of species j decreases the growth rate of species i, whereas if α_{ij} is positive the presence of species j increases the growth rate of species i. We have three paradigmatic cases:

- If α_{ij} and α_{ji} are both positive, we will call the interactions *competitive*. One example is plants that compete for sunlight.
- If α_{ij} and α_{ji} are both negative, we will call the relationship *mutualistic*. This is the case for plants and pollinators.
- If the two interaction coefficients have different signs, we will call the relationship *parasitic*. For example, if j is a predator and i its prey, we would find $\alpha_{ij} > 0$ and $\alpha_{ji} < 0$.

It is also possible that only one of the interaction coefficients is non-zero: we will then refer to *commensalism* if $\alpha_{ij} > 0$ (e.g. j consumes waste products of i), and to *amensalism* if $\alpha_{ij} > 0$ (e.g. i produces a toxin that kills j). If both interactions coefficients are zero, the two species have a *neutral* relationship. The different cases are summarized in Table 2.1.

	$\alpha_{ij} > 0$	$\alpha_{ij} = 0$	$\alpha_{ij} < 0$
$\alpha_{ji} > 0$	Competition	Amensalism	Parasitism
$\alpha_{ji} = 0$	Amensalism	Neutralism	Commensalism
$\alpha_{ji} < 0$	Parasitism	Commensalism	Mutualism

Table 2.1: Summary of the possible ecological relationship according to the signs of the interaction coefficients.

Thanks to the extreme simplicity of their assumptions, the Lotka-Volterra equations have found numerous applications in a variety of domains, from economics to immunology, and from genetics to evolutionary game theory [94–97].

A simpler version of the Lotka-Volterra model was independently proposed by Alfred Lotka in 1920 [98] and Vito Volterra in 1926 [99] for a predator-prey system. They assumed exponential

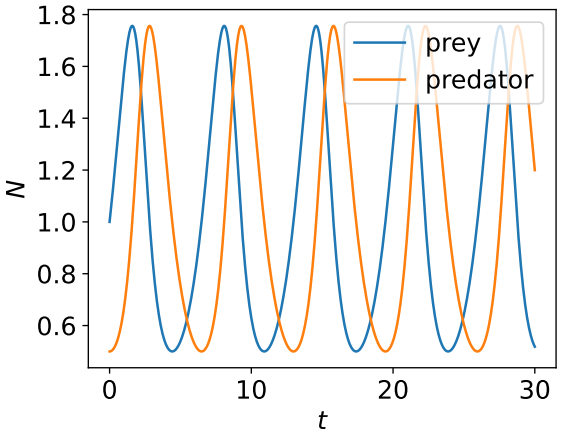

Figure 2.5: Evolution of the abundances of a predator and a prey species (Eq. (2.21)).

growth of the prey (species 1) in the absence of the predator, and exponential death of the predator (species 2) in the absence of the prey. Their simplified model reads:

$$\begin{aligned} \dot{N}_1 &= bN_1 - \alpha_{12}N_1N_2 \\ \dot{N}_2 &= -dN_2 - \alpha_{21}N_1N_2 \end{aligned} \tag{2.21}$$

b and d are positive constants, $\alpha_{12} > 0$ and $\alpha_{21} < 0$ consistently with the previous notation. In this model the abundances of the two species exhibit periodic out-of-phase oscillations (Figure 2.5): a depletion of the predators leads to a growth of the prey, which in turn stimulates the growth of the predators. Ultimately the predators become so abundant that they overconsume the prey, generating a decrease in their abundance. With fewer prey, the predators also decrease in abundance, restarting the cycle. The amplitude of the oscillations depends on the initial conditions.

The periodicity of the oscillations is a non-trivial consequence of the fact that these equations admit a conserved quantity [99], and it is not robust to small perturbations of the model, for example to the reintroduction of a logistic limitation to the growth of prey. However, the oscillatory behavior is a generic consequence of the *non-reciprocity* of the interactions, i.e. of the fact that predators and prey have opposite effects on each other. This will be discussed in detail in Chapter 5.

Going back to the full Equation (2.20), depending on the interactions coefficients, growth rates and carrying capacities, several outcomes are possible. Let us for simplicity consider two species with identical growth rates and carrying capacities, $r_1 = r_2 = r$, $k_1 = k_2 = k$. Without loss of generality we can set $r = 1$ and $k = 1$ by redefining the units of time and abundances. Figure 2.6 summarizes the possible outcomes as a function of the two interactions coefficients:

- *Coexistence*: if the interactions are not too strong (see below), the two species reach a fixed point in which they both have a finite abundance, $N_1 = \frac{1-\alpha_{12}}{1-\alpha_{12}\alpha_{21}}$, $N_2 = \frac{1-\alpha_{21}}{1-\alpha_{12}\alpha_{21}}$
- *Outcompetition*: if either of the interaction coefficients is larger than 1, the two species cannot coexist. If $\alpha_{ij} > 1$ and $\alpha_{ji} < 1$, j drives i to extinction and then reaches the fixed point $N_j = 1$.
- *Alternative fixed points*: if both interaction coefficients are larger than 1, the species that starts at higher abundance drives the other to extinction and then reaches a fixed point.

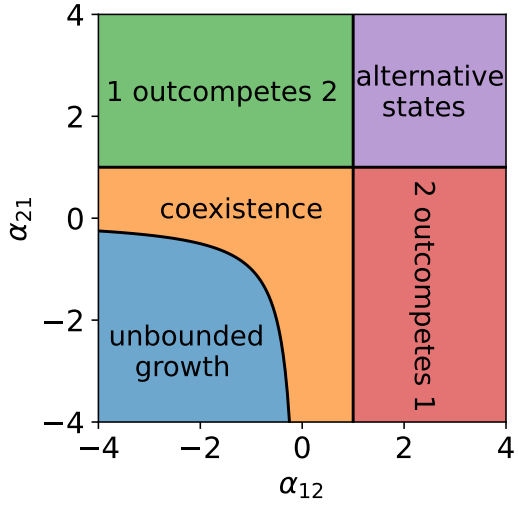

Figure 2.6: Phase diagram of a 2 species Lotka-Volterra system (Equation (2.20)) with $r_1 = r_2 = 1$, $k_1 = k_2 = 1$.

- *Unbounded growth*: if the two species have strong mutualistic interactions ($\alpha_{12}\alpha_{21} > 1$, $\alpha_{12} < 0$, $\alpha_{21} < 0$), they can overcome the quadratic limitation of growth, leading to exponentially diverging abundances. This is a pathology of the model, which can be fixed by including a stronger growth saturation, for example via the θ-logistic model (Eq. 2.8).

2.6 Many species and random interactions

Most natural ecosystems are composed by a very large number of species. We can easily generalize the Lotka-Volterra equations to include a generic number of species S:

$$\dot{N}_i = r_i N_i \left(k_i - N_i - \sum_j \alpha_{ij} N_j \right) \ . \tag{2.22}$$

We have arranged all interaction coefficients in the $S \times S$ matrix α_{ij}.

In principle, given the interaction coefficients, the growth rates and the carrying capacities of each species we can solve these deterministic equations, similarly to what we have done in the previous section in the case of two species. We nevertheless immediately encounter several problems.

First of all, we do not know all the relevant parameters. Measuring ecological interactions is extremely challenging [100], and, since the number of parameters scales as the square of the number of species, already for $S \sim 10$ this is an unfeasible task. Even if we did know all the interaction coefficients, as soon as the number of species is above 2 or 3, it is extremely hard to obtain analytical results: see already the complexity of the 2-species phase diagram in Figure 2.6. We could of course run numerical simulations of the dynamics, but it is not easy to make sense of such a high dimensional parameter space, and even scanning it via numerical simulations could soon become unfeasible. Not to mention the fact that the Lotka-Volterra equations are just a phenomenological description of the dynamics, and small modifications can lead to very different quantitative results.

The statistical physics approach consists in renouncing to make accurate predictions on the quantitative behavior of each of the species, and trying to predict some collective properties of the

ecosystem, based on a few macroscopic parameters. This is possible thanks to *universality*, which is the observation that in many-body systems the large-scale properties are often independent of the details of the dynamics.

A popular approach to study systems in which heterogeneity plays an important role, is to sample randomly the unknown parameters. This idea was pioneered by Wigner, who proposed to predict the statistics of the energy levels of heavy nuclei by considering statistical ensembles of Hamiltonians [101–104]. The approach has been so successful that the study of *disordered systems* has become a field on its own. Further strong motivation came from the analysis of *spin glasses* (see Chapter 5), and the analytical tools developed in that setting have since been applied in an incredible variety of problems, from amorphous solids to neural networks, and from constraints satisfaction problems to, as in this thesis, theoretical ecology [7, 105].

2.6.1 May's bound

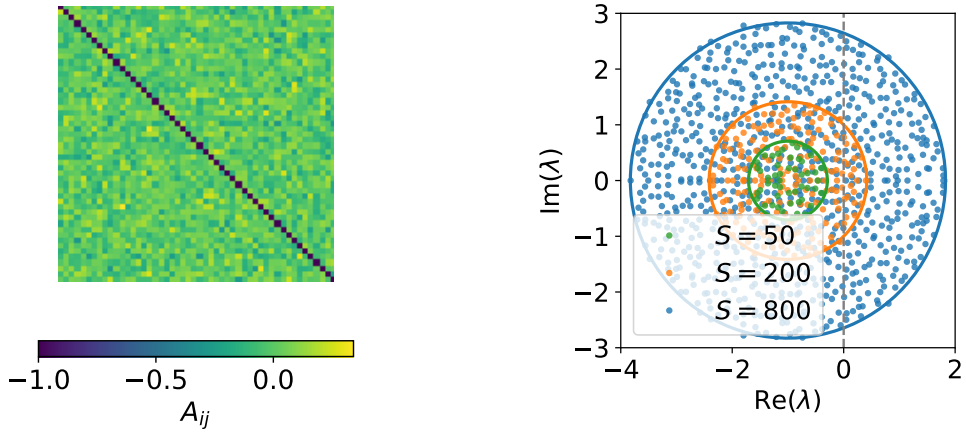

(a) Random matrix A_{ij}

(b) Spectrum of A_{ij} for various values of S

Figure 2.7: (a) A random matrix of the form considered by May ($A_{ij} \sim \mathcal{N}(0, \tilde{\sigma})$ if $i \neq j$, $A_{ii} = -1$) with $S = 50$, $\tilde{\sigma} = 0.1$. (b) Spectrum of A for $\tilde{\sigma} = 0.1$ and various values of S. The circles represent the corresponding analytical predictions for the edges of the spectrum.

A first question we can ask in this setting is: *Will a Large Complex System be Stable?* [106] In order to answer this question, Robert May studied the stability of a fixed point of an unspecified non-linear ecological dynamics. Around this equilibrium point, the dynamics can be linearized, obtaining:

$$\delta \dot{N}_i = \sum_j A_{ij} \delta N_j, \tag{2.23}$$

where A_{ij} is the Jacobian of the system at the fixed point and δN_i is the distance of the abundance of species i from its equilibrium value. He assumed that each species would return to the equilibrium point in the absence of interactions, and thus set all the diagonal elements to -1. All other elements were sampled randomly from a distribution with mean 0 and variance $\tilde{\sigma}^2$ (see Figure 2.7a).

The equilibrium point is stable if all eigenvalues of the matrix A have a negative real part[4], implying that a perturbation from the equilibrium point would be exponentially damped. In the large S limit, the spectrum of A is given by the circular law [106,107]: in the complex plane, the eigenvalues are uniformly distributed inside a circle centered in -1 and of radius $\tilde{\sigma}\sqrt{S}$ (Figure 2.7b). The fixed point will thus be stable if and only if $\tilde{\sigma}\sqrt{S} < 1$. The model can be easily generalized to allow each of the species to interact with only a fraction C of the others, by setting each off-diagonal element to zero with probability $1 - C$. The spectrum of A would then still be given by the circular law, with a modified radius $\tilde{\sigma}\sqrt{SC}$. The corresponding result that the fixed point will be stable if $\tilde{\sigma}\sqrt{SC} < 1$ is known as May's bound.

This indicates that more complexity – i.e. a larger number of species, a stronger heterogeneity and connectance – should lead to less stability, contradicting the previous expectation that complex ecosystems would be more resilient to external perturbations [108, 109]. May's bound also seems unreconcilable with the incredible diversity that is observed in natural ecosystems, and with the observation that ecosystems with few species, such as those in the Arctic, exhibit much stronger fluctuations than species-rich ones, like those in the tropics.

Over the more than fifty years of debate that followed, two main types of critiques have been moved to May's result. The first is that in a real ecosystems, interactions are not random and independent, since they are the result of both evolutionary processes and community assembly. Several works have been devoted to incorporating relevant features into the matrix structure, considering for example different interaction types, trophic levels, or spatial structure [82, 110–114]. The second line of criticism is that, by leaving the dynamics entirely unspecified, May's argument provides no insight into what happens to the ecosystem after it departs from the unstable fixed point. The ecosystem could reach another (possibly stable) fixed point, or enter a stationary chaotic state, as it has been experimentally observed both in synthetic and natural ecosystems. To address this issue, we need to go back to the full dynamics of our Lotka-Volterra model.

2.6.2 GLV phase diagram

In the following we will go beyond May's approach by studying the Generalized Lotka-Volterra (GLV) model with random interactions in the limit of a large number of species S. We will not consider related models that can be studied with similar approaches [115], such as the random replicators model [116–119] or MacArthur's consumer-resource model [38, 120].

In our GLV model, we will also include demographic fluctuations and a (small) immigration from an external reservoir, so that the complete dynamics we will consider reads:

$$\dot{N}_i = r_i N_i \left(k_i - N_i - \sum_j \alpha_{ij} N_j \right) + \eta_i \sqrt{N_i} + \lambda \ . \tag{2.24}$$

Demographic fluctuations can be eliminated by setting the effective temperature T that characterizes their amplitude ($\langle \eta_i(t)\eta_j(t')\rangle = 2T\delta_{ij}\delta(t-t')$) to zero.

We need to specify the distribution of the parameters of each species. For simplicity, we will consider constant growth rates $r_i = r = 1$ and carrying capacities $k_i = k = 1$. The results can be easily generalized to the case of Gaussian distributed carrying capacities.

We will assume that the moments of the distribution of the interactions coefficients scale with the inverse of the number of species S. Since we will consider a fully connected network of interaction, each species will interact with $S - 1$ other species. If the abundances are of order 1, in order to have a finite interaction term in the $S \to \infty$ limit we need the mean and the variance

[4]Unless the matrix is at an exceptional point (see Chapter 5), which we do not expect to occur in a large random matrix without fine-tuning

of α_{ij} to scale as $1/S$. This ensures that the effect of the intra-specific interactions (the logistic limitation of growth) and inter-specific ones (i.e. interactions with other species) are of the same order, so that both contribute to the dynamics. There are several ways to interpret this scaling of the interactions. The first is through the *niche* paradigm [121]: individuals of the same species have the same preferences and eating habits, and therefore compete more strongly than individuals of different species. This nevertheless does not justify why the interaction strength should decrease by adding more species in the system. A more agnostic approach consists in saying that whatever the distribution of the interactions, the combination of parameters that will be predictive of the behavior of the ecosystem when many species are present is, as we already saw in the previous section, the variance multiplied by the number of species. It then makes sense to define a parameter $\sigma^2 = \tilde{\sigma}^2 S$, and to study the system in the limit $S \to \infty$ at fixed σ. Applying the same reasoning also to the mean of the interactions, we obtain precisely the above mentioned scaling. Following this approach, it might be relevant to analyze what happens when the rescaled moments of the interactions diverge. This is the subject of a work that I completed before the beginning of this thesis [5], and that will not be discussed in detail here. Note that a different way to obtain a finite interaction term is to assume that each species interacts with only a finite number of others [122–126].

The interactions coefficients α_{ij} will thus be sampled from a distribution with mean μ/S and variance σ^2/S. For some of the results (the ones obtained by the replica method) we need to assume the distribution to be Gaussian, but most of them hold for a generic distribution with finite mean and variance. Different interaction coefficients are independent, except if they involve the same two species: α_{ij} and α_{ji} will have a correlation coefficient of $\gamma\sigma^2/S$. For $\gamma = 1$, the interaction matrix will be symmetric, $\alpha_{ij} = \alpha_{ji}$, whereas $\gamma < 0$ leads to an anticorrelation between the two interactions coefficients, which is characteristic of predator-prey systems.

In recent years, numerous generalizations of this model have been proposed, including extensions to non-fully connected interaction networks [122–129], the introduction of some additional structure in the interaction matrix [130, 131], a time-dependence of the interaction coefficients [132], and alternative growth laws [133, 134]. Here, we will restrict our discussion to a fully connected network of quenched, unstructured interactions, and Lotka-Volterra dynamics.

The phase diagram of this model, detailed below, can be obtained with several different methods borrowed from the disordered systems literature. The *replica method* [5, 11, 12, 105] allow us to obtain precious insights into the behavior of the system in the high heterogeneity regime, but is limited to symmetric interactions. The alternative approach is to use *Dynamical Mean Field Theory* [10, 131, 135–137], whose derivation will be described in Chapter 3.

Depending on the mean, variance and covariance of the interactions, the ecosystem exhibits four different dynamical regimes (see Figure 2.8). Representative time evolutions of the abundances in the four regimes are plotted in Figure 2.9.

The single equilibrium phase

When the heterogeneity of the interactions is small and their mean is not too negative, the ecosystem has a unique fixed point, which is reached no matter the initial conditions (Figure 2.9a) and is stable against perturbations. Relaxation to this fixed point is exponential in time.

At the fixed point a finite fraction of the species goes extinct. Taking this into account, May's bound is always satisfied in this phase, and we can show that it is saturated when the phase loses stability (to the multiple attractors phase). This instability line will be derived in Section 3.4.1.

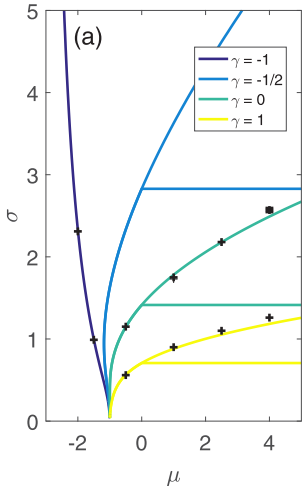

Figure 2.8: Phase diagram of the random Lotka-Volterra system without demographic noise, as a function of the mean and variance of the interactions, for different values of the correlation between opposite off-diagonal elements, reproduced from [10]. In the bottom right area the system is in the single equilibrium phase, crossing the horizontal line we enter the multiple attractors phase, beyond the curved line we have unbounded growth.

The unbounded growth phase

When interactions are strongly mutualistic (i.e. the mean interaction is below a certain threshold) or very heterogeneous, a subset of species can succeed in overcoming the quadratic saturation and grow unboundedly (Figure 2.9d), just as we saw in the case of two species. Again this is a pathology of the model, which can be cured by introducing a stronger saturation of growth.

The multiple attractors phase

Between the single equilibrium phase and the unbounded growth one, the dynamics of the system strongly depends on the initial conditions. The behavior is quite different for symmetric ($\gamma = 1$) and non-symmetric interaction matrices.

If $\gamma = 1$, the dynamics of the system can be described as a descent in a rugged landscape that has an exponential number (in S) of fixed points [12]. If we consider a finite number of species, at long times the system will approach one of these fixed points. Which fixed point will be selected depends on the initial conditions: restarting the dynamics from different values of the abundances we generally reach a different equilibrium point (Figure 2.9b). When the number of species is very large, the system will not manage to approach any of the fixed points, but its dynamics will dramatically slow down as time goes on. This phenomenon, called *aging* [138–140], is characteristic of conservative disordered systems, and it will be analyzed in detail in Chapter 5. In the presence of demographic noise, there are actually two distinct multiple equilibria phases: one, at moderate temperature, in which equilibria are locally stable (corresponding to a one-step replica symmetry broken phase [105]) [12], and one, at low temperature, in which all equilibria are posed at the edge of stability and are organized in a fractal hierarchical structure (corresponding to a full replica symmetry broken phase [105]) [11].

For $\gamma \neq 1$, the landscape descent is replaced by a chaotic dynamics, which was recently studied in detail in references [141–143].

In the presence of a finite immigration rate, the system reaches a dynamical steady state, in which the abundance of all species fluctuate over several orders of magnitude, going from $O(\lambda)$ to $O(1)$ (Figure 2.10a). Each species has long periods of time in which its total growth rate is

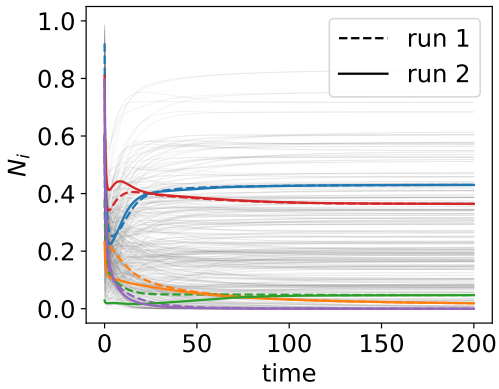

(a) Single equilibrium

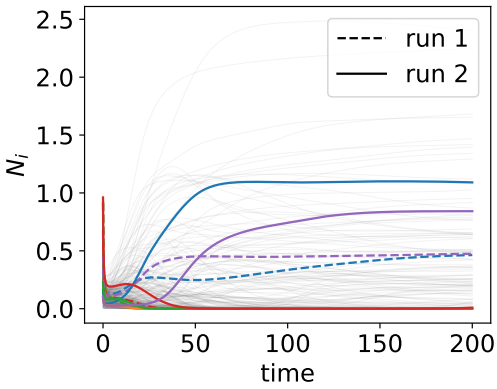

(b) Multiple equilibria

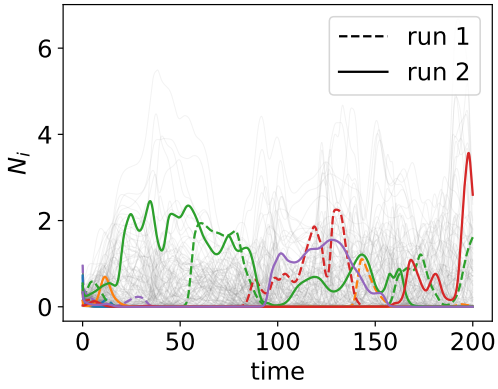

(c) Chaotic dynamics

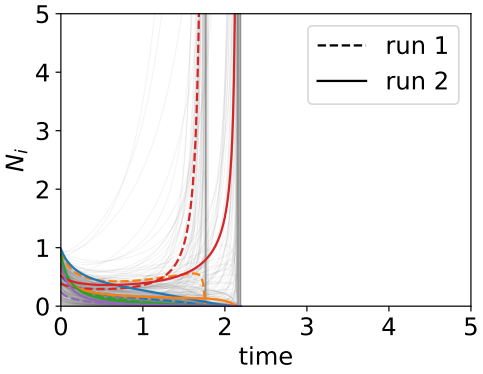

(d) Unbounded growth

Figure 2.9: Time evolution of the abundances in the 4 dynamical regimes, without demographic noise. 5 randomly selected species are highlighted in different colors. For each case, two runs of the simulation with the same interaction matrix but different random initial conditions are shown. Parameters:
(a) $S = 200$, $\mu = 4$, $\sigma = 0.6$, $\gamma = 0.5$, $\lambda = 10^{-4}$.
(b) $S = 200$, $\mu = 10$, $\sigma = 1.1$, $\gamma = 1$, $\lambda = 10^{-4}$.
(c) $S = 200$, $\mu = 10$, $\sigma = 2.5$, $\gamma = 0.1$, $\lambda = 10^{-4}$.
(d) $S = 200$, $\mu = 10$, $\sigma = 3$, $\gamma = 0.5$, $\lambda = 10^{-4}$.

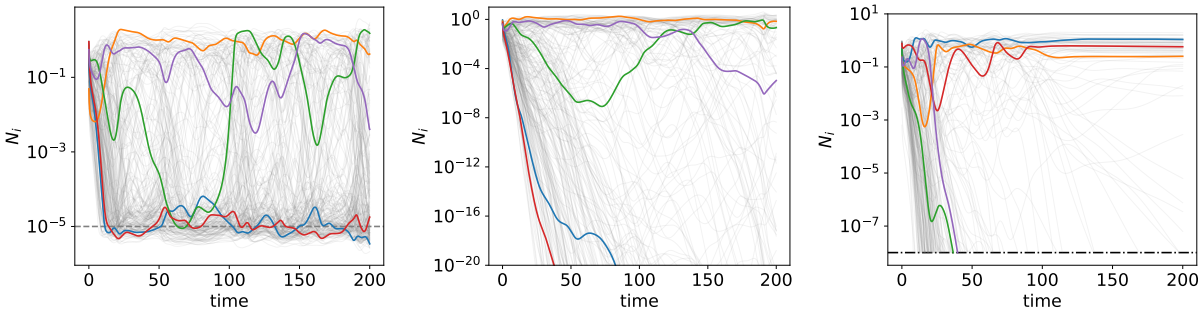

(a) $\lambda = 10^{-5}$, $N_c = 0$ (b) $\lambda = 0$, $N_c = 0$ (c) $\lambda = 0$, $N_c = 10^{-8}$

Figure 2.10: Time evolution of the abundances in the chaotic phase without demographic noise in log-scale. (a) With a finite immigration (indicated by gray dashed line), (b) with no immigration, (c) with a finite extinction threshold (indicated by black dotted line). 5 randomly selected species are highlighted in different colors. Parameters: $S = 200$, $\mu = 10$, $\sigma = 2.5$, $\gamma = 0$, $T = 0$.

negative and it is kept at $N_i \propto \lambda$ by the immigration. Occasionally, a reshuffling of the most abundant species renders conditions favorable, and the species starts to grow exponentially, until it reaches $N_i \sim 1$ and starts to experience self-limitation. This behavior resembles the bloom dynamics observed in planktonic communities [26, 144–146]. For very small λ, growing from $N_i \propto \lambda$ to $N_i \sim 1$ takes a time of order $\log \lambda$, therefore the reshuffling of the dominant species and the dynamics of the system is controlled by this (long) timescale.

Without immigration, the abundance of species continues to decay exponentially for as long as their growth rate is negative. If a reshuffling in the dominant community renders their growth rate positive, it takes them a very long time (of the order of the time expired since the preparation of the system) to grow back to abundances of order 1 (Figure 2.10b). The dynamics becomes therefore slower and slower in time, a phenomenon that has also been called aging, despite having a quite different origin from the one found in conservative disordered systems.

Clearly, abundances of the order of 10^{-20} cannot meaningfully represent our population, since in any realistic situation this would correspond to less than one individual. In order to take this into account, we should introduce an extinction threshold N_c, and declare extinct any species whose abundance becomes smaller than the threshold. In this case, fluctuations lead many of the species to extinction. This reduces the complexity of the ecosystem, effectively reducing the heterogeneity σ, until the fixed point solution becomes stable and abundances stop fluctuating (Figure 2.10c).

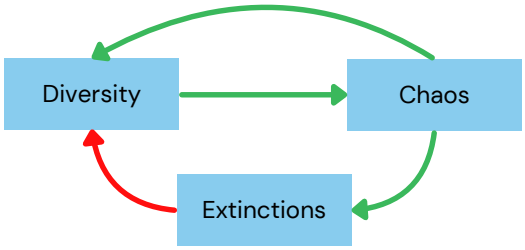

Figure 2.11: Scheme summarizing the relations of diversity, chaos, and extinctions: in the considered model, chaos is only realized in diverse enough communities, and in turn it allows the coexistence of more species than it would be possible at equilibrium. At the same time, chaos generates extinctions that reduce the diversity of the ecosystem, ultimately suppressing itself.

Chaotic dynamics is widely observed in natural and synthetic ecosystems [147–151], and, since it allows the ecosystem to escape May's bound, it has been proposed as an important ingredient in the stabilization of diversity, in particular in planktonic communities [152]. Nevertheless, this appears incompatible with the above described "self-defeating" mechanism, summarized in Figure 2.11: chaotic fluctuations generate extinctions, until the diversity decreases to the point that chaotic dynamics is not sustained anymore.

This puzzle could be solved by taking into account the spatial extension of ecosystems [153–156]. In a meta-community, local populations could exhibit desynchronized fluctuations, which, as in the case of demographic fluctuations, would lead to local and not global extinctions, maintaining the diversity of the ecosystem.

2.7 Ecosystems as a physical system

Throughout this chapter, I have highlighted the many contributions that Statistical Physics can bring to Theoretical Ecology. There is nevertheless another side of the medal: Ecology can be a source of inspiration for physicists to explore dynamics that are forbidden to more traditional physical systems. To conclude this introduction, I would like to briefly summarize which peculiar features of ecological systems make them interesting from the physical point of view.

Many individuals

The fact that populations are often composed of many individuals allows us to approximate the abundance with a continuous variable, and to write differential equations for its evolution. It also enables a statistical description of the many biological details that we do not wish to model.

Multiplicative processes

One of the essential features of living organism is *reproduction*. Since all individuals undergo reproduction and death events simultaneously, most ecological processes are *multiplicative*, and the dynamics is often dominated by exponential growths and decays. An important consequence is that a small difference in the growth rate can be much more important than the initial conditions, and advantageous mutations can easily spread to an entire population. It is also the origin of the unique "aging of chaos" phenomenon described in the previous section.

Extinctions

Another effect of the multiplicativity of growth is that a population always has an absorbing state: extinction. This leads to interesting connections to directed percolation, and has important consequences on the nature and stability of the chaotic dynamics.

Different kinds of stochasticity

Populations are subjected to different kinds of multiplicative stochasticity: environmental and demographic, white and colored. Each of them has different effects on the dynamics, for example causing or not extinctions, leading to a rich phenomenology.

Large number of species and heterogeneous interactions

Having many coupled degrees of freedom opens the way to collective phenomena and phase transitions. The heterogeneity in the interaction network leads to the fascinating emergent

behavior that I described in the previous section. Interestingly, this diversity is not just a given like in other many-body systems, but also a puzzle in itself: *why* are there so many species?

Non-reciprocal interactions

Predation is a very natural example of non-reciprocal interactions: the presence of the prey enhances the growth of the predator, whereas the predator suppresses the growth of the prey. As we will see in Chapter 5, non reciprocal interactions, that are forbidden in traditional physical systems by Newton's action-reaction principle, lead to a variety of fascinating non-equilibrium phenomena, from chaotic dynamics to oscillatory states.

Interaction network replicated across space

In a spatially extended ecosystem, each local community is controlled by the same (complex) interaction matrix. From the disordered systems perspective, we can see an ecological meta-community as a collection of coupled identical spin-glasses, each with the same microscopic realization of the disorder. In the multiple attractor phase (both in the landscape descent and in the chaotic case), this leads to very interesting questions on the synchronization of the dynamics of different communities.

Chapter 3

Dynamical Mean Field Theory and effective neutral models

In this chapter, I will present Dynamical Mean Field Theory (DMFT) [157–159], one of the main analytical tools throughout this thesis. As we will see, it allows us to replace a many-body system with an effective description of a single degree of freedom coupled to an additional noise source. In some cases this enables an analytical closure of the problem; we will in particular show how to obtain the transition from the single equilibrium to the multiple attractors phase in the absence of demographic noise. We will then study the stationary probability distributions that various forms of stochasticity give rise to, and discuss an approximate solution scheme for the DMFT equations.

The first part of the chapter is a review of the literature, whereas Sections 3.5 and 3.6 also contain original and ongoing work in collaboration with Jules Fraboul.

3.1 Dynamical Mean Field Theory

Dynamical Mean Field Theory (DMFT) is a powerful technique that allows one to study the complex dynamics of systems with many interacting degrees of freedom. Even though it was first developed to study mean-field spin-glasses [13, 157, 160–163], it has since been employed in several different contexts from quantum many-body systems to the ecological dynamics considered here [66, 164].

DMFT can be applied to systems in which each degree of freedom is coupled *weakly* to *many* others. When these two hypothesis are satisfied, correlations in the system remain small, and we can look for an effective dynamics for a single degree of freedom, considering everything else as a source of noise.

The procedure is analogous to the one used to derive Langevin's equation from Newtonian dynamics [165, 166], schematized in Figure 3.1. Imagine we want to describe the dynamics of a large particle immersed in a bath of smaller particles (Fig. 3.1a). Indicating with X the position of the large one, and with x_i the position of each of the small particles, we can write down Newton's equations of motion:

$$M\ddot{X} = \sum_i F_{int}(X, x_i) + F_{ext}(X) \ , \tag{3.1}$$

$$m\ddot{x_i} = F_{int}(x_i, X) + \sum_j F_{int}(x_i, x_j) + F_{ext}(x_i) \ . \tag{3.2}$$

We have indicated with F_{int} all the interaction forces, and with F_{ext} the external ones. Deriving the trajectory of every single particle from these equations of motion is not feasible when many

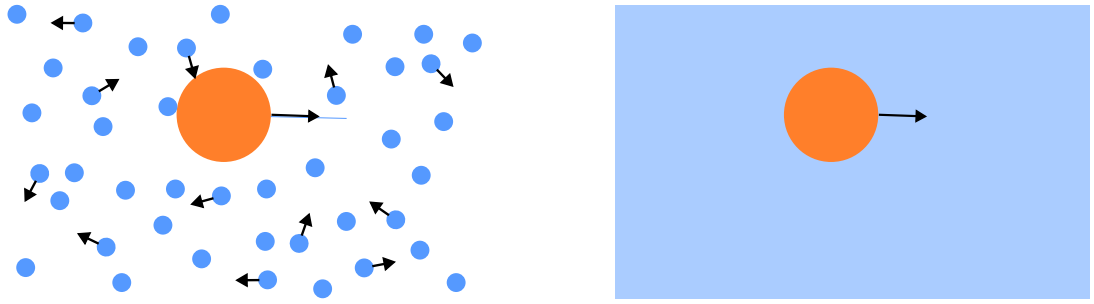

(a) Large particle surrounded by small ones.

(b) Large particle in a heat bath.

Figure 3.1: Integrating out the dynamics of the small particles, we can go from a many-body system to the description of a unique degree of freedom coupled to a colored heat bath.

particles are involved. If we are only interested in the large particle, we can try to give a statistical description of the force that all the small ones apply on it, and study the dynamics of the large particle under an effective non-interacting but stochastic model. This strategy is successful if the small particles are very numerous, their dynamics are not too strongly correlated, and they all apply small forces. In this case, we can apply the central limit theorem to claim that the sum of the forces they apply on the large particle will be Gaussian distributed.

Two further effects should be taken into account. First of all, the dynamics of the small particles takes place on some finite timescale. This implies that the forces they apply will be correlated at short times. If we want to replace them with a noise term, this noise should be colored, meaning it should have a finite correlation time. Furthermore, the force between the big and the small particles depends also on the dynamics of the big one: if we try to suddenly move it in one direction, it would collide with many small ones, experiencing an effective friction. Because the small particles respond on a finite timescale, this effective friction is not instantaneous, but has some memory. The resulting equation for the dynamics of the large particle will therefore be of the form:

$$M\ddot{X}(t) = -\int_0^t R(t,t')\dot{X}(t') + \Xi(t) + F_{ext}(X) \ . \tag{3.3}$$

Ξ is a Gaussian noise with mean 0 and correlation $\langle \Xi(t)\Xi(t') \rangle = C(t,t')$. The functions R and C depend on the dynamics of the small particles. At equilibrium, they are linked by the Fluctuation-Dissipation Theorem (FDT) [166]:

$$R(t+\tau,t) = -\frac{1}{T}\frac{dC(t+\tau,t)}{d\tau} \tag{3.4}$$

for $\tau > 0$. T is the *temperature* of the system, related to the amount of energy that is stored in the small particles.

Note that we have obtained a stochastic model from a deterministic one. The randomness of the noise signals our ignorance of the exact initial conditions of the degrees of freedom that we have integrated out: averaging over such initial conditions corresponds to an average over the noise.

The idea of DMFT is very similar: we want to replace the interactions between degrees of freedom with a noise and a memory term. The main difference is that in this case the degree of freedom we are interested in is equivalent to the ones we want to integrate out. This means that the noise and memory term must be computed *self-consistently*.

3.2 DMFT derivation

We here present a (non-rigorous) derivation of DMFT by the cavity method [66, 105] in a slightly generalized framework, that will be relevant both for the Lotka-Volterra system and for the spherical spin models that we will study in Chapter 6. We will consider S degrees of freedom x_i whose evolution is described by the stochastic differential equation:

$$\dot{x}_i = f(x_i) + g(x_i)\left(\sum_{j=1}^{S} \alpha_{ij} x_j + \zeta_i\right) + l(x_i)\eta_i \ . \tag{3.5}$$

f, g and l are generic and possibly non-linear functions, η_i is a noise that acts independently on each degree of freedom, of which we do not need to specify the distribution. ζ_i is an external field that we introduce to compute response functions, and that will be taken to zero at the end of the computation. The initial conditions are sampled independently from a distribution $P_0(x_i)$.

Note that the system contains three sources of randomness: the static interaction coefficients α_{ij} (which represent the *quenched disorder*), the dynamical noises η_i, and the initial conditions. $\mathbb{E}[\cdot]$ indicates an average over all sources of randomness.

The interactions α_{ij} are sampled from a distribution with mean, variance and covariance between opposite off-diagonal elements given by:

$$\mathbb{E}[\alpha_{ij}] = \frac{\mu}{S} \tag{3.6}$$

$$\mathrm{Var}[\alpha_{ij}] = \frac{\sigma^2}{S} \tag{3.7}$$

$$\mathrm{Cov}[\alpha_{ij}, \alpha_{ji}] = \frac{\gamma\sigma^2}{S} \ . \tag{3.8}$$

If we fix the interaction matrix and the realization of the noise at all times $\eta_i(t)$, Eq. (3.5) deterministically defines the trajectories of the S degrees of freedom, indexed from 1 to S. We will call these trajectories $x_i^0(t)$, or "unperturbed trajectories". Let us now imagine adding a new degree of freedom, with index 0, and drawing its initial conditions and interactions independently from the rest of the system. Since the interactions with each of the other components are of order $1/\sqrt{S}$, its introduction can be considered a small perturbation, and we can compute the linear response of each of the trajectories to it, denoted by $\delta x_i(t)$:

$$\delta x_i(t) = \sum_{j=1}^{S} \int_0^t dt' R_{ij}(t,t') \alpha_{j0} x_0(t') \ , \tag{3.9}$$

where $R_{ij}(t,t') = \frac{\delta x_i(t)}{\delta \zeta_j(t')}$ is the response of x_i at time t to a perturbation applied on x_j at time t'. The dynamics of x_0 will depend on the perturbed trajectories of all other degrees of freedom:

$$\dot{x}_0 = f(x_0) + g(x_0)\left(\sum_{j=1}^{S} \alpha_{0j}(x_j^0 + \delta x_j) + \zeta_0\right) + l(x_0)\eta_0 \ . \tag{3.10}$$

Note that since the trajectories (deterministically) depend on the random interactions, the initial conditions and the realization of the noise $\eta_i(t)$, they can also be considered random variables. In the limit $S \to \infty$ the interaction term $\sum_{j=1}^{S} \alpha_{0j}(x_j^0 + \delta x_j)$ will be the sum of many weakly correlated stochastic quantities. Its statistics will converge to a Gaussian, whose mean and variance can be evaluated by the central limit theorem. Since the unperturbed trajectories

are by definition uncorrelated from x_0, we can define $\Xi(t) = \sum_j \alpha_{0j} x_j^0(t)$ and consider it an additional independent noise term in the dynamics of x_0. Since we expect it to be Gaussian, we only need to compute its first two moments. Using the fact that the unperturbed trajectories are independent from the interactions with x_0, we obtain:

$$\mathbb{E}\left[\Xi(t)\right] = \frac{\mu}{S}\sum_j \mathbb{E}\left[x_j^0(t)\right] \tag{3.11}$$

$$\mathrm{Cov}\left[\Xi(t),\Xi(t')\right] \approx \sum_{j,j'} \mathrm{Cov}\left[\alpha_{0j}\alpha_{0j'}\right]\mathbb{E}\left[x_j^0(t)x_{j'}^0(t')\right] = \frac{\sigma^2}{S}\sum_{j,j'}\delta_{jj'}\mathbb{E}\left[x_j^0(t)x_{j'}^0(t')\right] \ . \tag{3.12}$$

We have neglected terms of higher order in $1/S$. The fact that off-diagonal terms (with $j \neq j'$) will not matter in the limit $S \to \infty$ is not trivial, despite their being of higher order, since they are much more numerous than the diagonal ones. This can nevertheless be shown to hold in perturbation theory in the interaction strength [66, 105].

Since all degrees of freedom are equivalent after averaging over the disorder, the averages in Eq. (3.11) and (3.12) do not depend on j. We can then define $h(t) = \mathbb{E}\left[x_j^0(t)\right]$ and $C(t,t') = \mathbb{E}\left[x_j^0(t)x_j^0(t')\right]$, so that:

$$\mathbb{E}\left[\Xi(t)\right] = \mu h(t) \ , \tag{3.13}$$

$$\mathrm{Cov}\left[\Xi(t),\Xi(t')\right] = \sigma^2 C(t,t') \ . \tag{3.14}$$

We will call $C(t,t')$ the averaged autocorrelation function of the system.

Unlike the unperturbed trajectories, the perturbations are correlated with the interactions with x_0. We can use their explicit expression from Eq. (3.9):

$$\sum_i \alpha_{0i}\delta x_i = \sum_i \alpha_{0i}\sum_j \alpha_{j0}\int_0^t dt' R_{ij}(t,t')x_0(t') \approx \frac{\gamma\sigma^2}{S}\int_0^t dt' \sum_j R_{jj}(t,t')x_0(t') \ . \tag{3.15}$$

We have again neglected higher order terms, which do not contribute in the $S \to \infty$ limit. We define the averaged response function $R(t,t') = \mathbb{E}\left[R_{jj}(t,t')\right]$, which also does not depend on j.

Substituting the results in the dynamics for x_0 we obtain:

$$\dot{x}_0 = f(x_0) + g(x_0)\left(\Xi + \gamma\sigma^2\int_0^t dt' R(t,t')x_0(t') + \zeta_0\right) + l(x_0)\eta_0 \ . \tag{3.16}$$

As in the case described in the previous section, we have managed to decouple the dynamics of x_0 from the rest of the system, by replacing the interactions with additional noise and memory terms. Indeed the structure of the equation is very similar to Equation (3.3).

It is now crucial to note that the added degree of freedom x_0 is statistically identical to all others, and that when S is large the systems composed of S or $S+1$ degrees of freedom are equivalent. Therefore the response and correlation functions that define the effective dynamics of x_0 can be computed as averages over the effective dynamics:

$$h(t) = \mathbb{E}[x_0(t)] \ , \tag{3.17}$$

$$C(t,t') = \mathbb{E}[x_0(t)x_0(t')] \ , \tag{3.18}$$

$$R(t,t') = \frac{\partial \mathbb{E}[x_0(t)]}{\partial \zeta_0(t')} \ . \tag{3.19}$$

The resulting equations do not depend on the index 0, so we will drop it in the following. The averages are now over η, Ξ and the initial conditions of the effective process. Because the effective process depends on the average response and correlation functions, h, C and R must be computed self-consistently: the functions measured on the effective process should match the ones used to define the process itself. This procedure can be shown to be exact in the thermodynamic limit $S \to \infty$ [167].

3.3 DMFT for Lotka-Volterra

We can now apply these results to the generalized Lotka-Volterra equations in the presence of demographic noise and immigration:

$$\dot{N}_i = r_0 N_i \left(k - N_i - \sum_j \alpha_{ij} N_j + \zeta_i \right) + \eta_i \sqrt{N_i} + \lambda \ . \tag{3.20}$$

η_i is a Gaussian white noise with mean zero and correlations $\langle \eta_i(t)\eta_j(t')\rangle = 2T\delta_{ij}\delta(t-t')$. As we discussed in Section 2.6.2, we will consider random interactions α_{ij} with mean μ/S, variance σ^2/S, and covariance between opposite off-diagonal elements $\gamma\sigma^2/S$. The external field ζ_i is introduced to compute response functions and will be taken to zero at the end of the computation. Note that because it acts additively on the carrying capacity, the response functions will measure how species react to an infinitesimal variation of their carrying capacity. In an experimental setting, this could correspond to a change in the availability of a limiting resource.

Applying the method described in the previous section, we obtain the DMFT equations for this system:

$$\dot{N} = r_0 N \left(k - N - \Xi + \sigma^2 \gamma \int_0^t R(t,t') N(t') dt' + \zeta \right) + \eta \sqrt{N} + \lambda \ . \tag{3.21}$$

The statistics of the noise Ξ and the response function R must solve the self-consistent equations:

$$\mathbb{E}[\Xi(t)] = \mu \mathbb{E}[N(t)] \tag{3.22}$$

$$\mathrm{Cov}[\Xi(t), \Xi(t')] = \sigma C(t,t') = \sigma \mathbb{E}[N(t)N(t')] \tag{3.23}$$

$$R(t,t') = \frac{\partial \mathbb{E}[N(t)]}{\partial \zeta(t')} \ . \tag{3.24}$$

In the single equilibrium phase and in the case of chaotic dynamics in the presence of a finite immigration, the system reaches a (possibly non-equilibrium) steady state. One-time observables become time-independent, and two-time ones only depend on the time difference. When this occurs, it will be convenient to break down Ξ in several contributions. We will first of all separate its mean μh. What remains has mean 0, but does not decorrelate at long times, because, since the abundances are strictly positive, $C(t+\Delta t, t)$ is finite in the limit $\Delta t \to \infty$. We can therefore also separate a static and a dynamical component:

$$\Xi(t) = \mu h + \sigma z \sqrt{q_0} + \sigma \xi(t) \ . \tag{3.25}$$

μh is a static deterministic contribution, $\sigma z \sqrt{q_0}$ a static random one that plays the role of quenched disorder. z is a time-independent random variable with mean 0 and variance 1, $q_0 = \lim_{\Delta t \to \infty} C(t+\Delta t, t)$. Therefore $\xi(t)$ has mean 0 and decorrelates at long times:

$$\mathbb{E}[\xi(t+\Delta t)\xi(t)] = C(t+\Delta t, t) - q_0 \xrightarrow[\Delta t \to \infty]{} 0 \ . \tag{3.26}$$

At steady state, averaging over ξ and η is equivalent to averaging over time (but not over disorder) the behavior of a single species[1]. We will indicate this average with angular brackets, $\langle \cdot \rangle$. The average over the quenched variable z corresponds instead to an average over disorder, or over species, which will be indicated with an overline $\overline{\cdot}$. The fact that averaging over degrees

[1] In deterministic systems (i.e. at zero temperature), the noise is generated by the chaotic dynamics of the system. Averaging over this noise corresponds to averaging over initial conditions.

of freedom at fixed disorder is equivalent to averaging over the disorder is a non-trivial property of these systems called *self-averaging*.

With this new notation, the DMFT equation becomes:

$$\dot{N} = r_0 N \left(k - N - \underbrace{\mu h}_{1.} - \underbrace{\sigma z \sqrt{q_0}}_{2.} - \underbrace{\sigma \xi}_{3.} + \underbrace{\sigma^2 \gamma \int_0^t R(s) N(t-s) ds}_{4.} + \zeta \right) + \eta \sqrt{N} + \lambda \ , \quad (3.27)$$

and the self-consistency conditions:

$$h = \overline{\langle N \rangle} \quad (3.28)$$

$$C(\Delta t) = \overline{\langle N(t+\Delta t) N(t) \rangle} \quad (3.29)$$

$$R(\Delta t) = \frac{\partial \overline{\langle N(t+\Delta t) \rangle}}{\partial \zeta(t)} \ . \quad (3.30)$$

For $\Delta t \gg 1$, the dynamical averages in Equation (3.29) decouple, so that we can express $q_0 = \lim_{\Delta t \to \infty} C(\Delta t) = \overline{\langle N \rangle}^2$.

We have obtained an effective model in which interaction between species are replaced by four terms:

1. A constant reduction (or increase, if $\mu < 0$) of the effective carrying capacity of all species: because of intraspecific competition, all species will saturate to a lower abundance. This reduction is equal to μh, the average interaction coefficient multiplied by the average abundance.

2. Again a constant shift of the effective carrying capacity, but different for each species. Because of the heterogeneity in the interaction network, some species will experience a more favorable effective environment. Indeed this random shift, with mean 0, is proportional to the heterogeneity σ.

3. A colored environmental noise (see Section 2.3.1). Its correlation function will not be exponential as in the simple case considered in Sec. 2.3.1, but will be self-consistently determined. We can nevertheless define a correlation time-scale τ, which should match the timescale of the dynamics of the abundances. This observation is at the basis of the approximate solution scheme proposed in Section 3.6. Note that this noise is also proportional to σ: without heterogeneity there is no environmental noise, even if the single species abundances do fluctuate because of the demographic noise η.

4. A memory term, linking the evolution at time t to the abundance at time t'. It is due to the feedback that each species has on itself through the interaction with other species: species i influences species j through the interaction coefficient α_{ji}, and this influence feedbacks on i through α_{ij}. If α_{ij} and α_{ji} are correlated (as expressed by $\gamma \neq 0$), all these feedbacks sum up to give a net contribution. This memory term will also have a timescale, which should match the one of the correlation of the noise.

In general, solving the DMFT equations requires the determination of the correlation and response functions as a function of time, which can only be done numerically [66].

There are two values of γ for which some simplifications occur. The first is $\gamma = 0$, in which case we do not have the memory term. This simplifies both the numerical solution of the DMFT equations, since it is not necessary to compute the response function [66], and the analytical treatment. The second special case is $\gamma = 1$, corresponding to symmetric interactions.

As we will explain in Sec. 3.5.1, when interactions are symmetric the system undergoes a reversible dynamics at temperature T. Below a critical value of the heterogeneity, equilibrium is reached and the response and correlation functions verify the Fluctuation-Dissipation Theorem (FDT) [11, 12, 158]. This allows us to explicitly compute the stationary probability distribution in terms of some self-consistently determined moments of N, obtaining analytical closure of the problem.

3.4 Single equilibrium phase without demographic noise

To demonstrate the effectiveness of DMFT as an analytical tool, we now apply it to analyze the single equilibrium phase in the absence of demographic noise. Without demographic noise, the single equilibrium phase is particularly simple because there is no dynamical fluctuation. The abundances converge to one of the fixed points of Equation (3.27). We fix $\lambda = 0$, since it does not have a strong effect in this phase.

$k - \mu h - \sigma z\sqrt{q_0}$ can be viewed as an effective carrying capacity. If it is positive, the species will converge (starting from any finite initial condition) to the "survival" fixed point:

$$N = \frac{k - \mu h - \sigma z\sqrt{q_0} + \zeta}{1 - \sigma^2 \gamma R_{int}} \ , \tag{3.31}$$

where $R_{int} = \int_0^\infty R(s)ds$ is the integrated response. If $k - \mu h - \sigma z\sqrt{q_0} < 0$, the species has instead a negative effective carrying capacity and will inevitably go extinct, converging to $N = 0$. By linear analysis, we can show that the survival fixed point is stable if and only if it is positive, so that we can compactly write the stable fixed point solution as:

$$N = N^*(z) = \max\left\{0, \ \frac{k - \mu h - \sigma z\sqrt{q_0} + \zeta}{1 - \sigma^2 \gamma R_{int}}\right\} \ . \tag{3.32}$$

The fixed point value N^* explicitly depends on the disorder z, meaning that it will be different from species to species. Since z is Gaussian, the abundances will be distributed according to a truncated Gaussian, with a δ-function in $N = 0$. A finite fraction of the species, those with $z > \frac{k-\mu h}{\sigma\sqrt{q_0}}$, are extinct at the fixed point. We will denote the fraction of surviving species, or *diversity*, with ϕ. Formally it can be computed as $\phi = \overline{\langle\theta(N)\rangle}$, where θ is the Heaviside step function. There is a good quantitative agreement between this Gaussian distribution and the distribution obtained from numerical integration of the original many-species Lotka-Volterra equations, without any fitting parameter (Figure 3.2).

Since the fixed point only depends on the integrated response and there are no dynamical fluctuations, we only need to self-consistently determine three static quantities:

$$h = \overline{N^*(z)} = \int \mathcal{D}z N^*(z) \tag{3.33}$$

$$q_0 = \overline{(N^*(z))^2} = \int \mathcal{D}z \left(N^*(z)\right)^2 \tag{3.34}$$

$$R_{int} = \overline{\frac{\partial N^*(z)}{\partial \zeta}} = \int \mathcal{D}z \frac{\partial N^*(z)}{\partial \zeta} \ . \tag{3.35}$$

We have introduced a compact notation for the Gaussian integration over the disorder $\int \mathcal{D}z = \int \frac{dz}{\sqrt{2\pi}} e^{-z^2/2}$. Note that the integrated response is obtained perturbing the average abundance with a constant field ζ, instead of an instantaneous one as for the time-dependent response.

These self-consistent equations can be solved by iteration: starting with some initial guesses for the values of the order parameters h, q_0 and R_{int}, we compute $N^*(z)$. Integrating it over the

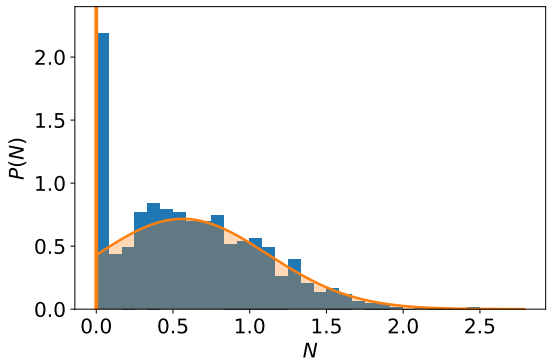

Figure 3.2: Comparison between the distribution of abundances obtained from numerical simulations of Eq. 3.20 (blue) and the truncated Gaussian predicted by DMFT (orange). The vertical orange line represents a delta function in $N = 0$, with weight $1 - \phi$. $T = 0$, $\lambda = 0$, $\mu = 1$, $\sigma = 0.5$, $\gamma = 1$, $S = 1000$. Self-consistently determined parameters: $h = 0.6078$, $q_0 = 0.6032$, $R_{int} = 1.2096$. h and q_0 match the result of numerical simulations within a 10% error margin ($h_{NUM} = 0.60$, $q_{0NUM} = 0.58$).

Gaussian distribution of z, we obtain an updated guess for the order parameters. We iterate this procedure until the difference between the old and updated guesses is below an error threshold, signaling we reached a self-consistent solution. To improve the stability of the method, we perform at each step a "soft injection", summing with weight ϵ and $1 - \epsilon$ the updated and previous guesses. It is with this procedure that the solutions for h, q_0 and R_{int} were obtained in Figure 3.2.

3.4.1 Stability of the fixed point solution

The transition line from the unique equilibrium phase to the multiple attractors one can be obtained studying the stability of the fixed point solution to perturbations. We consider as a perturbation a small white environmental noise $\zeta(t)$, with correlations $\langle \zeta(t)\zeta(t') \rangle = 2\epsilon\delta(t - t')$, $\epsilon \ll 1$. Let us first consider non extinct species. Linearizing around the non-zero fixed point of Eq. (3.27), we obtain:

$$\delta\dot{N} = r_0 N^* \left(-\delta N - \sigma\xi + \gamma\sigma^2 \int_0^t R(t - t')\delta N + \zeta \right) , \tag{3.36}$$

where $\delta N = N - N^*$. The perturbation ζ leads to fluctuations of the abundances of all species, generating an additional noise ξ. Its statistics is self-consistently determined by

$$\langle \xi(t)\xi(t') \rangle = C(t - t') = \overline{\langle \delta N(t)\delta N(t') \rangle} . \tag{3.37}$$

This linearization is valid for non extinct species. Extinct species have a negative effective carrying capacity, leading to exponential decrease of their abundance. Adding a small perturbation will not change this, so that they remain exponentially suppressed and do not exhibit any fluctuations.

We can Fourier transform the linearized equation:

$$i\omega\delta N(\omega) = r_0 N^* \left(-\delta N(\omega) - \sigma\xi(\omega) + \gamma\sigma^2 R(\omega)\delta N(\omega) + \zeta(\omega) \right) , \tag{3.38}$$

and solve for $\delta N(\omega)$:

$$\delta N(\omega) = \frac{\sigma\xi(\omega) + \zeta(\omega)}{i\omega/(r_0 N^*) + 1 - \gamma\sigma^2 R(\omega)} , \tag{3.39}$$

At the phase transition, we expect the behavior of the system to become singular in $\omega = 0$, we therefore focus on the small ω limit. The self-consistent equation on the correlation function becomes:

$$C(\omega = 0) = \overline{\langle |\delta N(\omega = 0)|^2 \rangle} = \frac{\sigma \langle |\xi(0)|^2 \rangle + \langle |\zeta(0)|^2 \rangle}{|1 - \gamma\sigma^2 R(0)|^2} \phi = \frac{\sigma C(0) + \epsilon}{|1 - \gamma\sigma^2 R(0)|^2} \phi \ . \tag{3.40}$$

As before, ϕ is the fraction of non-extinct species, or diversity. The ϕ factor is due to the fact that only non-extinct species fluctuate, so that when averaging over the disorder we need to multiply the result of Eq. (3.39) (which doesn't otherwise depend on z for $\omega = 0$) by the fraction of surviving species. The response and correlation functions evaluated in $\omega = 0$ correspond to their integrated value, $C_{int} = \int_{-\infty}^{\infty} dt C(t)$, $R_{int} = \int_{-\infty}^{\infty} dt R(t)$. Solving for C_{int} we obtain:

$$C_{int} = \frac{\phi\epsilon}{(1 - \gamma\sigma^2 R_{int})^2 - \sigma^2\phi} \ . \tag{3.41}$$

This diverges for

$$(1 - \gamma\sigma^2 R_{int})^2 = \sigma^2\phi \ , \tag{3.42}$$

Solving this equation together with the self-consistent equations (3.33)-(3.35) determines the critical point. We can check that at criticality the solution verifies:

$$h = \frac{k}{\mu} \ , \qquad q_0 = \frac{k\pi}{\mu(1+\gamma)^2} \ , \qquad R_{int} = \frac{1}{2} \ , \qquad \phi = \frac{1}{2} \ , \tag{3.43}$$

and the critical line is given by:

$$\sigma_c = \frac{\sqrt{2}}{1+\gamma} \ . \tag{3.44}$$

This is the horizontal line in the phase diagram in Figure 2.8 [10]. Interestingly, at the critical point May's bound [106] is exactly saturated in the surviving community. Indeed taking $\gamma = 0$, as in May's original work, we find

$$\tilde{\sigma}\sqrt{S^*} = \frac{\sigma}{\sqrt{S}}\sqrt{\phi S} = 1 \ . \tag{3.45}$$

$\tilde{\sigma}$ is the unnormalized standard deviation of the interactions, and $S^* = S\phi$ the number of surviving species.

Computing the correlation function to next order in ω, it is possible to show that at the transition it behaves as $1/\omega$ (for $\gamma \neq 1$), signaling that we are entering a chaotic phase [66, 117].

The computation can easily be generalized to a spatially extended model with local interactions (as the ones described in Sec. 2.4), both with a continuous and a discrete spatial structure. Performing an additional Fourier transform in space we would find that the most unstable mode is the uniform (infinite wavelength) one, so that the computation carries out identically and we obtain the same result for the critical point [168, 169].

3.5 Effective single species processes and SADs

Through DMFT, we have seen that the dynamics of a complex ecosystem can be mapped onto those of a single non-interacting species. This reveals an intriguing connection between two contrasting ecological paradigms: on the one hand, models, such as the niche model, that emphasize the importance of interaction networks; on the other, models, like the neutral theory,

that attribute ecological dynamics primarily to stochastic fluctuations. In fact, within the DMFT framework, the interactions generate a noise term: the entire ecosystem acts as a randomly fluctuating environment for each species [66, 115, 170]. This helps reconcile the two viewpoints and offers some insight into why they often yield similar predictions.

This mapping can be leveraged to derive the Species Abundance Distribution (SAD) in a complex ecosystem by analyzing much simpler single-species dynamics. The obtained distributions can then be compared to experimental SADs, which are often fitted with power laws with exponential cut offs [40, 171], or with gamma or lognormal distributions [170, 172–174].

In this section, we present the abundance distributions that emerge under several simplified stochastic dynamics. Our main tool will be the Fokker-Planck equation, which describes the time evolution of the probability distribution of a Markovian process. A stochastic process is called *Markovian* if its evolution only depends on its current state. This condition is violated in the presence of memory terms or of colored noise.

Let us consider a stochastic differential equation in the Ito convention [175]:

$$\dot{N} = f(N) + g(N)\xi(t) \ , \tag{3.46}$$

where f and g are generic functions and ξ is a white noise, with correlations $\langle \xi(t)\xi(t')\rangle = 2T\delta(t-t')$. The probability to associated Fokker-Planck equation reads [175]:

$$\frac{\partial P(N,t)}{\partial t} = -\frac{\partial}{\partial N}\left(f(N)P(N,t)\right) + T\frac{\partial^2}{\partial N^2}\left(g(N)^2 P(N,t)\right) \ . \tag{3.47}$$

3.5.1 Demographic noise

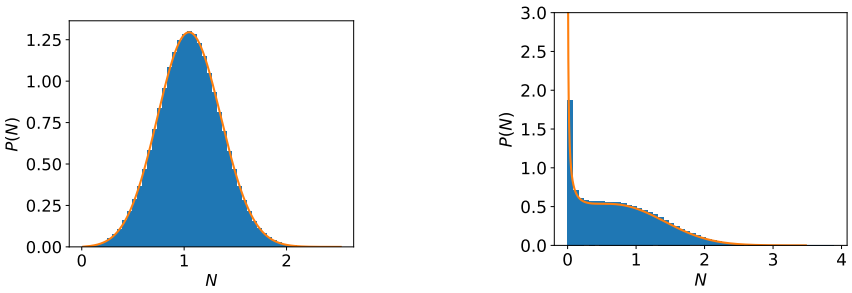

(a) $T = 0.05 < \lambda$ (b) $T = 0.2 > \lambda$

Figure 3.3: Stationary probability distribution of the abundance under white demographic noise for two values of the effective temperature, smaller (a) and larger (b) than the immigration. The histogram represents the result of numerical simulations, in orange the analytical prediction (Eq. 3.50). $\lambda = 0.15$, $r_0 = 1$, $k = 1$.

The first case we consider is the one of a single species undergoing logistic growth and demographic fluctuations, in the presence of immigration:

$$\dot{N} = r_0 N\left(k - N\right) + \eta(t)\sqrt{N} + \lambda \ . \tag{3.48}$$

The noise is defined according to the Ito convention.

The associated Fokker-Planck equation reads:

$$\frac{\partial P(N,t)}{\partial t} = -\frac{\partial}{\partial N}\left(\left(r_0 N\left(k-N\right)+\lambda\right)P(N,t)\right) + T\frac{\partial^2}{\partial N^2}\left(NP(N,t)\right) \ . \tag{3.49}$$

To obtain the stationary probability distribution, we set the time derivative to zero. The solution, up to a normalization factor, is:

$$P(N) \propto N^{-\frac{T-\lambda}{T}} \exp\left(-\frac{r_0}{T}\left(\frac{N^2}{2k} - N\right)\right) . \tag{3.50}$$

The result is plotted in orange in Fig. 3.3, and perfectly agrees with numerical results. For large N, the distribution is controlled by the exponential, and resembles a Gaussian, whereas at low abundances it is controlled by the power law. If $\lambda < T$ the distribution diverges in $N = 0$ (Figure 3.3b), and for $\lambda \to 0$ it becomes non integrable. This signals the fact that the only stationary solution in the presence of demographic noise and without immigration is a delta function in $N = 0$: the species goes extinct, and this is an absorbing state.

The stationary probability distribution can be written in the form of a Boltzmann weight $P \propto e^{-H_{eff}/T}$, with the effective Hamiltonian:

$$H_{eff} = r_0\left(\frac{N^2}{2k} - N\right) + (T - \lambda)\log N . \tag{3.51}$$

This is not a coincidence: the dynamics at stationarity is indeed a thermal equilibrium one [11, 12]. In order to prove this, we need to show that the system is symmetric under time reversal. In Appendix A.1 we prove it for a more general dynamics that also includes a colored environmental noise and a memory term:

$$\dot{N} = r_0 N\left(k - N - \xi + \int_0^t R(s)N(t-s)ds\right) + \eta(t)\sqrt{N} + \lambda , \tag{3.52}$$

with $\langle \xi(t)\xi(t')\rangle = C(t - t')$. If $\gamma = 1$, the DMFT equation (3.21) can be cast in this form by absorbing a σ^2 factor in R and C. In order for the system to be at equilibrium, the correlations of the noise and the response function in the memory term must satisfy a fluctuation-dissipation relation:

$$R(\tau) = -\frac{1}{T}\frac{dC(\tau)}{d\tau} . \tag{3.53}$$

The strategy, following reference [175], is to construct the Martin-Siggia-Rose-De Dominicis-Janssen (MSRDJ) action [176–178] that describes the probability of observing any given trajectory, and to show that if we take Eq. (3.50) as initial and final condition, the action is reversible under time reversal.

If the abundance undergoes an equilibrium dynamics, its correlation and response functions will also satisfy a fluctuation-dissipation relation. This means that if $\gamma = 1$, i.e. for symmetric interactions, equilibrium dynamics can be a self-consistent solution of the DMFT equation (3.21). In practice this will happen only if the system actually manages to relax to a steady state, which will be the case in the single equilibrium phase.

We can similarly prove equilibrium-like dynamics also for a many-species system with symmetric interactions and demographic fluctuations described by Eq. (3.20). In that case, the effective Hamiltonian reads

$$H_{eff} = \sum_i r_0\left(\frac{N_i^2}{2k} - N_i\right) + \frac{1}{2}\sum_{i,j}\alpha_{ij}N_iN_j + \sum_i (T - \lambda)\log N_i . \tag{3.54}$$

This mapping is exact even at finite S and for any choice of the symmetric interaction matrix α_{ij}. In this framework non symmetric interactions would correspond to non-conservative forces, driving the system out of equilibrium. This effective Hamiltonian is the starting point of the replica treatment of the random Lotka-Volterra system, which is therefore also restricted to symmetric interactions.

Solution without logistic growth

To better understand the role of demographic noise, it is instructive to look at the even simpler process,

$$\dot{N} = \eta(t)\sqrt{N} \ , \tag{3.55}$$

with initial condition $N(0) = N_0$. The solution of the associated Fokker-Planck equation is known for all times [179]:

$$P(N,t) = \delta(N)e^{-\frac{N_0}{Tt}} + \frac{e^{-\frac{N_0+N}{Tt}}}{Tt}\sqrt{\frac{N_0}{N}}I_1\left(\frac{2\sqrt{N_0 N}}{Tt}\right) \ . \tag{3.56}$$

I_1 is the modified Bessel function of the first kind of order 1. Note that even though the noise vanishes for $N \to 0$, the species has a finite probability rate to go extinct, and the distribution converges to a delta function in 0. This is a crucial difference between demographic and environmental noise: because the latter vanishes faster when $N \to 0$, it can never lead to extinctions, unless we introduce a finite extinction threshold.

As it was noted in reference [180], by Taylor expanding the Bessel function we can show that we can exactly sample $P(N,t)$ as:

$$N = Tt\text{Gamma}\left(\text{Poisson}\left(\frac{N_0}{Tt}\right)\right) \ . \tag{3.57}$$

In other words, we sample a Poisson distribution with parameter $\frac{N_0}{Tt}$, we sample a Gamma distribution with shape parameter given by the Poisson variable we have extracted, we multiply the result by Tt, and the random variable we obtain is exactly distributed according to $P(N,t)$ of Eq. (3.56). Since efficient Gamma and Poisson variables generators are widely available, this allows us to efficiently sample the demographic noise. To simulate numerically a more general process such as Eq. (3.48) or Eq. (3.20), we discretize time and we integrate separately at each time step the deterministic part of the equation and the demographic fluctuations:

$$\tilde{N}(t+dt) = N(t) + f(N)dt \tag{3.58}$$

$$N(t+dt) = Tdt\text{Gamma}\left(\text{Poisson}\left(\frac{\tilde{N}(t+dt)}{Tdt}\right)\right) \ , \tag{3.59}$$

where $f(N)$ denotes all the deterministic forces acting on N [180, 181]. This method has an error of order dt. Note that the naive integration of the stochastic differential equation through the Euler-Maruyama method [182], i.e.

$$N(t+dt) = N(t) + f(N)dt + \sqrt{Tdt}\tilde{\eta}(t)\sqrt{N(t)} \ , \tag{3.60}$$

with $\tilde{\eta}(t)$ a Gaussian variable with mean zero and variance 1, can lead to unphysical negative abundances, resulting in numerical instabilities.

3.5.2 Environmental noise

We have seen that in the DMFT framework, the interactions between species can be replaced by an environmental noise. This noise has in general non-trivial correlations, which should self-consistently match the ones of the abundance. We nevertheless expect the behavior of the system to be mainly controlled by the amplitude and the correlation time of the noise. The

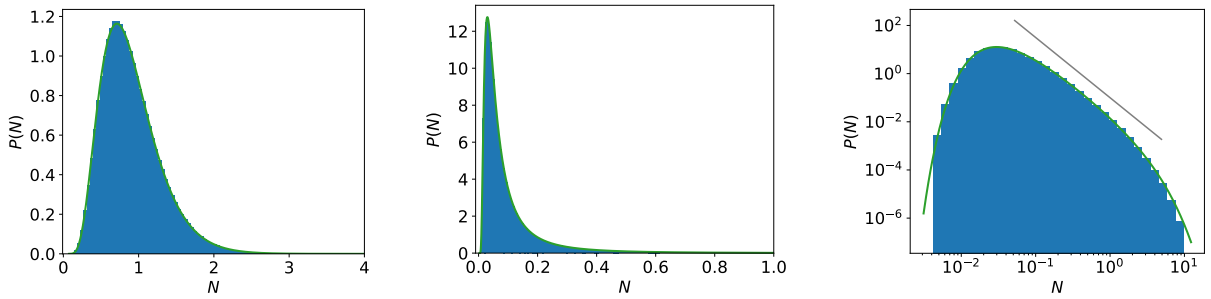

(a) $T_e = 0.1$ (b) $T_e = 2$, linear scale (c) $T_e = 2$, log-log scale

Figure 3.4: Stationary probability distribution of the abundance under white environmental noise for two values of T_e. The histogram represents the result of numerical simulations, the green curve the analytical prediction (Eq. 3.63). When the environmental noise is strong, the SAD exhibits a power law behavior at intermediate N, as can be appreciated from the log-log plot in (c). In gray we plot the slope of the power law $P \propto N^{-(1-r_0k/T_e)}$. The log-log scale the power law (or exponential) one at small N. $\lambda = 0.15$, $r_0 = 1$, $k = 1$.

effect of these two control parameters can be evaluated in the simplified cases of white and exponentially correlated noises.

Let us neglect for the moment demographic fluctuations, and consider the process:

$$\dot{N} = r_0 N\,(k - N) + \xi(t) N + \lambda\ . \tag{3.61}$$

We first assume that ξ is white, with correlations $\langle \xi(t)\xi(t')\rangle = 2T_e\delta(t-t')$. Since we will later be interested in the colored noise case, we use Stratonovich discretization, which can be seen as the limit of vanishing correlation time of the noise. This leads to an additional drift term in the Fokker-Planck equation, which in this case reads:

$$\frac{\partial P(N,t)}{\partial t} = -\frac{\partial}{\partial N}\left(\left(\left(r_0 N\,(k-N) + \lambda + T_e N\right) P(N,t)\right) + T_e \frac{\partial^2}{\partial N^2}\left(N^2 P(N,t)\right)\right)\ . \tag{3.62}$$

Its stationary solution is:

$$P \propto \exp\left(-\frac{1}{T_e}\left((T_e - r_0 k)\log N + r_0 N + \frac{\lambda}{N}\right)\right)\ . \tag{3.63}$$

The result is plotted in green in Fig. 3.4; again it perfectly matches numerical results. In this case the immigration leads to an exponential suppression in 0, and the decay at large N is exponential instead of Gaussian. When the environmental noise is strong, $T_e \gg r_0 k$, the SAD exhibits a power law behavior at intermediate N, with $P \propto N^{-(1-r_0k/T_e)}$ (see the log-log plot in Figure 3.4c). In this limit, the distribution reduces to Fisher's log-series [171], which was originally proposed to fit abundance distributions of British moths and Malaya butterflies, but has since been used on a variety of other datasets [183]. Fisher's log-series also arises from neutral models [46].

Colored environmental noise

In the Fokker-Planck equation, the evolution of the probability distribution only depends on its instantaneous value. It can therefore only describe Markovian processes, in which there is no dependence on the history of the system. This is notably not true in the presence of colored noise. The Unified Colored Noise Approximation (UCNA) [184, 185] allows us to obtain an

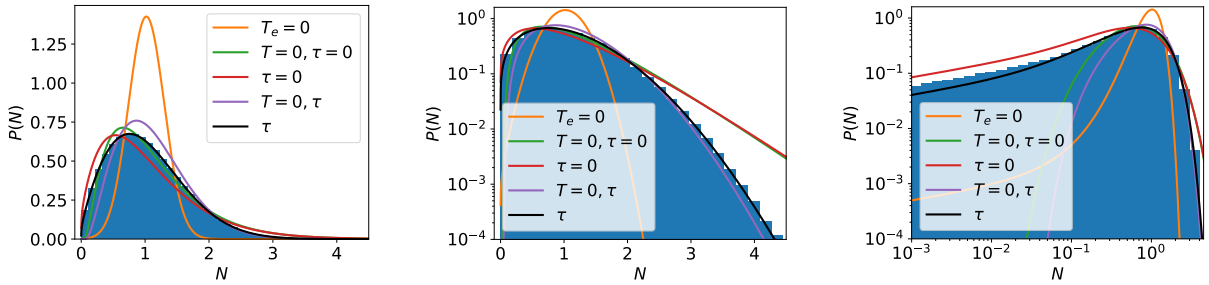

(a) Linear scale (b) Linear-log scale (c) Log-log scale

Figure 3.5: Stationary probability distribution of the abundance under white demographic noise and colored environmental noise. The histogram represents the result of numerical simulations, the black curve the analytical prediction under the UCNA. In orange the result considering only the demographic noise (Eq. 3.50), in green considering only white environmental noise (Eq. 3.63), in red neglecting the correlations of the environmental noise, in purple considering only the colored environmental noise (Eq. 3.65). The linear-log scale plot highlights the exponential decay at large N, the log-log one the power law (or exponential) one at small N. $\tau = 0.5$, $T_e = 0.5$, $T = 0.08$, $\lambda = 0.1$, $r_0 = 1$, $k = 1$.

approximate Fokker-Planck equation for exponentially correlated noise, which is exact in the limit of both small and large correlation time τ.

Let us then consider again equation (3.61), but with exponentially correlated noise:

$$\langle \xi(t)\xi(t') \rangle = \frac{2T_e}{\tau} e^{\frac{|t-t'|}{\tau}} \ . \tag{3.64}$$

Because of the length of the equations, we directly give the stationary solution under the UCNA:

$$\begin{aligned} P \propto \exp \Bigg\{ & -\frac{r_0 N}{T_e}(1 - r_0 k\tau) - \tau \frac{r_0^2 N^2}{2T_e} - \frac{T_e - r_0 k}{T_e} \log N + \\ & + \log\left(1 + \tau r_0 N + \frac{\lambda\tau}{N}\right) - \lambda \frac{1 + r_0 k\tau}{T_e N} - \lambda^2 \frac{\tau}{2T_e N^2} \Bigg\} \ . \end{aligned} \tag{3.65}$$

The result is plotted in purple in Fig. 3.5. In the limit $\tau \to 0$ we recover Eq. (3.63). For $\tau \to \infty$ the amplitude of the noise vanishes, and indeed we correctly obtain a δ-function centered in the fixed point of the deterministic equation, i.e. in $N = k$ for $\lambda = 0$. The results are quantitatively accurate for $\tau \lesssim 1$. After the completion of this study, we found that this result was similarly obtained in reference [170].

Combination of both noises

It is also possible to find the stationary probability distribution under the combination of white demographic noise and colored environmental noise, using again the UCNA to treat the latter. The result is plotted in Figure 3.5 and matches very well the distribution obtained from numerical simulations. The analytical distributions under some of the other discussed dynamics are also shown for comparison. The full analytical form of the distribution is reported in Appendix A.2. The behavior at large N is strongly affected by the presence of correlations in the environmental noise, and not too much by the demographic fluctuations (the black and purple curves have similar asymptotic behaviors in Fig. 3.5b), while the reverse is true at small N (the black and red curves have similar asymptotic behaviors in Fig. 3.5c). This analytical result was, to our knowledge, never before reported in the literature.

3.6 Towards an approximate closure of the DMFT equations

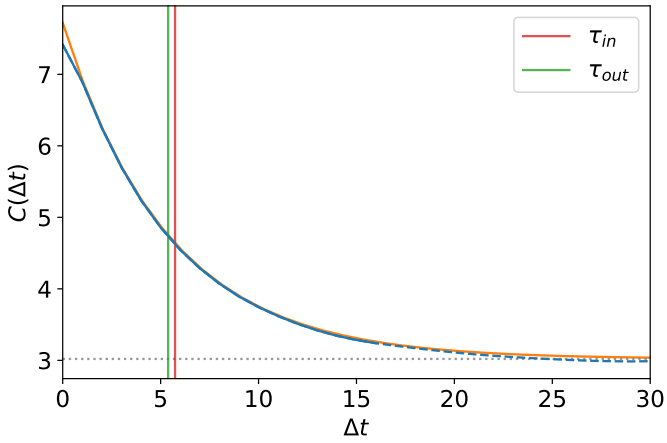

Figure 3.6: Numerical result (in blue) and exponential fit (in orange) of the correlation function of the dynamics of Eq. (3.61) with colored noise. The correlation time of the noise τ_{in} and of the dynamics τ_{out} are shown in red and green respectively. The dotted line is the asymptotic value of the correlation, $\langle N \rangle^2$. The exponential is only fitted to the first part of the curve (indicated by a continuous line) to increase numerical stability of the method. $\tau_{in} = 5.7$, $k = 1.2$, $T_e = 0.3$, $\lambda = 10^{-2}$.

The dynamics analyzed in the previous section are quite similar to the effective one resulting from DMFT, at least in the case of uncorrelated interactions ($\gamma = 0$), in which the memory term is not present. There are however two key points of DMFT that we haven't taken into account. The first is that every species should have a different effective carrying capacity, given by

$$k_{eff} = k - \mu h - \sigma z \sqrt{q_0} \ . \tag{3.66}$$

The heterogeneity in the ecosystem is reflected in the random term $\sigma z \sqrt{q_0}$, which differs from species to species. In the previous section we have focused on the distribution of the abundances of a single species, when repeatedly sampled over time. To obtain the distribution of the abundances that we would obtain by sampling all species at the same time, we need to average the previous result over a Gaussian distribution of effective carrying capacities. This is in principle quite simple, as we will see in Section 4.4.1 for a concrete example.

The second point that we have neglected in the previous section is that the parameters that appear in the effective carrying capacity and the statistics of the noise must be determined self-consistently. While static quantities can be easily derived from the abundance distribution, this is not true for the noise correlation function. As we have already discussed, we expect the system's behavior to primarily depend on the amplitude and correlation time of the noise. Thus, we can seek a self-consistent solution for just these two parameters, rather than for the entire correlation function. The amplitude of the noise is proportional to the average variance of the single species abundance abundance, $\overline{\langle N^2 \rangle - \langle N \rangle^2}$, which can be obtained from the abundance distribution. This is not the case for the correlation time, and we could not devise any useful approximation scheme that would allow us to compute it analytically. However, it can be easily obtained from numerical simulations of the dynamics.

Let us consider, as in Eq. (3.61), a species subjected to environmental noise:

$$\dot{N} = r_0 N \left(k_{eff} - N\right) + \xi(t) N + \lambda \ . \tag{3.67}$$

We have denoted the carrying capacity with k_{eff} to highlight that we are absorbing in this parameter all the static contributions that come from DMFT, as indicated in Eq. 3.66. We consider exponentially correlated noise:

$$\langle \xi(t)\xi(t') \rangle = \frac{2T_e}{\tau_{in}} e^{\frac{|t-t'|}{\tau_{in}}} \quad . \tag{3.68}$$

For a given value τ_{in} of the correlation time of the input noise, we simulate this dynamics. Once the system has reached stationarity, we compute the correlation function $C(\Delta t)$. The result, plotted in Figure 3.6, is indeed well fitted by an exponential (up to an additive constant, given by $\langle N \rangle^2$). From the exponential fit we can extract the correlation time of the dynamics τ_{out}. This allows us to obtain an approximate closure of the DMFT equations that is significantly less computationally demanding than the one proposed in [66]. The advantage lies not only in having to determine a single parameter self-consistently, rather than an entire function: the generation of the noise also becomes much more efficient when exponential correlations are imposed[2], with a cost that scales linearly rather than quadratically with the number of time steps.

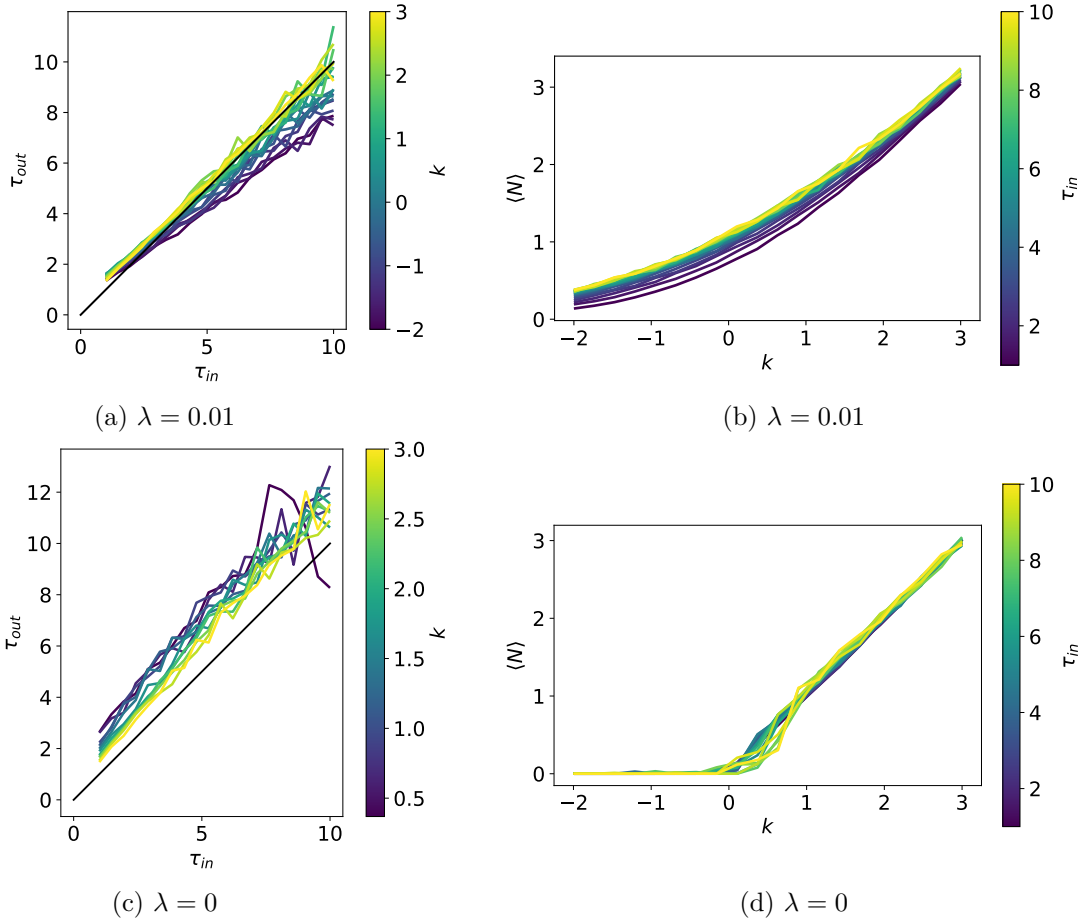

(a) $\lambda = 0.01$

(b) $\lambda = 0.01$

(c) $\lambda = 0$

(d) $\lambda = 0$

Figure 3.7: τ_{out} versus τ_{in} for various values of k (left) and $\langle N \rangle$ versus k for various values of τ_{in}, for $\lambda = 0.01$ (top) and $\lambda = 0$ (bottom). For $\lambda = 0$ the average abundance is very close to 0 for all negative values k, it is therefore not possible to reliably measure the correlation time. The exponential fit is also not as good for small k, leading to more uncertainty in the determination of τ_{out}. $T_e = 0.3$.

[2]The noise can be generated by simulating a Ornstein–Uhlenbeck process [186].

In Figure 3.7a-c we plot the measured correlation time of the dynamics τ_{out} as a function of the correlation time of the imposed noise τ_{in}. A first interesting observation is that it is only possible to find a matching $\tau_{out}(\tau_{in}) = \tau_{in}$ if we consider a finite immigration rate (Figure 3.7a). For $\lambda = 0$, $\tau_{out}(\tau_{in}) > \tau_{in}$ for all values of k and T_e considered (Figure 3.7c), meaning that the timescale of the dynamics is always larger than the timescale of the noise. This is due to the fact that when $\lambda = 0$ the species spends long periods of time close to $N = 0$ (see Figure 3.8).

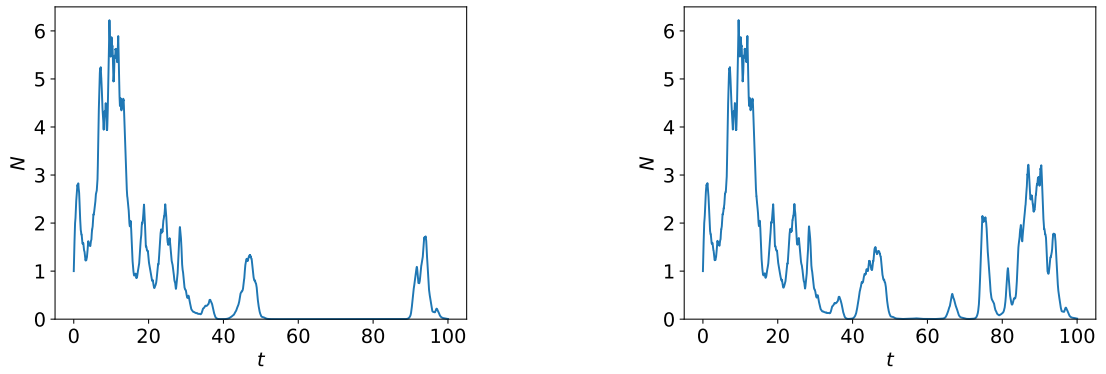

(a) $\lambda = 0$ (b) $\lambda = 0.01$

Figure 3.8: Numerical simulation of the dynamics of Eq. 3.67, with and without immigration, for the *same* realization of the noise $\xi(t)$. When $\lambda = 0$ (left) the species can reach exponentially small values of the abundance. Growing back then requires a long time, and, if the conditions are favorable just for a short time, the abundance remains close to 0. This is visible for example around $t = 80$: with immigration the species grows back to appreciable abundances, whereas without it it remains close to 0.

The mismatch between τ_{in} and τ_{out} is related to the phenomenon of aging of chaos that is found considering no immigration and no extinction threshold (see Section 2.6.2). To understand this, let us imagine starting the many-species dynamics from random initial conditions in the chaotic phase. Initially, each species is far from a fixed point, and grows or decays on a timescale of order 1. In the DMFT framework, this generates a noise with a $\tau_{in} \sim 1$. At longer times, the species is close to a fixed point, and its dynamics is primarily driven by the shifts of other species, or, in the DMFT framework, by the self-consistent noise. The dynamics of species subjected to this noise has a correlation time $\tau_{out} > \tau_{in}$, generating an increase in the noise timescale at later times. This mismatch leads to a continuous slowdown of the dynamics, which is precisely the aging of chaos phenomenon.

While matching $\tau_{out}(\tau_{in}) = \tau_{in}$ already gives some qualitative indications on the behavior of the system, this is not sufficient to determine the solution, because the statistic of the noise needs to be averaged over the quenched disorder, and all parameters must be self-consistently determined at the same time. The dynamics in Eq. (3.67) depends on five parameters: the effective carrying capacity k_{eff}, the amplitude of the noise T_e, the correlation time τ_{in}, the growth rate r_0 and the immigration rate λ. r_0 and λ are not affected by the DMFT treatment, so we do not need to vary them to find the self-consistent solution. Since the remaining parameters (k_{eff}, T_e and τ_{in}) are not very numerous and τ_{out} depends smoothly on them (see Figure 3.7a), it is convenient to simulate the dynamics in a grid of values of the three parameters, and fit the function $\tau_{out}(\tau_{in}, k_{eff}, T_e)$. The moments of the abundance could a priori be determined from the approximate distribution of abundances under correlated noise, Eq. 3.65. However, the approximation is not very good for the relevant values of τ, we therefore extract also the moments of the abundance from the numerical simulations, determining $\langle N \rangle$ and $\langle N^2 \rangle$ as a

function of τ_{in}, k_{eff} and T_e (Figure 3.7b). This completes the mapping from the parameters that define the process to the properties of the dynamics:

$$(\tau_{in}, k_{eff}, T_e) \to (\tau_{out}, \langle N \rangle, \langle N^2 \rangle) \ , \tag{3.69}$$

which contains all the information we need to find a self-consistent solution.

The next step is to make explicit the dependence of k_{eff} and T_e on the moments of the distribution and the disorder. As previously mentioned, $k_{eff} = k - \mu h - \sigma z \sqrt{q_0}$. Regarding T_e, we need to match the variance of the noise and of the abundances. In Eq. (3.68), we have normalized amplitude of the correlated noise by τ_{in} in order to recover the white noise limit when $\tau_{in} \to 0$. We therefore have to impose:

$$\frac{2T_e}{\tau_{in}} = \overline{\langle N^2 \rangle - \langle N \rangle^2} = q_d - q_0 \ , \tag{3.70}$$

where $q_d = \overline{\langle N^2 \rangle}$ is the value of the correlation function for equal times, i.e for $\Delta t = 0$. This means that we need to set $T_e = \frac{1}{2}(q_d - q_0)\tau_{in}$.

We now need to average the properties of the dynamics over the disorder contained in $k_{eff} = k - \mu h - \sigma z \sqrt{q_0}$. This gives us the self-consistent equations on the moments of the abundance:

$$h = \int \mathcal{D}z \langle N \rangle (\tau_{in}, k - \mu h - \sigma z \sqrt{q_0}, \frac{1}{2}(q_d - q_0)\tau_{in}) \tag{3.71}$$

$$q_d = \int \mathcal{D}z \langle N^2 \rangle (\tau_{in}, k - \mu h - \sigma z \sqrt{q_0}, \frac{1}{2}(q_d - q_0)\tau_{in}) \tag{3.72}$$

$$q_0 = \int \mathcal{D}z \langle N \rangle^2 (\tau_{in}, k - \mu h - \sigma z \sqrt{q_0}, \frac{1}{2}(q_d - q_0)\tau_{in}) \ . \tag{3.73}$$

The parentheses contain the arguments of the functions $\langle N \rangle(\tau_{in}, k_{eff}, T_e)$ and $\langle N^2 \rangle(\tau_{in}, k_{eff}, T_e)$, which we can fit from the numerical simulations. Averaging over the disorder is somewhat more subtle in the case of the correlation time. We need to compute the averaged correlation function:

$$C(\Delta t) = \int \mathcal{D}z \left(\langle N^2 \rangle - \langle N \rangle^2 \right) e^{-\Delta t / \tau_{out}} \ , \tag{3.74}$$

and extract from it the correlation time. We have omitted the dependence of $\langle N \rangle$, $\langle N^2 \rangle$ and τ_{out} on their arguments for compactness.

The four self-consistency equations can be solved by iteration, as explained in Section 3.4. Note that we do not need to simulate the effective single species processes at each iteration: once we know the mapping $(\tau_{in}, k_{eff}, T_e) \to (\tau_{out}, \langle N \rangle, \langle N^2 \rangle)$ we can solve the DMFT equations for all values of μ and σ, at fixed r_0 and λ. This constitutes a further strong simplification with respect to the method presented in [66]. Albeit in principle quite simple, this approximate self-consistent closure of the DMFT equations is still work in progress.

Perspectives: chaotic dynamics in meta-communities

The approximate DMFT closure scheme could be particularly useful for studying the chaotic dynamics in a spatially extended ecosystem (see Sec. 2.4), where the numerical method of [66] is computationally unfeasible. As we explained in Sec. 2.6.2, in an isolated community the chaotic phase is stable only in the presence of immigration: without it chaos slows down indefinitely (aging) and some species reach unrealistically small abundances; if we introduce an extinction threshold the system reaches an (unstable) fixed point. It has been proposed that a spatial

structure would allow chaotic dynamics to persist, thanks to unsynchronized fluctuations in different sites [153–156].

The DMFT treatment of a spatially extended ecosystem will be the subject of the next chapter. The result is analogous to the one obtained for a single community, but the response and correlation functions must be self-consistently determined also as a function of space (see Sec. 4.3.1).

As a first step, we could perform a mean-field approximation in space, which is exact in a fully-connected network with an infinite number of patches. This greatly simplifies the analysis, because it allows us to map the complex spatial process onto the dynamics of a single species in a single site, with a self-consistently determined immigration $\lambda = D\langle N\rangle$ (see Sec. 4.2.1 for more details). The solution scheme would then be analogous to the one presented here, albeit with some additional self-consistent equations to solve. Obtaining a fluctuating solution (i.e. a self-consistent solution with $T_e > 0$) would allow us to verify that indeed a spatial structure can stabilize chaotic dynamics.

In a finite dimensional system, for example a linear array of sites, the stability of this fluctuating solution would presumably depend on the diffusion strength D. We could then have a phase transition between an "inactive" fixed point phase and an "active" chaotic one. Whether this transition falls in the Directed Percolation universality class is an open question that could be addressed with our approximate DMFT closure scheme. In a finite dimensional system, we cannot neglect the correlation of the noise in neighboring sites. We could either try to self-consistently determine the entire spatial correlation function, or make an exponential ansatz also in space:

$$\langle \xi(x,t)\xi(x',t')\rangle = \frac{2T_e}{\tau\tau_x} e^{\frac{|t-t'|}{\tau}} e^{\frac{|x-x'|}{\tau_x}} \quad . \tag{3.75}$$

We would then have to self-consistently determine only the correlation length τ_x. One should pay extra caution to this ansatz in the proximity of any phase transition, since the correlation length usually diverges, and the correlation function can take a non-exponential form. The long range correlations that are then obtained would presumably play an important role at the transition.

3.7 Conclusions

Dynamical Mean Field Theory provides a description of a many-body system in terms of an effective dynamics for a single degree of freedom, which is subjected to an additional noise and memory term. This method can be fruitfully applied to complex ecological systems: it allows us to compute the distribution of the abundances in the single equilibrium phase, and to obtain the critical line at which this phase becomes unstable. Moreover it provides an insightful connection between deterministic models that highlight the role of interactions and non-interacting models in which the dynamics is driven by stochastic fluctuations. DMFT demonstrates that, if each species interacts *weakly* with *many* others, these interactions can have the same effect as a fluctuating environment. By linking complex deterministic models with simpler stochastic ones, this approach challenges the conventional divide between the two frameworks, which indeed often yeld similar results.

This mapping motivated us to study several stochastic single-species dynamics. By solving the Fokker-Planck equations associated to the various processes, we obtained the Species Abundance Distributions (SADs). In the case of exponentially correlated noise, the Fokker-Planck equation was obtained through the Unified Color Noise Approximation, which is exact for both long and short correlation times. In the limit of strong environmental noise, the SAD approaches

Fisher's log-series, which has been proposed to fit a variety of experimental datasets, and can also be derived from the neutral model.

DMFT leads to some self-consistent equations on the correlation and response functions that cannot in general be solved analytically. A numerical solution was performed in Reference [66], but it is very numerically intensive. One of the main results of this chapter is the proposition of a novel approximate solution scheme for the case of uncorrelated interactions ($\gamma = 0$), based on an exponential approximation of the correlations of the dynamics. The qualitative analysis of the conditions to obtain a matching between the correlation timescale of the noise and the one of the dynamics already provides some insights on the behavior of the system, and offers a new perspective on the "aging of chaos" phenomenon. The proposed approach could prove particularly valuable for the study of the chaotic dynamics in a spatially extended ecosystem.

Chapter 4

Interactions and disorder rescuing ecological diversity

In this chapter, we consider a system composed of many heterogeneously interacting species, living on a discrete network of sites and experiencing demographic fluctuations. Materials from this chapter can be found in reference [1]. The introduction section summarizes ideas already detailed in the previous chapters to allow the chapter to be read independently.

4.1 Introduction

Community ecology explores how the interactions between different species shape the diversity-rich ecosystems that characterize the natural world. Understanding the main mechanisms at play is a challenge that spans different scientific fields and it is relevant for human health [187].

There are three salient facts that one has to take into account in this endeavor. Many ecosystems of interest are *species-rich*. The interactions between these large sets of species, and the induced ecological dynamics, can lead to complex dynamical behaviors such as chaos and a very large number of possible equilibria [10–12, 65, 135, 150, 188]. Many ecosystems are *spatially extended*: the ecological dynamics takes place at some local scale, but individuals can then explore different spatial locations through migration [69]. This can lead to the appearance of complex ecological phenomena, such as traveling activity fronts, pattern formation, and persistent chaotic dynamics [79, 92, 93, 114, 155, 156, 168, 189, 190]. Ecosystems are subject to *noise*, in particular environmental and demographic (due to stochasticity in births and deaths). Both noises induce fluctuations which are a key factor in determining abundances distributions, and their time-dependence [57, 58, 60, 170, 191–197]. Understanding the interplay between these three properties of ecosystems is essential for answering many central questions in community ecology.

In this chapter, we consider spatially extended species-rich ecosystems subject to demographic noise. We will consider populations that are large but spatially structured, so that demographic fluctuations globally average out, but they have an important effect on the local dynamics. This is for example the case in semi-arid ecosystems: the total number of plants is such that global fluctuations are negligible, but at the local level stochasticity can play a fundamental role [194]. Our aim is to understand how in these cases interactions and spatial migration can allow for large diversity and finite abundances despite the adversarial role of demographic noise. In fact, in an isolated community demographic noise leads to extinctions, irreversibly reducing the ecosystem's diversity until there are no species left [195].

Previous works, following the classical theory of Island Biogeography by MacArthur and Wilson [64], proposed as a rescuing mechanism the immigration from a static reservoir (or "mainland", when thinking of an island-mainland system) [5, 11, 65, 195, 198]. Nevertheless,

this approach simply shifts the question from how diversity is maintained on the island to its maintenance on the mainland. Here we use a different approach. We consider ecosystems as a network of ecological communities (*a metacommunity*) coupled by passive dispersal. In this case, the immigration rates are not externally imposed, but they are the result of the internal dynamics. If a species goes locally extinct in one of the communities, immigrants from the neighboring ones can re-invade, providing an "insurance" (or "storage") effect [71, 72]. This makes the possibility of a global extinction much more unlikely, and it can allow the ecosystem to self-sustain at finite abundances and diversity. The stabilisation of high-diversity states by spatial structure is a very general phenomenon: it can arise in the presence of spatial heterogeneity of environmental conditions [69, 71, 72, 82, 199] or when abundances in different spatial locations exhibit unsynchronized fluctuations [79, 155, 156, 200]. Providing a theory for this mechanism for species-rich ecosystems subject to demographic noise, and assessing the role of interactions, is the main contribution of this chapter.

The situation is well understood in the case of a few species, in which depending on the competition between migration and death-birth rates the system is found to be either in a survival or in a extinct state. A transition separates the two regimes [92, 93, 201]. This phase transition falls in the universality class of Directed Percolation, a second-order out-of-equilibrium transition studied in statistical physics and widely used to describe spreading phenomena, from forest fires to epidemics [89–91].

In a many-species metacommunity with constant competitive interactions, it was recently shown that a similar second-order phase transition takes place and that it also belongs to the Directed Percolation universality class [79]. Because the transition is continuous with vanishing abundances, interactions, that are quadratic in the abundances, are subleading at the critical point. In consequence, the main mechanism at play in this case is still the competition between migration and death-birth rates. We shall show that the scenario for *heterogeneous interactions* is different and goes beyond the directed percolation paradigm. The transition can become discontinuous. The ecosystem can exhibit global bistability and tipping points between drastically different alternative states. Upon small changes in the environmental condition, the system can undergo catastrophic shifts from a state with large diversity and finite abundances to one in which all species are extinct. As in many other dynamical systems, from coral reefs to arid ecosystems and from Earth's climate to financial markets [202–205], it is important to find early warning signals of these kinds of transition in order to prevent them. We have identified a specific probe, which is based on the response of the ecosystem to perturbations, and that can be monitored in experiments. Our analytical framework shows that interactions play a key role both in the overall scenario and in promoting a self-sustained survival state, in agreement with results obtained for constant mutualistic interactions [206]. Remarkably, in our case, heterogeneous interactions of the pool of species are not necessarily mutualistic on average. It is the ecological dynamics that shapes the ecosystem in a self-sustained phase characterized by emergent mutualistic behavior among the non-extinct species.

In our work, we make use of several methods developed in statistical physics that are particularly well suited for species-rich ecosystems, which are complex systems formed by many interacting degrees of freedom undergoing stochastic dynamics. To model the heterogeneity in the interactions, we sample the coupling coefficients from a random ensemble. We have thus to deal with "disordered" ecosystems, which can be analyzed by transferring methods from spin-glass theory [105]. This disorder approach, which dates back to May's seminal paper [106], has recently inspired a growing body of work [10–12, 60, 132, 133, 135, 207, 208] and also received positive experimental confirmations [198, 209]. Previous works have explored within this framework the effect of heterogeneous interactions [10–12, 106, 135], demographic fluctuations [12, 60] and spatial structure [79, 93, 114, 155, 156, 168], but the analysis we present here is to our knowledge

the first analytical study in which the three ingredients are combined.

The model we focus on is a disordered Generalized Lotka Volterra (GLV) system of metacommunity subject to demographic noise. For one community, the disordered GLV has been shown to have a rich phase diagram, and to display several dynamical regimes: single equilibrium, multi-stability, and chaos [10–12, 135, 198]. We expect this complex behavior also in the case of spatially structured ecosystems [168]. In this work, we focus on the moderate-heterogeneity regime in which there is a single stable equilibrium. This allows us to disentangle the multistability due to the fragmentation of the basins of attraction of the ecological dynamics at strong heterogeneity from the bistability of the feedback mechanism between abundance and immigration. Our analysis is performed using a mean-field approximation on the spatial fluctuations, which is equivalent to considering that the community network is a fully connected graph.

Note that because of their generality, Lotka-Volterra equations have been applied to a variety of fields besides their original ecological interpretation, from immunology to economics and game theory [94–97]. Our results could therefore find applications beyond ecology, notably for the study of global bistability and crashes in economy.

4.2 The model

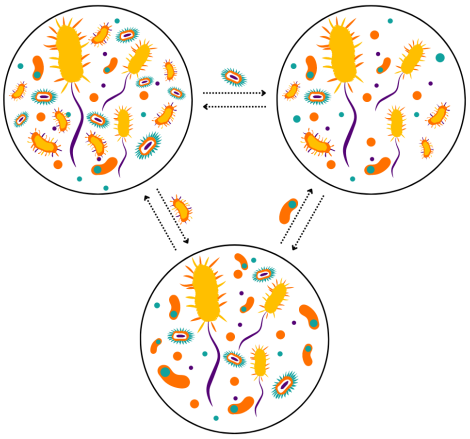

Figure 4.1: A metacommunity of 7 species living on 3 patches. Each individual interacts with the local community to which it belongs possibly migrating to neighboring patches with diffusion coefficient D.

We consider a meta-community of S species living on a network of L discrete spatial locations, or patches. The patches could represent islands or water sources, but also a population of hosts for their microbiomes [85] or the metastasis of a tumor [86]. A graphical representation of the system is given in Figure 4.1 in the case of a fully connected network of 3 patches. Each species is characterized by its abundance in each patch, which is modeled by a continuous variable, $N_{i,u}$, representing the total number of individuals divided by the typical size of the local population $\tilde{N}_{typ}$. The abundance of species i in patch u evolves according to the stochastic differential equation:

$$\dot{N}_{i,u} = \frac{r_0}{k} N_{i,u} \left(k - N_{i,u} - \sum_j \alpha_{ij}^u N_{j,u} \right) + \frac{D}{c} \sum_{v \in \partial u} (N_{i,v} - N_{i,u}) + \eta_i^u(t) \sqrt{N_{i,u}} \,, \tag{4.1}$$

which corresponds to Lotka-Volterra (LV) dynamics, with constant growth rate r_0 and carrying capacity k that are set to 1 throughout. The notation ∂u indicates the set of patch neighbors of

u (from and to which species in patch u can migrate). The growth of each species is influenced by the abundance of all the others through the interaction coefficients α_{ij}^u: if α_{ij}^u is positive species j inhibits the growth of species i in patch u and vice versa. Positive α_{ij}^u and α_{ji}^u correspond to two species competing for resources, whereas α_{ij}^u and α_{ji}^u both negative correspond to mutualistic behavior. Predation leads to opposite signs. The interaction network is fully connected, i.e. any two species interact, but we expect our results to hold also for other interaction networks with extensive connectivity [11].

To model the heterogeneity in the interactions of species-rich ecosystems, we follow [10, 65] and consider the disordered LV model. As already discussed in Section 2.6, the disorder approach has attracted recently a lot of attention [10–12, 60, 133, 135, 207] and also received positive experimental confirmations [198, 209]. In this framework, the interaction coefficients are random variables, with mean μ/S and variance σ^2/S. They are independent in each patch except for α_{ij}^u and α_{ji}^u, which have a correlation coefficient γ. In the following, we will first focus on the symmetric interactions case ($\gamma = 1$), and then show that a small asymmetry does not qualitatively change the results. As the interactions between species can depend on the environmental conditions (temperature, humidity, resources availability...) which differ in space, we consider interaction matrices fluctuating from one patch to another, i.e. they are not identical in different patches but corresponding elements α_{ij}^u and α_{ij}^v have a correlation coefficient ρ [155, 156].

We will restrict the choice of μ and σ to values for which an isolated Lotka-Volterra community only displays a single uninvadable equilibrium (the single equilibrium phase presented in Section 2.6.2). Without spatial heterogeneity the transition point is not modified by the introduction of a spatial structure [168, 169], and spatial heterogeneity decreases the effective complexity of the interaction network [82], favoring the single equilibrium phase. Therefore we also expect the metacommunity to be in the single equilibrium phase for all the allowed values of μ and σ. The effect of migration between patches in the strong heterogeneity regime with non symmetric interactions, in which a single community with fixed immigration exhibits chaotic dynamics, [10–12, 135, 198] was studied in [155, 156] in the absence of demographic noise. It leads to complex dynamical behavior with long-lived persistent fluctuations. Combining strong heterogeneity, demographic noise, and spatial migration is a challenge left for future studies.

In the model defined by Eq. (4.1) individuals can migrate on the patches network through diffusion, with a constant diffusion coefficient D/c, where c is the connectivity (or number of connections per site) of the network. We assume the network to be translationally invariant, therefore each site has the same connectivity. Migration is possible and equiprobable from patch u to any of its c nearest neighbors $v \in \partial u$.

Each species is subject to a white demographic noise η_i^u, accounting for the stochasticity in birth and death events in a continuum setting [12, 60]. We follow Ito's convention, according to which fluctuations in birth and deaths at time $t + dt$ depend on the abundance at the previous time step. The noise is uncorrelated and of constant amplitude across species and patches:

$$\langle \eta_i^u(t)\eta_j^v(t')\rangle = 2T\delta_{ij}\delta_{uv}\delta(t-t') \ . \tag{4.2}$$

The auto-correlation of the demographic noise defines the noise strength T which depends on the birth and death rates and on the typical size of the local population; T scales as $T \propto 1/\tilde{N}_{typ}$ [12, 60]: the smaller the local populations, the more important are demographic fluctuations. As we saw in the previous chapter, T can be interpreted as an effective temperature.

Some further insights into the effect of the demographic noise can be obtained considering it in the absence of all the other terms. In this case, an exact solution to the associated Fokker-Planck equation is available, showing that starting from any initial condition the population goes to zero abundance with some finite rate (see Sec. 3.5.1 and [179, 180]). Therefore also in

the continuous model, extinction is possible over finite times, and not only asymptotically as it would be the case for example with environmental noise.

4.2.1 Mean field Directed Percolation

As we explained in Section 2.4.1, a single species subject to birth, death and diffusion on a spatial network undergoes an out-of-equilibrium phase transition that falls in the Directed Percolation (DP) universality class. Let us for the moment neglect interactions, and consider the single species model:

$$\dot{N}_u = r_0 N_u \left(k - N_u\right) + \eta(t)\sqrt{N_u} + \frac{D}{c}\sum_{v\in\partial u}\left(N_v - N_u\right) . \tag{4.3}$$

When the migration is sufficiently strong, the species is able to self-sustain at finite abundances, whereas at small (or zero) dispersal, the species goes extinct due to demographic noise. We can study the DP phase transition under a mean field approximation in space. This amounts to replacing the empirical average over neighbors that appears in the diffusion term with its average over demographic fluctuations, $\frac{1}{c}\sum_{v\in\partial u} N_v \to \frac{1}{c}\sum_{v\in\partial u}\langle N_v\rangle$. Since the system is translationally invariant, the average abundance is the same in each site, and can be determined self-consistently:

$$\dot{N} = r_0 N \left(k - N\right) + \eta(t)\sqrt{N} + D(N^* - N) , \tag{4.4}$$

with $N^* = \langle N\rangle$ the average over fluctuation of the abundance under the effective single-site process. We have dropped the index u since the equation does not depend on it anymore. The mean field approximation becomes exact in the limit of large connectivity $c \to \infty$, and in particular in a fully connected network in the limit of infinite number of sites.

The equation we have obtained is formally equivalent to the one describing a species subject to demographic noise and migration from an external reservoir studied in Section 3.5.1. The migration term leads to a reduced carrying capacity $(k - D/r_0)$ and a self-consistently defined immigration $\lambda = D\langle N\rangle$. We can therefore use the probability distribution obtained in Eq. (3.50) to compute the average abundance:

$$N^* = \langle N\rangle = \int dN N P(N; \lambda = DN^*) . \tag{4.5}$$

We have made explicit the dependence of the probability distribution on the immigration to show the self-consistency of the equation. $N^* = 0$ is always a solution, because in the absence of immigration the probability distribution becomes a δ-function in 0. If D is above a critical threshold D_0, the equation also has a finite solution, signaling the onset of the active DP phase. The DP phase transition is continuous: N^*, the order parameter, goes to zero continuously approaching D_0 from above. Close to the transition, we can therefore expand Eq. (4.5) in powers of N^*:

$$N^* = a_1 N^* + a_2 (N^*)^2 , \tag{4.6}$$

where a_1 and a_2 are constants that depend on D, T, r_0 and k. a_2 is always negative, therefore the equation will develop a positive solution when $a_1 = 1$. This leads to an implicit equation for the critical point D_0:

$$D_0\sqrt{\frac{\pi}{2Tr_0}}\exp\left(\frac{(kr_0 - D_0)^2}{2Tr_0}\right)\left(1 + \operatorname{erf}\left(\frac{kr_0 - D_0}{\sqrt{2Tr_0}}\right)\right) = 1 . \tag{4.7}$$

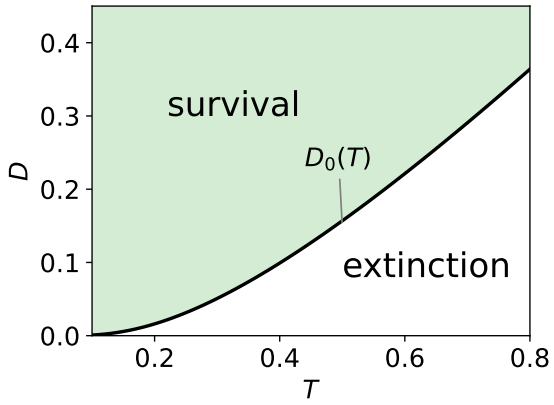

Figure 4.2: Phase diagram for Directed Percolation in the mean-field approximation: in green the active phase, in which at long times there is a finite density of particles, in white the inactive phase, in which all particles eventually die. $D_0(T)$ indicates the transition line (see Sec. 4.3 and App. A.5.1 for details).

The resulting phase diagram is plotted in Figure 4.2.

For $T \to 0$ we can expand Eq. (4.7) and show that D_0 vanishes exponentially:

$$D_0(T) \sim \sqrt{\frac{T r_0}{2\pi}} e^{-\frac{r_0 k^2}{2T}} \ . \tag{4.8}$$

The reason for this behavior is that at low demographic noise, the abundances of a species with carrying capacity k undergoes a fluctuation toward very low values very rarely. In fact, one needs to wait a rare fluctuation of the demographic noise that makes the species go against the force due to the logistic growth. This phenomenon is similar to the one encountered in the Kramers' problem for barrier crossing. Using the same line of arguments employed there, one finds that the timescale for this rare event is $e^{\frac{k^2}{2T}}$ (the "energy barrier" equals $k^2/2$). The equation above can be therefore interpreted as a balance between two inverse time-scales: the one needed for diffusion to operate and the one over which extinctions take place.

The aim of this work is to generalize these results to the case of species-rich ecosystems in the presence of heterogeneous interactions. Upon increasing the number of species in the pool and considering heterogeneous interactions, the set of directed percolation processes is no longer independent and the complexity of the model increases considerably. In fact, the system becomes equivalent to the collection of an infinite number of directed percolation processes, coupled by random interactions – an interesting and open statistical physics problem.

4.3 Methods

4.3.1 DMFT and coupled Directed Percolation processes

In this work, we aim to study systems in which both the number of species and the number of patches are very large. In order to obtain analytical results we follow the statistical physics "way" and take the limit of an infinite number of species and an infinite number of patches. In this double limit (whose order is irrelevant) the macroscopic properties of the system do not depend on the particular realization of the demographic noise and of the interactions: the macroscopic properties are *self-averaging* in the jargon of disordered systems [105].

As we explained in Chapter 3, the large S limit allows for an analytical treatment, as the dynamics of the S interacting degrees of freedom can be replaced by the effective dynamics

for a single representative species, through Dynamical Mean Field Theory (DMFT, see Section 3.3) [66]. The effect of interactions with other species is captured by an environmental noise and a memory term, which are defined in a self-consistent way. Thanks to DMFT, we can map an infinite number of randomly coupled DP processes – a formidable problem – into a *single* DP process with additional terms to be determined self-consistently (a colored noise and a memory term).

Our derivation follows the one developed in reference [66] and discussed in Section 3.2, and can be found in Appendix A.3 for generic values ρ of the spatial heterogeneity of the interactions. Here we outline the main steps in the special case of patch-independent interactions, $\rho = 1$. We expect that after a transient the system will settle in a steady state, we derive the effective dynamics assuming to be in this time-translationally invariant regime. For $S \to \infty$, DMFT allows one to replace the interaction term $-\sum_j \alpha_{ij} N_{j,u}$ by a stochastic expression that has the same statistical properties:

$$-\mu h - \sigma \tilde{\xi}^i_u(t) + \sigma^2 \gamma \int_0^t \sum_v R_{uv}(t,s) N^i_v(s) ds \ . \tag{4.9}$$

Since this allows us to decouple different species, we will for simplicity omit the species index i in the following. We now discuss the different contributions. Note that in the following empirical averages over species will be denoted as $\mathbb{E}[\cdot]$.

The first term represents the average interaction with all other species. It is given by the product of the mean of the interaction strength and the mean abundance, $h = \mathbb{E}[N_u]$, that in the steady state does not depend on the patch u thanks to translational invariance.

The second term represents the fluctuation of the interaction with all other species. It is given by the product of the standard deviation of the interaction coefficients and Gaussian noise with zero mean and correlation matching the time auto-correlation of the single species abundances:

$$\langle \tilde{\xi}_u(t) \tilde{\xi}_v(s) \rangle = \mathbb{E}[N_u(t) N_v(s)] := C_{u,v}(t-s) \ . \tag{4.10}$$

The noise $\tilde{\xi}_u(t)$ is multiplied by the abundance in the LV equations. Following the definitions of Sec. 2.3, we will call it *environmental* since its effect is to add fluctuations to the carrying capacity. Since the autocorrelation of the abundances generically decays to a positive plateau at large time separations [66], one can decompose the environmental noise into a fluctuating component and a static one. The former corresponds to the fluctuations due to ecological dynamics for a given species. The latter is characteristic of a given species and fluctuates from species to species [66]. We decompose the noise by rewriting $\tilde{\xi}_u(t) = z\sqrt{C_d^\infty} + \xi_u(t)$, where $C_d^\infty = \lim_{\tau\to\infty} C_{u,u}(t, t+\tau)$ is the value of the correlation function within the same patch at infinite times, z is a static Gaussian variable with zero mean and unit variance, that now plays the role of quenched disorder, and $\xi_u(t)$ is a fluctuating noise whose covariance vanishes at long times. Again C_d^∞ does not depend on the patch u thanks to translational invariance. The static part of the noise does not depend on the patch because we are considering interactions that do not depend on space ($\rho = 1$), see Sec. 4.3.4 for the extension to generic ρ.

To distinguish the roles of fluctuating and static noises in the GLV equation, we introduce two kinds of averages: $\langle\cdot\rangle$ indicates the average over the fluctuating noises ξ and η. It is an average over the ecological dynamics, or by ergodicity, over patches for a fixed species. In analogy with physical systems, we call it *thermal average*. The overline $\bar{\cdot}$ instead stands for the average over the static field z corresponds to averaging over species or over different instances of the interaction matrix. Again in analogy with the physical system, we call it *quenched disorder average*.

The last term in the dynamical mean-field treatment of the interactions is due to a feedback mechanism: a fluctuation of the abundance of species i influences species j, which in turn influences species i. These contributions sum up because of the correlation between α_{ij} and its reciprocal α_{ji}, leading to the factor γ. This feedback mechanism (called Onsager reaction in the spin-glass literature) generates a memory term, containing the response function of the abundance on patch u to a perturbation in the carrying capacity in patch v:

$$R_{u,v}(t,s) = \mathbb{E}\left[\left.\frac{\delta N_u(t)}{\delta \zeta_v(s)}\right|_{\zeta=0}\right] . \tag{4.11}$$

In the $S \to \infty$ limit, there is convergence in law between the statistics of the infinite number of randomly coupled DP processes and the effective one [165, 210], i.e. the dynamics of a species satisfying the GLV equation (4.1) is equivalent to the effective one of a *single species* living on the original spatial network:

$$\begin{aligned}\dot{N}_u = N_u\left(k - N_u - \mu h - \sigma\left(z\sqrt{C_d^\infty} + \xi_u\right) + \sigma^2\gamma\int_0^t \sum_v R_{uv}(t,s)N_v(s)ds\right) + \\ + \frac{D}{c}\sum_{v\in\partial u}(N_v - N_u) + \eta_u\sqrt{N_u} .\end{aligned} \tag{4.12}$$

We set $r_0 = 1$ here and in the following. The DMFT closure consists then in replacing the empirical averages over species $\mathbb{E}[\cdot]$ with the one with respect to the effective single-species one. Because the effective process itself depends on some averaged quantities, one ends up with a self-consistent stochastic equation.

Eq. (4.12) can also be interpreted as the Langevin equation associated with a Directed Percolation (DP) process, with the addition of a memory term (that is absent in the special case $\gamma = 0$) and environmental noise. The effect of the static part of the environmental noise z is to change the control parameter of the DP process, determining whether this is sub-critical or supercritical.

Interestingly, whereas a system of few species interacting and diffusing on a network was established to boil down to a standard DP problem [90, 92, 93, 201, 211], the case of *many* species is fundamentally different and belongs to a different class. Indeed, a system of *many* species is equivalent to a family of *many* DP processes, characterized by different values of static and fluctuating noises and coupled through the common self-consistently determined mean, correlation, and response functions. In this work, we study whether the DP transition can fundamentally change nature due to this self-consistent coupling. Even if the transition remained qualitatively DP-like (continuous and from an absorbing state to a fluctuating one) critical properties could change. In fact, although an environmental noise can be shown to be an irrelevant perturbation of the associated field theory [89], within DMFT the environmental noise inherits the time dependence of the correlation function through the self-consistency. It can therefore develop long-range correlations in time at the critical point, possibly altering the critical behavior and leading to a new universality class.

4.3.2 Mean-field approximation in space

Studying the coupled field theories of Eq. (4.12) is a formidable task. In the following, we simplify the problem by doing a mean-field approximation which allows us to obtain a general theory independent of the underlying network of patches.

As we did in Sec. 4.2.1 to study a single mean-field DP process, we replace the term $\frac{D}{c}\sum_{v\in\partial u} N_v$ by its thermal average $\frac{D}{c}\sum_{v\in\partial u}\langle N_v\rangle$. Thanks to translation invariance, $N^* = \langle N_v\rangle$

does not depend on the patch (nor on time since we are considering steady states). This procedure corresponds to a mean-field approximation of the spatially dependent DMFT Eqs. (4.12). Such DMFT^2 approximation becomes exact for a fully connected network. In fact, in this case, taking the $L \to \infty$ limit, the empirical average of the abundances over the patches concentrates around the thermal average $N^* = \langle N_u \rangle$. From now on, we shall focus on this case.

By substituting $\frac{D}{c}\sum_{v\in\partial u} N_v$ with DN^* in Equation (4.12), one obtains an equation on N_u only, with an additional parameter to be determined self-consistently. Note that N^* is obtained by averaging only over thermal fluctuations, and not over disorder: therefore, it will have to be determined as a function of z (see Figure 4.3). This means that different species will have different immigration rates (here, for simplicity, we are still focusing on the $\rho = 1$ case; generalizations will be discussed later).

This substitution allows us to decouple stochastic processes for the abundance in different patches. Since all patches are equivalent on a fully connected lattice, the R_{uv} and C_{uv} matrices (of functions) only have two independent elements: the diagonal ones, R_d and C_d, and the off-diagonal ones R_0/L and C_0. The off-diagonal response is of order $1/L$ because a perturbation in patch v influences the abundance in patch u through the diffusion term, that in a fully connected network scales as $1/L$. The sum over sites of these small contributions has a non-negligible effect on the system. Omitting for simplicity the index u, we obtain (for large times, i.e. in the steady state):

$$\begin{aligned}\dot{N} = N\Bigg(k - N - \mu h - \sigma z\sqrt{C_d^\infty} - \sigma\xi(t) + \\ + \sigma^2\gamma\left(\int_0^t R_d(t-s)N(s)ds + N^*\int_0^t R_0(t-s)ds\right)\Bigg) + D(N^* - N) + \eta(t)\sqrt{N}\,.\end{aligned} \tag{4.13}$$

4.3.3 Symmetric interactions and thermal equilibrium

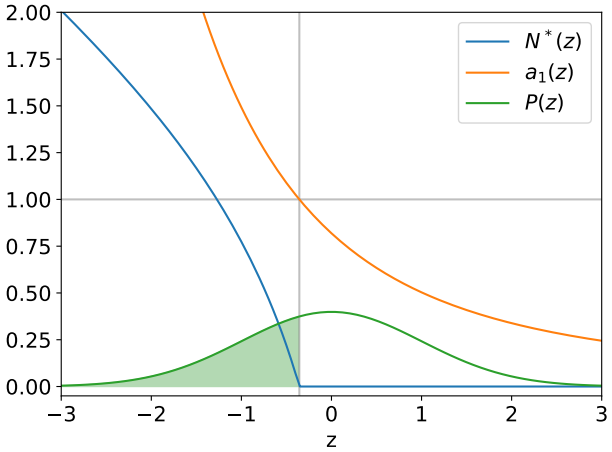

Figure 4.3: Self-consistent solution for $N^*(z)$ (blue) and Gaussian probability distribution $P(z)$ (green). In orange we plot $a_1(z)$, the coefficient of the first order expansion of the self-consistent equation for N^* defined in App. A.5, generalizing Eq. 4.6. $a_1(z) = 1$ defines the single species extinction threshold z^*, indicated by a gray vertical line. The highlighted region corresponds to the non-extinct species, its area is the diversity of the ecosystem. $T = 0.4$, $D = 0.15$, $\mu = 1$, $\sigma = 0.5$.

Equation (4.13) differs from the one obtained from DMFT on a single site in Section 3.3 only for the presence of two additional constant shifts of the carrying capacity ($\sigma^2\gamma N^* \int_0^t R_0(t-s)ds$

and $-D$), and for the fact that the immigration is self-consistently determined, $\lambda = DN^*$. As in that case, we show in App. A.1 that if the interactions are symmetric ($\gamma = 1$), the self-consistent solution maps to a thermal equilibrium process. In fact, one finds that the diagonal elements of the response and correlation functions obey a fluctuation-dissipation relation:

$$R_d(\tau) = -\frac{1}{T}\frac{\partial}{\partial\tau}C_d(\tau) \ . \tag{4.14}$$

The memory term and ξ therefore play the role of a friction term and the noise associated with a colored thermal bath at temperature T. The stochastic process maps then to a generalized Langevin equation whose stationary probability distribution is given by the Boltzmann distribution at temperature T and with the effective Hamiltonian:

$$H_{eff} = \left(1 - \frac{\sigma^2}{T}(C_d^0 - C_d^\infty)\right)\frac{N^2}{2} - (k - D - \mu h - z\sqrt{C_d^\infty}\sigma + \sigma^2 N^* R_0^{int})N + \\ +(T - DN^*)\ln N \ , \tag{4.15}$$

where C_d^0 is the equal-time correlation function, namely the second moment of the abundances over disorder and noise, $\overline{\langle N^2\rangle}$. The long time limit of the correlation function, C_d^∞, represents instead the second moment of the thermal-averaged abundances, $\overline{\langle N\rangle^2}$.

R_0^{int} is the integrated off-diagonal response, i.e. the response of the abundance in patch u to a perturbation of the carrying capacities of all other patches (all of them because we have included a factor L in its definition). Its determination requires a careful analysis of how the different patches influence each other.

Off-diagonal response

At equilibrium we can rewrite the integrated disorder-dependent responses to a perturbation of the carrying capacity (indicated by $\tilde{R}_d^{int}(z)$ in the following) and of the immigration rate ($\chi(z)$) in terms of connected correlation functions of N:

$$\tilde{R}_d^{int}(z) = \int_0^\infty d\tau \langle \frac{\delta N_u(\tau)}{\delta\zeta_u(0)}\rangle = \frac{\partial\langle N_u\rangle}{\partial\zeta_u} = \beta(\langle N^2\rangle - \langle N\rangle^2) \tag{4.16}$$

$$\chi(z) = \int_0^\infty d\tau \langle \frac{\delta N_u(\tau)}{\delta\lambda_u(0)}\rangle = \frac{\partial\langle N_u\rangle}{\partial\lambda_u} = \beta(\langle N\log N\rangle - \langle N\rangle\langle\log N\rangle) \ . \tag{4.17}$$

When the time dependence is not indicated we are considering a time independent perturbation.

Adding a perturbation in site v leads to a variation of the abundances in all other sites, because of the coupling by diffusion and the off-diagonal memory term. These variations are of order $1/L$, but since there are L of them they give a relevant contribution. When studying $\frac{\partial\langle N_u\rangle}{\partial\zeta_v}$ we need to take into account four contributions: there is a $O(1)$ variation of N_v that leads to a $O(1/L)$ perturbation of the immigration rate perceived by N_u and a $O(1/L)$ change in its off-diagonal memory term; there are $L-2$ variations of $O(1/L)$ of the N_w, with $w \neq u, v$, each leading to a $O(1/L^2)$ change in both immigration and memory term. Carefully taking into account all these contributions, we can write $\tilde{R}_0^{int}(z)$ in terms of $\tilde{R}_d^{int}(z)$, $\chi(z)$ and $\tilde{R}_0^{int}(z)$ itself:

$$\tilde{R}_0^{int}(z) = L\int_0^\infty d\tau\langle\frac{\delta N_u(\tau)}{\delta\zeta_v(0)}\rangle = L\frac{\partial\langle N_u\rangle}{\partial\zeta_v}$$

$$= L\langle\left(\frac{\partial N_v}{\partial\zeta_v}\left(\frac{D}{L}\frac{\partial N_u}{\partial\lambda_u} + \sigma^2 R_{uv}^{int}\frac{\partial N_u}{\partial\zeta_u}\right) + \sum_{w\neq u,v}\frac{\partial N_w}{\partial\zeta_v}\left(\frac{D}{L}\frac{\partial N_u}{\partial\lambda_u} + \sigma^2 R_{uw}^{int}\frac{\partial N_u}{\partial\zeta_u}\right)\right)\rangle = \tag{4.18}$$

$$= \left(D\chi(z) + \sigma^2\tilde{R}_d^{int}(z)R_0^{int}\right)\left(\tilde{R}_d^{int}(z) + \tilde{R}_0^{int}(z)\right) \ .$$

In the third line we used the fact that the correlations between different patches are subleading to take separately the thermal averages. Solving for $\tilde{R}_0^{int}(z)$ we obtain:

$$\tilde{R}_0^{int}(z) = \frac{\left(D\chi(z) + \sigma^2 \tilde{R}_d^{int}(z) R_0^{int}\right) \tilde{R}_d^{int}(z)}{1 - \left(D\chi(z) + \sigma^2 \tilde{R}_d^{int}(z) R_0^{int}\right)} \,. \tag{4.19}$$

We can then average over z to obtain R_0^{int}:

$$R_0^{int} = \overline{\frac{\left(D\chi(z) + \sigma^2 \tilde{R}_d^{int}(z) R_0^{int}\right) \tilde{R}_d^{int}(z)}{1 - \left(D\chi(z) + \sigma^2 \tilde{R}_d^{int}(z) R_0^{int}\right)}} \,. \tag{4.20}$$

Static self-consistency equations

The self-consistency equations can be expressed as averages with respect to the Boltzmann distribution:

$$N^*(z) = \langle N \rangle = \frac{\int_0^\infty dN N e^{-\beta H_{eff}}}{\int_0^\infty dN e^{-\beta H_{eff}}} \tag{4.21}$$

$$h = \overline{\langle N \rangle} = \int \mathcal{D}z \frac{\int_0^\infty dN N e^{-\beta H_{eff}}}{\int_0^\infty dN e^{-\beta H_{eff}}} \tag{4.22}$$

$$C_d^0 = \overline{\langle N^2 \rangle} = \int \mathcal{D}z \frac{\int_0^\infty dN N^2 e^{-\beta H_{eff}}}{\int_0^\infty dN e^{-\beta H_{eff}}} \tag{4.23}$$

$$C_d^\infty = \overline{\langle N \rangle^2} = \int \mathcal{D}z \left(\frac{\int_0^\infty dN N e^{-\beta H_{eff}}}{\int_0^\infty dN e^{-\beta H_{eff}}} \right)^2 \,. \tag{4.24}$$

and analogously for R_0^{int}. $\int \mathcal{D}z = \int \frac{dz}{\sqrt{2\pi}} e^{-z^2/2}$ indicates the average over the Gaussian field.

These equations can be solved iteratively: starting from a suitable initial condition for $N^*(z)$, h, C_d^0, C_d^∞ and R_0^{int}, one updates their values according to equations (4.21)-(4.24) until reaching a fixed point. Because very large values of z are exponentially suppressed by the Gaussian distribution, it is sufficient to determine $N^*(z)$ for z of $O(1)$. An example of the self-consistent solution for $N^*(z)$ is plotted in Figure 4.3.

In conclusion, within the DMFT^2 approximation and for the symmetric case, the formidable self-consistent stochastic equations (4.12) can be analyzed by studying a set of static self-consistent equations on four parameters $h, C_d^0, C_d^\infty, R_0^{int}$ and one function $N^*(z)$. Solving these equations (see next section) allows us to obtain a general picture of the interplay between migration and demographic noise for spatially extended metacommunities. In order to show that such a picture is valid beyond the simplified case we focus on, we have also considered several extensions that we shall present below.

4.3.4 Extensions

Spatial heterogeneity

In the case of a generic value of the spatial heterogeneity of the interactions ρ, an analogous procedure can be implemented, with some important differences. The static disorder is now a patch-dependent and correlated variable, that we can decompose as $\rho\sqrt{C_0^\infty} z + \sqrt{C_d^\infty - \rho^2 C_0^\infty} w_u$ where z is constant and w_u independent across locations, and C_d^∞ and C_0^∞ are the infinite time correlation function of the abundance on the same patch and on different patches, that for $\rho = 1$

coincide. Averaging the abundance across patches to obtain the immigration rate requires an additional step, *i.e.* averaging also over w_u. The solution of the self-consistent equations, albeit conceptually analogous to the $\rho = 1$ case, is for generic values of ρ much more numerically challenging, because of the need to integrate over two disorder fields, z and w_u. For this reason, we focused on the two extreme cases, $\rho = 1$ and $\rho = 0$, in which only one of the two disorder fields is present. The results are qualitatively similar so we expect our conclusions to hold also for intermediate values of ρ. We confirm it by numerical simulations at $0 < \rho < 1$.

Asymmetric interactions

The mapping to an equilibrium distribution requires symmetry in the interactions: non-symmetric interactions correspond to non-conservative forces, which explicitly break time reversal and lead to non-equilibrium steady states. In order to show that our results hold also in this case, at least if the asymmetry is not too strong, we have analyzed the case of small asymmetry in perturbation theory. The analysis of the Martin-Siggia-Rose-De Dominicis-Janssen action [175–178] allows us to conclude that a small degree of asymmetry ($\gamma = 1 - \epsilon$, $\epsilon \ll 1$) does not affect qualitatively the results we shall present in the next section, therefore establishing that our findings for the symmetric case also holds for small asymmetry (see Appendix A.4 for more details). We have also confirmed this result by numerical simulations for $\gamma < 1$.

4.4 Results

In the following we present our analytical results focusing on ecosystems with parameters $\sigma = 0.5$ and $\mu = 1$, hence a case in which interactions are in average competitive for the pool of species.

4.4.1 Characterization of the self-sustained phase

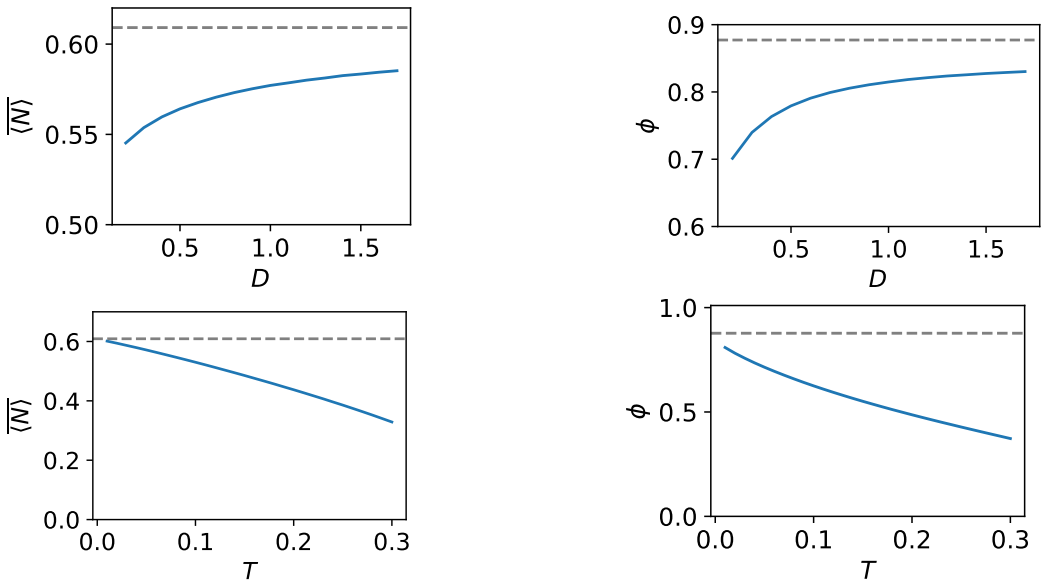

Figure 4.4: Average abundance $\overline{\langle N \rangle}$ and diversity ϕ as a function of the diffusion constant D for $T = 0.25$ (top) and as a function of temperature (strength of demographic noise) for $D = 0.1$ (bottom). The dashed lines represent the $T = 0$ well-mixed results. $\mu = 1$, $\sigma = 0.5$.

By solving the DMFT equations described in the previous section, one finds that when the diffusion constant is large enough the system is in a self-sustained phase (active phase in the

directed percolation jargon) in which a non-zero abundance is maintained despite the presence of demographic fluctuations. In this regime, although some species go globally extinct on all patches, others survive thanks to the migration from neighboring patches. This mechanism is sufficient to prevent extinctions due to demographic stochasticity and leads to a self-sustained metacommunity.

In the following, we discuss the salient properties of this phase, focusing on two ecologically relevant observables: the average abundance, $h = \overline{\langle N \rangle}$, and the ecosystem diversity ϕ, defined as the fraction of species that are not globally extinct, *i.e.* that have non zero abundance in at least one patch. At stationarity, we can compute the ecosystem diversity as $\phi = \overline{\theta(\langle N \rangle)}$. We also discuss the abundance distribution.

Average abundance and diversity

As expected, demographic noise is detrimental to survival: the fraction of surviving species, or diversity, and the average abundance decrease with the strength of demographic fluctuations, see bottom panels of Fig. 4.4. On the contrary, dispersal is beneficial, as shown in the top panels of Fig. 4.4. The behavior of the diversity for species-rich ecosystems with heterogeneous interactions in the presence of demographic noise is a novel result of our approach: in the case of fixed external immigration, previously often considered in the literature, all species are kept alive by the immigration, albeit some at very small abundances, it is therefore not possible to rigorously define the ecosystem diversity [5]. We find that the species that go extinct are those whose growth is on average more affected by the interactions with the rest of the ecosystem, as quantified by the static part of the environmental noise $-z\sigma\sqrt{C_d^\infty}$, which renormalizes the carrying capacity of a species. For $\rho = 1$, if z is lower than a critical value z^* the corresponding species goes extinct (Figure 4.3). In Appendix A.5, we show that at z^* the single DP process is critical: species with $z < z^*$ are in the active DP phase, whereas if $z > z^*$ the species is in the inactive DP phase. This argument can be generalized for smaller values of ρ.

The case of independent interactions across patches ($\rho = 0$) is special. Since all species are globally equivalent, they can only be all surviving or all extinct. In general, all species have some patches in which they are very abundant, immigrants from these patches can then save them from extinction in the rest of the system. This favorable role of dispersal through which spatial heterogeneity enhances diversity has been discussed in [69, 82, 156, 199].

The limits $D \to \infty$ and $T \to 0$ can be mapped to the well-mixed case. For $D \to \infty$ the timescale of spatial mixing is much smaller than all other timescales, therefore the abundances of each species are equal on all sites. The absence of spatial fluctuations allows one to write an evolution equation involving only the space-averaged abundances, that corresponds to an effective single local community without demographic fluctuations with interactions given by the spatial average of the original ones. The well-mixed result is also recovered (for $\rho = 1$) in the $T \to 0$ limit (see two bottom panels of Figure 4.4): because the abundances do not fluctuate there is no migration flux between patches, and the diffusion term plays no role.

As for the distribution of the abundances, we find an exponential decay, as it is the case in other models with random fully connected interactions [10–12, 212].

Abundance distribution

As noted before, two types of stochasticity contribute to the distribution of abundances. Each species is subjected to demographic and environmental noise, making their abundance a time-dependent random variable. For each species, the abundance is distributed according to the

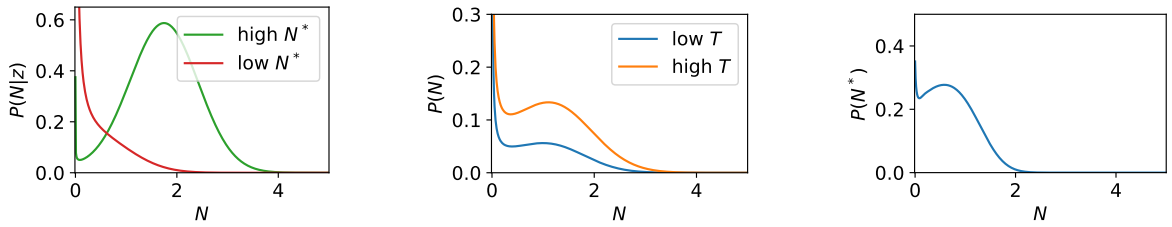

(a) (b) (c)

Figure 4.5: (a) Probability distribution of the abundance for a given species, i.e. at fixed z; in red for a species close to extinction ($z = -0.45$, $N^* = 0.148$), in green for a species far from extinction ($z = -2.45$, $N^* = 1.733$); $T = 0.4$, $D/D_0(T) = 0.84$. (b) Probability distribution of the abundance N; in orange deep in the survival phase ($T = 0.8, D/D_0(T) = 1.5$), in blue right before the discontinuous transition ($T = 0.4$, $D/D_0(T) = 0.84$). Note that the shown distributions do not integrate to 1 because a finite fraction of the species are extinct, leading to a delta function in zero with weight $1-\phi$. (c) Probability distribution of the space (or time) averaged abundance, because of extinct species we again have a delta function in zero with weight $1 - \phi$. $T = 0.4$, $D/D_0(T) = 0.84$. $\mu = 1$, $\sigma = 0.5$, $\rho = 1$.

Boltzmann distribution with Hamiltonian H_{eff} from Eq. (4.15):

$$P(N|z) = \frac{e^{-\beta H_{eff}(N;z,N^*(z))}}{\int_0^\infty dN e^{-\beta H_{eff}(N;z,N^*(z))}} \ . \tag{4.25}$$

Two examples of this distribution, for different values of z, are plotted in Figure 4.5a.

On top of this, because of disorder, different species experience different average interactions with the rest of the ecosystem. This corresponds to different values of z, which is Gaussian distributed, and leads to species-dependent factors in H_{eff}. If we want to study the distribution of the abundances of all species at a given time in one site ($P(N)$) we need to take into account both effects. We can compute $P(N)$ marginalizing over z:

$$P(N) = \int \mathcal{D}z P(N|z) \ . \tag{4.26}$$

We could also be interested in the distribution across species of the abundance averaged over patches or time (Figure 4.5c), given by:

$$P(N^*) = P(z) \left(\frac{dN^*(z)}{dz} \right)^{-1} \tag{4.27}$$

for $N^* > 0$. The probability that $N^* = 0$ is $1 - \phi$, where ϕ is the diversity.

4.4.2 Transition to complete extinction and meta-stability

Continuous transition

When demographic fluctuations are sufficiently strong, decreasing the diffusion constant leads to a continuous phase transition from an active phase in which some species are able to self-sustain to an inactive phase in which they are all extinct. The critical value of the diffusion constant is the same that would be obtained in the absence of interactions, where the system directly maps to directed percolation, or in the case of constant interactions [79] (see Figure 4.2 and Appendix A.5.1). This is to be expected: upon approaching the transition, the abundances tend to zero,

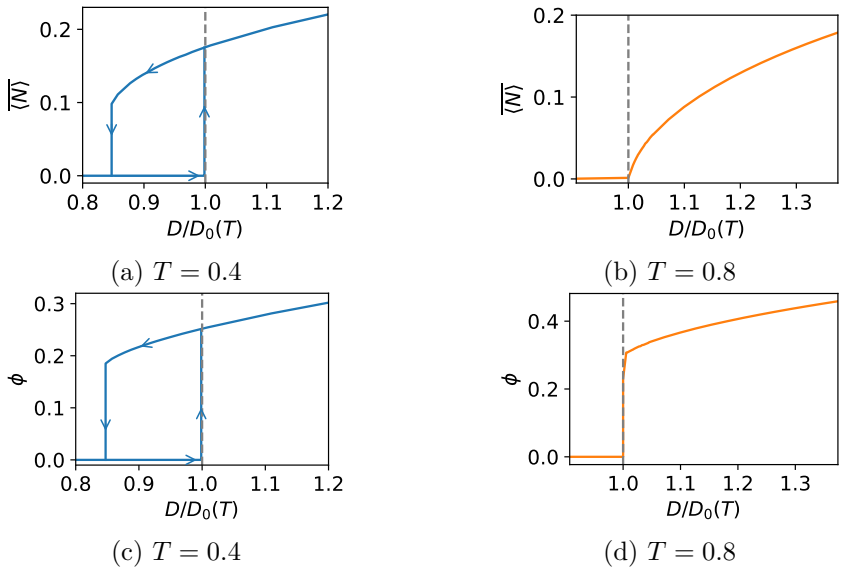

(a) $T = 0.4$ (b) $T = 0.8$

(c) $T = 0.4$ (d) $T = 0.8$

Figure 4.6: The average abundance $h = \overline{\langle N \rangle}$ and the diversity $\phi = \overline{\theta(\langle N \rangle)}$ as a function of D across a discontinuous (a, c) or continuous (b, d) transition. In (a) the arrows indicate the direction of the hysteresis cycle: decreasing D (starting from high values) the ecosystem would follow the finite solution until the discontinuous transition, where the abundances jump to zero. If we now increase D, it would follow the zero solution until this becomes unstable at $D_0(T)$. Gray dashed lines indicate the value of D at which a single species would go (continuously) extinct. Note that we have divided D by the critical value of the diffusion constant for Directed Percolation $D_0(T)$ in all plots, to emphasize the effect of interactions on the already known case. Because $D_0(T)$ vanishes exponentially for $T \to 0$ (App. A.5.1), the metastability region has a vanishing width in this limit and the system is always in the survival phase. $\mu = 1$, $\sigma = 0.5$.

and therefore the interactions, which have a quadratic dependence on the abundances, become irrelevant. The critical exponents indeed match the ones falling in the Directed Percolation universality class; in particular, the abundance goes to zero linearly (Figure 4.6b). Interestingly, approaching the transition the diversity does not go to zero and instead tends to a finite value (Figure 4.6d). This indicates that the average abundance goes to zero not because more and more species are going extinct, but because all surviving species are simultaneously decreasing their abundances. This homogenization in the behavior of species is yet another consequence of the irrelevance of the interactions, the only trait distinguishing one species from another in our model.

Discontinuous transition

At smaller demographic noise this picture changes drastically and interactions play a major role. The ecosystem is able to self-sustain at values of the diffusion constant for which in the absence of interactions it would be in the inactive phase. Further lowering D we encounter a discontinuous transition at which all species abruptly go extinct, i.e. species abundances suddenly jump to zero (Figures 4.6a and 4.6c). Before the discontinuous transition, there is an extended region in which the ecosystem is meta-stable (in grey in Figure 4.7): in this regime, the system reaches an equilibrium with high or low abundances depending on the initial conditions. As a consequence, it exhibits hysteresis (Figure 4.6a): if we slowly decrease the diffusion constant starting from $D > D_0$, the system will abruptly jump from finite to zero average abundance at the transition, and then remain in this degraded state even upon a subsequent increase of the diffusion constant. Indeed, only when we exit the metastability region the extinction state becomes unstable, and adding a small external immigration the system can go back to the diverse state. The phase diagram of the system is represented in Figure 4.7.

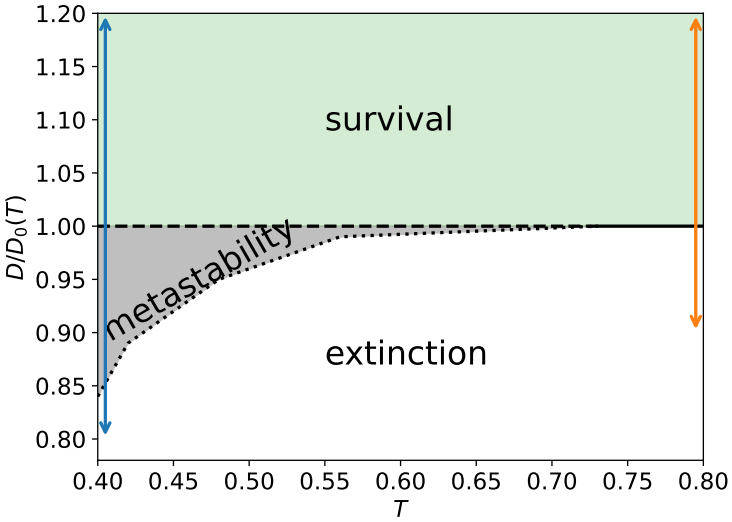

Figure 4.7: The phase diagram for constant interactions across patches ($\rho = 1$). The continuous line indicates the continuous transition, and the dotted and dashed lines are the limits of the metastability region, highlighted in grey. At the two limits of the metastability region one of the two solutions disappears and we have a discontinuous transition. The arrows indicate the parameters range in Figure 4.6.

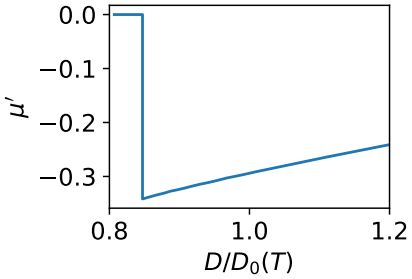

(a) Mean of the reduced interaction matrix

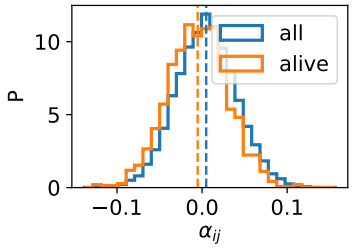

(b) Distribution of the interaction coefficients

Figure 4.8: Left: Analytical estimate of the mean of the reduced interaction matrix using Eq. (4.28) for $T = 0.4$. Right: Numerical results for the distribution of the interaction coefficients for all and surviving species. $T = 0.18$, $D/D_0 = 0.8$. In both cases in the initial species pool $\mu = 1$, $\sigma = 0.5$; if all species go extinct we say $\mu' = 0$.

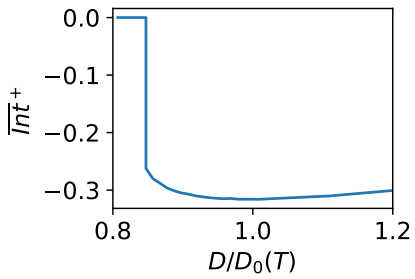

(a) Average interaction term

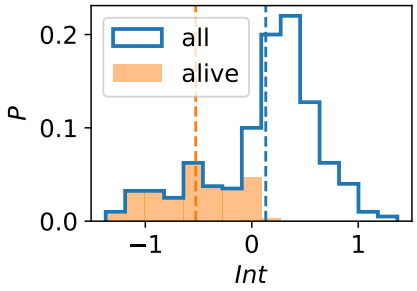

(b) Distribution of interaction terms

Figure 4.9: Thermal averaged interaction term, $Int = \langle \sum_j \alpha_{ij} N_j \rangle$, averaged over non extinct species (indicated by an overline with a $^+$ superscript), for two temperatures corresponding to the discontinuous regime. Left: analytical results for $T = 0.4$, $\rho = 1$ (as in Figures 4.6 a-c). Int^+ is negative in the metastability region, it jumps to zero when all species go extinct at the discontinuous transition. Right: Distribution of the thermal averaged interaction terms in a numerical simulation in the metastability region ($T = 0.18$, $D/D_0(T) = 0.8$, $S = 200$, $L = 400$, $t_{max} = 500$, averaged over 2 runs). Non extinct species are highlighted in orange, only species with negative (or close to zero) interaction terms manage to survive. Averaging only over non extinct species (orange dotted line) leads to a significantly lower (more mutualistic) value than averaging over all species (blu dotted line). $\mu = 1$, $\sigma = 0.5$

Emergence of mutualistic interactions

It was recently shown that a metacommunity subject to demographic noise and constant mutualistic interactions exhibits a similar discontinuous phase transition [206]. The authors of [206] also performed numerical simulations with random (patch-independent) interactions, showing that the surviving species have more mutualistic interactions than the total species pool. We find that a similar mechanism is at play in our case: it is an emergent phenomenon due to ecological dynamics which is present even though interactions are not on average mutualistic (in fact they are competitive, $\mu = 1$). Because of the symmetry in the interaction network, species that interact more competitively are more negatively affected by the interactions with the rest of the ecosystem, and will hence be more easily driven to extinction. This leads to a decrease of the mean of the interaction matrix restricted to surviving species.

Following reference [136], we can compute the statistics of the reduced interaction matrix at zero temperature as:

$$\mu' = \phi\mu - 2\frac{\sigma^2 h}{\phi}\frac{d\phi}{d\zeta} = \phi\mu - 2\frac{\sigma h}{\phi\sqrt{2\pi C_d^\infty}}e^{-(z^*)^2/2} \ . \tag{4.28}$$

Since we have a finite demographic noise, in our case this formula is only an approximation, but it provides an useful estimate of the variation of the mean interaction. We find that the interaction mean decreases (more mutualistic) when decreasing the diffusion coefficient (Figure 4.8a); it is negative in the entire metastability region. In Figure 4.8b we show the distribution of the interaction coefficients considering all species or only surviving ones in numerical simulations. The distribution of the interaction coefficients is slightly shifted to more negative values, and indeed the average changes from 0.96 to -0.28.

Another quantity of interest is the average interaction term for non-extinct species, $\overline{Int}^+ = \overline{\sum_j \alpha_{ij}\langle N_j\rangle}^+$ (the $^+$ indicates that the average is carried out only over non-extinct species, $\langle N_i\rangle > 0$), which we find to be negative in the entire metastability region (Fig. 4.9a). In order for a species to survive in conditions in which without interactions it would go extinct, we need the interaction term (that appears summed to the carrying capacity with a negative sign) to give on average a negative contribution. We indeed find numerically that only species with negative interaction terms manage to survive (Fig. 4.9b), thus leading to an enhancement of mutualism between surviving species.

To compute the average interaction term we can again use the cavity method and imagine to add a species (with index 0) to the community. With similar arguments to those employed in the DMFT derivation we obtain at stationarity:

$$Int_0 = \langle\sum_j \alpha_{0j}N_j^u\rangle = \mu h + \sigma\sqrt{C_d^\infty}z - \gamma\sigma^2\left(R_d^{int} + R_0^{int}\right)\langle N_0\rangle \ . \tag{4.29}$$

We can now average it over all species (all values of z, indicated by an overline), or over only non extinct ones ($z < z^*$, indicated by an overline with $^+$ superscript).

$$\overline{I} = \mu h - \gamma\sigma^2\left(R_d^{int} + R_0^{int}\right)h \tag{4.30}$$

$$\overline{I}^+ = \mu h - \sigma\frac{\sqrt{q_0}}{\phi}\frac{e^{-z^{*2}/2}}{\sqrt{2\pi}} - \gamma\sigma^2\left(R_d^{int} + R_0^{int}\right)\frac{h}{\phi} \ . \tag{4.31}$$

Note that we will always find $\overline{I}^+ < \overline{I}$; $\overline{I}^+$ is negative in the entire metastability region (Figure 4.9a in the main text). This is also confirmed by numerical simulations: the average interaction term is 0.13 considering all species, and -0.46 considering only non extinct ones (Figure 4.9b).

In the case of independent interaction matrices, all species survive, so that the interaction matrix is not modified.

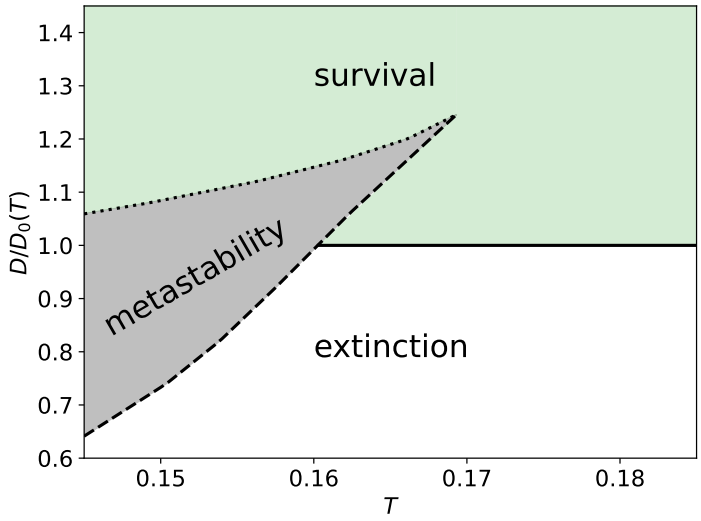

Figure 4.10: The phase diagram for independent interactions across patches ($\rho = 0$). The continuous line indicates the continuous transition, the dotted and dashed lines the limits of the metastability region, highlighted in grey. At the two limits of the metastability region one of the two solutions disappears and we have a discontinuous transition. $\mu = 1$, $\sigma = 0.5$

4.5 Assessing the generality of the scenario

To confirm the generality of our results, we now consider different variations of the model studied in the previous section. The aim is to show that our results hold in a broader setting. We shall be particularly interested in considering the case of a large but finite number of species, a large but finite number of patches, a small but finite asymmetry of interactions, as well as generic values of ρ.

4.5.1 Independent interaction matrices

As explained in Section 4.3.4, our analytical treatment can be generalized to arbitrary values of the spatial heterogeneity ρ. However, the numerical solution of the self-consistent equations is more challenging for intermediate values of ρ, because two distinct averages over the disorder need to be performed. We therefore obtained analytically the phase diagram only for the extreme values $\rho = 1$ and $\rho = 0$. Since the qualitative behavior is the same, we conjecture the same holds also for intermediate values of ρ. This is also confirmed by numerical simulations (see Figure 4.13).

The phase diagram in the case of independent ($\rho = 0$) interactions across patches is shown in Figure 4.10 (to be compared to the one of Figure 4.7 corresponding to constant ($\rho = 1$) interactions across patches). For $\rho = 0$ it is quite clear that the metastability region extends above $D_0(T)$ in some range of temperature. In the part of the metastability region above $D_0(T)$ the two metastable solutions are both finite: one is of order one and the other proportional to the distance from $D_0(T)$; the two solutions coalesce at the tip of the metastability region. This is actually also true for $\rho = 1$, but in such a small parameter range that it is very hard to access numerically. In both cases, the upper limit of the metastability region is bounded from below by the critical value of the diffusion constant in the absence of interactions, $D_0(T)$.

4.5.2 Finite number of species and finite number of patches

The case of finite number of species and finite number of patches could also in principle be studied analytically, but they would require very involved analysis. We therefore turn to direct numerical simulations of the Generalized Lotka-Volterra equation (4.1) and show that the results agree with and extend the theory presented in the previous section. The details on the numerical scheme implemented for the simulation can be found in Appendix A.7. These simulations are challenging as we are interested in considering both a large number of species and a large number of patches.

Some of the challenges become clear examining the time evolution of the average abundances (Figs. 4.11). At high temperature (top) the average abundance fluctuates significantly even with large number of species and patches ($S = 200$, $L = 400$); finite size effects on L lead to an excess of extinctions. At lower temperature (bottom) the dynamics strongly slows down, and at $t = 200$ some of the abundances (depending on the value fo D) have not yet reached their asymptotic value, leading to a smoothing of the discontinuous transition.

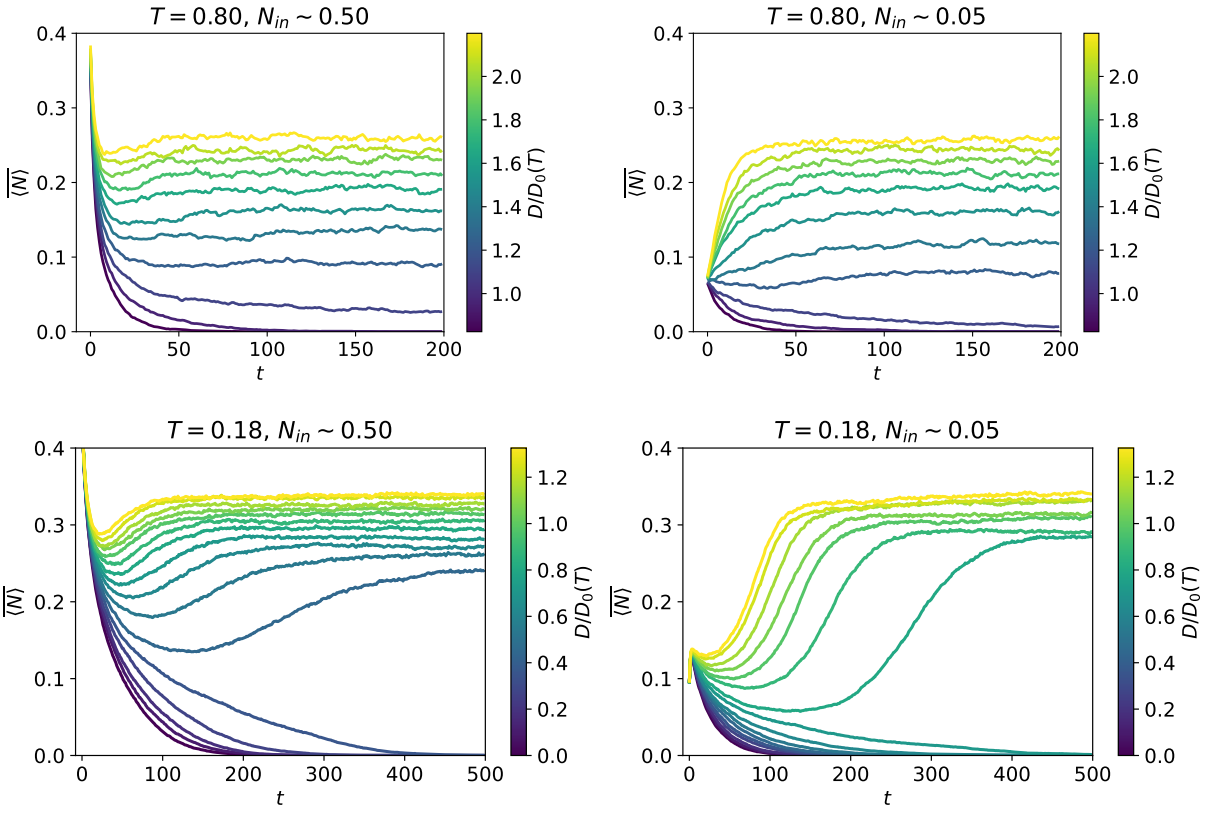

Figure 4.11: Time evolution of the average abundance for two different temperatures and two average values of the initial conditions. Note the different time ranges in the top and bottom figures: at high temperature the abundances have converged to their asymptotic values at $t_{max} = 200$, at lower temperature it is necessary to wait much longer ($t_{max} = 500$). $S = 200$, $L = 400$, $\mu = 1$, $\sigma = 0.5$.

Generically, for moderate system sizes ($S < 100$ and $L < 100$) we find strong fluctuations due to the quenched disorder in the interaction matrix, and quantitative finite size effects compared to the asymptotic $S, L \to \infty$ solution, in particular for $\rho = 1$ (for $\rho = 0$ each patch is characterized by an independent realization of the interaction matrix, thus leading to a faster

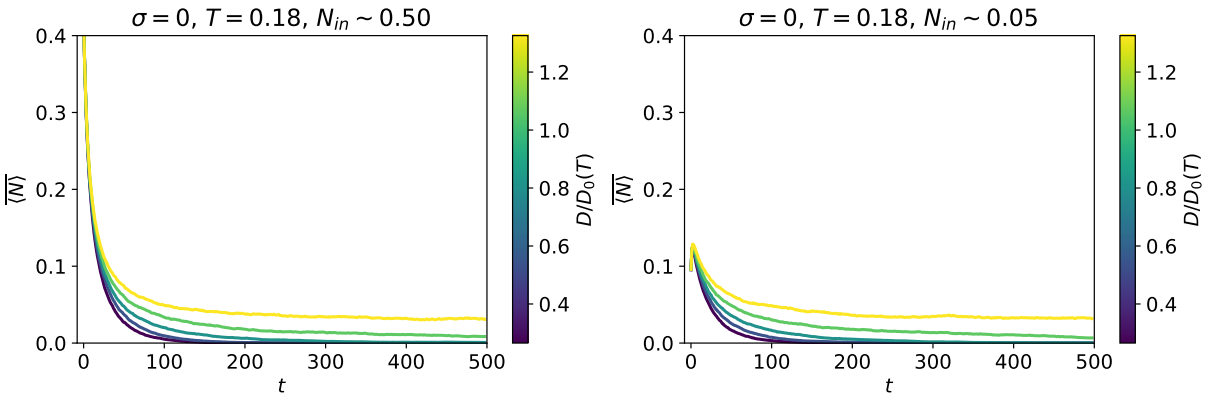

Figure 4.12: Time evolution of the average abundance without heterogeneity in the interaction network ($\sigma = 0$) at $T = 0.18$ and two average values of the initial conditions. For $D < D_0(T)$ the abundances converge to 0. $S = 200$, $L = 400$, $\mu = 1$.

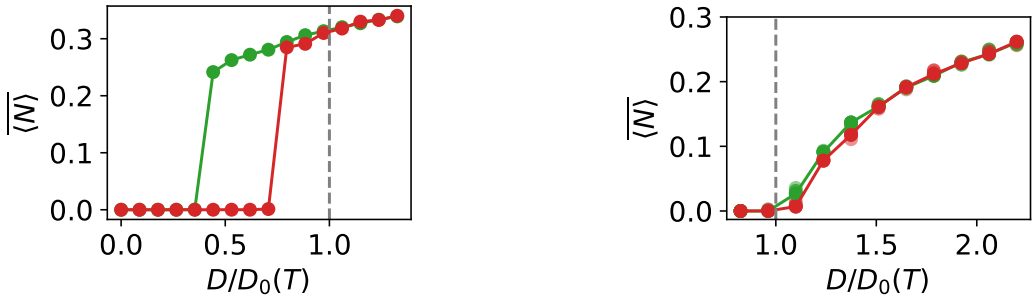

(a) $T = 0.18$ (b) $T = 0.8$

Figure 4.13: Average abundance $\overline{\langle N \rangle}$ as a function of the diffusion constant D for $T = 0.18$ and $T = 0.8$ at the end of the runs plotted in Figure 4.11. Green and red dots indicate the initial conditions of order 1 and of order 0.1. The dashed line indicates the analytical prediction for the critical value of the diffusion constant for the continuous transition. $\mu = 1$, $\sigma = 0.5$, $S = 200$, $L = 400$, $t_{max} = 500$ (left) and 200 (right).

(self-averaging) convergence of the system to its disorder average). For larger values of S and L, e.g. $S = 200$, $L = 400$, fluctuations and finite size effects are limited and one finds results that are in both qualitative and quantitative agreement with the analytical solution.

In figure 4.13 we show the behavior of the average abundance as a function of the diffusion constant for two different values of the temperature, starting from two different initial conditions. In order to probe the existence of hysteresis, and therefore a discontinuous transition and metastability, we numerically simulate systems with different initial conditions. For the green curves, the initial abundances were uniformly sampled between 0 and 1, for the red curves between 0 and 0.1. The former should therefore be more prone to evolve toward the self-sustained solution, if it exists, whereas the latter to the "all-extinct" solution.

We find that indeed at higher temperatures, $T = 0.8$, in agreement with the analytics and the phase diagram in Figure 4.7, the final abundances vary continuously when varying the diffusion constant, and they converge to the same value, no matter the initial condition. The value of D at which the final abundances significantly depart from zero quantitatively matches the analytical result for the critical value of the diffusion constant at the continuous transition.

Instead, at $T = 0.18$ the final abundances show a strong dependence on the initial condition in an extended interval of diffusion strengths; for a given initial condition the final abundance exhibits a very abrupt change. The discontinuous transition takes place slightly before the analytical prediction. Besides finite size effects, we note that this phenomenon is to be expected for this kind of transition. In fact, when the red curve (low initial condition) jumps to high abundance, this does not necessarily indicate that the $\overline{\langle N \rangle} = 0$ solution has become locally unstable, but rather that its basin of attraction has shrunk and does not include the considered initial condition anymore. It is therefore to be expected that this occurs for $D < D_0(T)$. A similar phenomenon takes place for spinodal transition in physics.

Interestingly, the dynamics strongly slows down in this regime, in particular for the decay of the abundances from large initial conditions. In fact, this process occurs via the rare extinctions of species that are asymptotically not able to self-sustain but can persist for very long times, especially in this regime in which demographic fluctuations are weak. The dynamics is not as slow without the heterogeneity in the interaction network (Figure 4.12) The strong dependence on the initial conditions cannot be explained just by the slowdown of the dynamics because the abundances with different initial conditions evolve in opposite directions (see Figure 4.11).

The heterogeneity in the interaction network is essential to allow the ecosystem to self-sustain below the single DP critical point: indeed if we consider the same parameters but take $\sigma = 0$ all species go extinct below $D_0(T)$, and there is no strong dependence on the initial conditions (Figure 4.12).

4.5.3 Asymmetric interactions and partial correlation between patches

We are now interested in focusing on cases in which the interactions between species are not fully symmetric, and the interaction matrices are partially correlated between patches, i.e. $0 < \rho < 1$.

One can analytically show that the phase diagrams remains qualitatively unchanged considering a small asymmetry in the interactions ($\gamma = 1 - \epsilon$, $\epsilon \ll 1$), see Appendix A.4. Thus, our results should qualitatively hold also for a finite, at least not too large, asymmetry.

To confirm this finding and study intermediate values of ρ (besides $\rho = 0$ and 1 considered analytically) we performed simulations with spatial heterogeneity $\rho = 0.9$ and asymmetry in the interactions $\gamma = 0.9$, and as before for $L = 400$, $S = 200$. Also in this case at $T = 0.8$ we find a continuous transition and no strong dependence on the initial conditions, while at $T = 0.18$ we find a discontinuous transition and a hysteresis region (Figure 4.15) [1]. Although the curves

[1] At $T = 0.18$ the dynamics is so slow (especially close to the tipping points) that at $t_{max} = 500$ some of

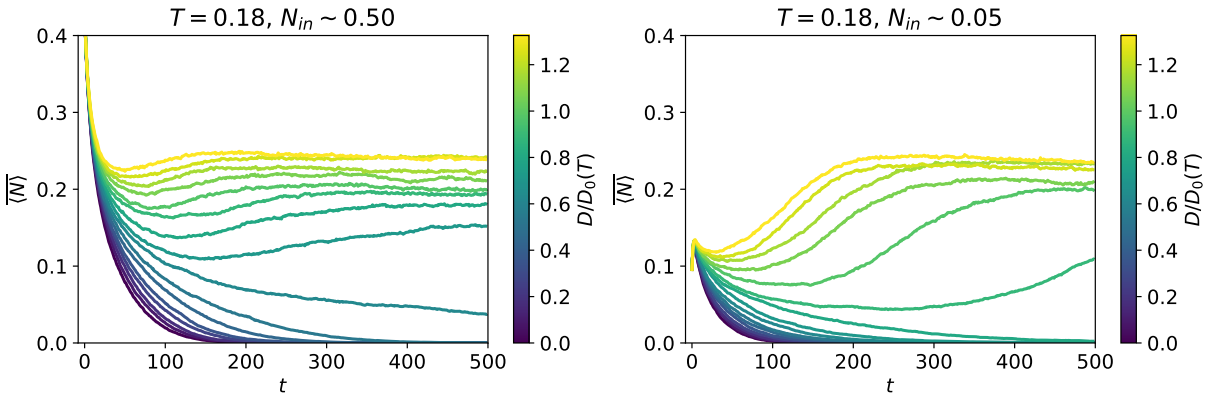

Figure 4.14: Time evolution of the average abundance with partial correlation between patches ($\rho = 0.9$) and non symmetric interactions ($\gamma = 0.9$) at $T = 0.18$ and two average values of the initial conditions. At $t = 500$ the abundances have not yet reached their asymptotic value, leading to an apparent smoothing of the discontinuous transition. Nevertheless this is ensured by the abrupt change of behaviour of the evolution of the average abundance: for one value of the diffusion constant at long times the abundance is decaying to 0, whereas for the next it shows a (slow) increase. We conclude that the asymptotic values would likewise show an abrupt change. $S = 200$, $L = 400$, $\mu = 1$, $\sigma = 0.5$.

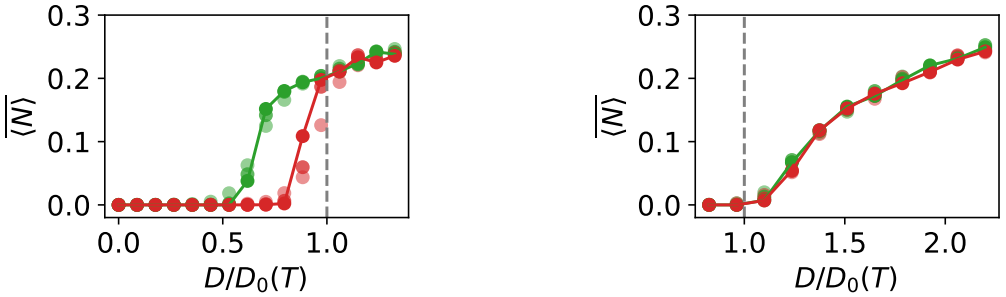

(a) $T = 0.18$ (b) $T = 0.8$

Figure 4.15: Average abundance $\overline{\langle N \rangle}$ as a function of the diffusion constant D for $T = 0.18$ and $T = 0.8$ with some spatial heterogeneity ($\rho = 0.9$) and some asymmetry in the interactions ($\gamma = 0.9$). Green and red lines indicate the initial conditions of order 1 and of order 0.1, lighter dots show the average abundance at intermediate times (50% and 75% of t_{max}). $\mu = 1$, $\sigma = 0.5$, $S = 200$, $L = 400$, $t_{max} = 500$ (left) and 200 (right).

quantitatively change with respect to their $\gamma = \rho = 1$ counterparts, as expected, the results and in particular the existence of a discontinuous transition do remain qualitatively unaltered.

In conclusion, combining all these numerical tests, we conclude that the scenario obtained from the analytical solution is robust and holds broadly. We will come back to this point in the conclusion to suggest other extensions and tests.

4.6 Precursor of the instability toward extinction

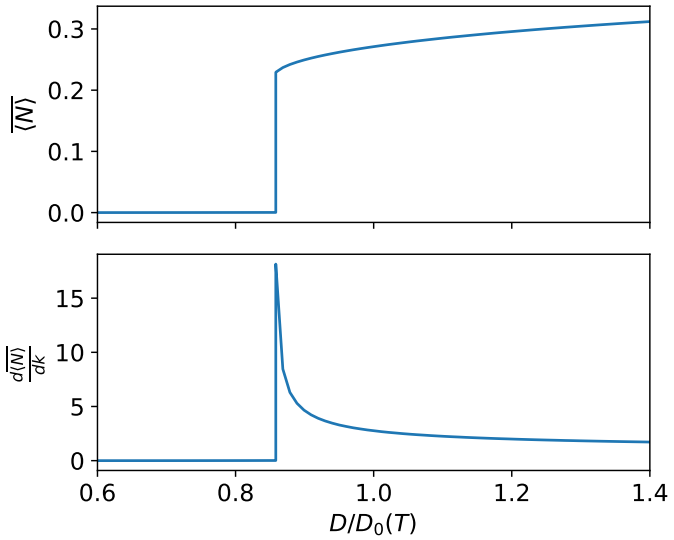

Figure 4.16: Average abundance and its response to a perturbation of the carrying capacity k at $T = 0.153$ for $\rho = 0$ approaching the instability of the self-sustained phase. $\mu = 1$, $\sigma = 0.5$.

In the previous section, we have shown that dispersal can rescue complex and large ecosystems from extinction due to demographic noise. Depending on the strength of the demographic noise, the transition from the self-sustained to the extinct phase can be either continuous or discontinuous. The latter takes place for low demographic noise and low dispersal. In this regime, we have found that the transition is accompanied by a metastable regime and hysteresis. Such transition is what is called in ecology, in environmental and social sciences a *tipping point* or regime-shift [202, 213] and in physics a spinodal. Tipping points are often catastrophic events, as the abrupt rapid shifts almost always lead to negative consequences and a less favorable state of the system. Our case is no exception, as the system's transition is from a self-sustained state with high diversity to one in which all species are extinct. As done for several other tipping points [214, 215], it is therefore important to find early signs or precursors that can allow one to detect the closeness of the system to the tipping point before the catastrophic shift actually takes place.

In our case, following intuition that comes from the physics of spinodal points, we focus on responses to perturbations as probe of closeness to the tipping point. Indeed the divergence of response functions is a generic feature of saddle node bifurcations [214]. Let us consider a generic dynamical system, described by

$$\frac{d\vec{x}}{dt} = F(\vec{x}, k) \ . \tag{4.32}$$

the abundances have not yet converged to their asymptotic values. This leads to an apparent smoothing of the discontinuous transition, whose existence is nevertheless ensured by the abrupt change of behavior of the evolution of the abundance (see Figure 4.14), analogous to the one observed for $\rho = 1$, $\gamma = 1$.

$\vec{x}$ contains all the degrees of freedom of the system, whereas k is a control parameter. The zeros of F yield the stationary states x^*:

$$F(x^*, k) = 0 \ . \tag{4.33}$$

The stationary point is stable if the Jacobian of F has only negative eigenvalues, ensuring that x returns to x^* upon small perturbations. In a saddle node bifurcation, a stable and an unstable stationary point collide and annihilate each other. Since the Jacobian at the stable stationary point has only negative eigenvalues whereas the one at the unstable stationary point has at least a positive eigenvalue, one of the eigenvalues has to cross zero at the bifurcation. The existence of a zero mode leads to a diverging response to perturbation.

In Appendix A.6, we show how this mechanism is at play in our case when approaching the tipping point of the self-sustained phase. We study the response of the system to a perturbation in the environmental conditions in the case of independent interaction coefficients ($\rho = 0$). We will consider for concreteness a perturbation to the carrying capacity k, but we expect the same qualitative behavior for perturbations to the diffusion constant, the moments of the interactions, or the strength of the demographic fluctuations. Such response, which can be measured in controlled lab experiments, does diverge approaching the discontinuous transition, see Figure 4.16 for the $\rho = 0$ case. A similar behavior is expected for generic values of ρ. This probe can therefore be used as an early warning signal of the proximity to the tipping point of the self-sustained phase. In natural ecosystems, where measuring responses to perturbation can be challenging, one could instead monitor the long-term fluctuations of average abundance due to environmental noise affecting the carrying capacity on a long time. This would be a proxy for the response proposed above. It is important to focus on long-times since the processes at play are slow: at low temperature, extinctions are due to rare fluctuations of the demographic noise, as discussed at the end of Section 4.2.1.

4.7 Conclusions

We uncovered a rich phase diagram for many-species Lotka-Volterra metacommunities subject to heterogeneous symmetric interactions, demographic noise and diffusion. If the demographic fluctuations are too strong they drive all species to extinctions, but when the diffusion constant is large enough these extinctions can be compensated by recolonizations from neighboring sites, and the ecosystem is able to self-sustain at finite abundance and diversity. The system exhibits a phase transition between an extinction and a survival phase. The transition can be either continuous or discontinuous, depending on whether the behaviour of the system is dominated by the demographic fluctuations or the heterogeneous interaction network.

When the demographic fluctuations are strong the transition is continuous and interactions play a secondary role. In fact, the transition is completely analogous to what one would have in the absence of the interactions (even the critical value of the diffusion constant coincides). This is because when the abundances tend to zero the interactions become sub-dominant and the system falls in the standard Directed Percolation universality class.

The situation is drastically different at lower demographic noise. In this case the transition becomes discontinuous and the system exhibits novel features, that are a signature of the complexity of the ecosystem and the major role played by the interactions. There is an extended range of parameters in which without interactions, i.e. for single species, the system would be driven to extinction but the metacommunity is instead able to self-sustain at finite abundances. This is possible because strongly competing species are eliminated from the community, while surviving species cooperate to self-sustain in such harsh conditions. Lowering the diffusion constant, the ecosystem reaches a tipping point at which all surviving species go extinct; close

to this point the ecosystem is subject to collapses upon small perturbations and its dynamics exhibits hysteresis. We therefore find that mutualism naturally emerges from a (on average) competitive pool of species when conditions become harsher. This has a double effect: it allows the ecosystem to survive in conditions in which all species in isolation would go extinct, but it also makes it fragile to perturbations. In this regime, it is not possible to predict the vicinity of the catastrophic shift of the ecosystem by looking at the average abundance. As early warning sign, we propose to monitor the response of the system to perturbations. We have shown that this is a suitable probe, as it diverges approaching the discontinuous transition.

We confirm and complement our analytical approach with numerical simulations, which show that our results are quite robust to modifications of the model, in particular to the introduction of a small asymmetry in the interactions, to various degrees of correlation of the interaction network between different spatial locations, and for system with a finite number of species and patches.

There are several directions worth future investigations. We focused on a fully connected spatial system, which provides a mean-field analysis for generic spatial lattices. On the other hand, our DMFT treatment of the interactions is directly generalizable to any other spatial network, including finite dimensional ones. It would be very interesting to study cases in which the patches are located in finite dimensional lattice or on random structures. In particular, it would be interesting to find out (1) whether the discontinuous transition is also present in this case or finite dimensional fluctuations destroy the metastable region, and (2) whether the continuous transition can still be described in terms of directed percolation or interactions, although secondary, can alter its universality class. It would also be worth analysing stronger asymmetries in the interactions, e.g. lowering the value of γ. We expect that a significant positive correlation between reciprocal interactions is needed to induce metastability. This ensures that species that interact more competitively are also more negatively affected by the interactions with the rest of the ecosystem and hence go extinct, thus leading to mutualism for the surviving species.

Finally, species rich LV model with heterogeneous and strong interactions display multiple equilibria and chaotic dynamics [10–12, 65]. The possibility of different patches to converge to different stationary states could strongly modify the behaviour of the system; in particular allowing the system to experience higher values of the global diversity, possibly violating May's bound [106].

Part II

Non-reciprocal interactions

Chapter 5

Non-equilibrium dynamics: from slow relaxation to non-reciprocity

In this chapter, I review the literature on two different classes of non-equilibrium systems: aging systems and systems driven out of equilibrium by the presence of non-reciprocal interactions.

In Section 5.1 I recapitulate some properties of equilibrium systems. This allows me to better define two distinct reasons why a system can be out of equilibrium: either its dynamics is reversible, but it has not yet relaxed to equilibrium, or its dynamics is irreversible, and no equilibrium distribution exists. Aging systems, introduced in Section 5.2, fall in the first category: their dynamics is reversible, but their relaxation is so slow that in the thermodynamic limit they do not manage to reach equilibrium on any finite timescale. Over the past 60 years, an extensive body of literature on aging and glasses has been developed. Here, I will only focus on topics that are directly relevant to the following chapters. In Section 5.3, I introduce a paradigmatic example of systems with an irreversible dynamics: system that are driven out of equilibrium by the presence of non-reciprocal interactions. In Section 5.4 I discuss what happens when combining two kinds of non-equilibrium dynamics: slow relaxation and non-conservative forcing. The non-reciprocal coupling of aging systems will be the subject of Chapters 6 and 7.

5.1 Equilibrium

Equilibrium statistical physics provides a framework for understanding the large-scale properties of systems composed of many interacting degrees of freedom. While thermodynamics studies the relations between macroscopic observables, statistical physics provides a framework to connect the microscopic dynamics of the constituents of the system to its large-scale properties. This is achieved by considering a statistical *ensemble* of systems, describing the probability of being in any of the microscopic states. At equilibrium, statistical properties do not depend on time, so that observables can be computed by averaging over a static probability distribution. The distribution only depends on conserved quantities, such as the energy, as it can be justified through the ergodic hypothesis or maximum entropy arguments. This allows one to easily compute it, up to a multiplicative normalization factor.

5.1.1 Time reversal and detailed balance

The hallmark of equilibrium systems is their invariance under time translation and time reversal. Time translational invariance implies that the system should be in a stationary state, in which its probability distribution P_{st} is independent of time. Let us indicate with x all the (potentially many) degrees of freedom of our system, and consider a trajectory $x(t)$ between times t_0 and t_f.

At equilibrium the probability to observe a given trajectory should be equal to the probability to observe the time-reversed one. We can separate two contributions: $P_{st}(x(t_0))$ is the probability that the system is in $x(t_0)$ at the initial time, and $\mathcal{P}[x(t)|x(t_0)]$ is the probability that, given the initial condition, it follows the trajectory $x(t)$. With this notation, we can express reversibility under time reversal as:

$$P_{st}(x(t_0))\mathcal{P}[x(t)|x(t_0)] = P_{st}(x(t_f))\mathcal{P}[x_R(t)|x(t_f)] \ , \tag{5.1}$$

where $x_R(t) = x(t_f - t)$ is the time-reversed trajectory, which starts from $x(t_f)$. This condition is known as *detailed balance*; it should hold for every possible trajectory. If the system is described by a stochastic differential equation, the probability of a given trajectory can be computed with a path integral formalism such as the Martin-Siggia-Rose-De Dominicis-Janssen (MSRDJ) action [175–178]. The verification of Equation (5.1) via the MSRDJ formalism was already used in Part I of this thesis (see Sections 3.5.1, 4.3.3 and Appendix A.1) to prove equilibrium for an ecosystem with symmetric interactions subjected to demographic noise.

Detailed balance implies that the flux of probability from any configuration x_1 to any other x_2 is perfectly balanced by the one from x_2 to x_1, so that there are no *probability currents* in the system. This condition is more stringent than the minimal requirement for a stationary distribution, known as *global balance*, which only demands that the total incoming and outgoing probability fluxes for each configuration be balanced. Indeed in a stationary state probability currents can be present, as long as their divergence is equal to zero.

We will say that a dynamics is *reversible* [216] if it exists a function of the state of the system $H(x)$ such that:

$$\frac{W[x_1 \to x_2]}{W[x_2 \to x_1]} = e^{-(H(x_2)-H(x_1))/T} \ , \tag{5.2}$$

where $W[x_i \to x_j]$ is the probability rate to go from x_i to x_j. In physical systems $H(x)$ is the *energy*. Equation (5.2) corresponds to requiring detailed balance with respect to the Boltzmann measure:

$$P_{st}(x) \propto e^{-H(x)/T} \ , \tag{5.3}$$

which indeed turns out to be the equilibrium distribution associated with such a dynamics. Note, however, that (5.2) can be satisfied even if the system is *not* in the stationary state. If the system is ergodic, it will converge to the Boltzmann distribution, but this could take a long time.

We can now better precise the statement we made in the introduction on the two reasons why a system might be out of equilibrium: either its dynamics is irreversible or the system does not manage to reach its stationary distribution. Of course, both things could also happen, and we will be particularly interested precisely in this case.

5.1.2 Equilibrium properties

Stationarity and time reversal symmetry allow one to demonstrate a number of other properties. By definition of stationarity, at equilibrium one time observables must be constant, and two times ones can only depend on the time difference. This holds for example for the correlation function:

$$\langle x(t)x(t')\rangle = C(t-t') \tag{5.4}$$

and for the response:

$$\left.\frac{\partial\langle x(t)\rangle}{\partial h(t')}\right|_{h=0} = R(t-t') \ . \tag{5.5}$$

We have indicated with angular brackets the average over the stochastic dynamics; $h(t)$ is a small field that modifies the Hamiltonian as $H(x) + h(t)x$.

From time-reversal symmetry we can show that the response and correlation functions are also constrained by the Fluctuation-Dissipation Theorem (FDT):

$$R(t-t') = \frac{1}{T}\frac{dC(t-t')}{dt'}\theta(t-t') \ . \tag{5.6}$$

5.2 Aging

In this section we will consider systems which, despite undergoing a reversible dynamics, do not reach equilibrium. Let us imagine to prepare our system at time $t = 0$ in a random configuration; this corresponds to equilibrating it at infinite temperature. If the system is ergodic and we let it evolve under a finite temperature reversible dynamics, it relaxes exponentially to the equilibrium distribution. The relaxation time is finite in a finite system, but it could diverge in the thermodynamic limit. If this is the case, a system with many degrees of freedom could remain out of equilibrium on any reasonable timescale. Time translational invariance is violated: the dynamics of the system explicitly depends on its *age*, which is the waiting time since its preparation t_w. We call this behavior *aging* [160–163, 217]. This effect is visible for example in the correlation function, which explicitly depends on t_w. In the cases that we will consider in this thesis, the correlation function exhibits a plateau that becomes longer and longer as time goes on: the system needs increasingly more time to decorrelate. The length of the plateau defines an effective timescale of the dynamics, which is a function of the age of the system. If we wait an *infinite* time, the system remembers forever its configuration:

$$\lim_{\Delta t\to\infty}\lim_{t_w\to\infty} C(t_w+\Delta t, t_w) = q_{EA} > 0 \ . \tag{5.7}$$

q_{EA} is called the Edwards-Anderson order parameter [218, 219]. However, for any *finite* waiting time, the system will eventually manage to decorrelate[1]:

$$\lim_{t_w\to\infty}\lim_{\Delta t\to\infty} C(t_w+\Delta t, t_w) = 0 \ . \tag{5.8}$$

This situation is called *weak ergodicity breaking* [138, 160, 222–224]. The system eventually forgets what happened at any finite time ("weak long-term memory" [160]); this allows one to obtain an asymptotic solution for the slow component of the dynamics. At long times, aging only modifies the timescale of the dynamics: the asymptotic behavior of the correlation function becomes self-similar upon a rescaling of time. The fluctuation-dissipation theorem is violated; however the response and correlation functions remain linked by an FDT-like relation, albeit with an effective temperature that differs from that of the bath [225].

5.2.1 Physical systems and beyond

To give a qualitative understanding of why a system might fail to equilibrate, we now present three paradigmatic cases: structural glasses, spin-glasses and coarsening systems.

Structural glasses

Glass is an amorphous solid, formed by rapid cooling (*quenching*) of suitable melt materials, such as silica. Even though glassmaking dates back several thousands of years, the nature of glass is still not fully understood.

[1] This is not true in spin-glass models that exhibit *strong ergodicity breaking* [220, 221]. The study of such systems is beyond the scope of this thesis.

The main difference between a liquid and a solid is that a liquid flows, whereas a solid does not. In a liquid, particles are free to move. Let us imagine to record the positions of all particles at an initial time t_1 and to compare to the ones at a later time t_2. If t_1 and t_2 are sufficiently separated, more than a certain relaxation time τ, most particles will have moved, and the two configurations will be very weakly correlated. If we lower the temperature, the relaxation time generically increases; this is also associated with an increase in viscosity.

If we cool our liquid very slowly, at the melting temperature it undergoes a first order phase transition to a solid crystal phase. Below the melting point, the liquid is still an equilibrium state, but becomes metastable with respect to the crystal. If we cool fast enough [226], the system doesn't have time to nucleate crystals and remains in the liquid phase, exhibiting no order in its structure. A liquid below its melting temperature is called *supercooled*. Further lowering the temperature (with a non-linear cooling rate that allows the liquid to relax, but avoiding the nucleation of crystals), we encounter a sharp increase in the relaxation time of the supercooled liquid. This can be truly dramatic, spanning up to 14 orders of magnitude, until on any reasonable experimental time-scale the supercooled liquid cannot relax anymore. When the super liquid falls out of equilibrium it becomes a *glass*. The glass transition is conventionally defined as the temperature at which the relaxation time reaches 100 seconds. Whether there is a true thermodynamic phase transition at some lower temperature at which the relaxation time diverges is still an open question [7].

Because a glass is a supercooled liquid that has fallen out of equilibrium, it doesn't exhibit any long-range order. Unlike a liquid, nevertheless, it does not flow on any reasonable timescale, and its mechanical properties resemble those of a solid. This dramatic shift in physical properties from a liquid to a glass, upon minimal structural changes, is also still a puzzle.

Right before the glass transition, the dynamical correlation function of the system develops a characteristic plateau [227]. The relaxation of any particle occurs in two steps: at short times it vibrates inside a "cage" formed by its neighbors, and after some time it manages to escape and diffuses freely. We can then interpret the sharp increase in relaxation time as an indication that escaping the cage becomes increasingly difficult when lowering the temperature. Relaxation actually actually occurs through collective events: after vibrating around fixed position for some time, many particles suddenly rearrange into a new configuration. This can take a long time, either because they have to find a rare path from one favorable configuration to another, or because they have to climb an energy barrier to rearrange.

Because many degrees of freedom are strongly correlated in glasses, it is sometimes useful to think of the system in its (high-dimensional) configuration space. The dynamics of our many-body system can then be seen as the evolution of a single particle in a complex and high-dimensional landscape. This allows for example to better visualize the collective rearrangement events as barrier-crossings (or valley explorations) in a high-dimensional space.

Once the supercooled liquid falls out of equilibrium, it performs aging: physical properties, such as the susceptibility, explicitly depend on the time elapsed since the quench [228, 229].

Spin-glasses

Spin glasses are magnetic alloys in which the random position of impurities generates interactions between spins that have random sign and intensity [230]. This randomness gives rise to *frustration*. In a ferromagnet there are two states (the ground states) in which all interaction energies are minimized. In a spin-glass, instead, no such configurations exist: some of the spins will always be "unhappy" (see Figure 5.5a). This leads to a complex free-energy landscape, with many minima and saddles. Below a critical temperature, spin-glasses fail to equilibrate, and exhibit extremely slow relaxation. This can be experimentally verified by studying the decay of magnetization after a field change [231–233]. The system is quenched from a temperature

above the critical point to one below it, in the presence of a small field. After a time t_w from the quench, the field is switched off. The magnetization exhibits a two-step relaxation. The second decay strongly depends on the waiting time: different curves approximately collapse if plotted as a function of t/t_w. More complex temperature protocols reveal other interesting effects, such as rejuvenation and memory, which offer additional insights in the hierarchical organization of the free-energy landscape [234, 235].

A number of models have been developed to understand the behavior of spin-glasses. They generally include random interactions between pairs, or groups, of spins. Spins can be of Ising type or continuous. The most realistic models embed the spins in a finite-dimensional space, and only allow for short-range interactions. However, important insights can be gained by studying fully-connected models, in which all spins interact with each other. These simplified models still exhibit a very rich phenomenology, and they enable analytical solutions via the replica and cavity methods. One of their main drawbacks is that they cannot describe barrier-crossings, because in a fully-connected system energy barriers are extensive, and therefore in the thermodynamic limit their crossing rate goes to zero.

Coarsening after a phase transition

Another case in which aging is observed, somewhat simpler than the previous ones, is when a system undergoes a second-order phase transition from a disordered phase to one in which some symmetry is spontaneously broken [139, 236]. Let us consider for example a 3-dimensional ferromagnetic Ising system that is quenched from a very high temperature to a temperature below the critical point. Immediately, the system starts to evolve towards the equilibrium configuration, in which it will exhibit a macroscopic magnetization of a randomly chosen sign. Because in the initial condition the magnetization is zero, both positive and negative domains will form and coarsen. Their growth is due to the surface tension of the interface between domains with opposite magnetization, which generates effective forces that are proportional to the curvature of the interface. As time progresses, domains grow increasingly larger, and the associated forces become weaker: the system undergoes aging. If the system is infinite, it never manages to choose between positive and negative magnetization, and is forever divided in ever-growing opposite domains. In contrast, in a finite system, once the typical size of the domains becomes larger than the system size, one of the two magnetizations will be selected.

Beyond physical systems

Aging is not limited to classical physical systems. Optimization or constraint satisfaction problems can be solved by defining a "cost" function, and searching for its minima. This is equivalent to looking for the ground state of and energy landscape, and indeed many algorithms implement dynamics inspired by physical ones [237]. These problems can undergo a transition from an "easy" to a "hard" phase, in which the solution cannot be found in polynomial time. This computational hardness is related to the slow relaxation in glassy systems [238]. The minimization of a very complex and high dimensional loss function is also at the basis of many machine learning algorithms [239–243]. A better understanding of aging phenomena could thus have numerous concrete applications in computational problems and machine learning.

Physical aging also arises in biological systems. Dramatic slowdowns of the dynamics are observed experimentally in motile cells tissues [244–246], and in models and numerical simulations of dense active particles [246–250]. As we described in Part I, aging is also found in diverse ecological systems [7, 12, 133, 142, 251], and it arises in models of neural networks [252–257] and of cell's metabolic and genetic networks [258]. Note that the dynamics of these systems is not necessarily reversible. We will later come back to the question of how to interpret aging in the

absence of an energy landscape.

5.2.2 Self-generated disorder and mode coupling theory

Spin-glasses and structural glasses have many intriguing similarities: they become very "stiff" despite exhibiting no long-range order, and they undergo slow relaxation and aging. An important difference is that, unlike structural glasses, spin-glasses are described by Hamiltonians with *quenched* disorder. Nevertheless, in structural glasses, because of the lack of order in the configuration, each particle sees a different – and in some measure random – potential, so that the disorder is in some sense self-generated by the system. A formal link between the two is provided by Mode Coupling Theory (MCT). MCT was developed as an approximate quantitative description of supercooled liquids. It provides some self-consistent equations on the dynamical correlation functions of the density fluctuations of the supercooled liquid. These were found to be formally equivalent to those obtained in a class of mean-field spin-glass models, the *p-spin* [259] (see Section 7.3).

5.2.3 Energy barriers and flat directions

The slowdown of relaxation can be due to two different mechanisms: either the system has to overcome growing (free) energy barriers, or it becomes progressively harder to find decreasing directions in the energy landscape, because they are increasingly rare and flat [138]. Both mechanisms could be at play in finite dimensional systems.

Let us consider a particle undergoing Langevin dynamics at finite temperature in a complex energy landscape. If the landscape has many local minima, the particle could end up trapped in one of them for some time. To escape, it would then have to wait for a random fluctuation of the thermal noise to push it outside of the basin of attraction of the local minima. Such a process is called *thermal activation* and at low temperature it has an exponentially small rate given by Arrhenius law:

$$W \propto e^{\Delta E/T} \ . \tag{5.9}$$

ΔE is the *energy barrier* that the particle has to overcome, i.e. the difference between the energy at the minimum and the energy at the closest saddle point. If descending the landscape the particle encounters deeper and deeper minima, and has to climb higher and higher energy barriers, this can lead to a slowdown of its dynamics: the system undergoes aging.

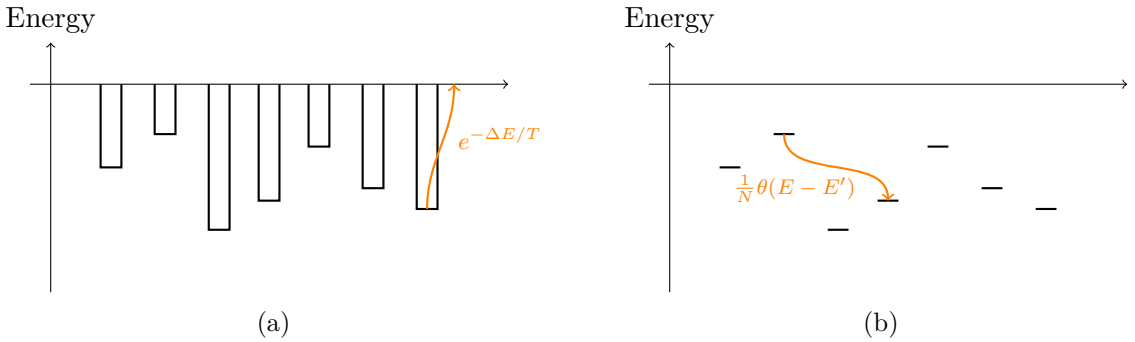

Figure 5.1: Sketches of the energy landscape and transition rates in Bouchaud's trap model (a) and in the case considered by Barrat and Mézard in [260] (b).

This effect can be studied in the simplified setting of Bouchaud's trap model [222, 261]. Let us consider a particle moving in a landscape full of "traps", i.e. of low-laying local equilibria

from which the particle can only escape by thermal activation (see the sketch in Figure 5.1a). Each trap has a random energy depth ΔE extracted from a distribution $\rho(\Delta E)$; the escape rate from the trap is proportional to $e^{-\Delta E/T}$. Once the particle escapes the trap, it immediately falls into another one, with energy depth $\Delta E'$ extracted again from ρ. If the energies are exponentially distributed, there is a sharp phase transition: at high temperature the system equilibrates, whereas at low temperature it undergoes aging. In the low temperature phase, the particle explores increasingly deep traps, leading to a slowdown of the dynamics as the escape rate continuously decreases.

Aging can nevertheless also occur in systems that have no energy barriers at all [138,260,262]. In [260], Barrat and Mézard consider again a model with random energy levels, but with a different dynamics (see the sketch in Figure 5.1b). The particle can hop from energy E to any lower energy $E' < E$ with rate proportional to $1/N$, where N is the total number of states. This corresponds to the zero temperature limit of the Glauber dynamics, which does (at finite temperature) satisfy detailed balance with respect to the Boltzmann distribution. As times goes on, the dynamics slows down because there are fewer and fewer states the particle can jump to. When N goes to infinity, the particle never reaches the ground state: there are always moves that allow it to decrease the energy, but the probability rate of finding one goes to zero.

In mean-field spin-glass models, the energy barriers are extensive, so that the escape rate from a minimum vanishes in the thermodynamic limit. These systems therefore fall in the second scenario: they are "trapped" by saddle points with fewer and fewer decreasing directions [160]. In this models, an additional ingredient comes into play: these rare directions through which the system can decrease the energy become increasingly flat. This can be seen from the Hessian of the energy around the saddle points, whose eigenvalues approach zero at long times. We will call these states (and by extension, also the systems) *marginal*. In finite dimensional systems, energy barriers are instead sub-extensive, and activated jumps play an important role. This is believed to be the source of some of the discrepancies between mean-field and finite dimensional models, and between mode coupling theory and supercooled liquids.

5.2.4 The spherical Sherrington-Kirkpatrick model

Some further understanding of the aging phenomenon can be gained by studying simple exactly solvable models, such as the spherical Sherrington-Kirkpatrick model [263–268]. It consists of a fully-connected network of continuous spins, interacting through two-body random interactions. Despite having a relatively simple landscape with only two minima, it displays interesting dynamical phenomena such as aging and weak-ergodicity breaking [160]. Since this model will be central in the next chapter, we here present it in some detail.

The model

The spherical Sherrington-Kirkpatrick spin-glass model is composed of N continuous spins with random all-to-all symmetric interactions and a spherical constraint, imposing $\sum_{i=1}^{N} s_i^2 = N$. The dynamics of the system is defined by the Langevin equation:

$$\dot{s}_i = \sum_{j=1}^{N} J_{ij} s_j - \ell s_i + \eta_i + h_i \ , \tag{5.10}$$

in which s_i is the state of the spin $i = 1, \dots, N$. The quenched interaction matrix J_{ij} is symmetrical; the elements of J_{ij} are drawn from a Gaussian distribution with zero mean. Their variance is assumed to scale with the inverse of the number of spins N, so that in the thermodynamic limit $N \to \infty$ the interaction term remains of order 1 and the energy (Eq. (5.11)) is extensive.

By appropriately rescaling all terms, we can ensure that the variance of J_{ij} is $1/N$; thus in the following we will assume this holds without loss of generality. Each spin is also subject to a thermal Gaussian white noise η_i with covariance $\langle \eta_i(t)\eta_j(t')\rangle = 2T\delta_{ij}\delta(t-t')$, where T denotes the temperature. h_i is an external field that will be taken to zero at the end of the computation. Finally, ℓ is a Lagrange multiplier used to enforce the spherical constraint.

Energy landscape and stationary points

Equation (5.10) can be shown to describe the thermal dynamics at temperature T of the system in the energy landscape

$$E = -\frac{1}{2}\sum_{ij} J_{ij}s_i s_j + \frac{\ell}{2}\sum_i s_i^2 \ . \tag{5.11}$$

The stationary points of this potential solve the eigenvalue equation

$$\sum_j J_{ij}s_j = \ell s_i \ . \tag{5.12}$$

The stationary points are therefore the eigenvectors of J, that we denote as $\vec{v}_\mu$. At zero temperature the Lagrange multiplier at the fixed point has to be equal to the corresponding eigenvalue μ. J belongs to the Gaussian Orthogonal Ensemble (GOE), and in the thermodynamic limit $N \to \infty$ its spectrum is given by the Wigner semicircle with support in $[-2, 2]$ [269]:

$$\rho(\mu) = \frac{1}{2\pi}\sqrt{4-\mu^2} \qquad \text{for } \mu \in [-2,2] \ . \tag{5.13}$$

We can use the basis that diagonalizes J to write the energy:

$$E = -\frac{1}{2}\sum_\mu (\mu - \ell)s_\mu^2 \tag{5.14}$$

and the Langevin dynamics:

$$\dot{s}_\mu = (\mu - \ell)s_\mu + \eta_\mu + h_\mu \ . \tag{5.15}$$

s_μ is the projection of the system on the eigenvector $\vec{v}_\mu$. Note that in this basis the different modes are only coupled through the Lagrange multiplier. The statistics of the noise is unchanged. Eq. (5.14) tells us that in a stationary state the Lagrange multiplier must be larger than the maximum eigenvalue of J, $\ell \geq \mu_{max} = 2$, otherwise the system would not be bounded.

We can study the stability of the fixed point $\vec{v}_\mu$ to a perturbation in the direction $\vec{v}_{\mu'}$ by looking at the Hessian of the energy:

$$H_{\mu,\mu'} = -\mu' + \ell = -\mu' + \mu \ . \tag{5.16}$$

If μ is the largest eigenvalue of J, $\vec{s} = \pm N\vec{v}_\mu$ are minima of the potential. All other fixed points have at least one unstable direction (one for each mode with a larger eigenvalue), and are therefore saddle points (except for the two fixed points corresponding to the lowest eigenvalue, which are maxima). In the thermodynamic limit, the gap between the first and successive eigenvalues goes to zero as an inverse power of N. The ground state becomes therefore marginally stable.

The energy landscape is thus relatively simple: it exhibits only two minima, related by inversion symmetry. For this reason the spherical SK model has been called a "ferromagnet in disguise" [267].

Dynamical Mean Field Theory

In the thermodynamic limit $N \to \infty$, the dynamics of the system can be analyzed by Dynamical Mean-Field Theory (DMFT) [13,157–159], which has already been presented in Chapter 3. The derivation by the cavity method is standard and analogous the one outlined in Section 3.2, but we sketch it here for the convenience of the reader.

Given the noise realizations $\eta_i(t)$, Eq. (5.10) deterministically defines the trajectories $s_i(t)$ for the N spins, indexed from 1 to N. Let us now imagine adding a new spin, with index 0, and drawing its initial conditions and interactions independently from the rest of the system. Since the interactions with each of the other components are of order $1/\sqrt{N}$, its introduction can be considered a small perturbation, and we can compute the linear response of each of the trajectories to it, $\delta s_i(t)$:

$$\delta s_i(t) = \sum_j \int_0^t dt' R_{ij}(t,t') J_{j0} s_0(t') \ , \tag{5.17}$$

where $R_{ij}(t,t') = \frac{\delta s_i(t)}{\delta h_j(t')}$ is the response of spin i to a perturbation applied on spin j.

The dynamics of s_0 will depend on the new trajectories of all other spins:

$$\dot{s}_0 = \sum_{j=1}^{N} J_{0j}(s_j + \delta s_j) - \ell s_0 + \eta_0 + h_0 \ . \tag{5.18}$$

We now want to describe the statistic of the interaction term $\sum_{j=1}^N J_{0j}(s_j + \delta s_j)$ in the limit $N \to \infty$. Because it is the sum of many weakly correlated terms, we expect it to be Gaussian, so that we only need to compute its first two moments. The unperturbed trajectories contribute a colored noise $\sum_j J_{0j} s_j \sim \xi$. Since the s_j are by definition uncorrelated from the interactions with spins 0, we can easily compute the statistics of ξ:

$$\langle \xi(t) \rangle = 0 \ , \tag{5.19}$$

$$\langle \xi(t)\xi(t') \rangle = N\overline{J_{0j}^2}\, \mathbb{E}\left[s_j(t) s_j(t') \right] = C(t,t') \ . \tag{5.20}$$

$C(t,t')$ is the autocorrelation function of the system.

The perturbations of the trajectories are instead correlated with the interactions with spin 0. We can use their explicit expression from Eq. (5.17):

$$\begin{aligned} \sum_i J_{0i}\delta s_i = \sum_i J_{0i} \sum_j J_{j0} \int_0^t dt' R_{ij}(t,t') s_0(t') \sim \\ \sim \int_0^t dt' \overline{R_{jj}(t,t')} s_0(t') = \int_0^t dt' R(t,t') s_0(t') \ . \end{aligned} \tag{5.21}$$

We have used the Central Limit Theorem to claim that the sums over spins concentrate around their averages, and used the fact that $\overline{J_{0i}J_{j0}} = \frac{1}{N}\delta_{ij}$, where the overline indicates an average over spins. $R(t,t')$ is the average response function of a spin to a perturbation of its own dynamics. It is possible to show that the off-diagonal terms give subleading contributions [66].

Substituting the results in the dynamics for s_0 we obtain:

$$\dot{s}_0 = -\ell s_0 + \eta_0 + h_0 + \xi + \int_0^t dt' R(t,t') s_0(t') \ . \tag{5.22}$$

It is now crucial to note that spin 0 is statistically identical to all others, and that when N is large the systems composed of N or $N+1$ spins are equivalent. Therefore the response and

correlation functions that define the effective dynamics of spin 0 can be computed as averages over the effective single spin dynamics:

$$C(t,t') = \langle s(t)s(t')\rangle, \qquad R(t,t') = \frac{\partial\langle s(t)\rangle}{\partial h(t')} \ . \tag{5.23}$$

The resulting equations do not depend on the index, so we have dropped the index 0 here and in the following. The angular brackets indicate an average over η, ξ and the initial conditions of the effective process. Because the effective process depends on the average response and correlation functions through the statistics of ξ and the last term of equation (5.22), C and R must be computed self-consistently: the correlation and response functions measured on the effective process must match the ones used to define the process itself. This procedure can be shown to be exact in the thermodynamic limit $N \to \infty$ [167].

Spin-glass phase transition

At sufficiently high temperature, the system reaches a time translational invariant state, in which two times observables only depend on the difference between the two times, and the Lagrange multiplier ℓ is constant. In this regime, the DMFT equations greatly simplify in Fourier transform:

$$(-i\omega + \ell - R(\omega))s(\omega) = \xi(\omega) + \eta(\omega) + h(\omega) \ . \tag{5.24}$$

Differentiating both sides with respect to $h(\omega)$ we obtain:

$$(-i\omega + \ell - R(\omega))R(\omega) = 1 \ . \tag{5.25}$$

We can solve this equation as a function of the still unknown Lagrange multiplier ℓ:

$$R(\omega) = \frac{\ell - i\omega - \sqrt{(\ell - i\omega)^2 - 4}}{2} \ . \tag{5.26}$$

We have excluded one of the two solutions, because the response function has to decay to 0 for $\omega \to \infty$. Since the problem is linear, $s(\omega) = R(\omega)(\xi(\omega) + \eta(\omega))$. This allows us to compute the correlation functions:

$$\begin{aligned} \delta(\omega+\omega')C(\omega) = \langle s(\omega)s(\omega')\rangle = R(\omega)\langle(\xi(\omega)+\eta(\omega))(\xi(\omega')+\eta(\omega'))\rangle R(\omega') = \\ = \delta(\omega+\omega')|R(\omega)|^2(C(\omega)+2T) \ . \end{aligned} \tag{5.27}$$

We can solve this self-consistent equation on C:

$$C(\omega) = \frac{2T}{|R(\omega)|^{-2} - 1} \ . \tag{5.28}$$

The spherical constraint imposes that

$$C(t=0) = \frac{1}{2\pi}\int d\omega C(\omega) = 1 \ . \tag{5.29}$$

This equation determines the Lagrange multiplier ℓ, on which C depends through R. In practice, it is easier to fix a given value of ℓ and find which temperature it corresponds to, through the relation

$$T^{-1} = \frac{1}{2\pi}\int d\omega \frac{2}{|R_\ell(\omega)|^{-2} - 1} \ , \tag{5.30}$$

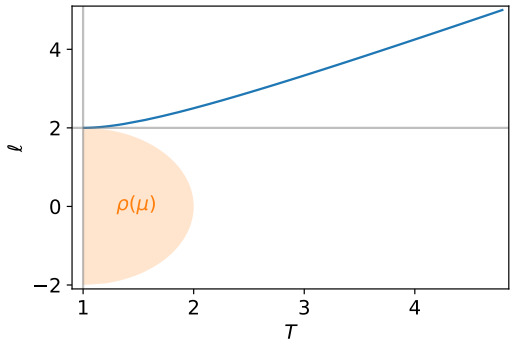

Figure 5.2: Lagrange multiplier ℓ a a function of temperature T. The shaded region sketches (not in scale) the eigenvalues density of J, from Eq. (5.13). When $T \to 1$, ℓ touches the edge of the spectrum.

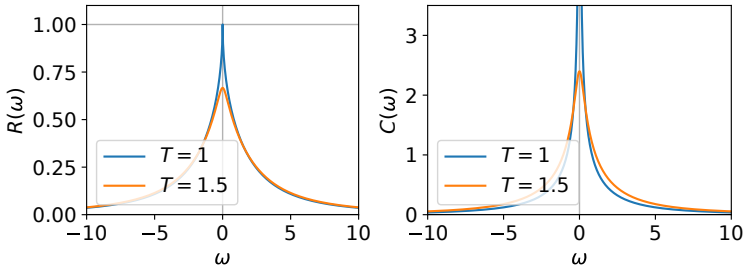

Figure 5.3: Response (left) and correlation (right) functions in the time-translational invariant phase ($T = 1.5$) and at the critical point ($T = 1$).

where $R_\ell(\omega)$ is the response function for a fixed value of ℓ. As we noted in the previous section, at stationarity the Lagrange multiplier must be larger or equal than 2. Solving numerically the self-consistent equations at high temperature, we find that ℓ monotonously decreases when decreasing T (Fig. 5.2).

Both response and correlation functions are peaked in $\omega = 0$ (Figure 5.3). If the system undergoes a phase transition, we expect these peaks to become singularities. From equation (5.28), we see that C has a divergence if $|R(\omega)| = 1$. The largest value of ℓ for which this occurs is $\ell = 2$, leading to:

$$R(\omega) = 1 - i\omega - \sqrt{i\omega - \omega^2}\ . \tag{5.31}$$

For this value of ℓ, $R(\omega)$ is non analytic in $\omega = 0$, since $R(\omega) - 1 \sim \sqrt{\omega}$. This results in an integrable divergence of $C \sim \omega^{-1/2}$. If this was not the case, the integral on the right side of Eq. (5.30) would diverge for $\ell \to 2$, meaning that the critical point could only be reached for $T \to 0$. The matching of the singularities of R and C allows instead a finite temperature critical point for $T_c = 1$.

It is not a coincidence that at the critical point the Lagrange multiplier touches the edge of the spectrum of J: this signals the fact that the mode corresponding to the leading eigenvector of J is not damped anymore, and indeed below the transition it will acquire (asymptotically, see later) a macroscopic weight.

In the time domain, one finds a relaxation time to equilibrium that diverges as $1/\sqrt{T - T_c}$ and critical relaxation at T_c, corresponding to a behavior $C(t) \sim 1/t^{1/2}$.

Aging

Since the relaxation time diverges at T_c, the dynamics after quenches below T_c are not expected to relax to a steady state. As we show below, indeed they do not — instead aging ensues (on timescales that do not diverge with N). To study the aging regime we follow Ref. [265] and consider again the dynamics in the basis that diagonalizes the interaction matrix J, Eq. (5.15):

$$\dot{s}_\mu = (\mu - \ell) s_\mu + \eta_\mu + h_\mu \ . \tag{5.32}$$

The different modes are now coupled only through the Lagrange multipliers, which will now be time-dependent, since the system is not time-translationally invariant anymore. We can formally write the solution in terms of the realization of the noise $\xi_\mu(t)$ and the (unknown) time evolution of the Lagrange multipliers:

$$s_\mu(t) = e^{\mu t - \int_0^t \ell(t')dt'} s_\mu(0) + \int_0^t dt' e^{\mu(t-t') - \int_{t'}^t \ell(t'')dt''} \xi_\mu(t') \ . \tag{5.33}$$

We consider a quench from infinite temperature, corresponding to uniform initial conditions on the sphere, to $T < T_c$. In order to find an equation for $\ell(t)$, we compute the sum of the squares of the spins:

$$\begin{aligned} \left\langle \sum_\mu (s_\mu(t))^2 \right\rangle &= \sum_\mu e^{2\mu t - 2\int_0^t \ell(t')dt'} \langle s_\mu^2(0) \rangle + 2T \sum_\mu \int_0^t dt' e^{2\mu(t-t') - 2\int_{t'}^t \ell(\tau)d\tau} = \\ &= \frac{N}{2} \int d\mu \rho(\mu) e^{2\mu t - 2\int_0^t \ell(t')dt'} + 2TN \int d\mu \rho(\mu) \int_0^t dt' e^{2\mu(t-t') - 2\int_{t'}^t \ell(\tau)d\tau} \ . \end{aligned} \tag{5.34}$$

We have neglected all terms that do not contribute when averaging over the initial conditions or the noise, and used $\langle s_\mu^2(0) \rangle = 1$. $\rho(\mu)$ is the eigenvalue density of J, the Wigner semicircle of Eq. (5.13). Imposing that the constrain is satisfied at all times we obtain:

$$\int d\mu \rho(\mu) e^{2\mu t - 2\int_0^t \ell(t')dt'} + 2T \int d\mu \rho(\mu) \int_0^t dt' e^{2\mu(t-t') - 2\int_{t'}^t \ell(\tau)d\tau} = 1 \ . \tag{5.35}$$

This determines the value of ℓ at all times, and hence the solution for $s_\mu(t)$ is fully specified. We can now compute the correlation function:

$$\begin{aligned} C(t,t') = \left\langle \sum_\mu \mathbf{s}_\mu(t) \mathbf{s}_\mu(t')^T \right\rangle &= \int d\mu \rho(\mu) e^{\mu(t+t') - \int_0^t \ell(\tau)d\tau - \int_0^{t'} \ell(\tau')d\tau'} + \\ &+ \int d\mu \rho(\mu) \int_0^t dz \int_0^{t'} dz' e^{\mu(t-z+t'-z') - \int_z^t \ell(\tau)d\tau - \int_{z'}^{t'} \ell(\tau')d\tau'} \ . \end{aligned} \tag{5.36}$$

An asymptotic solution is available when t, t' and $\Delta t = t - t' \gg 1$ [265]:

$$C(t' + \Delta t, t') = q_{EA} \left(\frac{2\sqrt{1 + \Delta t/t'}}{2 + \Delta t/t'} \right)^{\frac{3}{2}} \ . \tag{5.37}$$

q_{EA} is a temperature-dependent constant, called the Edwards-Anderson order parameter (see below). This correlation function, plotted in Fig. 5.4, only depends on time through the ratio $\Delta t/t'$, and hence it is translationally invariant in log-time.

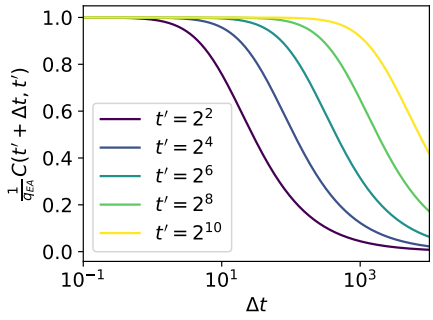

Figure 5.4: Asymptotic solution for the correlation function of the spherical Sherrington-Kirkpatrick model at long times in the aging regime.

Asymptotic behavior

When $t \to \infty$ at fixed but large N, the system equilibrates to one of the two states (related by inversion symmetry) with a macroscopic overlap with the leading eigenvector of J, denoted as v_{μ_0} (in replica language, this reflects a simple replica symmetric spin-glass phase) [265, 267]. On time-scales exponentially large in $N^{1/3}$ [270, 271] the system switches from one state to the other by activated barrier hopping. The equilibrium value of the overlap of the system with the leading eigenvector is the Edwards-Anderson order parameter q_{EA} that appears in the asymptotic correlation function of Eq. (5.37). It depends linearly on temperature, as

$$q_{EA} = 1 - \frac{T}{T_c} \,. \tag{5.38}$$

At $T = 0$ it is equal to 1, indicating that the system perfectly aligns with the leading eigenvector of J, whereas it tends to 0 at the transition.

5.3 Non reciprocity

Newton's third law, also known as *action-reaction* principle, states that the forces that two bodies apply on each other must have same intensity but opposite signs [272]. This constraint comes from the fact that these forces are assumed to derive from a common potential energy, and implies that momentum is conserved in the system. As we explained in the introduction, this principle can be violated when we give coarse-grained descriptions of a system: integrating out some degrees of freedom can lead to an apparent non-conservation of the momentum. Consider for example two bacteria that swim in a medium and regulate each other's motility by releasing and sensing chemicals. Their interactions can be described as effective forces, but, since they exchange momentum with the medium, these forces will generically violate the action-reaction principle [273, 274]. This is even more evident in systems where the connection to physical dynamics is less direct, as in the case of neural networks, ecosystems, opinion dynamics or economic models. In all these cases, effective forces will generically violate the action-reaction principle, exhibiting what we will call non-symmetric or *non-reciprocal* interactions. Non-reciprocal interactions also arise in open quantum systems, where they are referred to as *non-hermitian* [275–277].

Non-reciprocal interactions generate a variety of fascinating phenomena that would be forbidden at equilibrium, such as persistent oscillatory or chaotic states in dissipative systems [13, 252, 257, 273, 278–292], "non-reciprocal phase transitions" with distinctive signatures [291–301],

odd elasticity and odd viscosity [302, 303], and long-range order in 2-dimensional systems with continuous symmetries [284].

These phenomena have been studied at length in the case in which the units interacting non-reciprocally are "simple", meaning that they do not have a complex internal dynamics. In the following we will be interested instead in the non-reciprocal coupling of *complex* agents. Examples include neural networks with incompatible goals, or bipartite networks of predators and preys.

5.3.1 Frustration

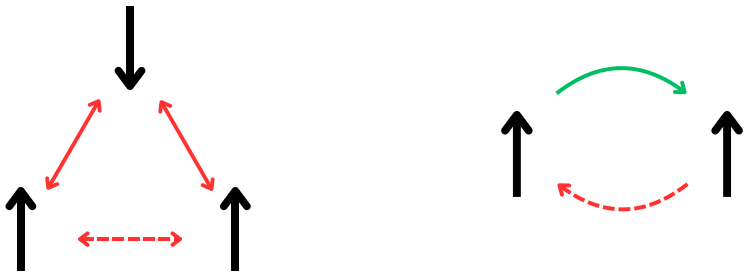

(a) Geometric frustration (b) Non-reciprocal frustration

Figure 5.5: Sketch of two spin systems with (a) geometric and (b) non-reciprocal frustration. Double-headed arrows indicate reciprocal interactions, single-headed ones one-way interactions. Red indicates anti-aligning interactions, green aligning ones. Unsatisfied interactions are dashed.

Non-reciprocal interactions often derive from agents having incompatible objectives. Let us consider two soft spins s^a, labeled by $a = 1, 2$. s^1 wants to align with s^2, whereas s^2 wants to antialign with s^1 (see the sketch in Figure 5.5b). We can model such a system through the following coupled differential equations:

$$\begin{cases} \dot{s}^1 = -\nabla V(s^1) + \alpha s^2 \\ \dot{s}^2 = -\nabla V(s^2) - \alpha s^1 \end{cases} \tag{5.39}$$

V is a double well single spin potential, α is the strength of the non-reciprocal coupling. It is not possible to write these evolution equations as a gradient descent in a common energy landscape. However, it is possible to define a "selfish energy" for each of the two spins individually [291]:

$$E_1(s^1, s^2) = V(s^1) - \alpha s^1 s^2 \tag{5.40}$$

$$E_2(s^1, s^2) = V(s^2) + \alpha s^1 s^2 \tag{5.41}$$

so that the dynamics of each spin can be written as a gradient descent in its own selfish energy. The fact that it is not possible to define an energy for the entire system is an illustration of the incompatibility of the goals of the two spins. This is sometimes referred to as *frustration*. In this context this has a different meaning than in the case of spin-glasses, to avoid confusion we will call them non-reciprocal frustration and geometrical frustration [293] (see Figure 5.5). Non-reciprocal frustration derives from two agents having incompatible goals: there is no configuration that satisfies both of them. To have geometrical frustration we need to have at least three spins. Each interaction link can be satisfied individually (and we can write a global energy), but it is not possible to satisfy all of them at the same time. There is nevertheless a deep analogy between the two kinds of frustration, since both give rise to marginal and degenerated

states: in Figure 5.5a flipping one of the bottom spins leads to a state with the same energy; an "equivalent" state (we cannot define an energy) can be found by flipping any of the two spins in 5.5b. These degeneracies can be lifted by noise, generating in both cases an order-by-disorder phenomenon [293].

5.3.2 Two simple agents

We will now review what happens when non-reciprocally coupling two *simple* agents. We will consider systems with a spherical constraint, since this will be relevant for the next chapter.

Two 2-dimensional systems

Let us consider two XY spins, i.e. two-dimensional unit vectors, with components s_i^a, where a indexes the spin and i the component. The two spins are coupled non-reciprocally and antagonistically: spin 1 wants to align with spin 2 with coupling strength $\alpha_1 > 0$, whereas spin 2 wants to anti-align with spin 1 with coupling strength $\alpha_2 > 0$. This setting is described by the following dynamical equation:

$$\begin{cases} \dot{s}_i^1 = -\ell^1 s_i^1 + \eta_i^1 + \alpha_1 s_i^2 \\ \dot{s}_i^2 = -\ell^2 s_i^2 + \eta_i^2 - \alpha_2 s_i^1 \end{cases} \tag{5.42}$$

The spherical constraints, enforced by the Lagrange multipliers ℓ^a, are independently imposed on the two spins, $(s_1^a)^2 + (s_2^a)^2 = 1$. η_i^a is a thermal noise of temperature T.

If the interactions are anti-symmetric, $\alpha_1 = \alpha_2 = \alpha$, at zero temperature the two spins rotate indefinitely at constant angular velocity, with direction of motion and angular separation completely determined by initial conditions. We can express the positions in polar coordinates

$$\vec{s^a} = \begin{pmatrix} s_1^a \\ \\ s_2^a \end{pmatrix} = \begin{pmatrix} \sin\phi_a \\ \\ \cos\phi_a \end{pmatrix} . \tag{5.43}$$

Projecting the dynamics on the direction orthogonal to each vector, we find that the polar angles ϕ_a satisfy

$$\dot{\phi}_a = -(-\ell^a s_1^a + \epsilon_{ab}\alpha s_1^b)s_2^a + (-\ell^a s_2^a + \epsilon_{ab}\alpha s_2^b)s_1^a \ , \tag{5.44}$$

where $\epsilon = \begin{pmatrix} 0 & 1 \\ \\ -1 & 0 \end{pmatrix}$ is the fully anti-symmetric Levi-Civita symbol. Expressing the components in polar coordinates we obtain:

$$\dot{\phi}_1 = \dot{\phi}_2 = -\alpha \sin(\phi_1 - \phi_2) \ . \tag{5.45}$$

The two spins rotate at the same constant velocity $\alpha \sin(\phi_1 - \phi_2)$, which is maximum and equal to α if they have a phase separation of $\pi/2$. The velocity is 0 if the two spins are perfectly aligned or antialigned. Since the angular velocity only depends on the angular separation between the two spins, which does not change during the dynamics, it is solely determined by initial conditions.

This zero temperature chiral phase is only possible if the coupling is exactly anti-symmetrical: otherwise the two spins would have different angular velocities, and they would reach either the aligned (if $\alpha_1 > \alpha_2$) or antialigned (if $\alpha_1 < \alpha_2$) fixed points. In the following we will always consider anti-symmetrical coupling unless specified.

At any finite temperature, the fluctuations can stochastically exchange the positions of the two spins, leading to a change in the direction of rotation. This means that the system is not chiral if we observe it on a long enough timescale.

Two N-dimensional systems

We can also consider two non-reciprocally coupled spherical many-body systems, still with no random interactions between components, described by Eq. (5.42), where now i runs from 1 to N, and $\alpha_1 = \alpha_2 = \alpha$. At $T = 0$, the two systems rotate indefinitely in the plane spanned by the two initial conditions. If the initial conditions are randomly and independently sampled on the sphere, they will in general be orthogonal when $N \to \infty$, and the angular velocity will be equal to α.

At finite temperature the directions of oscillation will diffuse freely, so that the correlation function will only exhibit damped oscillations. After a short transient, we expect the system to reach a stationary state. The Lagrange multipliers correspond to the force that the constraints need to apply on the systems in order to keep them on the sphere. Because of the symmetry of the model under the transformation $(s_1, s_2) \to (-s_2, s_1)$ (and under inversion) the two systems are completely equivalent. Whenever this equivalence is not broken, the force on the constraint is the same in the two systems, and therefore the two Lagrange multipliers are equal, $\ell^1 = \ell^2 = \ell$. We expect this to be true as long as an extensive number of modes contribute to the dynamics, allowing us to interpret the sum of the force over modes as an average.

Collecting the i-th component of each system in the two-dimensional vectors $\mathbf{s}_i$, we can formally solve Eq. (5.42) as a function of the unknown Lagrange multiplier ℓ:

$$\mathbf{s}_i(t) = e^{-\ell t}\mathcal{R}_{\alpha t}\mathbf{s}_i(0) + \int_0^t dt' e^{-\ell(t-t')}\mathcal{R}_{\alpha(t-t')}\eta_i(t') \ . \tag{5.46}$$

We have introduced the rotation matrix

$$\mathcal{R}_{\alpha t} = e^{\alpha \epsilon t} = \begin{pmatrix} \cos\alpha t & \sin\alpha t \\ -\sin\alpha t & \cos\alpha t \end{pmatrix} \ , \tag{5.47}$$

and η_i is a two-dimensional vector containing the noises on components i of the two systems. We will see that at finite temperature $\ell > 0$, so that at stationarity we can neglect the first term. We can impose the spherical constraint to determine the Lagrange multiplier:

$$\begin{aligned} N &= \sum_i \langle (s_i^1)^2 \rangle = \sum_i \langle \left(\int_0^t dt' e^{-\ell(t-t')} \left(\cos\alpha(t-t')\eta_i^1(t') + \sin\alpha(t-t')\eta_i^2(t') \right) \right)^2 \rangle = \\ &= 2TN \int_0^t dt' e^{-2\ell(t-t')} \left(\cos^2\alpha(t-t') + \sin^2\alpha(t-t') \right) = \frac{2TN}{2\ell} \left(1 - e^{-2\ell t} \right) \to \frac{TN}{\ell} \ . \end{aligned} \tag{5.48}$$

We thus obtain $\ell = T$, so that now Eq. (5.46) fully determines $\mathbf{s}_i(t)$. We can use it to compute the 2×2 matrix of the correlation functions $C_{ab} = \frac{1}{N}\sum_i \langle s_i^a(t) s_i^b(t') \rangle$. With a computation analogous to the one just done we obtain:

$$C(t, t') = e^{-\ell(t-t')}\mathcal{R}_{\alpha(t-t')} \ . \tag{5.49}$$

This tells us that the systems exhibit exponentially damped oscillations.

In Chapter 6, our goal will be to study what happens when the two non-reciprocally coupled agents have a complex internal dynamics.

5.3.3 Non-reciprocal phase transitions

In other systems composed of *many* non-reciprocally coupled simple agents, many-body effects can lead to a stabilization of the chiral phase in the presence of noise, and to an increased

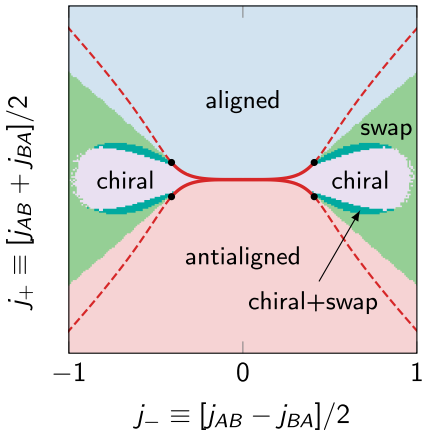

Figure 5.6: Phase diagram for the non reciprocal flocking model of [292] at low temperature, reproduced from the same reference. j_+ and j_- indicate the symmetric and anti-symmetric components of the interactions. The red lines correspond to lines of exceptional points.

robustness with respect to non perfect anti-symmetry of the interactions [279, 280, 291, 292, 304, 305]. Let us consider $2N$ XY spins, evenly divided in two species, in the thermodynamic limit $N \to \infty$. Spins of the same species tend to align, whereas we have non-reciprocal interactions between spins of different species. Varying the strength of the symmetric and anti-symmetric components of the interactions, the system undergoes a finite-temperature phase transition between a static aligned (or anti-aligned) phase in which the continuous rotational symmetry is broken, to a time-dependent phase in which rotational symmetry is dynamically restored, but chirality is spontaneously broken [292] ("chiral" phase in Figure 5.6). The system also exhibits a phase in which the absolute value of the order parameter oscillates ("swap" phase), and one in which both the absolute value and the direction depend on time ("chiral + swap" phase). The aligned-chiral transition occurs when a damped mode coalesces with the Goldstone mode associated with rotational symmetry. At the critical point, not only the two modes have both zero eigenvalues, but also their eigenvectors become parallel, so that the Jacobian of the system becomes non-diagonalizable. This spectral singularity is called *exceptional point* and is characteristic of non-reciprocal phase transitions. Exceptional points also arise in contexts ranging from optics to open quantum systems [277, 306, 307].

Phases analogous to the chiral and swap ones described in [292] were also reported in [294, 295]. The authors study a single $O(N)$ model driven out of equilibrium by negative damping, but show that it can be mapped onto a pair of overdamped $O(N)$ models with non-reciprocal interactions. They show that for $N = 1$ (i.e. for the Ising model) only the swap phase exists, in agreement with the results of [291, 304], and the phase transition from disorder to oscillations corresponds to an equilibrium XY phase transition (as also conjectured in [291, 304]). Indeed all oscillating phases have a broken $SO(2)$ symmetry, corresponding to a phase shift of the oscillations (time translations inside a period). For $N > 1$, instead, both swap and chiral phases exist, and can be reached from the disordered one. The transition from disorder to swap is first order for all $N > 1$, whereas the transition to the chiral phase is of the second order, and described by a novel non-equilibrium universality class. By performing a Renormalization Group analysis, the authors show that the equilibrium critical point is unstable with respect to infinitesimal non-equilibrium perturbations.

In Ref. [278, 308] it has been shown that the oscillatory dynamics often encountered in non-reciprocal systems persists in mean-field Mattis-like models in which disorder can be gauged

away by a change of variables [309, 310].

5.4 Aging and non-conservative forces

In the next chapter we will study what happens if we couple non-reciprocally two systems that, if isolated, would undergo aging. Since non-reciprocal interactions are a special case of non-conservative forces, let us first review what happens if we add some generic non-conservative forces on a single aging system. In models in which aging is due to the "trapping" in flat regions of the phase space, it is believed that an infinitesimal non-conservative force will be sufficient to drive the system away from marginal states, generically destroying aging.

5.4.1 The Crisanti and Sompolinsky model

This was first evidenced by Crisanti and Sompolinsky in [13]. Drawing inspiration from neural networks, in which interactions between neurons are generically non-reciprocal, they proposed to consider a spherical Sherrington-Kirkpatrick model in which the interaction matrix J_{ij} is not symmetrical. As in Eq. 5.10, the system is described by:

$$\dot{s}_i = \sum_{j=1}^{N} J_{ij} s_j - \ell s_i + \eta_i + h_i \ , \tag{5.50}$$

but now $\mathbb{E}[J_{ij}J_{ji}] = \gamma/N$, so that for $\gamma \neq 1$ $J_{ij} \neq J_{ji}$. This is the kind of reciprocity that is often considered in ecological models, as we have seen in Part I. They found that even an infinitesimal degree of asymmetry has a dramatic effect on the behavior of the system: at any finite temperature the system reaches a time translational invariant phase, so that aging can only occur at zero temperature.

As in the reciprocal case, the system can be analyzed with DMFT. The derivation is completely analogous, the only difference arises when treating the term coming from the perturbation of the trajectories, in Eq. (5.21), because now an additional γ factor appears. The DMFT equation then becomes:

$$\dot{s} = -\ell s + \eta + h + \xi + \gamma \int^t dt' R(t,t') s(t') \ . \tag{5.51}$$

At high temperature the system is again time translational invariant, so that we can as before obtain an equation on the Fourier transform of R, that carries along the extra γ factor:

$$(-i\omega + \ell - \gamma R(\omega))R(\omega) = 1 \ . \tag{5.52}$$

The equation on C is instead unchanged:

$$C(\omega) = \frac{2T}{|R(\omega)|^{-2} - 1} \ . \tag{5.53}$$

The additional γ factor in Eq. (5.52) generates a mismatch between the singularities of R and C: when R becomes equal to one, generating a divergence of C in $\omega = 0$, it is analytic, so that the divergence of $C \sim 1/\omega$ will not be integrable. Because of the spherical constraint (see Eq. (5.30)), this critical behavior can only be reached at zero temperature. At any finite temperature the system will then be time-translationally invariant.

At zero temperature, the model does have a spin-glass phase transition: at low temperature it exhibits critical slowing down of the dynamics, whose characteristic timescale diverges as $1/T$, and is completely frozen for $T = 0$. This freezing can be seen from the correlation function, which

remains equal to 1 at all times. While the finite temperature behavior qualitatively extends to non-linear systems, this zero-temperature phase transition is believed to originate from the fact that a linear system must relax to a static limit in the absence of external sources [13]. Indeed non-linear systems with random asymmetric interactions exhibit a non-trivial dynamics even at zero temperature [285, 311]: the system is able to decorrelate from its initial conditions even in the absence of thermal fluctuations, which demonstrates that it must be undergoing a *chaotic dynamics*. At finite temperature the dynamics combines chaoticity and thermal fluctuations.

5.4.2 Marginal and non marginal models

These results on the fate of aging when the system is explicitly driven out of equilibrium by non conservative forces were extended to more general glassy models in Refs. [312–319]. In the case of the p-spin (see Section 7.3), it was shown that aging is interrupted on a time scale that diverges as a power law of the asymmetry coefficient [315]. The connection between marginality of the system and interruption of aging upon the introduction of non-reciprocity was confirmed by reference [313]. They considered a p-spin initialized at an energy below the threshold, which means that it is in a non-marginal state, and found that in this case the phenomenology is unchanged. Reference [316] studied a p-spin model (for both $p = 2$ and $p > 2$) under an oscillating driving force applied on a random direction. They found that aging is maintained below a finite frequency-dependent amplitude of the forcing; the correlation function exhibits small oscillations superimposed to the slow aging behavior. This is not in contradiction with the picture that aging is destroyed whenever the marginal modes of the system are perturbed by a non-conservative force, since a generic random direction in the p-spin is not marginal.

These results were believed to be relevant also for supercooled liquid under shear, thanks to the link provided by the Mode Coupling Approximation [315]. This was confirmed by molecular dynamics simulations in reference [314], which showed that in a sheared supercooled liquid below the glass transition temperature, aging is interrupted on a timescale proportional to the inverse of the shear rate. This is not true if the non-conservative force acts locally on each particle, as it is the case in active matter. Indeed aging has been observed in models and experiments of dense active particles [244–250, 320]

In non marginal models, a finite amount of non-reciprocity is generally needed to destroy aging behavior [321, 322].

Chapter 6

Non reciprocal spin-glass transition and aging

In this chapter, we couple non-reciprocally two spin-glass models and investigate whether they still exhibit aging. The introduction summarizes key concepts from the previous chapter to ensure that this chapter can be read independently. Materials from this chapter have already been presented in reference [2], and will be discussed in greater detail in a forthcoming publication [3].

6.1 Introduction

Disordered systems – i.e. systems composed of many randomly interacting units – can exhibit *aging*: they can fail to equilibrate [217, 323, 324], and their dynamics then becomes slower and slower in time [138–140], explicitly depending on the age of the system. In systems whose dynamics can be described as the minimization of an energy, this is usually attributed to the *complexity* of the energy landscape: when interactions between components are heterogeneous and *frustrated* – i.e. no configuration can minimize all interaction energies – the landscape can exhibit many saddle points, where the curvature is small and the system is trapped for long times. As shown in [160], aging can be induced by flat directions in the energy landscape: as time goes on, the system approaches saddle points with increasingly scarce and flat unstable modes, therefore the typical relaxation time scale of a sample increases with the time elapsed since its preparation. This slowdown of the dynamics has been observed in physical systems ranging from disordered magnets to dense liquids and active matter [138–140, 325]. In order to investigate the properties of this out-of-equilibrium aging dynamics, several spin-glass models have been introduced. Spin-glasses are spin systems with disordered and frustrated interactions, that exhibit a transition between a high temperature disordered phase and a low temperature aging – or *glassy* – phase.

Aging can also arise in many-body systems whose basic constituents are not classical physical objects such as spins or simple particles. Biologically-inspired examples include active matter [244–250, 326, 327], ecological systems [7, 12, 133, 142, 251], neural networks [241–243, 252–257] and cell's metabolic and genetic networks [258]. The coarse-grained dynamics of these many-body systems can be described with the tools of statistical physics, but they do not have to obey many of the constraints imposed on classical physical systems. In particular, they are often found to exhibit non-reciprocal interactions between constituents, thereby violating detailed balance. Consider, for example, predator-prey relationships in ecology: the presence of the prey enhances the growth of the predator, whereas the predator inhibits the growth of the prey, so that the two species have opposite effects on each other. Non-reciprocal interactions have been studied in a variety of contexts where they generate a rich phenomenology ranging from oscillatory

states and traveling waves [278–284, 291, 292] to chaotic states [13, 252, 273, 285–287] and non-equilibrium phase transitions [291–300]. Crucially, the dynamics of systems with non-reciprocal interactions can in general not be described as the minimization of a potential energy. Whether such systems can exhibit aging, and how to interpret such a dynamics when no potential energy can be defined, is an open question that goes beyond the rich literature developed in the last decades on glassy systems [7, 105].

Since the slowdown of the dynamics relies on the trapping of the system in very flat regions of the landscape, it is believed that the introduction of non-conservative forces, which would drive the system away from these flat regions, will generically destroy aging [13,315]. Pioneering studies by Crisanti and Sompolinsky (CS) [13] considered a spherical Sherrington-Kirkpatrick (SK) model [263–267] to which they added random *all-to-all* non-reciprocal interactions between spins. They showed that non-reciprocity suppresses the finite temperature spin-glass transition and, hence, also aging dynamics. Instead, chaotic dynamics is observed. These results were extended to more general glassy models in Refs. [311–319]. The emerging picture is that any amount of non-reciprocity then tends to destroy glassiness in marginally stable models[1].

Here we demonstrate that the aforementioned conclusions crucially depend on the structure of the system. Instead of coupling non-reciprocally many simple components, we consider the non-reciprocal coupling of two macroscopic agents with a complex internal dynamics, modeled by a spin-glass. This scenario could be relevant for many biological system, since non-reciprocal interactions often appear at a high organizational level. Examples include predators and preys, adversarial neural networks or robots, etc. The combination of a deterministic macroscopic structure and fine-grained disorder is also relevant for ecological systems, in particular when species can be organized in a small number of "functional groups" [130, 131].

Specifically, we consider a bipartite many-body spin-glass system with random symmetric interactions in each part, and fixed antisymmetric interactions between the two parts. We find that in this system, the finite temperature spin-glass transition is not destroyed by the introduction of non-reciprocity, but simply dressed by oscillations. Below the transition the system oscillates on a finite timescale that only depends on the non-reciprocity strength, but a long time-scale also emerges, determining the coherence time of the oscillations. As in the reciprocal case, this long time-scale is proportional to the time elapsed since preparation. We dub this behavior "non-reciprocal aging". The mechanism underpinning the destabilization of the usual spin glass in favor of the non-reciprocal one is a spectral singularity called exceptional point.

We contrast these results with the case of random non-reciprocity, where aging is suppressed at any finite temperature, and propose that the two cases correspond to two broader classes of systems, with "microscopic" versus "macroscopic" non-reciprocity, with aging surviving only in the second case. We also consider several extensions of our model, to probe which features of the model are essential to obtain the non-reciprocal spin-glass phase. We find that non-reciprocal aging is also present if the two systems only interact through the respective magnetizations, whereas no true finite-temperature transition occurs if the two spin-glasses are not identical. We describe the rich phenomenology that arises in both cases.

6.2 Non-reciprocally coupled spherical SK models

The system we will focus on combines features of several models described in Chapter 5. While Crisanti and Sompolinsky (see Section 5.4.1) studied a random network in which each microscopical component can interact non-reciprocally with all the others, we are interested in a situation

[1] In discrete models, a finite amount of non-reciprocity is instead generally needed to destroy aging behavior [321, 322].

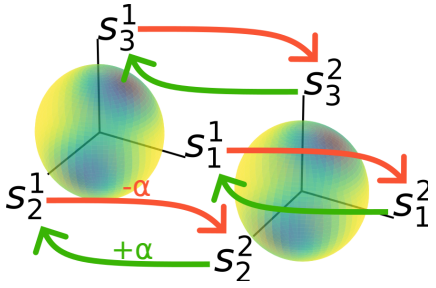

Figure 6.1: Sketch of the non-reciprocal spin-glass model: two (N-dimensional, in the plot $N = 3$) spherical spin systems, corresponding degrees of freedom are coupled non-reciprocally. The sphere's colors sketch the identical random potential in the two systems.

in which two complex units, each composed of many randomly interacting components, interact in a non-reciprocal way at the macroscopic level.

We consider *two* spherical Sherrington-Kirkpatrick (SK) spin-glass systems, each composed of N continuous spins. The dynamics of a single spherical SK model in described in Section 5.2.4. The two systems represent two distinct species, denoted by 1 and 2, with random all-to-all symmetric interactions within the same species plus a non-reciprocal (i.e. asymmetric) deterministic coupling between the two species. Their dynamics is defined by the coupled Langevin equations:

$$\begin{cases} \dot{s}_i^1 = \sum_j J_{ij} s_j^1 - \ell^1 s_i^1 + \alpha s_i^2 + \eta_i^1 + h_i^1 \\ \dot{s}_i^2 = \sum_j J_{ij} s_j^2 - \ell^2 s_i^2 - \alpha s_i^1 + \eta_i^2 + h_i^2 \end{cases} \tag{6.1}$$

in which s_i^a is the state of the spin $i = 1, \dots, N$ in the system $a = 1, 2$. The quenched interaction matrix J_{ij} is symmetrical and assumed to be the same in both systems (we will relax this assumption in Section 6.7.2). As before, the elements of J_{ij} are drawn from a Gaussian distribution with zero mean and variance $1/N$. The spins s_i^1 and s_i^2 in each system are coupled anti-symmetrically, with a coupling strength $\alpha > 0$: system 1 wants to align with system 2, whereas system 2 wants to anti-align with system 1. See Figure 6.1 for a graphical sketch. Each spin is also subject to a thermal Gaussian white noise η_i^a with covariance $\langle \eta_i^a(t) \eta_j^b(t') \rangle = 2T\delta_{ab}\delta_{ij}\delta(t - t')$, where T denotes the temperature. h_i^a is an external field that will be taken to zero at the end of the computation. Finally, ℓ^a are two Lagrange multiplier used to independently enforce the spherical constraint in the two systems, $\frac{1}{N}\sum_{i=1}^N (s_i^a)^2 = 1$. This model can be interpreted as describing the dynamics of two identical agents that are antagonistically coupled and whose internal complexity is modeled by spin-glass dynamics.

In the following, we analyze the effect of non-reciprocity on the steady-state dynamics by progressively decreasing the temperature.

6.2.1 Dynamical Mean Field Theory

In the thermodynamic limit $N \to \infty$, the dynamics of the system can again be analyzed by Dynamical Mean-Field Theory (DMFT) [13, 157–159]. The derivation is analogous to the one in Section 5.2.4, we report its adaptation to our bipartite model in Appendix B.1. The main difference is that we will now add a spin to each of the two systems, and we will study their coupled dynamics. As a result, we will have to consider not only the response and correlation function of each system separately, but also the cross-response and cross-correlation. It will be

convenient to organize them in 2×2 matrices:

$$R_{ab}(t,t') = \frac{\delta \langle s^a(t) \rangle}{\delta h^b(t')} \ , \tag{6.2}$$

$$C_{ab}(t,t') = \langle s^a(t) s^b(t') \rangle \ . \tag{6.3}$$

We can then write the DMFT equation in vectorial form as:

$$\dot{\mathbf{s}} = -\Lambda \mathbf{s} + \alpha \epsilon \mathbf{s} + \eta + \xi + \int_0^t dt' R(t,t') \mathbf{s}(t') + \mathbf{h} \ , \tag{6.4}$$

where $\mathbf{s} = [s^1, s^2]^T$ is a two-dimensional vector that contains the two spins, $\Lambda = \mathrm{diag}(\ell^1, \ell^2)$ is the diagonal matrix of the Lagrange multipliers. The noise vector ξ is Gaussian with zero mean and variance $\langle \xi_a(t) \xi_b(t') \rangle = C_{ab}(t,t')$. In addition to the terms already found in the single system case (Sec. 5.2.4), the two components are coupled by a term proportional to α, in which $\epsilon = \begin{pmatrix} 0 & 1 \\ -1 & 0 \end{pmatrix}$ is the fully anti-symmetric Levi-Civita symbol. As in the previous cases, the average correlation and response matrices have to be determined self-consistently.

6.3 Non-reciprocal spin-glass transition

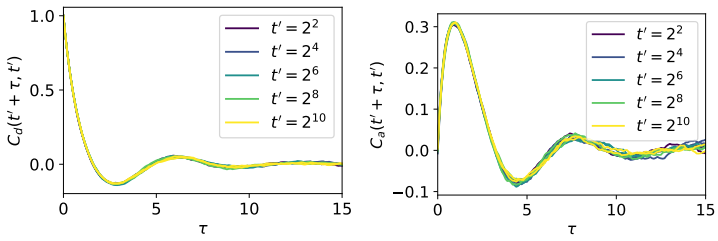

Figure 6.2: Auto- (left, $C_d = C_{11} = C_{22}$) and cross- (right, $C_a = C_{12} = -C_{21}$) correlation functions for different values of the initial time t', from numerical simulations of the equations (6.1), at $T = 1.4$. $\alpha = 1$, $N = 20000$, averaged over 5 runs.

At sufficiently high temperature, as in the case of a single system, we expect a time translational invariant state, in which two times observables only depend on the times difference. In order to verify this, we performed numerical simulations by direct integrations of Eq. (6.1) by Euler–Maruyama method. The spherical constraints are imposed by normalizing each spherical system after each time step: $s_i^a = \tilde{s}_i^a / \left(\frac{1}{N} \sum_i (\tilde{s}_i^a)^2 \right)$, where $\tilde{s}_i^a$ is the value obtained integrating the equations without taking into account the spherical constraint. This introduces an error of order dt, which does not change the precision of the method. If needed, the Lagrange multipliers can be computed as the force that would be needed to keep the systems on the sphere: $\ell_a = \frac{1}{dt} \left(\sqrt{\frac{1}{N} \sum_i (\tilde{s}_i^a)^2} - 1 \right)$.

As expected, at high temperature after a short transient the auto-correlation function of the system $C(t'+\tau, t')$ for different values of the initial time t' only depends on the time difference τ (Fig. 6.2), signaling that indeed the system is time translationally invariant.

Since the model is still symmetric under the transformation $(s_1, s_2) \to (-s_2, s_1)$ and under inversion, the two Lagrange multipliers are equal, $\ell^1 = \ell^2 = \ell$. Thanks to time-translational-invariance, we can conveniently Fourier transform the DMFT equations:

$$((-i\omega + \ell)\mathbb{1} - R - \alpha\epsilon)\mathbf{s} = \xi + \eta + \mathbf{h} \ . \tag{6.5}$$

Differentiating both sides with respect to $\mathbf{h}$ we obtain:

$$((-i\omega + \ell)\mathbb{1} - R - \alpha\epsilon)R = \mathbb{1} \ . \tag{6.6}$$

If we knew the Lagrange multiplier ℓ, this equation would determine R. Because of the aforementioned symmetry under the transformation $s_1 \to -s_2$, $s_2 \to s_1$, R has the form

$$R = \begin{pmatrix} R_d & R_a \\ -R_a & R_d \end{pmatrix} . \tag{6.7}$$

All matrices of this form are diagonalized in the basis

$$v^{\pm} = \frac{1}{\sqrt{2}} \begin{pmatrix} \mp i \\ 1 \end{pmatrix} . \tag{6.8}$$

This leads to a simple expressions of the eigenvalues of R:

$$R_+ = R_d + iR_a \ , \qquad\qquad R_- = R_d - iR_a \ . \tag{6.9}$$

We can write the self-consistent equation on R in its eigenbasis:

$$(\ell - i(\omega \pm \alpha) - R_\pm)R_\pm = 1 \ , \tag{6.10}$$

and easily solve it:

$$R_\pm = \frac{\ell - i(\omega \pm \alpha) - \sqrt{(\ell - i(\omega \pm \alpha))^2 - 4}}{2} \ . \tag{6.11}$$

These equations are the same that would be found in the single system case (Eq. (5.25) and (5.26)), except for a shift of $\pm\alpha$ in ω.

As before, we can use the linearity of the the problem to claim that $\mathbf{s}(\omega) = R(\omega)(\xi(\omega)+\eta(\omega))$ and compute the correlation functions:

$$\begin{aligned} \delta(\omega + \omega')C(\omega) = \langle \mathbf{s}(\omega)\mathbf{s}(\omega')^T \rangle = \\ = R(\omega)\langle(\xi(\omega) + \eta(\omega))(\xi(\omega') + \eta(\omega'))^T\rangle R(\omega')^T = \\ = \delta(\omega + \omega')R(\omega)(C(\omega) + 2T)R^\dagger(\omega) \ . \end{aligned} \tag{6.12}$$

This gives us the self-consistent equation on C:

$$R^{-1}C(R^\dagger)^{-1} - C = 2T \ . \tag{6.13}$$

As R, also C is of the form

$$C = \begin{pmatrix} C_d & C_a \\ -C_a & C_d \end{pmatrix} . \tag{6.14}$$

This means that it is diagonalized in the same basis $v^\pm$ as R, which ensures that C and R commute. We then obtain:

$$C(\omega)((R(\omega)^\dagger R(\omega))^{-1} - \mathbb{1}) = 2T \ . \tag{6.15}$$

If $(R(\omega)^\dagger R(\omega))^{-1} - \mathbb{1}$ is invertible,

$$C(\omega) = 2T((R(\omega)^\dagger R(\omega))^{-1} - \mathbb{1})^{-1} \ . \tag{6.16}$$

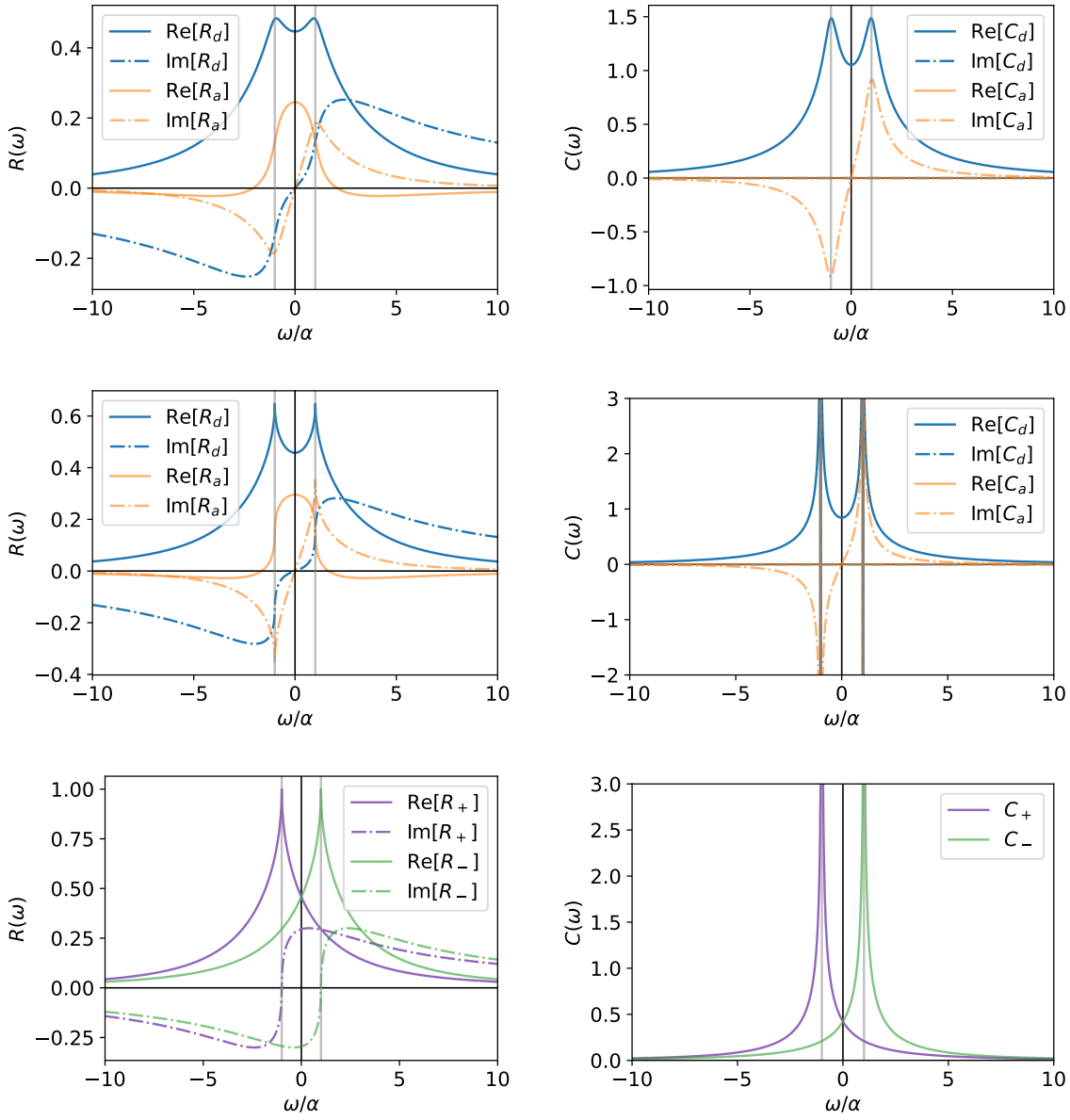

Figure 6.3: Real and imaginary parts of the response (left) and correlation (right) functions, in the original basis at $T = 1.5$ (top) and at $T = T_c$ (center), and in the diagonalizing basis at $T = T_c$(bottom). $\omega = \alpha$ indicated in gray.

Using again the diagonalizing basis, we have:

$$C_{\pm}(\omega) = \frac{2T}{|R_{\pm}(\omega)|^{-2} - 1} \ . \tag{6.17}$$

This is again the same equation as in the single system case, Eq. (5.28). Because the ω dependence is only through $R_{\pm}$, also $C_{\pm}$ behave in the same way as in the single system case except for the $\pm\alpha$ shift in ω.

The spherical constraint imposes that

$$C_d(t=0) = \frac{1}{2\pi}\int d\omega C_d(\omega) = 1 \ . \tag{6.18}$$

Since C_a is an odd function of ω, it does not contribute to the integrals:

$$\int d\omega C_d = \int d\omega (C_d \pm iC_a) = \int d\omega C_{\pm}(\omega) \ . \tag{6.19}$$

Because the non-reciprocal coupling only introduces a shift in the ω dependence of $C_{\pm}$, it does not change the integral either, which will then be the same as in the single system case (Sec. 5.2.4), that we can indicate with $C_{\alpha=0}(\omega)$:

$$C_d(t=0) = \frac{1}{2\pi}\int d\omega C_{\pm} = \frac{1}{2\pi}\int d\omega C_{\alpha=0} = 1 \ . \tag{6.20}$$

The equation imposed by the spherical constraint determines the Lagrange multiplier ℓ, which will therefore be at all temperatures the same as in the single system case, following the same curve as in Figure 5.2. This leads to the same critical point $T_c = 1$, where $\ell \to 2$ and touches the edge of the spectrum of J.

For $T > T_c$, response and correlation functions are peaked around $\omega = \pm\alpha$ (Fig. 6.3, top). This is the frequency at which the system would exhibit regular oscillations in the absence of disordered interactions (Sec. 5.3.2). Strikingly, in their presence, the disordered system does not exhibit macroscopic oscillations but responds more strongly if excited at this frequency. These peaks become singularities when $T \to T_c = 1$ (Figure 6.3): the one of $R(\omega)$ approaches a finite limit with a square root behavior, whereas the one of $C(\omega)$ diverges as $(\omega \pm \alpha)^{-1/2}$. In the time domain, one finds a relaxation time to the non-equilibrium steady state that diverges as $1/\sqrt{T - T_c}$ and critical relaxation at T_c, corresponding to a behavior $C(t) \sim \cos(\alpha t)/t^{1/2}$. The transition shares crucial similarities to the transition to an ordinary spin glass phase that is found in the reciprocal single system case (Sec. 5.2.4) except for the superposition of oscillations that shift the singularity of correlation and response functions from $\omega = 0$ to $\omega = \pm\alpha$.

Note again the crucial matching of the singularities of R and C for $\ell = 2$ for obtaining a critical point at finite temperature. For $\ell = 2$ the eigenvalues of R behave around $\omega = \mp\alpha$ as $R_{\pm} - 1 \sim \sqrt{|\omega \pm \alpha|}$. The corresponding eigenvalues of C therefore behave as $2T|\omega \pm \alpha|^{-1/2}$, leading to integrable singularities. If this was not the case (as in the case of Crisanti and Sompolinsky, Sec. 5.4.1 and [13]), the integral in equation (6.20) would be diverging at criticality, implying that criticality can only be reached at 0 temperature.

The analysis of the steady state dynamics therefore reveals a first important result: adding non-reciprocal interactions to the spherical spin-glass model does lead to a dynamical phase transition, which generalizes the spin-glass transition found in the symmetric case. This is in contrast with what is found for all-to-all non-reciprocal interactions à la CS, which instead wipe out the finite temperature transition (Sec. 5.4.1 and [13]). We will now show that the different form of non-reciprocity also leads to a very different physical behavior for the non-equilibrium dynamics.

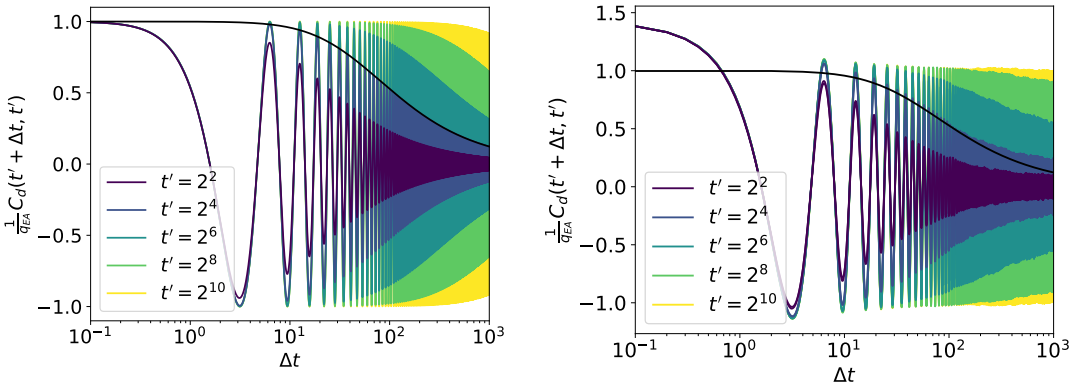

(a) Analytical results

(b) Numerical results

Figure 6.4: Analytical (a) and numerical (b) results for the diagonal component of the correlation function, normalized by the Edward-Anderson order parameter, for different values of the waiting time. The numerical results are obtained from simulations of the dynamical equations (6.1) with $T = 0.3$ (so that $q_{EA} = 0.7$). Note that the time axis is in log-scale to better visualize the slow aging evolution, leading to an apparent acceleration of the oscillations, which are instead of constant period in linear time. The analytical prediction for the envelop of the oscillations is shown in black for $t' = 2^4$. The asymptotic solution for the correlation function does not describe the initial relaxation (on a timescale of order 1) from $C_d(t', t') = 1$ to oscillations of amplitude q_{EA}. $\alpha = 1$.

6.4 Non-reciprocal aging

As in the single system case (Sec. 5.2.4), after quenches below T_c we do not expect the dynamics to relax to a steady state. To verify whether aging survives in this case, we again analyze the dynamics in the basis that diagonalizes the interaction matrix J. This leads to:

$$\dot{\mathbf{s}}_\mu = (\mu \mathbb{1} - \Lambda + \alpha\epsilon)\, \mathbf{s}_\mu + \eta_\mu \ , \tag{6.21}$$

in which the eigenvalues μ of J are used to label the two-dimensional vectors $\mathbf{s}^\mu$ composed of the projections of s^1 and s^2 on the corresponding eigenvector. η_μ is also a two-dimensional vector containing both components of the noise.

In this basis different modes are only coupled through the (now time-dependent) Lagrange multipliers. We can formally write the solution in terms of the realization of the noise $\eta_\mu(t)$ and the (unknown) time evolution of the Lagrange multipliers:

$$\mathbf{s}_\mu(t) = e^{(\mu\mathbb{1}+\alpha\epsilon)t - \int_0^t \Lambda(t')dt'} \mathbf{s}_\mu(0) + \int_0^t dt' e^{(\mu\mathbb{1}+\alpha\epsilon)(t-t') - \int_{t'}^t \Lambda(t'')dt''} \eta_\mu(t') \ . \tag{6.22}$$

On time scales that do not diverge with N, an extensive number of modes will contribute to the dynamics of the Lagrange multipliers. As before, and because of the randomness in the initial conditions, we then expect them to be equal at all times, $\ell^1(t) = \ell^2(t) = \ell(t)$. This greatly simplifies the analysis, because now Λ and ϵ commute and we can separate their exponentials:

$$\mathbf{s}_\mu(t) = e^{\mu t - \int_0^t \ell(t')dt'} \mathcal{R}_{\alpha t} \mathbf{s}_\mu(0) + \int_0^t dt' e^{\mu(t-t') - \int_{t'}^t \ell(t'')dt''} \mathcal{R}_{\alpha(t-t')} \eta_\mu(t') \ . \tag{6.23}$$

We have introduced the rotation matrix $\mathcal{R}_{\alpha t} = e^{\alpha\epsilon t} = \begin{pmatrix} \cos\alpha t & \sin\alpha t \\ -\sin\alpha t & \cos\alpha t \end{pmatrix}$. Note that this rotation matrix acts on the 2-dimensional space of the projection of the two systems on a given

mode, and it describes the out-of-phase oscillation of each mode of the two systems. The vector $\mathbf{s}_\mu$ rotates at constant angular velocity α, while its radius undergoes a slow aging evolution akin to the one found in the absence of non-reciprocity.

We can express the initial conditions in polar coordinates: $\mathbf{s}^\mu(0) = r_\mu(0)\begin{pmatrix}\sin\theta_\mu(0)\\ \cos\theta_\mu(0)\end{pmatrix}$. We consider uniform initial conditions on the two spheres, which corresponds to taking uniform and independent $\theta_\mu(0)$.

In order to find an equation for $\ell(t)$, we impose the spherical constraint on system 1:

$$\begin{aligned}\langle\sum_\mu (s^1_\mu(t))^2\rangle &= \frac{1}{2}\sum_\mu e^{2\mu t - 2\int_0^t \ell(t')dt'} r^2_\mu(0) + \\ +2T\sum_\mu \int_0^t dt' e^{2\mu(t-t')-2\int_{t'}^t \ell(\tau)d\tau}(\cos^2\alpha(t-t') + \sin^2\alpha(t-t')) &= \\ = \frac{N}{2}\int d\mu\rho(\mu)e^{2\mu t-2\int_0^t \ell(t')dt'} r^2_\mu(0) + 2TN\int d\mu\rho(\mu)\int_0^t dt' e^{2\mu(t-t')-2\int_{t'}^t \ell(\tau)d\tau} &= N\ .\end{aligned} \tag{6.24}$$

As expected, we would have obtained the same result using system 2, self-consistently confirming that $\ell^1(t) = \ell^2(t) = \ell(t)$. We have neglected all terms that do not contribute when averaging over the initial conditions or the noise, and used $\langle r^2_\mu(0)\rangle = \langle (s^1_\mu(0))^2\rangle + \langle (s^2_\mu(0))^2\rangle = 2$. $\rho(\mu)$ is the eigenvalue density of J from Eq. (5.13). Imposing that the constrain is satisfied at all times we obtain:

$$\int d\mu\rho(\mu)e^{2\mu t-2\int_0^t \ell(t')dt'} + 2T\int d\mu\rho(\mu)\int_0^t dt' e^{2\mu(t-t')-2\int_{t'}^t \ell(\tau)d\tau} = 1\ . \tag{6.25}$$

This is the same equation on the Lagrange multiplier that would be obtained in the uncoupled case [265], therefore we can use the known result for the spherical constraint. We can now compute the correlation function:

$$\begin{aligned}C(t,t') &= \langle\sum_\mu \mathbf{s}_\mu(t)\mathbf{s}_\mu(t')^T\rangle = \\ &= \left(\int d\mu\rho(\mu)e^{\mu(t+t')-\int_0^t \ell(\tau)d\tau-\int_0^{t'} \ell(\tau')d\tau'} + \right. \\ &\left. + 2T\int d\mu\rho(\mu)\int_0^t dt'' e^{\mu(t+t'-2t'')-\int_{t''}^t \ell(\tau)d\tau-\int_{t''}^{t'} \ell(\tau')d\tau'}\right)\mathcal{R}_{\alpha(t-t')}\ .\end{aligned} \tag{6.26}$$

The factor in parentheses is precisely the expression that we have derived for the correlation function in the uncoupled case $C_{\alpha=0}(t,t')$ in Equation (5.36). Therefore we find:

$$C(t,t') = C_{\alpha=0}(t,t')\mathcal{R}_{\alpha(t-t')}\ . \tag{6.27}$$

The self-correlation functions, C_{11} and C_{22}, plotted in Figure 6.4a for different values of the initial time t', read in the asymptotic regime $t, t' \gg 1$, $\Delta t = t - t' \gg 1$:

$$C(t,t') = q_{EA}\left(\frac{2\sqrt{1+\Delta t/t'}}{2+\Delta t/t'}\right)^{\frac{3}{2}}\begin{pmatrix}\cos\alpha\Delta t & \sin\alpha\Delta t\\ -\sin\alpha\Delta t & \cos\alpha\Delta t\end{pmatrix}\ , \tag{6.28}$$

where $q_{EA} = 1 - \frac{T}{T_c}$ is the non-reciprocal counterpart of the Edwards-Anderson order parameter or self-overlap [219, 265, 267, 328]. This form is in very good agreement with the simulation results (Figure 6.4b).

In summary, the correlation function after a quench displays regular oscillations at the same frequency that would be obtained in the absence of the disordered potential. The envelope of these oscillations performs a slow aging evolution – with a dependence on $\Delta t/t'$, which remarkably turns out to be the same as in the single system case (Sec. 5.2.4) [265, 267]. This means that the oscillations have a coherence time that increases linearly with the time elapsed since the preparation of the system in random conditions. We refer to the emergence of this long timescale, which coexists with the order 1 timescale set by the non reciprocity, as *non-reciprocal aging*. Notably, aging survives for all values of the non-reciprocity α, contrarily to previously studied cases in which aging is interrupted above some critical value of the driving [316,321,322].

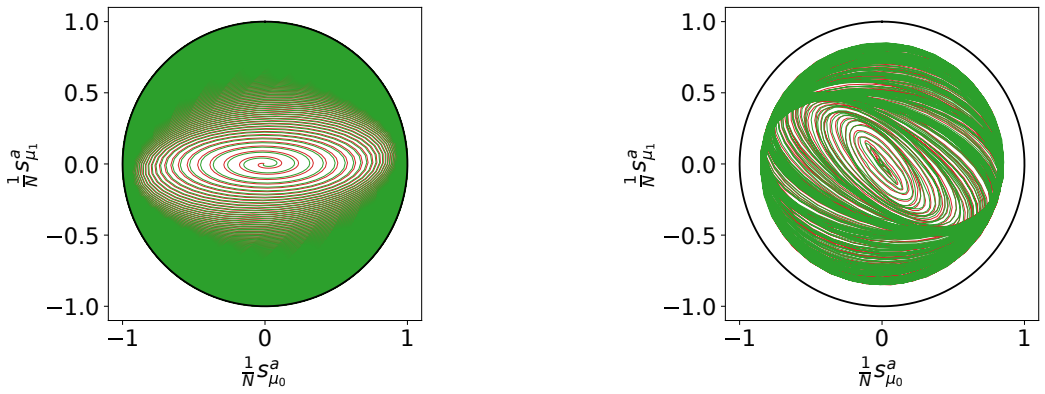

(a) $T = 0$ (b) $T = 0.3$

Figure 6.5: Projection on the two leading eigenvectors of the interaction matrix J of the trajectories (green and red) of the two systems for $T = 0$ (left) and $T = 0.3$ (right). Random initial conditions, $\alpha = 0.2$, $N = 20000$. The black circle represents the spherical constraint $(s^a_{\mu_0})^2 + (s^a_{\mu_1})^2 \leq N$: at $T = 0$ this constraint is saturated at long times, whereas at finite temperature it is not, because of fluctuations on all other modes having a finite total weight. The radius of the orbit at long times is $A(\omega = \alpha)$.

6.5 Asymptotic behavior

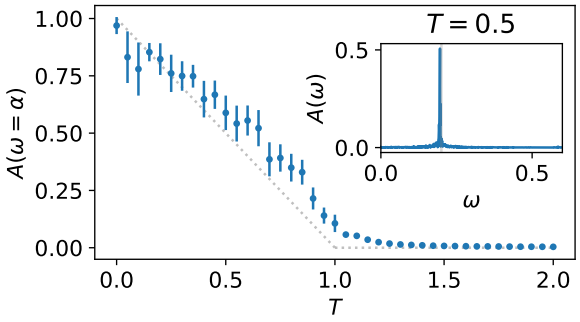

Figure 6.6: Numerical results for the amplitude of the Fourier component at $\omega = \alpha$ of the projection of one of the two clones on the leading eigenvector, as a function of temperature. The amplitude goes to zero continuously for $T \to T_c = 1$; in gray we show $q_{EA} = 1 - \frac{T}{T_c}$. In the inset, the amplitude of the Fourier transform as a function of ω for $T = 0.5$. $\alpha = 0.2$

Let us now consider the asymptotic behavior, i.e. the regime $t \to \infty$ at fixed but large N.

By numerically integrating the equations of motion (6.1), we find that once the non-reciprocity is switched on the situation is drastically different from the single system case described in Sec. 5.2.4. Activated barrier hopping between the two ground states (related by inversion symmetry) is wiped out by the non-reciprocity and each of the systems oscillates on timescales of order one between the two states. More precisely, at zero temperature each system performs a periodic orbit in the circle spanned by the two lowest eigenvectors of J (Figure 6.5) with angular frequency α and relative phase $\pi/2$. At finite temperature, the Fourier transform of the projection of the spin configuration of any of the two systems on the leading eigenvector has a delta peak in $\omega = \alpha$, whose amplitude $A(\omega = \alpha)$ goes to zero continuously at the transition (Figure 6.6). The two systems perform periodic orbits with macroscopic overlap on the two lowest eigenvectors of J ($s^a_{\mu_0}, s^a_{\mu_1} \propto N$), and exhibit noise-driven order 1 fluctuations on all other modes. At finite N the sense of rotation can be stochastically inverted, much like in the uncoupled case the system can jump between the two ground states, but only on timescales that diverge with N, so that this is never observed in numerical simulations with $N = 20000$.

This oscillating phase, which we call *non-reciprocal spin-glass*, is the counterpart of the low-temperature static phase found in the uncoupled case. The observable $A(\omega = \alpha)$ generalizes the Edwards-Anderson parameter q_{EA} that in the uncoupled case describes the overlap of the system with the ground state. The numerical dependence on temperature of $A(\omega = \alpha)$ indicates a phase transition at $T_c = 1$, and it behaves in a quantitatively similar way to q_{EA}, $A(\omega = \alpha) = 1 - \frac{T}{T_c}$.

In the equilibrium case, there is a symmetry breaking corresponding to the choice of one of the two pure states. In the non-reciprocal case, there is spontaneous chiral symmetry breaking: the direction of rotation is randomly selected, and with a rotation plane that is disorder-dependent. As a result, similarly to what was found in references [279, 308] for a related model, the oscillations are not visible in the magnetization of the system, that is zero in this phase, or other disorder-independent one-time observables. Instead, they are visible in the auto-correlation function. In practice, to determine the plane of rotation one can perform a principal component analysis (PCA) of the trajectory of the system.

6.5.1 Non antisymmetric coupling

We have seen in Section 5.3.2 that if each system has only two spins oscillations are only possible at zero temperature and if the non-reciprocal interactions are exactly antisymmetrical. In our model the oscillating phase does not have these limitations. We already mentioned the persistence at finite temperature of the oscillations on timescales that diverge with N. This is a many-body effect, analogous to the one discussed in Section 5.3.3 [292], and, as shown in section 5.3.2, it would not be present without the random interactions.

The non-reciprocal spin-glass phase also exists for non exactly antisymmetrical coupling. We performed numerical simulations with two different coupling strengths α_1 and α_2 as in Eq. (5.42). In Fig. 6.7, we summarize the result of simulations for different values of α_2 and T at fixed $\alpha_1 = 1$. The colors represent the frequency of the peak of the Fourier transform of the projection of the trajectory of one of the two systems on the leading eigenvector of J (as in the inset of Fig. 6.6), that we refer to as ω_{max}. If the peak $A(\omega_{max}) < 0.05$, the corresponding point is left white. The system exhibits three different phases: (i) disordered, in white, (ii) static spin-glass, in purple, and (iii) oscillating spin-glass. If $\alpha_2 = \alpha_1 = 1$, the peak frequency is $\omega_{max} = 1$ for all values of the temperature, until for $T > 1$ the system enters the disordered phase. At $T = 0$, oscillations are only possible for anti-symmetrical couplings: if $\alpha_2 \neq \alpha_1 = 1$, the peak of the Fourier transform is in $\omega = 0$, signaling a static spin-glass phase. Interestingly, at finite temperature the oscillating spin-glass phase extends up to $\alpha_2 \sim 0.5$. Similarly to what was reported in Ref. [292], the thermal fluctuations drive the system away from the aligned or antialigned fixed points, continuously restarting the run-and-chase dynamics. Nevertheless

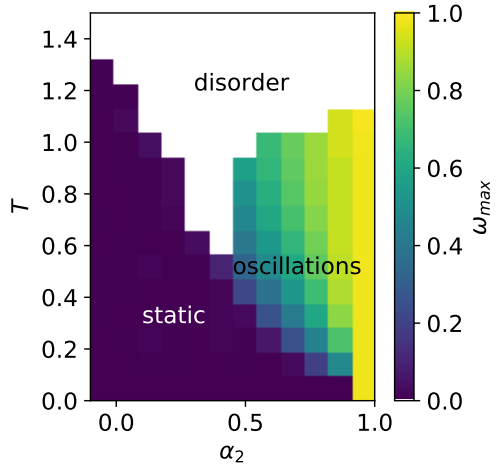

Figure 6.7: Phase diagram of the system with non-anti-symmetrical interactions, obtained from numerical simulations with $\alpha_1 = 1$, $N = 20000$. For each value of T and α_2, 5 numerical simulations were performed and we consider their average. The colors represent the frequency of the peak of the Fourier transform of the projection of the trajectory of one of the two systems on the leading eigenvector of J (as in the inset of Fig. 6.6). If the peak $A(\omega_{max}) < 0.05$, the corresponding point is left white (note that $A(\omega) \leq 1$).

the deviation from anti-symmetry can destabilize the oscillating spin glass phase, shifting the transition to disorder to lower values of the temperature.

6.6 Stability

6.6.1 Exceptional-point mediated transition

To investigate analytically the existence of the oscillating phase described above, we now analyze the stability of the equilibrium points at zero temperature, considering again anti-symmetrical interactions. We write the dynamics in the basis that diagonalizes the interaction matrix J:

$$\begin{cases} \dot{s}^1_\mu = (\mu - \ell_1)\, s^1_\mu + \alpha s^2_\mu = 0 \\ \dot{s}^2_\mu = (\mu - \ell_2)\, s^2_\mu - \alpha s^1_\mu = 0 \end{cases} \tag{6.29}$$

We have $4N$ stationary points; in each only one of the modes contributes, and we will indicate it with μ^*:

$$s^{*1}_\mu = \pm s^{*2}_\mu = \pm\sqrt{N}\delta_{\mu,\mu^*} \ . \tag{6.30}$$

Let us consider a fixed point with positive projections on the mode μ^* for both systems (the other equilibria are completely equivalent thanks to symmetries). Imposing stationarity in Eq. (6.29) and choosing the signs in Eq. (6.30) determines the Lagrange multipliers

$$\ell^1 = \mu^* + \alpha \ , \qquad\qquad \ell^2 = \mu^* - \alpha \ . \tag{6.31}$$

Note that $\ell^1 \neq \ell^2$ in this particular case.

To study the stability of this fixed point we can look at the linearized dynamics:

$$\delta \mathbf{s}_\mu = \mathbf{s}_\mu - \mathbf{s}^*_\mu \ , \tag{6.32}$$

$$\delta \dot{\mathbf{s}}_\mu = M_\mu \delta \mathbf{s}_\mu \ , \tag{6.33}$$

$$M_\mu = \begin{pmatrix} \mu - \mu^* - \alpha & \alpha \\ -\alpha & \mu - \mu^* + \alpha \end{pmatrix} . \tag{6.34}$$

The stability matrix M_μ has only one eigenvalue $\lambda_\mu = \mu - \mu^* = \Delta\mu$, with only one associated independent eigenvector $(1,1)^\top$: it is a *defective* matrix. This situation is known as an exceptional point [329]. Exceptional points, where two or more eigenstates coalesce, also arise in contexts ranging from optics to open quantum systems [277, 306, 307].

If μ^* is not the maximum eigenvalue, a finite number of the stability eigenvalues λ_μ will be positive, and therefore the system will depart exponentially from the fixed point. If μ^* is the maximum eigenvalue, all the stability eigenvalues will be negative, except for the one associated with mode μ^* which will be zero, exactly as in the uncoupled case (Sec. 5.2.4). Nevertheless, for non-normal matrices (such as those close to or at an exceptional point), looking at the eigenvalues of the stability matrix is not sufficient to determine the behavior of the system around the equilibrium point [330]. To clarify this point, we can explicitly solve the linearized equation:

$$\delta \mathbf{s}_\mu = e^{Mt} \delta \mathbf{s}_\mu(0) = \begin{pmatrix} e^{\Delta\mu t}(1-\alpha t) & \alpha e^{\Delta\mu t} t \\ -\alpha e^{\Delta\mu t} t & e^{\Delta\mu t}(1+\alpha t) \end{pmatrix} \delta \mathbf{s}_\mu(0) .$$

Even though at long times the behavior is controlled by the decaying exponential, at short times we can indeed see a growth of the perturbation (note that since we are linearizing around a fixed point, it is the initial behavior that we are interested in). Since we are interested in short times, we can expand the exponential:

$$\delta \mathbf{s}_\mu \sim \begin{pmatrix} 1 + (\Delta\mu - \alpha)t & \alpha t \\ -\alpha t & 1 + (\Delta\mu + \alpha)t \end{pmatrix} \delta \mathbf{s}_\mu(0) . \tag{6.35}$$

Let us take for example the perturbation $\delta \mathbf{s}^\mu(0) = \varepsilon \begin{pmatrix} 0 \\ 1 \end{pmatrix}$, with $\varepsilon \ll 1$. Because we are considering a configuration in which the two systems are perfectly aligned, while system 2 would tend to antialign with system 1, we expect that this perturbation on system 2 could destabilize the stationary point. Indeed at short times we obtain

$$\delta \mathbf{s}^\mu(t) = \varepsilon \begin{pmatrix} \alpha t \\ 1 + (\Delta\mu + \alpha)t \end{pmatrix} . \tag{6.36}$$

Therefore a perturbation on the mode μ is initially amplified as long as $\mu^* - \mu < \alpha$, although M_μ has only non-negative eigenvalues. Indeed $\mu^* - \mu$ is the energetic prize that system 2 has to pay to move from mode μ^* to mode μ, which needs to be compensated by its repulsion from system 1, i.e. α. In the thermodynamic limit, the gap between the first and subsequent eigenvalues vanishes, therefore for any finite value of α there will be an extensive number of unstable modes destabilizing the condensed phase.

This mechanism changes the nature of the low-temperature regime compared to the equilibrium case, and it leads to the rotating non-reciprocal spin-glass phase studied here. This exceptional-point mediated transition is reminiscent of the non-reciprocal phase transitions studied in Ref. [292]. Our results provide an extension of that mechanism to simple disordered systems.

6.6.2 Stability of the rotating state

The most unstable mode is the one associated with the second largest eigenvalue of J, μ_1. As a result, each system will start to rotate in the circle spanned by the two leading eigenvectors of

J, v_{μ_0} and v_{μ_1}. We can study the dynamics of the system restricted to this subspace, and then show that this solution is stable to perturbations.

We indicate the projections on the two leading eigenvectors with s_0^a and s_1^a, and group them in the two-dimensional vectors $\vec{s}^a = \begin{pmatrix} s_0^a \\ s_1^a \end{pmatrix} = N \begin{pmatrix} \sin\phi_a \\ \cos\phi_a \end{pmatrix}$. Projecting the dynamics on the direction orthogonal to each vector, we obtain an equation on the polar angles ϕ_a:

$$\dot{\phi}_a = -((\mu_0 - \ell^a)s_0^a + \epsilon_{ab}\alpha s_0^b)s_1^a + ((\mu_1 - \ell^a)s_1^a + \epsilon_{ab}\alpha s_1^b)s_0^a = \tag{6.37}$$

$$= -\frac{\Delta\mu_1}{2}\sin 2\phi_a - \alpha\sin(\phi_1 - \phi_2) \ . \tag{6.38}$$

In the thermodynamic limit the first term is negligible, and the two systems rotate at constant velocity $\alpha\sin(\phi_1 - \phi_2)$. From numerical simulations we see that the system always converges to a rotating phase in which the two vectors are perpendicular, so that the angular speed is maximal.

Using that thanks to the spherical constraint $\frac{d}{dt}((s_0^a)^2 + (s_1^a)^2) = 0$ we can obtain an equation on the Lagrange multipliers:

$$0 = \dot{s}_0^a s_0^a + \dot{s}_1^a s_1^a = (\mu_0 - \ell^a)N - \Delta\mu_1 (s_1^a)^2 + \alpha\epsilon_{ab}\vec{s}^a \cdot \vec{s}^b \ , \tag{6.39}$$

$$\ell^a = \mu_0 - \Delta\mu_1 \frac{(s_1^a)^2}{N} + \alpha\epsilon_{ab}\frac{\vec{s}^a \cdot \vec{s}^b}{N} \ , \tag{6.40}$$

where $\Delta\mu_1 = \mu_1 - \mu_0$ is of order $N^{-2/3}$ [271]. The Lagrange multipliers are thus dynamically determined by the values of $\vec{s}^a$. We can again linearize the dynamics around the (time-dependent) rotating solution. The stability matrix for mode $\mu \neq \mu_0, \mu_1$ now reads:

$$M'_\mu = \begin{pmatrix} \mu - \ell^1 & \alpha \\ -\alpha & \mu - \ell^2 \end{pmatrix} \ , \tag{6.41}$$

with eigenvalues

$$\lambda = \mu - \frac{\ell^1 + \ell^2}{2} \pm \sqrt{\left(\frac{\ell^1 - \ell^2}{2}\right)^2 - \alpha^2} \ . \tag{6.42}$$

In the thermodynamic limit in which $\Delta\mu_1 \to 0$, the two eigenvalues can only be equal if the two systems are either aligned or antialigned, bringing the system back to the previously studied unstable static solution. In all other cases, the stability matrix is not singular, and since again it has only eigenvalues with positive real part (except for the two lowest modes on which the system rotates), the system is stable with respect to perturbations outside of its rotating trajectory. The system is instead marginal with respect to a perturbation on the two lowest modes, corresponding to a phase shift.

6.7 Extensions

In the following we discuss several extensions of our model, to probe which features are essential to obtain the non-reciprocal spin-glass phase.

6.7.1 Random non-reciprocity

We emphasize that our non-reciprocal coupling α introduces a unique timescale for oscillations, in contrast with the random non-reciprocity in CS model, which leads to a continuous timescale distribution.

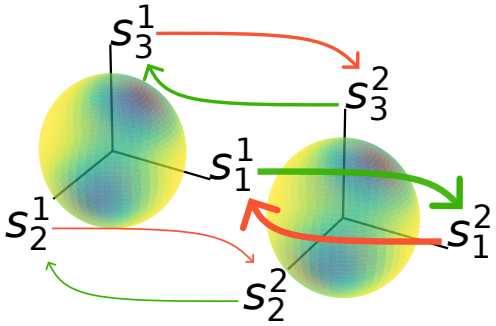

Figure 6.8: Sketch of the non-reciprocal spin-glass model in the random non-reciprocity case: two (N-dimensional, in the plot $N = 3$) spherical spin systems, corresponding degrees of freedom are coupled anti-symmetrically, with a *different* random coupling for each pair (indicated by different widths of the arrows). The sphere's colors sketch the identical random potential in the two systems.

In order to investigate whether the introduction of a continuous distribution of oscillations timescales can destroy aging we modify our system to consider random independent values of the non-reciprocal coupling α_i for each pair of spins s_i^1, s_i^2. The dynamical equation becomes:

$$\dot{s}_i^a = \sum_{j=1}^{N} J_{ij} s_j^a - \ell^a s_i^a + \sum_b \alpha_i \epsilon_{ab} s_i^b + \eta_i^a + h_i^a \ . \tag{6.43}$$

We can replicate the DMFT computation as in the previous case. The main difference is that the response and correlation functions are now α-dependent, but only their average enters the effective two-spin equations. We will indicate with R_α and C_α the α-dependent quantities, and with R and C their average over α. The DMFT equations read as before:

$$\dot{\mathbf{s}} = -\Lambda \mathbf{s} + \alpha \epsilon \mathbf{s} + \xi + \int_0^t dt' R(t,t') \mathbf{s}(t') + \mathbf{h} \ , \tag{6.44}$$

An analogous computation to the previous one now gives:

$$R(\omega) = \overline{((-i\omega + \ell)\mathbb{1} - R - \alpha\epsilon)^{-1}} \ , \tag{6.45}$$

$$C(\omega) = 2T \left(\overline{(R^\alpha(\omega)^\dagger R^\alpha(\omega))}^{-1} - \mathbb{1} \right)^{-1} \ . \tag{6.46}$$

We have indicated with an overline the average over α.

As before, C would have a critical point if $\overline{(R^\alpha(\omega)^\dagger R^\alpha(\omega))}$ had an eigenvalue equal to 1. Nevertheless, while before when this happened R also had a singularity in $\omega = \pm\alpha$, if α has a continuous distribution, this singularity is smoothed out by the integration over α. This means that at the critical point C would behave as $1/\omega$. Because this singularity would not be integrable, in order to satisfy the spherical constraint $C_d(t = 0) = 1$ this cannot happen at finite temperature.

In the case of a Gaussian and centered distribution of the α_i, it is possible to compute analytically the response and correlation functions at all temperatures, verifying that indeed they are analytic for all $T > 0$.

Since no phase transition can occur at finite temperature, we find that for continuous distributions of random anti-symmetrical coupling α_i the aging behavior is destroyed, leading to chaotic dynamics as in the CS model. This is reminiscent of what was found for slowly pulsating poly-disperse particles [331], that exhibit an arrested phase only if all particles pulsate

at the same frequency. For a continuous but sharp distribution, a sharp crossover is expected, that would be indistinguishable from a phase transition except in extremely large systems at extremely long times. In this case the system would display interrupted aging, i.e. aging only up to extremely large time-scales [138].

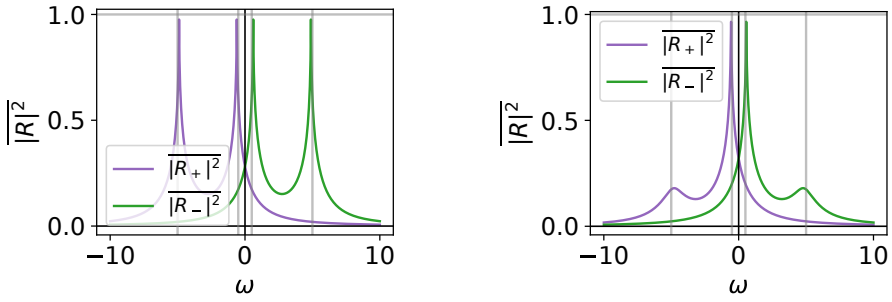

(a) $p_{\alpha=0.5} = p_{\alpha=5} = 0.5$ (b) $p_{\alpha=0.5} = 0.7$, $p_{\alpha=5} = 0.3$

Figure 6.9: Eigenvalues of $\overline{(R^\alpha(\omega)^\dagger R^\alpha(\omega))}$ at criticality, for two different discrete distributions of α. If α can take two values with equal probability (a), response and correlation functions exhibit two singularities, whereas if the two possible values have different probabilities (b), only the peak close to the most probable one becomes a singularity.

We have also considered anti-symmetric couplings which can only assume two different values with different probabilities. In this case, a genuine transition still exists: $\overline{(R^\alpha(\omega)^\dagger R^\alpha(\omega))}$ develops a singularity and an eigenvalue equal to 1 for the same value of ℓ (Fig. 6.9). This raises the intriguing possibility of two different scenarios for non-reciprocal interactions: (i) one characteristic of continuous distributions first evidenced by Crisanti and Sompolinsky, (ii) one characteristic of discrete distributions, whose simplest incarnation is the system analyzed in this paper. Physically, continuous vs discrete distributions indeed correspond to quite different situations, that we dub "microscopic" versus "macroscopic" non reciprocity. In the first case, we can think of the degree of non-reciprocity being independently fixed by each microscopic component. In the second case, we can decompose the systems in a finite number of sub-systems, each with a degree of non-reciprocity that is macroscopically fixed at the sub-system level.

6.7.2 Different interaction matrices

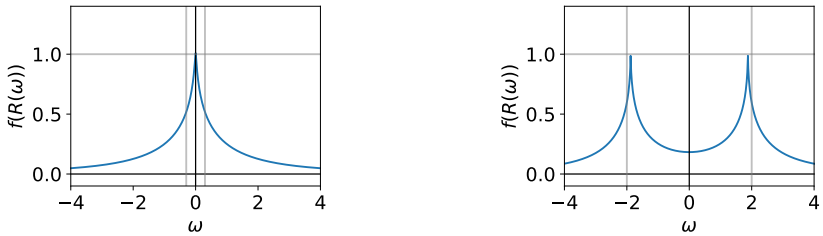

(a) $p_{\alpha=0.5} = p_{\alpha=5} = 0.5$ (b) $p_{\alpha=0.5} = 0.7$, $p_{\alpha=5} = 0.3$

Figure 6.10: $f(R)$ defined in Eq. (6.56) at the critical point (i.e. when it reaches 1) for $\rho = 0$, $\alpha = 0.3 < \alpha^*(0)$ (left) and $\alpha = 2$ (right). In both cases the functions are analytic, but very close to being singular at their peaks.

In many cases, it could be more realistic to consider two different interaction matrices for the two systems. To be as general as possible, we consider the case in which there is any amount

of correlation between J^1_{ij} and J^2_{ij}:

$$\overline{J^a_{ij}J^b_{ij}} = \frac{1}{N}(\delta_{ab} + (1-\delta_{ab})\rho) \ . \tag{6.47}$$

The dynamical equation becomes:

$$\dot{s_i}^a = \sum_j J^a_{ij}s^a_j - l_a s^a_i + \alpha \sum_b \epsilon_{ab}\sigma^b_i + \eta^a_i + h^a_i \ . \tag{6.48}$$

We can replicate the DMFT computation as in the previous cases. The main difference is that some ρ factors arise in the off-diagonal components of the memory terms and of the correlation of the noise:

$$\begin{aligned} \dot{s}^a = -l_a s^a + \sum_b \epsilon_{ab}\alpha s^b + \eta^a + h^a + \xi_a + \int_0^t dt' R_{aa}(t,t')s^a(t') + \\ + \sum_b (1-\delta_{ab})\rho \int_0^t dt' R^{ab}(t,t')s^b(t') \ , \end{aligned} \tag{6.49}$$

$$\langle \xi_a(t)\xi_b(t')\rangle = N\overline{J^a_{0j}J^b_{0j}}\mathbb{E}\left[s^a_i(t)s^b_i(t')\right] = \delta_{ab}C_{aa}(t,t') + (1-\delta_{ab})\rho C_{ab}(t,t') \ . \tag{6.50}$$

In order to write down in matrix form the self-consistent equations on R and C, it is convenient to define the matrices:

$$\tilde{R} = \begin{pmatrix} R_d & \rho R_a \\ -\rho R_a & R_d \end{pmatrix} \ , \qquad \tilde{C} = \begin{pmatrix} C_d & \rho C_a \\ -\rho C_a & C_d \end{pmatrix} \ . \tag{6.51}$$

The self-consistent equations, obtained as before, then read:

$$R(\omega) = ((-i\omega + l)\mathbb{1} - \tilde{R}(\omega) - A)^{-1} \ , \tag{6.52}$$

$$C(\omega) = (2T + \tilde{C}(\omega))R(\omega)R^\dagger(\omega) \ . \tag{6.53}$$

At small but finite α the response and correlation functions are peaked in $\omega = 0$ at all temperatures, whereas for $\alpha > \alpha^*(\rho)$ they develop two symmetric peaks at finite values of ω (Figure 6.10), signaling a damped oscillating behavior as in the case in which the two species have the same J. For $\rho = 0$ the equations simplify, and we can show that this crossover occurs at $\alpha^*(0) = 1/\sqrt{8}$.

The system has a critical point when the correlation function diverges. The solution for the diagonal and off-diagonal elements of C read:

$$C_d(\omega) = \frac{2T(|R_d|^2 + |R_a|^2 - \rho|R_d^2 + R_a^2|^2)}{1 - ((\rho+1)(|R_d|^2 + |R_a|^2) - \rho|R_d^2 + R_a^2|^2)} \ , \tag{6.54}$$

$$C_a(\omega) = \frac{2T(R_a R_d^* - R_d R_a^*)}{1 - ((\rho+1)(|R_d|^2 + |R_a|^2) - \rho|R_d^2 + R_a^2|^2)} \ . \tag{6.55}$$

Therefore the critical point will be when

$$f(R) = (\rho+1)(|R_d|^2 + |R_a|^2) - \rho|R_d^2 + R_a^2|^2 = 1 \ . \tag{6.56}$$

At any value of $\rho < 1$, when this condition is met the response function is not singular. As discussed before, this means that the system does not have a critical point at any finite temperature. Nevertheless, both for small ($\alpha \lesssim 0.3$) and large ($\alpha \gtrsim 1$) values of α, the response function is extremely close to being critical (Figure 6.10): in fact it would become critical for (unphysical) values of the Lagrange multipliers just below those reached when the correlation function diverges. This means that at moderate system sizes and not too long times the situation would be indistinguishable from a real phase transition to a spin glass phase at small α and an amorphous oscillating one at large α.

6.7.3 Coupling magnetization

Another possible coupling mechanism between the two clones is through their magnetization. Without ferromagnetic interactions inside each clone the magnetization is zero throughout the phase diagram, therefore the addition of non-reciprocity has no effect at all. Let us then consider the case in which each spin wants to align with the magnetization of its own system, and either align or antialign with the magnetization of the other:

$$\begin{cases} \dot{s}_i^1 = \sum_j J_{ij} s_j^1 - \ell^1 s_i^1 + \frac{\alpha_+}{N} \sum_j s_j^1 + \frac{\alpha_-}{N} \sum_j s_j^2 \\ \dot{s}_i^2 = \sum_j J_{ij} s_j^2 - \ell^2 s_i^2 + \frac{\alpha_+}{N} \sum_j s_j^2 - \frac{\alpha_-}{N} \sum_j s_j^1 \end{cases} \tag{6.57}$$

α_+ and α_- are the strengths of the reciprocal and non-reciprocal interactions. For simplicity we do not consider thermal fluctuations, but we do not expect a small temperature to dramatically change the behavior of the system.

The system exhibits a quite rich phenomenology. Its phase diagram, obtained from numerical simulations of Eq. (6.57), is represented in Figure 6.11. The colormaps represent different observables: $m^a = \frac{1}{N}\sum_j s_j^a$ is the magnetization of each of the systems, $m_{gs}^a = \frac{1}{N}\sum_j v_{\mu_0 j} s_j^a$ is the projection on the leading eigenvector of J. We indicate with $\langle m^a \rangle_t$ (and $\langle m_{gs}^a \rangle_t$) their average over time, and with $\Delta m^a = \frac{\max(m^a) - \min(m^a)}{2}$ (and Δm_{gs}^a) the amplitude of their oscillations. The same observables are also plotted as a function of α_- at constant $\alpha_+ = 1.7$ in Figure 6.12.

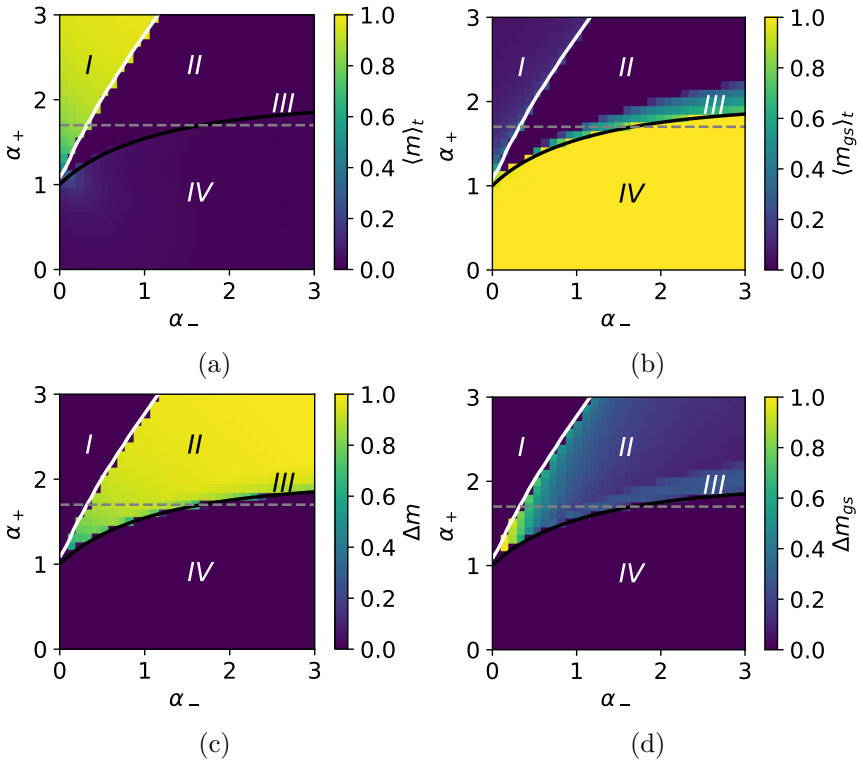

Figure 6.11: 4 phases: (I) finite static magnetization ($\langle m \rangle_t > 0$, $\Delta m = 0$). (II) magnetizations oscillate periodically ($\Delta m > 0$) and $\langle m_{gs} \rangle = 0$. (III) m_{gs} oscillates around a non zero value. (IV) $\langle m \rangle = 0$, $\langle m_{gs} \rangle \sim 1$. The black line indicates condition (6.61), the white line the disappearance of the solution of eq. (6.62), the gray dashed line the parameters used in Fig. 6.12. $N = 1500$.

At small values of α_+ (phase *IV* in the figures), the non-reciprocity plays no role, and the system converges at long times to the leading eigenvector of the interaction matrix. The absolute

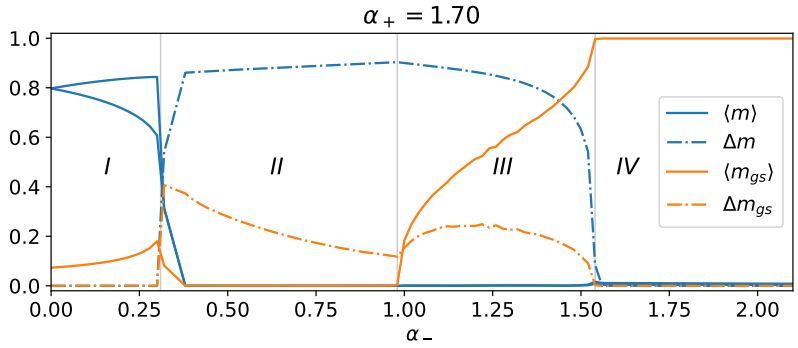

Figure 6.12: Order parameters as a function of α_- at fixed $\alpha_+ = 1.7$. $N = 4000$.

value of the projection of each of the clones on this eigenvector, m_{gs}, is asymptotically equal to 1 (Figure 6.11b). The dynamics is very similar to the one that we would find without non-reciprocity: the system exhibits aging. We can study the stability of this fixed point solution by linearizing around it:

$$\delta \dot{s}_i^a = \sum_j J_{ij} \delta s_j^a - \ell \delta s_i^a + \frac{\alpha_+}{N} \sum_j \delta s_j^a + \sum_b \epsilon_{ab} \frac{\alpha_-}{N} \sum_j \delta s_j^b \ . \tag{6.58}$$

At the fixed point $\ell^1 = \ell^2 = \ell = 2$. We define the $(2N \times 2N)$ stability matrix M such that

$$\delta \dot{\mathbf{s}} = M \delta \mathbf{s} \ . \tag{6.59}$$

If M has any positive eigenvalue, the fixed point is unstable (as we have seen before, the reverse is not true). The eigenvalues of M are the poles of its resolvent:

$$G(z) = (z\mathbb{1} - M)^{-1} \ . \tag{6.60}$$

If an instability occurs, because it would be due to the magnetization-mediated interactions, we expect the unstable mode to have some overlap with the vector of the fully magnetized states, that we denote as $|1_1\rangle$ and $|1_2\rangle$. We project the resolvent on this 2-dimensional space

$$\langle 1_1, 1_2 | \, G(z) \, | 1_1, 1_2 \rangle = \frac{1}{(z + \ell - g(z+\ell))\mathbb{1} - \begin{pmatrix} \alpha_+ & \alpha_- \\ -\alpha_- & \alpha_+ \end{pmatrix}} \ .$$

$g(z) = \frac{z - z\sqrt{1-4/z^2}}{2}$ is the Stieltjes transform of J [269]. Solving for the poles of the projected resolvent we find:

$$z = -\ell + \alpha_+ \left(1 + \frac{1}{\alpha_+^2 + \alpha_-^2}\right) \pm i\alpha_- \left(1 - \frac{1}{\alpha_+^2 + \alpha_-^2}\right) \ .$$

The real part of the eigenvalue becomes positive when

$$\alpha_+ \left(1 + \frac{1}{\alpha_+^2 + \alpha_-^2}\right) = 2 \ . \tag{6.61}$$

This condition is plotted in black in Figure 6.11, it perfectly agrees with numerical results. For non-zero α_- the transition is retarded, and when it occurs the unstable eigenvalue is complex, hinting to a transition to an oscillating phase. For $\alpha_- = 0$ we recover the known result for

the phase transition to a ferromagnetic state at $\alpha_+ = 1$; for $\alpha_- \to \infty$ the ground state of the interaction matrix loses stability at $\alpha_+ = 2$.

At very strong values of α_+ (phase I in the figures) the system converges to a fixed point with finite magnetizations m_1 and m_2. At the fixed point the magnetizations and the Lagrange multipliers satisfy:

$$\begin{cases} (\alpha_+^2 + \alpha_-^2) g(\ell^1) g(\ell^2) - \alpha_+ (g(\ell^1) + g(\ell^2)) + 1 = 0 \\ m_1 = \frac{\alpha_- g(\ell^1)}{1 - \alpha_+ g(\ell^2)} m_2 \\ (\alpha_+ m_1 + \alpha_- m_2)^2 \frac{g(\ell^1)}{\sqrt{(\ell^1)^2 - 4}} = 1 \\ (\alpha_+ m_2 - \alpha_- m_1)^2 \frac{g(\ell^2)}{\sqrt{(\ell^2)^2 - 4}} = 1 \end{cases} \tag{6.62}$$

Studying when this system of equations stops having a solution, we find the phase boundary of the magnetized phase, indicated in white in Figure 6.11. Again there is very good agreement with numerical simulations.

Between the two phases described so far, there is an extended region in which the system exhibits strong oscillations. This region is actually composed of two phases. In phase *II*, each clone rotates around the origin: both m and m_{gs} show strong oscillations, but their time average is zero. In phase *III*, each clone rotates around a vector with a finite projection on the leading eigenvector of J, so that $\langle m_{gs} \rangle_t \neq 0$. By Principal Component Analysis we see that in phase *II* the system explores a space spanned by two vectors, whereas in phase *III* it explores a space spanned by three vectors. Also in phase *III* we encounter aging behavior.

6.8 Conclusions

In this Chapter, we have studied a system composed of two antagonistically coupled complex agents, whose internal dynamics we modeled as spin-glasses. Contrary to what was believed after the seminal work [13], we showed that non-reciprocal interactions do not necessarily destroy glassy dynamics, but they can enrich it with novel features. The phase transition associated with the emergence of a simple spin-glass order is replaced by a different kind of symmetry breaking, in which the system starts to oscillate. The destabilization of the ordinary spin-glass phase is mediated by a spectral singularity called exceptional point. The oscillations have a frequency that is uniquely controlled by the non-reciprocity, while their envelope exhibits a slow evolution akin to the one found in a single spin-glass. At long times the two spin-glasses rotate on their two lowest energy modes, spontaneously breaking chiral symmetry. This rotating state shares certain similarities with the one observed in the absence of internal spin-glass dynamics, yet it also exhibits important differences: it is robust to the introduction of thermal fluctuations and to the departure from perfect antisymmetry in the interactions; the plan of rotation is fixed and independent of initial conditions, but depends on the realization of the internal dynamics, so that the oscillations would not be visible in the magnetization.

Crucially, this behavior only arises if all microscopical components of the two spin-glasses have the same non-reciprocal coupling, or if they can be divided in a finite number of subsets with the same couplings. This leads us to hypothesize the existence of two classes of non-reciprocally coupled disordered systems: one in which the non-reciprocity is coherently set on macroscopic portions of the systems, and one in which each microscopic component independently chooses its degree of non-reciprocity from a continuous distribution, with aging only surviving in the first case.

How these results generalize to more complex glassy systems is an open question certainly worth further investigation, and with potential implications for many complex biological systems.

In the next Chapter, we present some preliminary results on the non-reciprocal coupling of other aging systems.

Chapter 7

Non reciprocal couplings in other aging models

In this chapter, I discuss some preliminary results and ongoing work on the effect of non-reciprocal interactions in other aging models, namely coarsening Ising models, the p-spin model and the trap model. As we will see, the aging behavior in coarsening systems has some deep analogies to the one of the spherical SK model. This analogy carries on to the non-reciprocal case, which is found to be a simple generalization of the results of the previous chapter. We expect the picture to be more complex in systems in which the aging behavior relies on different mechanisms. Indeed, new phenomena emerge when coupling non-reciprocally two p-spin models. To extend our results to systems in which aging is due to barrier crossings, we propose to study two non-reciprocally coupled trap models. These projects are carried out in collaboration with Raphael Urfin for the p-spin model, and with Mattia Scandolo for the trap model.

7.1 Limitations of the spherical Sherrington-Kirkpatrick model

In the previous chapter, we have seen that if we couple non-reciprocally two identical spherical Sherrington-Kirkpatrick (SK) models, below a critical temperature they undergo aging, while also exhibiting oscillations. The system has two independent timescales: a short one, which only depends on the non-reciprocity and sets the frequency of the oscillations, and a long one, proportional to the age of the system, which controls the decay of correlations. In this chapter, we investigate how this behavior generalizes to other aging systems. We first review some limitations that already emerged from the study of the spherical SK model, which could hint at potential challenges in extending our results to more complex models.

We have seen that aging is only found if the non-reciprocity introduces a finite set of oscillation timescales. In our model the linearity of the dynamical equations guarantees that if we impose the same non-reciprocal coupling to all components, a single oscillation frequency is generated. However, in strongly non-linear systems, such as the p-spin model, even if we introduce a unique non-reciprocal coupling, the non-linearities in the system can generate other frequencies, possibly leading to more complex behavior.

It is also essential that the two parts of the system experience the same disorder, so that they can push and pull each other along the same soft modes. In models with more complex energy landscapes, such as the p-spin model, it would not be sufficient to impose the same realization of the interaction tensor: two systems starting from independent initial conditions could end up in very different regions of the phase space, in which their soft modes would be completely unrelated.

Lastly, in the spherical SK model aging derives solely from the presence of marginal directions. As we have discussed in the introduction, aging can also be due to trapping in increasingly deep states, which require longer and longer times to escape from. How the non-reciprocity would impact such an activated dynamics is still an open question.

7.2 Coarsening Ising models

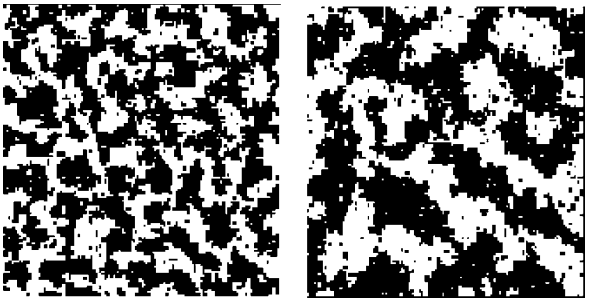

Figure 7.1: Snapshots at two different times ($t = 10^3$ and $t = 10^5$, measured in Monte Carlo steps) of a 2D section of a three-dimensional Ising model evolving with Glauber dynamics after a quench from a high temperature to a temperature below the ferromagnetic transition. Reproduced from reference [139].

As we explained in Section 5.2.1, if we quench a system below a second order phase transition it will generically fall out of equilibrium and display aging, because it takes a long time (diverging with the number of degrees of freedom) to equilibrate from a symmetric to a symmetry-broken state. This phenomenon can be studied in detail in the case of a three-dimensional Ising model quenched from a temperature above to one below the phase transition [236]. Interestingly, the out-of-equilibrium dynamics of this system shares many analogies with the aging behavior of a spherical SK model [267]. Both systems have only two minima of the energy, related by inversion symmetry. Starting from an initial condition with a macroscopic overlap with one of the two, they relax exponentially to it, but if instead we initialize them in a random configuration they remain forever undecided on which state to pick. These analogies become a formal mapping if we perform a Hartree-Fock approximation on the coarsening dynamics [332]. The connection carries on to the non-reciprocal case: we will see that the correlation functions of two non-reciprocally coupled quenched Ising models are also simply dressed by some oscillations of frequency α.

We now review the derivation of the aging behavior of a single Ising model under the Hartree-Fock approximation, adapted from [139].

7.2.1 Aging dynamics

In Figure 7.1, we report two snapshots of the dynamics of an Ising model quenched from a very high temperature to one below the critical point. As time goes on (from the left to the right picture), the system separates in uniform domains of positive or negative magnetization (represented in white and black respectively) of increasing size.

For simplicity we will consider a quench from infinite to zero temperature, but the results are easily generalizable to finite temperatures. The large-scale behavior of the system can be understood by studying the coarse grained magnetization ϕ, whose dynamics is described by:

$$\partial_t \phi = \nabla^2 \phi - V'(\phi), \tag{7.1}$$

where $V(\phi) = -\frac{m^2}{2}\phi^2 + \frac{g}{4}\phi^4$ is a double well potential. The potential is minimized for $\phi = \pm\sqrt{m^2/g}$, whereas the Laplacian term will favor uniform configurations. The initial condition $\phi(x,0)$ is uniformly sampled at infinite temperature, so that it is delta correlated in space:

$$\langle \phi(x,0)\phi(x',0)\rangle = \sigma\delta(x-x') \ . \tag{7.2}$$

These random initial conditions play the role of quenched disorder in this system. To obtain some analytical understanding of the behavior of the system, we perform a Hartee-Fock approximation, replacing the non-linear term $g\phi^3$ by $g\phi\langle\phi^2\rangle$, where $\langle\phi^2\rangle$ is a self-consistently determined average over initial conditions. This approximation becomes exact if we generalize the field ϕ to an N-components field $\vec{\phi}$ with potential $V(\vec{\phi}) = -\frac{m^2}{2}\vec{\phi}^2 + \frac{g}{4N}(\vec{\phi}^2)^2$ (which is known as the $O(N)$ model [333]), and we take the limit $N \to \infty$. Under this approximation the dynamics becomes:

$$\partial_t\phi(x) = \nabla^2\phi(x) + m^2\phi(x) - g\langle\phi^2\rangle\phi(x) \ . \tag{7.3}$$

We can diagonalize it by going to Fourier space:

$$\partial_t\vec{\phi}(k) = (-k^2 + m^2 - g\langle\phi^2\rangle)\vec{\phi}(k) = (-k^2 + a(t))\vec{\phi}(k) \ , \tag{7.4}$$

where $a(t) = m^2 - g\langle\phi^2(x,t)\rangle$ has to be computed self-consistently. The situation is very similar to the spherical SK model: we have a linear dynamics, and different modes are only coupled through a coefficient that has to be computed self-consistently. In 3 spatial dimensions, the density of states of plane waves is $\rho(k) \propto k^2$. If we define $\mu = k^2$, we find $\rho(\mu) = \rho(k)dk/d\mu \propto \sqrt{\mu}$: as for the spherical SK model, the density of states vanishes as a square root at the border of the spectrum. This, together with the self-consistency conditions, turns out to be a crucial feature, leading to the same aging behavior in the two models. Indeed, as for the spherical SK model, we can formally write the time-dependent solution in terms of the unknown function $a(t)$:

$$\phi(k,t) = \phi(k,0)e^{-k^2t + \int_0^t a(t')dt'} \ . \tag{7.5}$$

We can then compute the averaged squared field:

$$\langle\phi^2(x,t)\rangle = \sigma\int\frac{dk^3}{(2\pi)^3}e^{-2k^2t+2\int_0^t a(t')dt'} = \frac{\sigma}{(8\pi)^{3/2}}e^{2\int_0^t a(t')dt'}t^{-3/2} \ . \tag{7.6}$$

We expect $\langle\phi^2(x,t)\rangle$ to converge at long times to a finite value, m^2/g. This is only possible if the two time-dependent factors compensate each other:

$$e^{2\int_0^t a(t')dt'} \propto t^{3/2} \ , \tag{7.7}$$

which means that $a(t)$ has to scale as:

$$a(t) \simeq \frac{3t_0}{4t} \ . \tag{7.8}$$

By imposing $\langle\phi^2(x,t)\rangle \to \frac{m^2}{g}$, we can also obtain the constant $t_0 = \frac{1}{8\pi}\left(\frac{\sigma g}{m^2}\right)^{2/3}$. We can now compute the correlation function:

$$\begin{aligned}\langle\phi_i(x,t)\phi_i(x',t')\rangle &= \sigma\left(\frac{t}{t_0}\right)^{3/4}\left(\frac{t'}{t_0}\right)^{3/4}\int\frac{dk^3}{(2\pi)^3}e^{ik(x-x')}e^{-k^2(t+t')} = \\ &= \frac{m^2}{g}\frac{(tt')^{3/4}}{((t+t')/2)^{3/2}}e^{-\frac{(x-x')^2}{4(t+t')}} = \frac{m^2}{g}\left(\frac{2\sqrt{1+\Delta t/t'}}{2+\Delta t/t'}\right)^{\frac{3}{2}}e^{-\frac{(x-x')^2}{4(t+t')}} \ ,\end{aligned} \tag{7.9}$$

where $\Delta t = t - t'$. The power law dependence on time is exactly the same found in Eq. (5.37) for the spherical SK model. Let us analyze the various regimes in time and space separation. If we take a fixed $x - x' \sim O(1)$, and long, not very separated times $t' \gg 1$, $\Delta t/t' \ll 1$, we find $\langle \phi_i(x,t)\phi_i(x',t')\rangle \sim m^2/g$: at long times any finite region has constant magnetization $\pm\sqrt{m^2/g}$. At fixed times, correlations decay in space over a growing length scale $L(t) \sim \sqrt{t}$. Correlations also fall to zero if $\Delta t \gg t'$: the time scale of the dynamics is proportional to age of the system. In conclusion, at long times the system is composed of uniform domains of constant magnetization $\pm\sqrt{m^2/g}$ and size $L(t) \sim \sqrt{t}$, which rearrange over times proportional to the age of the system.

7.2.2 Non-reciprocal aging

Let us now take *two* Ising systems, and couple non-reciprocally corresponding spins in the two systems. This is precisely the "non-reciprocal Ising model" introduced in references [291, 304]. Their coarsening dynamics from infinite to zero temperature is described by the coupled field theories:

$$\partial_t \phi_1(x) = \nabla^2 \phi_1(x) + m^2 \phi_1(x) - g\phi_1^3(x) + \alpha \phi_2(x) \tag{7.10}$$

$$\partial_t \phi_2(x) = \nabla^2 \phi_2(x) + m^2 \phi_2(x) - g\phi_2^3(x) - \alpha \phi_1(x) \tag{7.11}$$

The initial conditions are sampled independently at infinite temperature, so that they are as before δ-correlated in space:

$$\langle \phi_i(x,0)\phi_j(x',0)\rangle = \sigma \delta_{ij}\delta(x-x') \ . \tag{7.12}$$

We again perform an Hartree-Fock approximation (which can be justified in a $O(N)$ model in the limit $N \to \infty$), and replace the non-linear term $g\phi_a^3$ by $g\phi_a\langle\phi_a^2\rangle$, where $\langle\phi_a^2\rangle$ is a self-consistently determined average over initial conditions. We can then diagonalize the dynamics in Fourier space. Collecting the two fields in a vector $\Phi(k,t) = \begin{pmatrix}\phi_1(k,t)\\ \phi_2(k,t)\end{pmatrix}$, we obtain:

$$\partial_t \Phi(k) = \begin{pmatrix} -k^2 + a_1(t) & \alpha \\ -\alpha & -k^2 + a_2(t)\end{pmatrix} \Phi(k) \ , \tag{7.13}$$

where $a(t) = m^2 - g\langle\phi^2(x,t)\rangle$. Because of the symmetry of the system under the exchange of the two fields and the reversal of one of the two, we expect $a_1(t) = a_2(t) = a(t)$. As for the Lagrange multipliers in the case of the SK model, this simplifies the analysis because the diagonal and off-diagonal components of the matrix commute. We therefore obtain the formal solution for Φ:

$$\Phi(k,t) = e^{-k^2 t + \int_0^t a(t')dt'} \begin{pmatrix} \cos\alpha t & \sin\alpha t \\ -\sin\alpha t & \cos\alpha t\end{pmatrix} \Phi(k,0) \ . \tag{7.14}$$

As in the single system case, this is finite at long times only if $a(t) \simeq \frac{3t_0}{4t}$. Computing as before the auto-correlation function, we find:

$$\langle \phi_a(x,t)\phi_a(x',t')\rangle = \frac{m^2}{g}\left(\frac{2\sqrt{1+\Delta t/t'}}{2+\Delta t/t'}\right)^{\frac{3}{2}} e^{-\frac{(x-x')^2}{4(t+t')}} \cos(\alpha(t-t')) \ . \tag{7.15}$$

The cross-correlation function $\langle \phi_1(x,t)\phi_2(x',t')\rangle$ has the same form, with the cosine replaced by a sine function. As in the single system case, there is a growing length scale $L(t) \sim \sqrt{t}$. Each of the two systems is composed of domains of size $L(t)$ and uniform magnetization, which

rearrange over a timescale proportional to the age of the system. However, their magnetization is not constant in time anymore, but oscillates at frequency α.

The coarsening dynamics of two non-reciprocally coupled 3D Ising models starting from random initial conditions was numerically studied in [304]. They report that an important role is played by lines of topological defects, around which scroll waves rotate. Defect lines, initially arranged in a complex mixture, gradually merge into rings that shrink and disappear, until a uniform oscillating phase is reached ("swap phase"). Sometimes the system remains trapped in long-lived metastable states with macroscopic scroll waves or planar waves.

This interesting dynamics is not captured by our analysis. However, as we discussed in Section 5.3.3, the non-reciprocal Ising model strongly differs from the non-reciprocal $O(N)$ one for $N > 1$, and our analysis is only exact in the limit $N \to \infty$. First of all, for $N > 1$ in addition to the swap phase, in which the order parameter oscillates in magnitude, there is also a chiral phase, in which the order parameter has fixed modulus and rotates in a plane [294, 295]. We expect this second behavior to occur in the case we are considering, in analogy to the behavior of two non-reciprocally coupled vectors described in Section 5.3.2. Moreover, for $N = 1$ the system only has to break the $O(2)$ symmetry related to the phase of the periodic oscillations, and indeed the system falls in the equilibrium XY universality class. For $N > 2$, instead, the system also needs to select a (hyper-)plane on which to rotate. Selecting this plane requires breaking an $O(N)$ symmetry, and could therefore lead to a coarsening dynamics more similar to the one found in the uncoupled case. This could be well described by our results. For $N = 2$ there is no freedom in the choice of the plane of rotation, but the sense of rotation has to be selected, which corresponds to breaking a $\mathbb{Z}_2$ symmetry. The coarsening dynamics could therefore also be qualitatively well captured by our analysis.

The coarsening dynamics in a non-reciprocal $O(N)$ model for $N > 1$, has never been studied numerically done to our knowledge; this would be an interesting direction for future research.

7.3 Spherical p-spin models

The spherical p-spin model [160, 334] is a generalization of the spherical SK model in which instead of 2-body interactions we consider p-body ones, with $p > 2$ (for $p = 2$ we recover the SK model):

$$\dot{s}_i = \frac{1}{(p-1)!} \sum_{i_2,\dots i_p} J_{i,i_2,\dots i_p} s_{i_2} \dots s_{i_p} - \ell s_i + \eta_i^s \ . \tag{7.16}$$

The interaction tensor J is symmetric under any permutation of the indices. Its elements have mean zero and variance $\frac{1}{N^{p-1}}$, where N is the number of spins, to ensure a well-behaved $N \to \infty$ limit. While for $p = 2$ the energy landscape is very simple, with only 2 ground states related by inversion symmetry and separated by sub-extensive barriers, in the p-spin a crucial role is played by metastable states. The energy landscape features many saddle points, whose number of unstable modes depends on their energy. Under a given energy density threshold E_{th}, typical saddle points have no unstable mode, meaning they are minima. At E_{th} the saddle points are *marginal*: they have some modes with vanishing eigenvalues, just as the ground state of the spherical SK model. The system undergoes a thermodynamic phase transition between a paramagnetic and a spin-glass phase at a temperature T_s, which can be obtained by studying the equilibrium Boltzmann distribution, for example through the replica method. However, at $T_d > T_s$ there is a *dynamical* phase transition, at which the relaxation time diverges. Starting from random initial conditions, in the $N \to \infty$ limit the system approaches asymptotically the threshold energy, but never penetrates below it, so that it is always in a marginal state. For

$p > 2$, the qualitative behavior of the system does not change with p (at least if a single value of p is considered [220, 221]).

The divergence of the relaxation time can be shown by studying the self-consistent equations on the response and correlation functions that can be obtained through Dynamical Mean Field Theory [160]:

$$\begin{aligned}\frac{\partial C(t,t')}{\partial t} &= -\ell(t)C(t,t') + 2TR(t',t) + \\ &+ \int_{-\infty}^{t'} dt'' R(t',t'')D(t,t'') + \int_{-\infty}^{t} dt'' \Sigma(t,t'')C(t'',t')\end{aligned} \tag{7.17}$$

$$\frac{\partial R(t,t')}{\partial t} = -\ell(t)R(t,t') + \delta(t,t') + \int_{t'}^{t} dt'' \Sigma(t,t'')R(t'',t') \tag{7.18}$$

$$\ell(t) = T + \frac{p^2}{2}\int_0^t dt'' R(t,t'')C(t,t'')^{p-1} \ , \tag{7.19}$$

where

$$D(t,t') = \frac{p}{2}C(t,t')^{p-1} \ , \tag{7.20}$$

$$\Sigma(t,t') = \frac{p(p-1)}{2}R(t,t')C(t,t')^{p-2} \ . \tag{7.21}$$

These are the same kind of equations that can be obtained from the Mode Coupling Approximation in supercooled liquids. Since they are non-linear, their solution is not as simple as for the $p = 2$ case considered in the previous chapter. They can however be integrated numerically.

7.3.1 Non-reciprocal coupling

As a first step in the study of non-reciprocal aging in more complex glassy systems, we can consider two non-reciprocally coupled spherical p-spin models[1]:

$$\dot{s}_i^a = \frac{1}{(p-1)!}\sum_{i_2,\dots i_p} J_{i,i_2,\dots i_p} s_{i_2}^a \dots s_{i_p}^a - \ell^a s_i^a + \sum_b \alpha \epsilon_{ab} s_i^b + \eta_i^a \ . \tag{7.22}$$

Even though we are again considering only one value of the non-reciprocal coupling α, the non-linearities in the system can now lead to the generation of many timescales, possibly destroying aging.

7.3.2 Numerical simulations

We first studied numerically the dynamics of two non-reciprocally coupled p-spin systems (Eq. (7.22)), for $p = 3$. The simulations are numerically challenging because the 3-body fully connected interactions lead to a scaling as N^3 of the simulation time. For this reason, we could only explore moderate system sizes ($N = 100$) and times ($t_{max} = 600$).

In Figure 7.2 we plot the autocorrelation function for different waiting times t_0 as a function of the time interval τ, averaged over many runs of the dynamics. For $\alpha = 0$ (top) the system exhibits aging both at $T = 0.1$ (left) and at $T = 0.5$ (right). Indeed the dynamical phase transition temperature for this model is $T_d = \sqrt{\frac{p(p-2)^{p-2}}{2(p-1)^{p-1}}} \approx 0.61$. For strong non-reciprocal coupling ($\alpha = 1$, bottom), aging is suppressed at both temperatures: the correlation functions

[1] This study was conducted in collaboration with Raphael Urfin, who carried out the numerical integration of the DMFT equations, while I contributed to the analysis of the results and performed the numerical simulations.

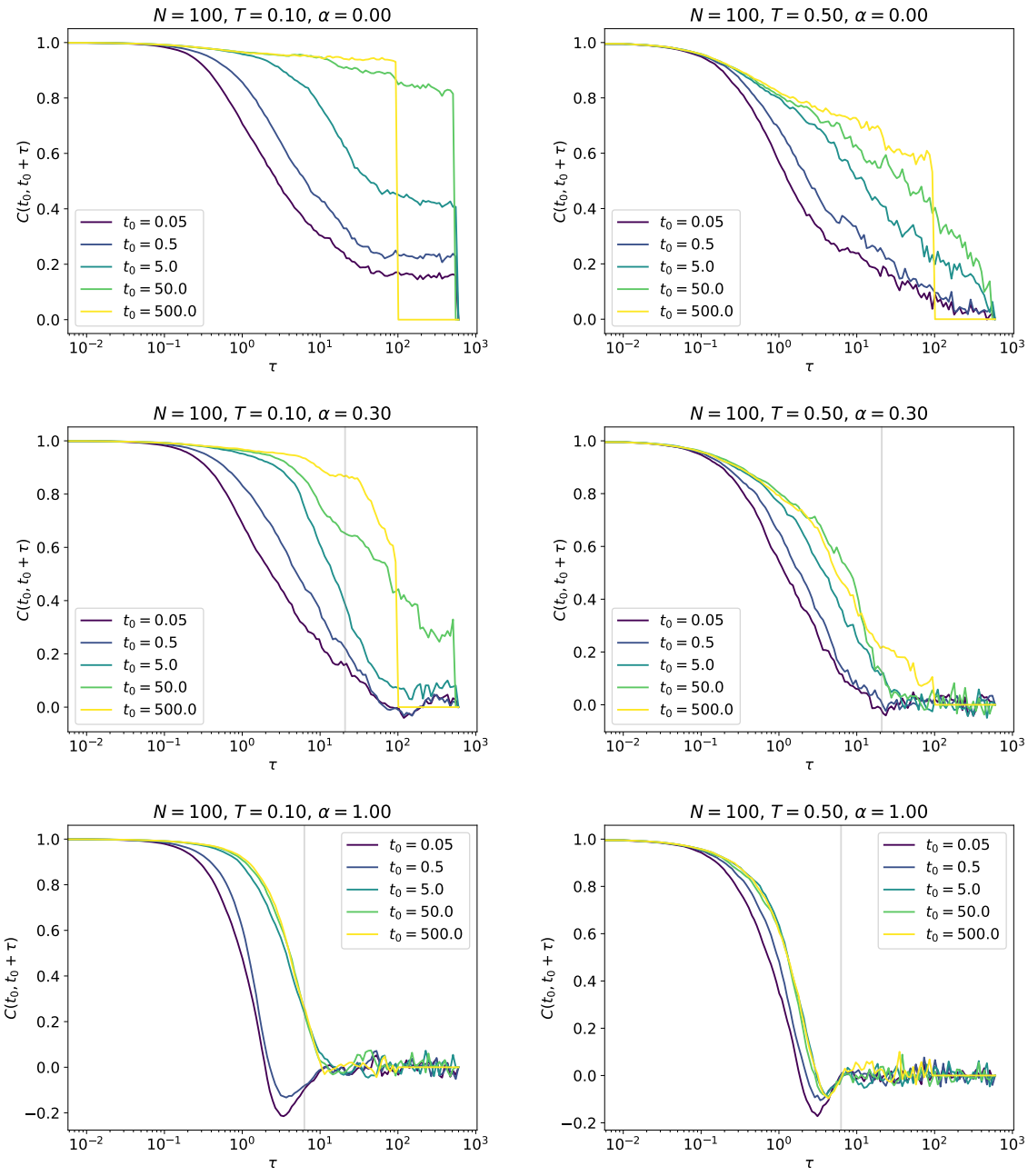

Figure 7.2: Correlation function in log time, averaged over 55 runs with the same interaction tensor J. The gray line represents the timescale associated with the non reciprocity $\frac{2\pi}{\alpha}$. The fact that for $\alpha = 0$ the plateau of the correlation function seems to depend on the waiting time could indicate that the system has penetrated below the threshold energy, and is exploring stable minima, which is expected at finite N [335].

reach a time-translational invariant regime, in which they decay on the timescale associated with the non-reciprocity $\frac{2\pi}{\alpha}$. However, at moderate values of the non-reciprocal coupling ($\alpha = 0.3$, middle), we see that the correlation functions do not reach a time-translational invariant regime (at least at $T = 0.1$) and in particular do not decay on the timescale $\frac{2\pi}{\alpha}$. This could be an indication that aging can survive the introduction of a finite but moderate non-reciprocity, possibly under an interaction-dependent dynamical temperature $T_d(\alpha)$.

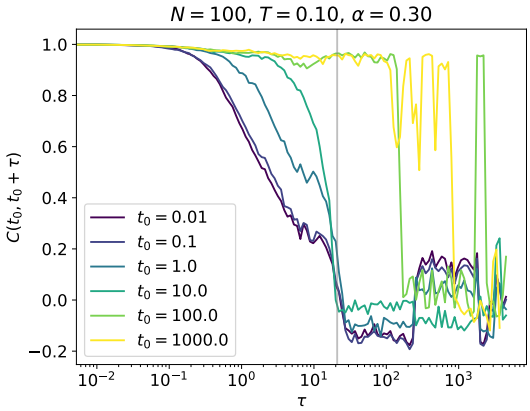

Figure 7.3: Correlation function in log time in a single run. The gray line represents the timescale associated with the non reciprocity $\frac{2\pi}{\alpha}$.

However, looking at the correlation function in a single run of the dynamics, we sometimes observe a peculiar behavior, shown in Figure 7.2, that could be indicative of strong finite size effects in our system. The correlation function exhibits at long times sudden jumps from small values to values close to 1, indicating that the system is jumping back to a state it had previously visited. This intermittent dynamics suggests that the system is exploring stable minima, and not marginal saddles, as it should do in the thermodynamic limit. This phenomenology is reminiscent of the one described in [313] for a finite size p-spin ($N = 50$) with random non-reciprocal interactions. In that case, however, the system explored a different minima at each jump. The fact that our system returns over and over again to the same minima, is a non trivial effect of the run and chase dynamics, which would require more careful exploration.

Note also that for $p = 3$ the single-system energy landscape is not symmetric under the reversal of all spins. This breaks the equivalence between the two systems: there is no symmetry operation that exchanges their labels. Moreover, it makes it impossible for the system to rotate in some low-energy manifold, as it was the case for $p = 2$, because during the rotation the energy would change sign from a very negative value to a very positive one.

The equivalence of the two systems and the symmetry of the energy landscape under spin reversal can be recovered by considering $p = 4$. However, this would lead to a scaling as N^4 of the simulation time, which makes it unfeasible to explore sufficiently large system sizes and times.

7.3.3 Numerical integration of the equations on correlation and response

To avoid finite size effects and to be able to study arbitrary values of p, we turned to the numerical solution of the DMFT equations, which are derived in Appendix B.2 via the cavity method:

$$\dot{s}_a = -l_a s_a + \alpha \sum_b \epsilon_{ab} s_b + \eta_a + \xi_a + \frac{p(p-1)}{2} \int_{-\infty}^{t} dt' \sum_b R_{ab}(t,t') C_{ab}(t,t')^{p-2} s_b(t') \ , \qquad (7.23)$$

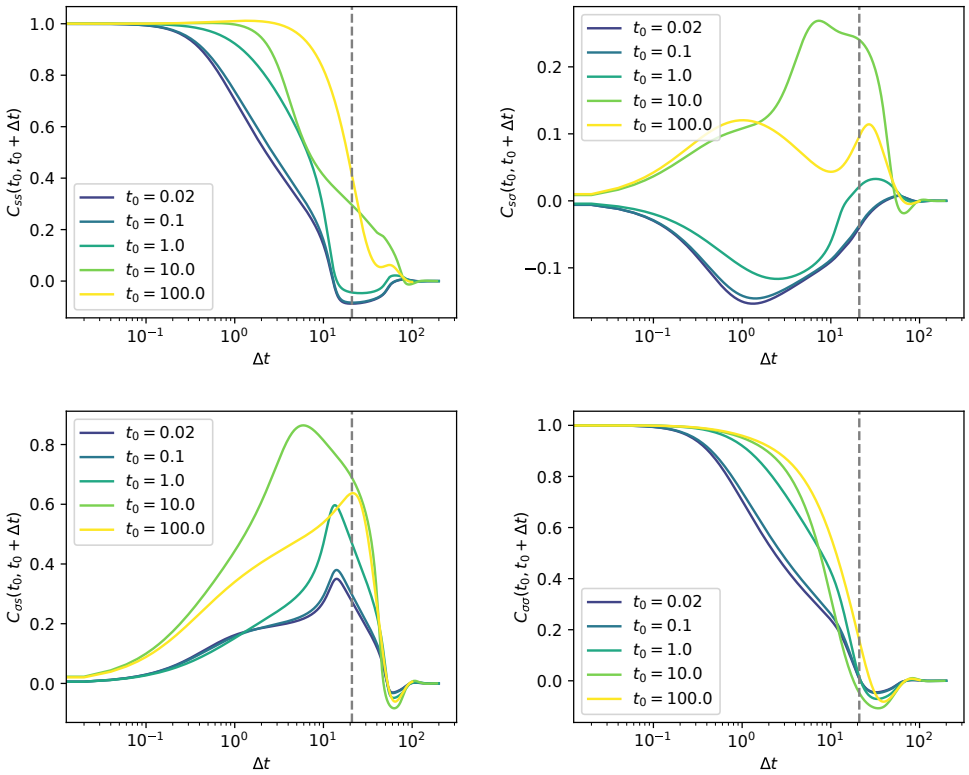

Figure 7.4: The four elements of the correlation function for $p = 3$, obtained by integrating numerically the DMFT equations (7.24)-(7.25). Since for odd p the two systems are not equivalent, all for correlation functions are different. s labels system 1, σ system 2. The gray line represents $\frac{2\pi}{\alpha}$, which is the timescale associated with the non reciprocity. $\alpha = 0.3$, $T = 0$.

where R and C are the matrices containing the response and correlation functions, to be computed self-consistently, and ξ is a Gaussian noise with correlations $\langle \xi_a(t)\xi_b(t')\rangle = C_{ab}(t,t')$.

Two different approaches are possible to obtain the correlation and response functions. The first, following reference [66], consists in simulating Eq. (7.23) with some initial ansatz of C and R, updating the ansatz with the measured correlation and response function, and iterating the procedure until convergence.

In the case of the p-spin, we can also obtain closed integro-differential equations on C, R and ℓ:

$$\begin{aligned}\frac{\partial C(t,t')}{\partial t} &= -\Lambda(t)C(t,t') + \alpha\epsilon C(t,t') + 2TR(t',t) + \\ &+ \frac{1}{2}\int_{-\infty}^{t'} dt'' R(t',t'')\left(D(t,t'') + D(t,t'')^T\right) + \int_{-\infty}^{t} dt'' \Sigma(t,t'')C(t'',t') \ ,\end{aligned} \tag{7.24}$$

$$\frac{\partial R(t,t')}{\partial t} = -\Lambda(t)R(t,t') + \alpha\epsilon R(t,t') + \delta(t,t')\mathbb{1} + \int_{t'}^{t} dt'' \Sigma(t,t'')R(t'',t') \ , \tag{7.25}$$

where Λ is the diagonal matrix containing the two Lagrange multipliers, which are given by

$$\ell_a(t) = T + \frac{p}{2}\left(p - \frac{1}{2}\right)\sum_b \int_0^t dt'' R_{ab}(t,t'')C_{ab}(t,t'')^{p-1} + \tag{7.26}$$

$$+ \frac{p}{4}\sum_b \int_0^t dt'' R_{ab}(t,t'')C_{ba}(t,t'')^{p-1} \ , \tag{7.27}$$

and

$$D(t,t') = \frac{p}{2}\begin{pmatrix} C_{11}(t,t')^{p-1} & C_{12}(t,t')^{p-1} \\ C_{21}(t,t')^{p-1} & C_{22}(t,t')^{p-1}\end{pmatrix} \tag{7.28}$$

$$\Sigma(t,t') = \frac{p(p-1)}{2}\begin{pmatrix} R_{11}(t,t')C_{11}(t,t')^{p-2} & R_{12}(t,t')C_{12}(t,t')^{p-2} \\ R_{21}(t,t')C_{21}(t,t')^{p-2} & R_{22}(t,t')C_{22}(t,t')^{p-2}\end{pmatrix} \ . \tag{7.29}$$

With both approaches the numerical complexity does not scale with N anymore (we are working in the thermodynamic limit), but it becomes quadratic with the number of time steps. We were therefore only able to go to $t_{max} = 200$. The second approach, solving the integro-differential equations on C and R, is more numerically efficient.

A first striking observation is that the behavior of the system is dramatically different for p even and odd, unlike in the case of a single p-spin model, whose qualitative behavior does not depend on p for $p > 2$.

For $p = 3$ the correlation functions never exhibit long-lived oscillations, and always converge to zero (Figure 7.4). For large α, the system becomes time-translational invariant, and decorrelates from initial conditions on a timescale proportional to $1/\alpha$. The fact that the system decorrelates from initial conditions even at zero temperature indicates that it is undergoing chaotic dynamics [285]. For smaller values of α, the correlation function does not attain a time-translationally invariant form within the accessible time window. However, we conjecture that aging is interrupted on a timescale that grows faster than $1/\alpha$.

In Figure 7.5, we plot the diagonal element of the correlation function for $p = 4$, for different values of α and T. We distinguish three different qualitative behaviors.

At small values of the temperature and of the non-reciprocal coupling (in blue in Figure 7.5), the decay of the correlation function becomes increasingly slow with time, and the system never becomes time-translational invariant (TTI) in the available time window. However, we cannot exclude that aging is interrupted on a timescale that diverges faster than $1/\alpha$.

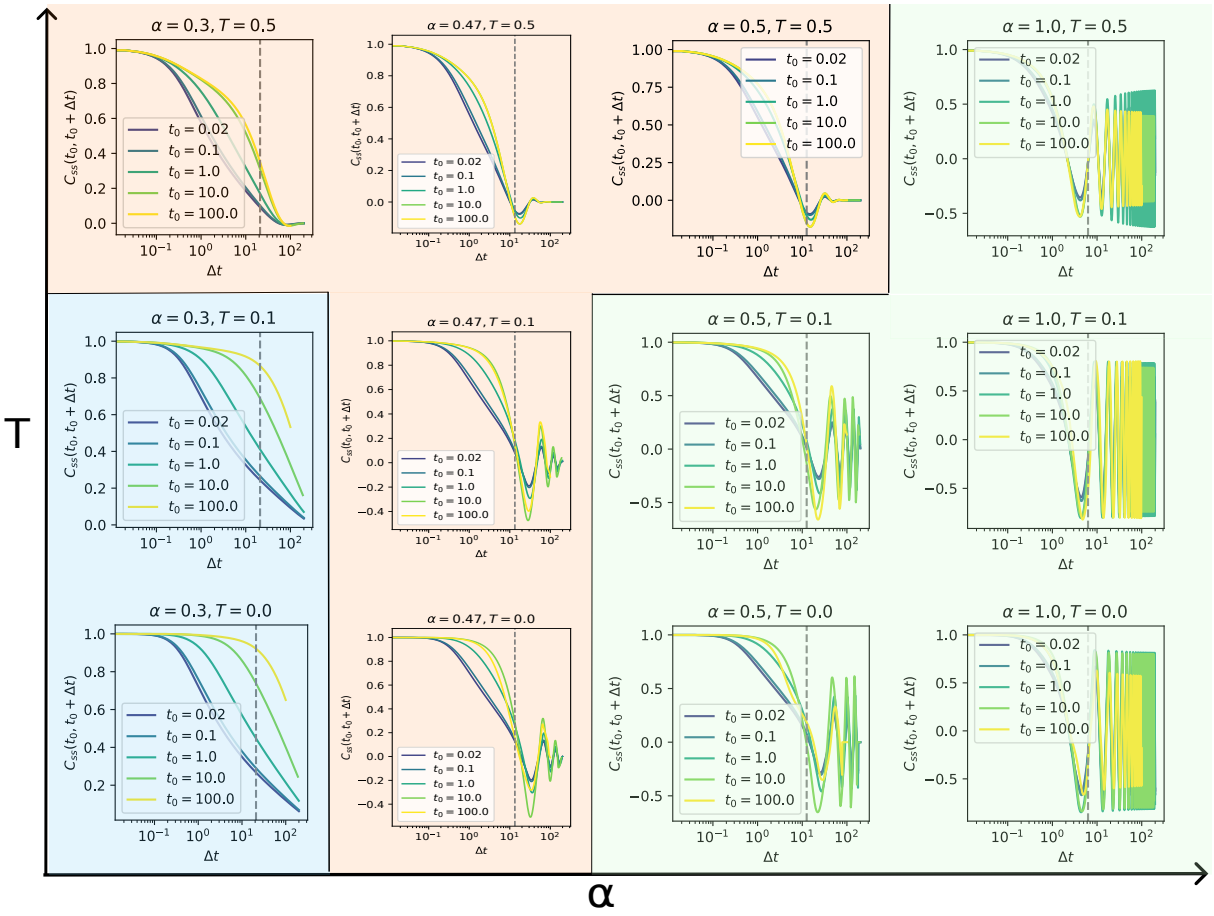

Figure 7.5: Auto-correlation function for $p = 4$, obtained by integrating numerically the DMFT equations (7.24)-(7.25), for different values of α and T. Different colors represent different qualitative regimes: in the blue region we have aging in the available time frame, in the orange region the system becomes time-translationally invariant, in the green region we have undumped oscillations, with oscillating envelope. The gray line represents $\frac{2\pi}{\alpha}$, which is the timescale associated with the non reciprocity. The values of α and T are not linearly scaled.

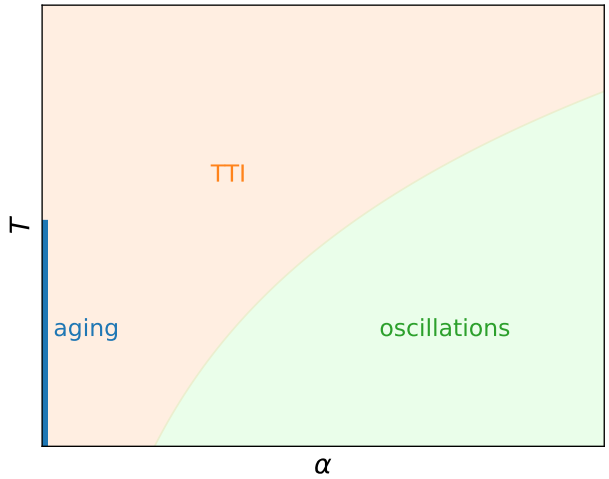

Figure 7.6: Qualitative phase diagram for $p = 4$. In the orange region the system becomes time-translationally invariant, in the green region we have undumped oscillations, with oscillating envelope.

At high values of α (in green in Figure 7.5), the system exhibits undamped oscillations, with an envelope that *oscillates* with the initial time t_0. The oscillations have a frequency smaller than $2\pi/\alpha$, which is the one we would find in the absence of random interactions, but their frequency seems to tend to this value for $\alpha \to \infty$. Surprisingly, the correlation with the random initial condition $C(t, 0)$ never decays to zero: the two systems oscillate indefinitely in a plane that has a macroscopic overlap with both their initial conditions. This is a non-trivial effect of the random interactions: without them, as we have seen in Section 5.3.2, the plane of rotation would freely diffuse in the N-dimensional space. How is it possible that the interactions allow the system to remember some random initial conditions, which are completely uncorrelated from the energy landscape, is an open question worth further investigations. The coherent rotations in the plane spanned by the two initial conditions are also the source of the oscillations of the envelope of the correlation function with the initial time t_0.

Between the two regimes (in orange in Figure 7.5), the system becomes TTI. When approaching the oscillating phase, the correlation function exhibits exponentially damped oscillations, with a decay time that appears to diverge at some finite α (around $\alpha \sim 0.5$). This suggests that there is a true phase transition between a phase in which the system forgets the initial conditions and one in which these are remembered forever. Note that the correlation function is non-trivial even at zero temperature, indicating that the system fluctuates (and decorrelates from its initial condition) even if it is not submitted to noise. This means that it is undergoing a chaotic dynamics [13, 285]. At finite temperature, the dynamics combines chaos and thermal fluctuations.

Whether there is also a finite-α phase transition between the TTI and the aging regime is also still an open question. Since we see no signature of such a phase transition, we conjecture that at finite α there is only a strongly non-linear increase of the timescale on which aging is interrupted, and that the true aging regime is only for $\alpha = 0$. The qualitative phase diagram for even p is sketched in Figure 7.6.

7.4 Random Energy Models and Trap models

In order to investigate how non-reciprocity affects system in which aging is not due to flat directions, but to the presence of growing energy barriers, we propose to study the non-reciprocal coupling of two trap models [222, 261]. This project, in collaboration with Mattia Scandolo, is still at a preliminary stage. Here we describe the general idea and the set-up. We first introduce the Random Energy Model and the trap model, two well-studied aging systems that will serve as inspiration for our non-reciprocal model.

7.4.1 Random Energy Model and trap model

In the Random Energy Model (REM) [336–338], we consider N spins with an up and a down state. We assign independent random energies to each of the 2^N configurations of the system, from a given distribution $\rho(E)$. In the original model by Derrida [336, 337], ρ is a Gaussian distribution with mean zero and variance $N/2$. However, we can also consider generalizations in which the energies are sampled from a different distribution. We will in particular also be interested in the exponential case, in which $\rho(E) = e^E \theta(-E)$ (Exponential Random Energy model, or EREM) [338].

The Gaussian REM can be obtained as the $p \to \infty$ limit of an Ising spin model with fully-connected random p-body interactions. It exhibits a phase transition at a critical temperature $T_c = \frac{1}{2\sqrt{\ln 2}}$ between an equilibrium phase in which no state has a macroscopic weight, to a spin-glass phase in which the Boltzmann distribution acquires a macroscopic weight on the ground

state. If we endow the system with a single spin flip Metropolis dynamics, below T_c it does not manage to relax to equilibrium on times that do not diverge with N, and instead performs aging. The aging dynamics at long times is well captured, at a coarse grained level, by the simplified trap model introduced by Bouchaud [222,338,339], which we have already described in Section 5.2.3.

In the trap model, we again consider 2^N configurations with randomly assigned energies, but the dynamics is determined as follows. When the system is in a trap with energy E (with $E < 0$), it escapes from it with a probability rate proportional to $e^{E/T}$, and then immediately falls in another trap, randomly chosen from the 2^N. The main differences with respect to the REM are that the escape rate only depends on the initial configuration, and that the system is not constrained to jump to one of the N states that could be reached through a single spin flip. These differences turn out to be irrelevant for a coarse-grained description of the long times dynamics, in which both the REM and the trap model spend most of their time in rare low laying states. In the original model considered by Bouchaud [222], the energies are sampled from an exponential distribution, which means that its dynamics will be more similar to the one of the EREM. It is also possible to consider Gaussian distributed energies, obtaining a model closer to the original REM.

7.4.2 Phase diagram of the EREM and the trap model

Since the EREM and the exponential trap model only differ for their dynamical rules, their equilibrium properties must be the same, and in particular they must fall out of equilibrium at the same temperature. Let us show that this occurs for $T = 1$ in both cases.

Trap model

In the trap model, the dynamics is defined by the escape rate:

$$r = \Gamma_0 e^{\beta E} \ , \tag{7.30}$$

where $\beta = 1/T$ is the inverse temperature, and Γ_0^{-1} sets the microscopic timescale. We can write the Fokker-Planck equation for the probability distribution $P(E,t)$ of finding the system at an energy E at time t:

$$\frac{1}{\Gamma_0}\frac{\partial}{\partial t}P(E,t) = -e^{\beta E}P(E,t) + \rho(E)\int dE' P(E',t)e^{\beta E'} \ . \tag{7.31}$$

The first term is the probability rate that the system is found at energy E at time t and then jumps away. The second one is the probability rate to jump to energy E from any other energy E'. The total probability rate that the system performs a jump at time t (from any energy) is $\omega(t) = \int dE' P(E',t)e^{\beta E'}$. With this notation we can rewrite the Fokker-Planck equation as:

$$\frac{1}{\Gamma_0}\frac{\partial}{\partial t}P(E,t) = -e^{\beta E}P(E) + \rho(E)\omega(t) \ . \tag{7.32}$$

Its stationary probability distribution is given by:

$$P(E) = \rho(E)\omega(t)e^{-\beta E} \propto e^{-(\beta-1)E} \ . \tag{7.33}$$

$\rho(E) = e^E\theta(-E)$ is the probability that a state has energy E. This distribution is only normalizable (for $E \in (-\infty, 0)$) if $\beta < 1$, i.e. for $T > 1$. Below $T = 1$ the non-normalizability of the distribution signals the fact that the system falls out of equilibrium. For finite N an equilibrium distribution still exists, but thermalization requires a time that diverges with N.

EREM

In the EREM the dynamics is not as simple as in the trap model, so the Fokker-Planck equation cannot be as easily derived. The equilibrium properties can be obtained from the study of the partition function. Indicating with $n(E)$ the density of states at energy E, the partition function can be expressed as:

$$Z = \int_{-\infty}^{0} dE n(E) e^{-\beta E} \ . \tag{7.34}$$

The average density of states is

$$\overline{n(E)} = \rho(E) 2^N = e^{E + N \log 2} \ . \tag{7.35}$$

The overline indicates an average over the disorder (i.e. the realization of the energy levels). If $\overline{n(E)} \gg 1$, thanks to the central limit theorem we expect $n(E) \sim \overline{n(E)}$. If $\overline{n(E)} \ll 1$, we expect that around most energies $n(E) = 0$, and very rarely there is an energy level. For large N, there is a critical energy $E_0/N = -\log 2$ such that for $E > E_0$, $n(E) = \overline{n(E)}$, and for $E < E_0$, $n(E) = 0$, so that E_0 is the ground state. Note that while the typical energies are of order 1, the ground state is extensive, i.e. of order N.

We can express the partition function in terms of the intensive energy $\varepsilon = E/N$:

$$Z \sim \int_{-\log 2}^{0} d\varepsilon e^{N(\log 2 + (1-\beta)\varepsilon)} \ . \tag{7.36}$$

For large N, it will be dominated by the value of the energy that minimizes the free energy. Since the density of states is exponential, the minimum will be in one of the two extremes of the interval: in $\varepsilon = 0$ for $T > 1$, and in the ground state $\varepsilon = -\log 2$ for $T < 1$. This confirms that there is a phase transition at $T_c = 1$. The transition is discontinuous: the intensive energy jumps from $\epsilon = 0$ to $\epsilon = -\log 2$.

7.4.3 Non-reciprocal coupling

In order to study the effect of non-reciprocity on aging in systems with activated dynamics, we propose to consider *two* particles hopping in the same disordered energy landscape. We first of all need to decide *how* to couple them in a non-reciprocal (and non-trivial) way, since several possibilities are available.

We will assume that the two particles undergo a thermal dynamics trying to minimize two different "selfish energies", in the sense introduced in Section 5.3.1. These selfish energies contain the random potential, which is the same for the two particles, and a function of the two positions, which will have different signs for the two particles to introduce non-reciprocal frustration in the systems.

In a trap model there is not really a notion of space, since all sites are connected. In order to define the non-reciprocal coupling, we will assume to have 2^N states arranged in a N-dimensional hypercube, as in the REM, but still allowing jumps from any site to any other, as in the trap model. The position of the two particles can be identified by N binary variables, $s_i^a = \pm 1$, where i runs from 1 to N and a indicates the identity of the particle, we collect them in vectors $\vec{s}_a$. The non-reciprocity can then be introduced by imposing that one particle wants to minimize the overlap $q = \frac{1}{N}\vec{s}_1 \cdot \vec{s}_2$, and the other wants to maximize it. Let us then define the selfish energies:

$$E_1 = E(\vec{s}_1) - \alpha \vec{s}_1 \cdot \vec{s}_2 \tag{7.37}$$

$$E_2 = E(\vec{s}_2) + \alpha \vec{s}_1 \cdot \vec{s}_2 \tag{7.38}$$

α is the strength of the non-reciprocal coupling. Each particle undergoes a dynamics that would satisfy detailed balance with respect to its own selfish energy at temperature T if the position of the other one was fixed.

$$\frac{r_{\vec{s}_1 \to \vec{s_1'}}}{r_{\vec{s_1'} \to \vec{s}_1}} = \exp\left(\beta\left(E(\vec{s}_1) - E(\vec{s_1'}) + \alpha(\vec{s_1'} - \vec{s}_1)\cdot\vec{s}_2\right)\right) \ , \tag{7.39}$$

$$\frac{r_{\vec{s}_2 \to \vec{s_2'}}}{r_{\vec{s_2'} \to \vec{s}_2}} = \exp\left(\beta\left(E(\vec{s}_2) - E(\vec{s_2'}) - \alpha(\vec{s_2'} - \vec{s}_2)\cdot\vec{s}_1\right)\right) \ . \tag{7.40}$$

This constraint does not yet unambiguously determine the transition rates. We propose two different dynamics:

1. Each particle jumps out of its trap with a probability rate proportional to $\exp(\beta(E(\vec{s}_a) - N\epsilon_{ab}\alpha q))$, and then select a new state uniformly from all the existing ones.

2. Each particle jumps out of its trap with a probability rate proportional to $\exp(\beta E(\vec{s}_a))$, and then select a new state with weight proportional to $\exp(N\beta\epsilon_{ab}\alpha q)$, which would be the Boltzmann weight of the overlap between two spin systems coupled by (anti-)aligning interactions.

If we want our model to be as close as possible to a REM, the second choice is more appropriate: when the system performs a spin flip, the overlap changes by an infinitesimal amount, so that its change does not really influence the escape rate. After the system has escaped a deep trap, it performs many jumps at high energy, macroscopically changing its overlap, before finding another low laying state. If we want to give a coarse-grained description of the dynamics between the deep traps, it is therefore more appropriate to assume that the escape rate only depends on the energy of the trap, and the overlap of the next state is sampled from an (egoistically) equilibrated distribution. We assume that the two particles never move at the same time, since in the aging phase they spend most of their time trapped in low energy states.

The first dynamics could however also be of interest to understand the behavior of more realistic spin glasses. In particular, if neighboring states have correlated energies, crossing a barrier can require many spin flips. This would lead to a macroscopic change of the overlap, which could then influence the barrier crossing rate.

The two dynamics can be seen as the two extreme cases of a continuum of models, in which the overlap influences partially the escape rate, and partially the selection of the following state.

7.4.4 Phase diagram of two reciprocally coupled EREM

To show that the coupling we have chosen induces a non-trivial effect, we can study the phase diagram of two *reciprocally* coupled trap models. This also allows us to gain some intuition on the behavior of the system in the non-reciprocal case.

If the coupling is reciprocal, we can write an energy for the entire system:

$$E_{TOT} = E(\vec{s}_1) + E(\vec{s}_2) - \alpha\vec{s}_1\cdot\vec{s}_2 \ . \tag{7.41}$$

We can express the partition function in terms of the intensive energies $\varepsilon_i = (\vec{s}_1)/N$ and the overlap:

$$Z \sim \int d\varepsilon_1 d\varepsilon_2 dq n(\varepsilon_1, \varepsilon_2, q) e^{-\beta N(\varepsilon_1+\varepsilon_2-\alpha q)} \ . \tag{7.42}$$

To compute the average density of states we need to distinguish two cases: if the two particles are in the same trap, i.e. if $q = 1$, they must also have the same energy (we will call this "attached" state), whereas if they are in different traps they have independent energies ("detached" state):

$$\overline{n(\varepsilon_1, \varepsilon_2, q)} = \rho(\varepsilon_1)\rho(\varepsilon_2)e^{NS(q)}2^N + \delta(q-1)\rho(\varepsilon_1)\delta(\varepsilon_1 - \varepsilon_2)2^N = \overline{n_D} + \overline{n_A} \ . \tag{7.43}$$

$e^{NS(q)}$ is the number of configurations that have overlap q with a reference one; for $N \gg 1$ $S(q)$ reads:

$$S(q) = -\left(\frac{1+q}{2}\log\frac{1+q}{2} + \frac{1-q}{2}\log\frac{1-q}{2}\right) \ . \tag{7.44}$$

As expected, $S(q)$ is maximal in $q = 0$.

As before, if one of the two average densities is much larger than 1, the density will be close to the mean, whereas if it is much smaller than 1, the density will be zero except for very rare states. We can find the ground state in the detached and attached cases by looking for the configuration that minimizes the total energy and has $\overline{n_{D/A}} = 1$. For the detached case we find:

$$\varepsilon_0^D = -\alpha q_0 - (\log 2 + S(q_0)) \ , \tag{7.45}$$

where $q_0 = \tanh\alpha$, namely the value that maximizes $S(q) + \alpha q$. This result has a simple interpretation. We put the first particle in the lowest energy level available ($-\log 2$, as we have seen for a single EREM). For the second particle there is a trade off: states with large overlap minimize the interaction energy, but, since there are very few of them, it is less likely that one of them will have a very low random energy. The optimal solution is found precisely by maximizing $S(q) + \alpha q$.

For the attached case we have:

$$\varepsilon_0^A = -\alpha - 2\log 2 \ , \tag{7.46}$$

meaning that the two particles are both in the lowest energy level.

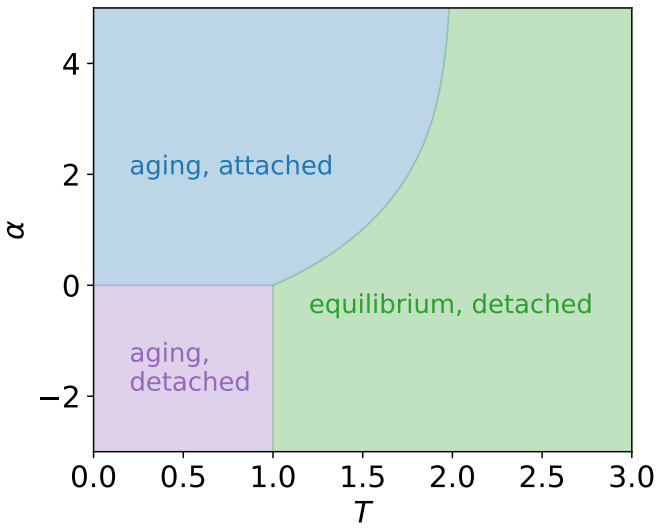

Figure 7.7: Phase diagram of two reciprocally coupled REM.

The partition function is dominated by the state that minimizes the free energy. As in the previous case, we find that either the system goes to the ground state, in which it has a

macroscopic energy and no entropy, or has 0 intensive energy and finite entropy. To obtain the configuration it is then sufficient to compare the four following free energies, corresponding to attached and detached states, either at the ground state ($f^{GS}_{A/D}$) or at zero energy ($f_{A/D}$):

$$f_A = -\alpha - \frac{\log 2}{\beta} \ , \tag{7.47}$$

$$f_D = -\frac{\log 2}{\beta} - \alpha q^*(\beta) - \frac{S(q^*(\beta))}{\beta} \ , \tag{7.48}$$

$$f^{GS}_A = -\alpha - 2\log 2 \ , \tag{7.49}$$

$$f^{GS}_D = -\alpha q_0 - (\log 2 + S(q_0)) \ . \tag{7.50}$$

$q^*(\beta) = \tanh \beta\alpha$ is the equilibrium value of the overlap, which maximizes $S(q) + \beta\alpha q$.

The phase diagram of the system is represented in Figure 7.7. For all values of β and α, $f_A > f_D$, so the two particles will never be in the same state, except if this is the ground state. On the other hand, for $\alpha > 0$, $f^{GS}_A < f^{GS}_D$: at low temperature the optimal solution is to put both particles in the same state. The opposite is true if $\alpha < 0$: if the particles repel each other, they will look for two different low energy states. Therefore for $\alpha < 0$ the particles are always detached, and they undergo a phase transition between an equilibrium and an aging phase for $T = 1$, as in the single REM case (see Figure 7.7). For $\alpha > 0$, instead, at high temperature we have a detached equilibrium phase, and at low temperature an attached non-equilibrium one. The phase transition can be located by imposing $f^{GS}_A = f_D$, leading to:

$$\alpha\beta + (2\beta - 2)\log 2 - \log\cosh(\alpha\beta) = 0 \ . \tag{7.51}$$

This condition determines the line between the blue and the green region in Figure 7.7.

Interestingly, the coupling leads the system to fall out of equilibrium at higher temperatures than it would do otherwise. This is because the ground state is further stabilized by the attraction. For $\alpha \to \infty$, the transition occurs for $T = 2$. The system becomes equivalent to a single REM with all energies levels multiplied by a factor 2. For $\alpha < 0$ instead the coupling has no effect. This is a particularity of the EREM, and would for example not be the case for Gaussian distributed energies.

7.4.5 Scenarios for non-reciprocal case

In the non-reciprocal case, since a global energy cannot be defined, we must rely on a dynamical approach. It is in principle possible to study the Fokker-Planck equation that describes the evolution of the probability distribution of the two energies and the overlap, but this computation is quite involved and it is currently ongoing. From the Fokker-Planck equation it would be possible to obtain the phase diagram of the system (by studying when the stationary distribution becomes non-normalizable, as done for the single trap model), but also to study the aging dynamics. Since the system is always out of equilibrium, the phase diagram could depend on the type of dynamics we choose.

We can however already hypothesize some scenario for what happens in the non-reciprocal case. Consider first the case in which particle 1 is attracted to particle 2, whereas particle 2 is not influenced at all by particle 1. Particle 2 undergoes the usual transition at $T = 1$, and, for $T > 1$, is typically in states with intensive energy equal to 0. The attraction to particle 2 cannot then help particle 1 to find states of extensive energy, particle 2 must then also undergo the phase transition for $T = 1$.

Let us now consider the non-reciprocally interacting case. It is hard to imagine that if particle 2 was repelled by particle 1 this would help them finding low energy states, therefore

the transition cannot occur at temperatures higher than 1. On the other hand, we have seen that if the two particles repel each other, they still undergo the phase transition at $T = 1$. We therefore conjecture that the non-reciprocal system undergoes a phase transition for $T = 1$, no matter the value of α.

As in the case of the p-spin for $p = 3$, the two non-reciprocally coupled traps are not equivalent: while chasing another particle can help in finding low energy states, running away from it doesn't have a strong effect. This is also evident from the fact that the phase diagram is not symmetric upon the reversal of α. Inspired by even-p spin models, whose energy is invariant under flipping of all spins in the system, we wonder what would happen if we imposed a similar symmetry to our energy levels, i.e. if $E(\vec{s}) = E(-\vec{s})$. Since the REM can be obtained as the limit for $p \to \infty$ of the (Ising) p-spin, such a model could be obtained as the limit $p \to \infty$ restricted to *even* p. In the reciprocal case, the phase diagram would become symmetric under the reversal of α (and analogous to the one already obtained for $\alpha > 0$). The non-reciprocal system would be invariant under the exchange of the two particles, given that the position of one of the two is reversed as well ($\vec{s}_1 \to -\vec{s}_2$, $\vec{s}_2 \to \vec{s}_1$). This could lead to an aging behavior similar to the one found for reciprocal coupling, but with oscillations between "attached" and "anti-attached" states.

7.5 Conclusions

In this chapter, we have described some preliminary results on the effect of a non-reciprocal coupling on pairs of aging systems. A general remark, which will also be relevant for the next chapter, is that the phenomenology strongly depends on whether the single system is invariant under reversal of all its degrees of freedom. In fact this invariance generates an "equivalence" between the two parts, and allows for rotations in phase space that would otherwise not be possible.

For two non-reciprocally coupled $O(N)$ models we find that aging is not destroyed by the coupling, but simply dressed by oscillations. This is exactly what we have already seen in the case of the spherical SK model. This is not a coincidence, and is linked to the formal similarity between the aging behavior in these two systems.

In the case of the p-spin model, we conjecture that aging is always destroyed. However, since aging is interrupted on timescales that diverge much faster than $1/\alpha$, this wouldn't be visible if we observed the system only until moderate times, and in particular it is not visible in the available numerical simulations. For odd p the systems always decorrelate from initial conditions and undergo chaotic dynamics. For even p there is instead a phase transition between a chaotic phase and a phase in which the systems rotate indefinitely in the plane spanned by their two random initial conditions. The mechanism enabling this long memory in the presence of thermal fluctuations is still not well understood, and would deserve further investigations.

We also propose to consider two non-reciprocally coupled trap models to study the effect of non-reciprocity on activated dynamics. We describe a coupling scheme that leads to a non-trivial modification of the phase diagram in the reciprocal case, and propose some scenarios for the behavior of the non-reciprocally coupled systems.

Chapter 8

Relevance of non-reciprocity at a phase transition

In this Chapter, we investigate under which conditions the introduction of a non-reciprocal perturbation can dramatically change the behavior of a system undergoing a phase transition. The presented results were obtained in collaboration with David Martin, Yael Avni, Daniel Seara, Michel Fruchart and Vincenzo Vitelli, and they will be the subject of a forthcoming publication [4].

8.1 Introduction

In non-equilibrium systems, microscopic components can interact in a *non-reciprocal* way: the effect of A on B need not be equal to the one of B on A. Such interactions arise across a wide range of systems, including predator-prey dynamics [292, 340] excitatory-inhibitory neuronal circuits [341, 342], open quantum systems [343, 344] and socially-driven human dynamics [345]. Non-reciprocal interactions have been identified as a key mechanism driving a variety emergent behaviors, among which the formation of traveling waves [282,283] and time crystals [291] or the presence of odd elasticity [303, 346]. In many-body systems, non-reciprocity can strongly affect phase transitions, as was recently shown for non-reciprocal versions of the Ising model [291] and as we discussed in the previous chapters for the spherical Sherrington-Kirpatrick model and other aging systems. In these models, non-reciprocity either completely destroys the phase transition (two dimensional Ising), changes its universality class (three dimensional Ising) or dresses the ordered state with persistent oscillations (spherical SK). In other systems, however, the introduction of non-reciprocity seems to have no effect. This is the case for a pair of coupled three-dimensional Ising models, with some finite reciprocal interactions and small non-reciprocal ones [304]. Despite these recent results, there is yet no generic understanding of when does the addition of non-reciprocal interactions change the critical properties of the system.

To answer this question, we propose a set of simple criteria, summarized in the table in Figure 8.1, to determine the relevance of infinitesimal non-reciprocity on a phase transition. These criteria only depend on the critical properties of the unperturbed system, and in particular on its critical exponents in the absence of non-reciprocal interactions. This is similar in spirit to the Harris criterion [347, 348], which was derived to assess whether the critical behavior of the Ising model at the ferromagnetic transition would be modified by the addition of a local random perturbation in the inter-spin interactions. In the Renormalization Group (RG) framework, this corresponds to asking whether the critical fixed point is stable with respect to the perturbation. As in the case of the Harris criterion, our criteria allow us to predict if the phase transitions will be modified, but they do not determine how: the universality class could change, or the

transition could be completely destroyed.

As in the previous chapters, we will consider pairs of identical systems, and add non-reciprocal interactions between corresponding components. The setup is sketched in Figure 8.1. Since we are interested in the critical behavior of these systems, we will work with field theories that describe the coarse grained dynamics of the local order parameters.

Before considering non-reciprocal interactions, we review the classical Harris criterion. We will derive it through a dynamical approach which allows us to generalize the criterion to non-equilibrium systems.

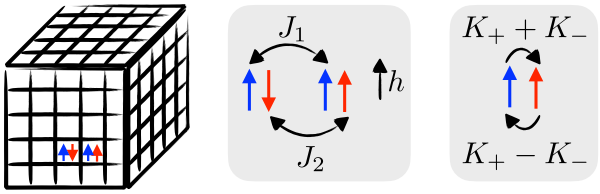

System	Perturbation	Irrelevant if	Conclusion
One field (Harris [347])	Random δJ	$\nu d > 2$	Depends
Uncoupled identical fields $K_+ = K_- = 0$, $J_1 = J_2$	δK_-	$\gamma < 0$	Relevant ✓
Uncoupled non-identical fields $K_+ = K_- = 0$, $J_1 \neq J_2$	δK_-	Always	Not relevant
Reciprocally coupled fields $K_+ \neq 0$, $K_- = 0$, $J_1 = J_2$	δK_-	Always	Not relevant ✓
Uncoupled identical fields $K_+ = K_- = 0$, $J_1 = J_2$	Random δK_-	$\nu d > 4\beta$	Not relevant for 3D Ising
Non-reciprocally coupled fields $K_+ = 0$, $K_- \neq 0$, $J_1 = J_2$	Random δK_-	$\nu d > 2$	Not relevant for swap

Figure 8.1: Top: Schematic drawing of a two coupled Ising model that our results apply to. Bottom: Summary of the results. The first line is the Harris criterion. A checkmark (✓) indicates results we have numerically tested.

8.2 Non-equilibrium Harris criterion

The general idea, applicable to both Harris and our case, is to introduce a small perturbation and compute the correction it induces to the order parameter. Its scaling when approaching the phase transition can in many cases be estimated in terms of the critical exponents of the unperturbed system. If this correction is small compared to the unperturbed order parameter, the critical behavior will remain unchanged, otherwise it might be modified. This approach does not require the system to be at equilibrium, as the correction can be computed directly from the dynamics of the system. This allows us to generalize the classical Harris criterion to non-equilibrium systems. This approach is similar to the one used in Reference [349] to generalize the Harris criterion to arbitrary spatio-temporal disorder.

Harris consider a d-dimensional Ising model with ferromagnetic interactions to which he

added a small, random perturbation [347]. The critical behavior of the Ising model is described by the field theory:

$$\partial_t \phi = \nabla^2 \phi - V'(\phi) + \eta \ , \tag{8.1}$$

where $V(\phi)$ is a double-well potential function and η is a Gaussian white noises with amplitude T. A local perturbation in the inter-spin coupling would result in a perturbation of the Laplacian term. However, we can equivalently consider some random variations of the mass term $\delta m(\mathbf{x})$:

$$\partial_t \phi = \nabla^2 \phi - V'(\phi) + \eta + \delta m(\mathbf{x})\phi \ . \tag{8.2}$$

The Gaussian disorder $\delta m(\mathbf{x})$ is δ-correlated in space:

$$\overline{\delta m(\mathbf{x}) \delta m(\mathbf{x}')} = \delta \sigma_m \delta(\mathbf{x} - \mathbf{x}') \ . \tag{8.3}$$

The overline indicates averaging over quenched disorder. Using the Martin-Siggia-Rose-De Dominicis-Janssen (MSRDJ) approach [175–178], the probability of observing a given configuration of the field can be expressed as:

$$\mathcal{P}\left(\{\phi\}\right) = \int D[\hat{\phi}] e^{-\int d\mathbf{x} dt \mathcal{S}} \ , \tag{8.4}$$

where $\hat{\phi}$ is an auxiliary field. The action $\mathcal{S}$ can be decomposed as

$$\mathcal{S} = \mathcal{S}_0[\hat{\phi}, \phi] + \delta \mathcal{S}[\hat{\phi}, \phi] \ , \tag{8.5}$$

with $\mathcal{S}_0$ being the action in the absence of perturbations and $\delta\mathcal{S}$ containing terms that derive from the perturbation:

$$\mathcal{S}_0 = \hat{\phi}\left(\partial_t \phi - \boldsymbol{\nabla}^2 \phi + V'(\phi)\right) + \frac{T}{2}\hat{\phi}^2 \ , \tag{8.6}$$

$$\delta\mathcal{S} = \delta m(\mathbf{x}) \hat{\phi} \phi \ . \tag{8.7}$$

To see whether the perturbation modifies the critical properties of the system, we compute the correction to the order parameter, the average magnetization $\langle \phi(\mathbf{x}, t) \rangle$, to first order in $\delta\sigma_m$. Expanding the exponential of the action, we obtain at first order:

$$\langle \mathcal{O}(\mathbf{x}, t) \rangle = \int D[\hat{\phi}] \mathcal{O}(\mathbf{x}, t) e^{-\int d\mathbf{x} dt \mathcal{S}} \left(1 + \int \delta \mathcal{S}|_{\mathbf{x}', t'} d\mathbf{x}' dt'\right) + O(\delta \sigma_m^2) \ . \tag{8.8}$$

We will omit the $O(\delta\sigma_m^2)$ in the following, all computations will be to first non-zero order in the perturbation. The first term is the unperturbed average value of the observable, the second the first order correction we are interested in. Indicating with $\langle \cdot \rangle_0$ the average with respect to the unperturbed action, we can express it as:

$$\delta \langle \mathcal{O}(\mathbf{x}, t) \rangle = -\langle \mathcal{O}(\mathbf{x}, t) \int \delta \mathcal{S}|_{\mathbf{x}', t'} d\mathbf{x}' dt' \rangle_0 \ . \tag{8.9}$$

Using the form of the perturbation of the action, the correction can be rewritten as:

$$\delta \langle \mathcal{O}(\mathbf{x}, t) \rangle = -\int \delta m(\mathbf{x}') G(\mathbf{x} - \mathbf{x}') d\mathbf{x}' \ , \tag{8.10}$$

where $G(\mathbf{x} - \mathbf{x}') = \langle \frac{\delta \mathcal{O}(\mathbf{x})}{\delta m(x')} \rangle_0$ is the response function of $\langle \mathcal{O} \rangle$ when perturbing it with a local variation of the linear term. Since δm is a random variable, the first order correction will also be random. Its average is equal to zero, to obtain its typical size we can compute its variance:

$$\overline{\delta \langle \mathcal{O} \rangle^2} = \delta \sigma_m^2 \int G(\mathbf{x})^2 d\mathbf{x} \ , \tag{8.11}$$

The response function G can be shown to scale, near the transition, as [350]:

$$G(\mathbf{x}) \sim \xi^{-(d+(\beta-1)/\nu)} f\left(\frac{\mathbf{x}}{\xi}\right) . \tag{8.12}$$

where β is the exponent characterizing the critical behavior of $\langle \mathcal{O} \rangle \sim |T - T_c|^\beta$, ξ is the correlation length, and ν is the critical exponent describing its divergence, $\xi \sim |T - T_c|^{-\nu}$. Inserting this expression in (8.11) we obtain that the typical size of the correction is:

$$\sqrt{\overline{\delta \langle \mathcal{O} \rangle^2}} \sim \delta\sigma_m |T - T_c|^{d\nu/2+\beta-1} . \tag{8.13}$$

Comparing this correction to the behavior of $\langle \mathcal{O} \rangle$ in the pure system, we see that the correction will be dominant if

$$d\nu/2 < 1 . \tag{8.14}$$

This is the Harris criterion. We have never used the fact that the system is at equilibrium. In fact, the same derivation can be used to determine the stability of a generic (even non-equilibrium) symmetry-breaking phase transition with respect to a perturbation that locally favors one of the two phases (the symmetric or the symmetry-broken one) over the other, without explicitly breaking the symmetry of the system.

Note that also a perturbation that only changed the critical point of the transition would lead to a dominant correction, without affecting the critical behavior. For example, a deterministic perturbation $\delta m > 0$ would simply lead to a shift of the critical point, but would similarly generate a strong correction of the order parameter. Here, symmetry guarantees that the perturbation does not shift the critical point to first order. Indeed, since the distribution of δm is symmetric around 0, reversing the sign of the perturbation leaves the system unchanged. Therefore we would expect a shift in the critical temperature to be at least quadratic in the perturbation amplitude.

8.3 Non-reciprocal coupling of two uncoupled systems

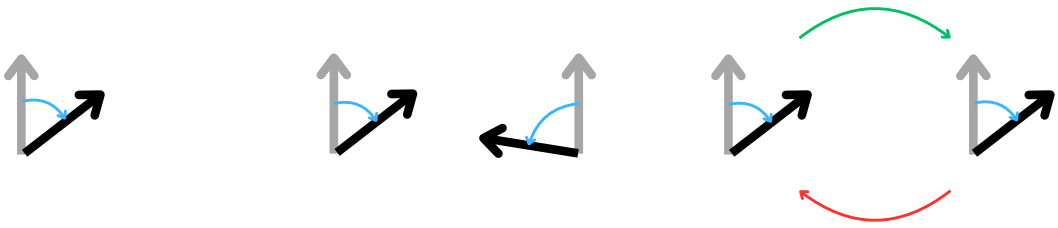

(a) A single system. Here, $O(2)$ symmetry

(b) Two uncoupled systems. Here, $O(2) \times O(2)$ symmetry

(c) Two NR coupled systems. Here, $O(2)$ symmetry

Figure 8.2: Illustration of the symmetries of our problem. (a) The single field is invariant under a certain symmetry, which will be spontaneously broken at the phase transition. Here we consider rotations in the plane ($O(2)$ symmetry). (b) Two uncoupled fields can be rotated independently. (c) Two (non-reciprocal) fields are only invariant under the simultaneous rotation of *both* fields. Green and red arrows indicate non-reciprocal interactions, blue arrows the symmetry transformation.

The simplest system with non-reciprocal interactions is composed of two species. We first focus on the case in which the two species are identical and independent before the introduction of non-reciprocity. Both species are described by a field with a given symmetry, which is spontaneously broken at the phase transition point (Figure 8.2a). Two uncoupled fields have a larger symmetry group, since we can independently transform each of them (Figure 8.2b). As soon as we introduce (non-reciprocal) interactions, however, the system is only invariant under the simultaneous rotation of *both* fields (Figure 8.2c): it therefore has the same symmetry as a single field. We can then ask whether the phase transition that will break this symmetry would be the same as the one in the original model. For the described class of systems, we will show that the introduction of non-reciprocity strongly affects the phase transition if the susceptibility of the system diverges when approaching the critical point. This is the case for most physical systems, and in particular for all the equilibrium ones.

Even though our results hold more generally, let us consider for concreteness two Models A [351]. A natural way to introduce non-reciprocal interactions is by adding to the evolution of each field a term linear in the other, with opposite signs:

$$\begin{aligned}\partial_t\phi_1 &= \nabla^2\phi_1 - V'(\phi_1) + \eta_1 + h_1 + \delta K_-\phi_2 \\ \partial_t\phi_2 &= \nabla^2\phi_2 - V'(\phi_2) + \eta_2 + h_2 - \delta K_-\phi_1\end{aligned} \tag{8.15}$$

ϕ_1 and ϕ_2 are two real-valued fields, η_1 and η_2 are Gaussian white noises of amplitude T, h_1 and h_2 are fields that we will use to compute response functions and we will take to zero at the end of the derivation. $V(\phi)$ is a symmetric double-well potential. The coefficient δK_- characterizes the strength of the non-reciprocal coupling; we will assume it to be small, and treat it as a perturbation. In systems that are symmetric under inversion, this choice of the non-reciprocal interaction maintains the equivalence of the two fields, because the system is symmetric under the exchange of the two fields and the reversal of one of the two ($\phi_1 \to \phi_2$, $\phi_2 \to -\phi_1$). This ensures that the fields still have the same critical point after the introduction of the non-reciprocity. This unique critical point cannot be shifted at linear order in δK_-. Changing the sign of the perturbation δK_- is equivalent to exchanging the identities of the two fields, and therefore cannot change the properties of the system. If the critical point was linearly shifted by the perturbation, a reversal of the perturbation would reverse this shift. Since this cannot happen, such a shift must be at least of order δK_-^2. As in the case considered by Harris, we are therefore ensured by the symmetry of the system that if we find a linear correction of the order parameter this does not derive from a trivial shift of the critical point.

Using the Martin-Siggia-Rose-De Dominics-Janssen (MSRDJ) formalism, we can express the joint probability of observing a given configuration of the two field as

$$\mathcal{P}\left(\{\phi_1,\phi_2\}\right) = \int D[\hat\phi_1,\hat\phi_2]e^{-\int d\mathbf{x}dt\mathcal{S}}\ , \tag{8.16}$$

where $\hat\phi_i$ are auxiliary response fields. The action $\mathcal{S}$ can be decomposed in an unperturbed part and a perturbation:

$$\mathcal{S} = \mathcal{S}_0[\hat\phi_1,\phi_1] + \mathcal{S}_0[\hat\phi_2,\phi_2] + \delta\mathcal{S}[\hat\phi_1,\phi_1,\hat\phi_2,\phi_2]\ . \tag{8.17}$$

The unperturbed part $\mathcal{S}_0$, which acts independently on the two fields, is the same as in the previous section, Eq. 8.6. The perturbation is given by:

$$\delta\mathcal{S} = \delta K_-\left(\hat\phi_1\phi_2 - \hat\phi_2\phi_1\right)\ . \tag{8.18}$$

To see whether the perturbation modifies the critical properties of the system, we compute the average magnetization of one of the two fields $\langle\phi_1(\mathbf{x},t)\rangle$, to first order in δK_-. Expanding the

exponential of the action, the correction can be written as:

$$\delta\langle\phi_1(\mathbf{x},t)\rangle = -\langle\phi_1(\mathbf{x},t)\int \delta\mathcal{S}|_{\mathbf{x}',t'}d\mathbf{x}'dt'\rangle_0 \,. \tag{8.19}$$

We have again indicated with $\langle\cdot\rangle_0$ the average with respect to the unperturbed action. Using the form $\delta\mathcal{S}$, we obtain:

$$\delta\langle\phi_1(\mathbf{x},t)\rangle = -\delta K_-\langle\phi_1(\mathbf{x},t)\int_{\mathbf{x}',t'}\left(\hat{\phi}_1\phi_2 - \hat{\phi}_2\phi_1\right)\Big|_{\mathbf{x}',t'}\rangle_0 \,. \tag{8.20}$$

Because under the unperturbed dynamics the two fields are independent, we can average them separately. Since $\langle\hat{\phi}_2\rangle_0 = 0$, only the first term contributes. Using

$$\langle\phi_i(\mathbf{x},t)\hat{\phi}_i(\mathbf{x}',t')\rangle_0 = \frac{\delta\langle\phi_i(\mathbf{x},t)\rangle_0}{\delta h_i(\mathbf{x}',t')}\Big|_{h_i=0} \,, \tag{8.21}$$

and that the integral of this response function gives the susceptibility χ, we find:

$$\delta\langle\phi_1\rangle = -\delta K_-\langle\phi_2\rangle_0\chi \,. \tag{8.22}$$

We need to compare the scaling of this correction with the one of the unperturbed order parameter when $T \to T_c$. Because the correction is proportional to $\langle\phi_j\rangle_0$ and the two fields are identical before the introduction of the perturbation, the correction will dominate as long as the susceptibility diverges at the transition. This is generally the case, and in particular always holds for systems that were in equilibrium before the introduction of the perturbation. Calling γ the critical exponent describing the divergence of the susceptibility at the transition, our first criterion tells us that the perturbation can modify the critical behavior of the system when $\gamma > 0$.

This result is confirmed by numerical simulations of two non-reciprocally coupled Ising models [291]: in 2D the transition to order is destroyed while in 3D the ordered phase exhibits persistent oscillations ("swap" phase in Figure 8.3a) and the critical exponents are significantly modified, becoming compatible with the ones of the XY transition (see Figure 8.4).

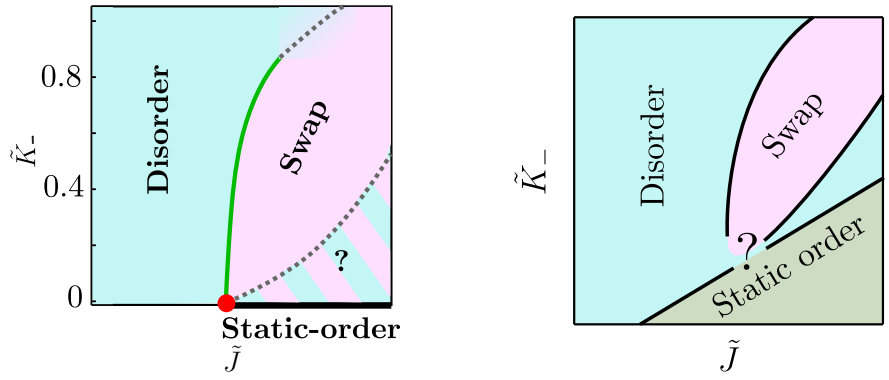

(a) $K_+ = 0$ (b) $K_+ > 0$

Figure 8.3: Phase diagram of the non-reciprocal Ising model in three spatial dimensions, reproduced from [304]. (a) If the reciprocal component of the interactions (K_+) is zero, the introduction of an infinitesimal amount of non-reciprocity changes the nature of the transition. (b) In the presence of a reciprocal component of the interactions ($K_+ > 0$), the transition to static order is not modified by the introduction of weak non-reciprocal interactions.

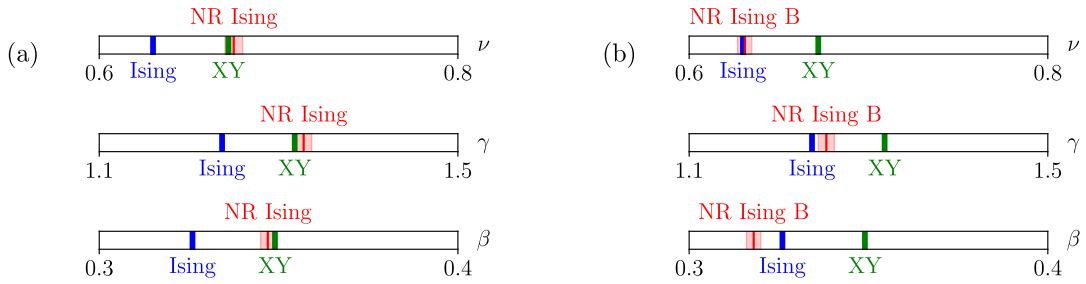

Figure 8.4: Critical exponents of the 3D non-reciprocal Ising model (red), with (a) $K_+ = 0$ and $\delta K_- = 0.1$ taken from Ref. [304] and (b) $K_+ = 0.5$ and $\delta K_- = 0.1$, which results from a new calculation. Results are obtained using finite-size scaling, as described in Ref. [304]. Standard deviation is represented by a semi-transparent red rectangular. The values of the critical exponents in the 3D Ising model and in the 3D XY model critical exponents are shown in blue and green, respectively, for comparison. Without reciprocal coupling, non-reciprocal coupling changes the universality class of the phase transition, while with a reciprocal coupling, non-reciprocity (when weaker than the reciprocal coupling) does not change universality class, in agreement with our analytical results.

Note that we have never used the form of the unperturbed action. Indeed our results hold for all systems that are symmetric under inversion, and that have a continuous phase transition which can be detected by studying a local order parameter. The precise symmetry conditions required for the validity of our results will be formalized in the next section. This class of systems includes for example $O(N)$ models for any value of N, but also non-equilibrium systems such as the incompressible Vicsek model. In all such systems, the phase transition to the ordered phase would be strongly modified by the introduction of non-reciprocity. In the case of the $O(N)$ model, this has been recently confirmed by a renormalization group analysis [294, 295]. These works show that the equilibrium critical point is destabilized by any infinitesimal non-equilibrium drive. With our approach, the same result is obtained through a much simpler computation. Moreover, it applies to a broader class of systems, though under a more specific form of the perturbation.

8.3.1 Symmetry requirements

Let us consider a system whose dynamics can be described, under the MSRDJ formalism, by an action $\mathcal{S}_0(\phi, \hat{\phi})$. ϕ is not necessarily scalar anymore. We will suppose that the action is invariant under a symmetry group $\mathcal{G}$, meaning that $\forall \mathcal{R} \in \mathcal{G}$, $\mathcal{S}_0(\mathcal{R}(\phi, \hat{\phi})) = \mathcal{S}_0(\phi, \hat{\phi})$. We only consider symmetry groups that contains the inversion operation $(\phi, \hat{\phi}) \to (-\phi, -\hat{\phi})$; examples include the $O(N)$ symmetry, but also the dihedral group D_n for n even (the symmetry group of a regular polygon with n sides), which characterizes the "clock model" [352, 353]. We also suppose that the system undergoes a phase transition, after which the considered symmetry is spontaneously broken.

We then consider two identical copies of the system, ϕ_1 and ϕ_2. If they are not coupled, their dynamics is described by the sum of the two actions,

$$\mathcal{S}_0(\phi_1, \hat{\phi}_1, \phi_2, \hat{\phi}_2) = \mathcal{S}_0(\phi_1, \hat{\phi}_1) + \mathcal{S}_0(\phi_2, \hat{\phi}_2) \ . \tag{8.23}$$

This action is clearly invariant under the exchange of the two fields:

$$\mathcal{S}_0(\phi_1, \hat{\phi}_1, \phi_2, \hat{\phi}_2) = \mathcal{S}_0(\phi_2, \hat{\phi}_2, \phi_1, \hat{\phi}_1) \ , \tag{8.24}$$

and under the independent transformation of each of the two fields:

$$\forall \mathcal{R}_1, \mathcal{R}_2 \in \mathcal{G}, \quad \mathcal{S}_0(\mathcal{R}_1(\phi_1, \hat{\phi}_1), \mathcal{R}_2(\phi_2, \hat{\phi}_2)) = \mathcal{S}_0(\phi_1, \hat{\phi}_1, \phi_2, \hat{\phi}_2) \ . \tag{8.25}$$

We now consider a perturbation $\delta\mathcal{S}(\phi_1, \hat{\phi}_1, \phi_2, \hat{\phi}_2)$ that respects the following conditions:

1. After the perturbation, the system is still invariant under a *simultaneous* transformation of the two fields. This can be imposed by requiring that $\forall \mathcal{R} \in \mathcal{G}$, $\delta\mathcal{S}(\mathcal{R}(\phi_1, \hat{\phi}_1), \mathcal{R}(\phi_2, \hat{\phi}_2)) = \delta\mathcal{S}(\phi_1, \hat{\phi}_1, \phi_2, \hat{\phi}_2)$

2. After the perturbation, the system is *not* invariant under two independent transformations of the two fields, meaning that $\exists \mathcal{R}_1, \mathcal{R}_2 \in \mathcal{G}$ such that $\delta\mathcal{S}(\mathcal{R}_1(\phi_1, \hat{\phi}_1), \mathcal{R}_2(\phi_2, \hat{\phi}_2)) \neq \delta\mathcal{S}(\phi_1, \hat{\phi}_1, \phi_2, \hat{\phi}_2)$

3. The two fields are still "equivalent" after the perturbation, in the sense that their identities can be exchanged if a transformation belonging to the symmetry group is applied to one of the two: $\exists \mathcal{R} \in \mathcal{G}$ such that $\delta\mathcal{S}(\phi_2, \hat{\phi}_2, \phi_1, \hat{\phi}_1) = \delta\mathcal{S}(\mathcal{R}(\phi_1, \hat{\phi}_1), \phi_2, \hat{\phi}_2)$

4. Exchanging the two fields changes the sign of the perturbation, $\delta\mathcal{S}(\phi_2, \hat{\phi}_2, \phi_1, \hat{\phi}_1) = -\delta\mathcal{S}(\phi_1, \hat{\phi}_1, \phi_2, \hat{\phi}_2)$

5. $\delta\mathcal{S}$ is an analytic function of its arguments

The first two conditions ensure that the system has the same symmetry as one of the two original fields. The last 3 conditions ensure that the perturbation doesn't shift the critical point at linear order. The two fields are still equivalent, so we expect them to have the same critical point (see the next section for the discussion of a case in which this condition is violated). This unique critical point is not shifted at linear order: we expect the shift to be analytic in the parameters defining the perturbation, since the perturbation is analytic, and a reversal of the perturbation leads to an "equivalent" system (i.e. only exchanges the labels of the two fields), so that as in the previous case the shift must be at least quadratic.

We conjecture that for all systems and perturbations that respect the above conditions, the introduction of the perturbation is relevant whenever the susceptibility diverges at the phase transition. A proof based solely on the system's symmetries is currently in progress.

In systems with $O(N)$ symmetry, a quite general form that can be taken by the perturbation of the action is:

$$\delta\mathcal{S} = \delta K_- \left(\hat{\phi}_1\phi_2 - \hat{\phi}_2\phi_1\right) f\left(\phi_1^2, \phi_2^2, \left(\hat{\phi}_1\phi_2 - \hat{\phi}_2\phi_1\right)^2\right) \ , \tag{8.26}$$

where f is any analytic function that is symmetric under the exchange of the first two arguments. For such a form of the perturbation, we can use scaling arguments to show that the dominant contribution is the same as in the simpler case considered in the previous section. Let us consider for example $f = \phi_1^2 + \phi_2^2$. This corresponds to the following perturbed dynamics:

$$\begin{aligned} \partial_t\phi_1 &= \nabla^2\phi_1 - V'(\phi_1) + \eta_1 + h_1 + \delta K_-\phi_2\left(\phi_1^2 + \phi_2^2\right) \\ \partial_t\phi_2 &= \nabla^2\phi_2 - V'(\phi_2) + \eta_2 + h_2 - \delta K_-\phi_1\left(\phi_1^2 + \phi_2^2\right) \end{aligned} \tag{8.27}$$

We can compute as before the correction to the order parameter:

$$\delta\langle\phi_1(\mathbf{x}, t)\rangle = -\delta K_-\langle\phi_1(\mathbf{x}', t')\int_{\mathbf{x}',t'}\left(\hat{\phi}_1\phi_2 - \hat{\phi}_2\phi_1\right)\left(\phi_1^2 + \phi_2^2\right)\Big|_{\mathbf{x}',t'}\rangle_0 \ . \tag{8.28}$$

As before the averages can be computed independently for the two fields. The terms with $\hat{\phi}_2$ do not contribute, because $\hat{\phi}_2(x,t)$ corresponds to the response to a perturbation at a time infinitesimally successive to t, and therefore $\langle \hat{\phi}_2 \phi_2^2|_{\mathbf{x}',t'} \rangle_0 = 0$. Since ϕ_1^2 and ϕ_2^2 are not critical fields, they do not change the critical behavior of the dominant term. As in the previous case, the perturbation is then relevant whenever the susceptibility diverges.

8.3.2 Directed percolation

To see what happens if the system lacks the reversal symmetry, let us consider the case of Directed Percolation. This well-studied statistical physics model, which we have already encountered in Section 2.4.1 and in Chapter 4, is used to describe spreading phenomena such as forest fires or epidemics, or particles reproducing and annihilating on a lattice. It undergoes an out-of-equilibrium phase transition between an active and an inactive phase. Any phase transition with a unique absorbing phase is conjectured to fall in the universality class of directed percolation.

The Langevin equation of motion for the density of particles is [89]:

$$\partial_t \rho = \nabla^2 \rho + m\rho - \lambda \rho^2 + \sqrt{\rho}\eta \ , \tag{8.29}$$

η is a white Gaussian noise with amplitude T.

In the case of Directed Percolation, a natural way to introduce non-reciprocal interactions between two species is via a quadratic term: the two species interact only if both are present. The model becomes then equivalent to a Lotka-Volterra system with space and demographic fluctuations.

$$\partial_t \rho_1 = \nabla^2 \rho_1 + m\rho_1 - \lambda \rho_1^2 + \sqrt{\rho_1}\eta_1 + \delta K_- \rho_1 \rho_2 \ , \tag{8.30}$$

$$\partial_t \rho_2 = \nabla^2 \rho_2 + m\rho_2 - \lambda \rho_2^2 + \sqrt{\rho_2}\eta_2 - \delta K_- \rho_1 \rho_2 \ . \tag{8.31}$$

Note a crucial difference with respect to the previously studied case: the ρ_i are densities, and as such must be positive. This means that the system is not symmetric under the inversion of the two fields, and we cannot exchange the identities of the two species by reversing one of the two fields. The two species therefore need not be equivalent, and in particular there is no guarantee that they have the same critical point. Indeed what we expect to happen in this case is that the species that is unfavored by the interaction (the "prey" if we think of Lotka-Volterra) will encounter the transition to the absorbing phase before than it would have in the unperturbed case. After that, the "predator" undergoes the same transition as in the unperturbed case, since the interaction term is zero if the other species is not present. Our criterion is therefore not applicable to this case.

It could be possible to recover the equivalence between species by considering three of them, with cyclic non-reciprocal interactions, forming a rock-paper-scissors game [354, 355]. Our criterion could be generalizable to this case, but we leave this perspective open for future studies.

8.4 Generality of the approach

The method presented here, which we have already used to derive both the Harris criterion and our non-reciprocal one, can be applied to assess whether a generic perturbation will change the critical behavior of a phase transition. The essential steps are: (i) writing down the MSRDJ action and its perturbation for the system of interest; (ii) assessing whether the perturbation will shift the critical point (iii) computing the first order correction of the order parameter (iv) express its scaling in terms of the unperturbed critical exponents (v) compare the correction to the unperturbed order parameter.

To elucidate the generality of our approach, we will now apply it to several other relevant cases of non-reciprocally coupled systems. The different cases we will consider are summarized in Fig. 8.1,where K_+ and K_- refer respectively to the symmetric and antisymmetric components of the interactions.

8.4.1 Two critical points

What happens if the two fields have different critical points, for example two different critical temperatures? Let us suppose that ϕ_1 is the first to encounter the symmetry-breaking transition. We can carry out the same computation for the correction to $\langle\phi_1\rangle$ as in the previous case, arriving again at Eq. (8.22). Nevertheless, around the transition of ϕ_1, ϕ_2 would still be deep in the disordered phase, so that $\langle\phi_2\rangle_0 = 0$, and there would be no correction at linear order in δK_-. In general, the coupling to a subcritical field is an irrelevant perturbation, this also holds in the non-reciprocal case.

8.4.2 Reciprocally coupled fields

In the previous section, ϕ_1 and ϕ_2 were independent in the absence of the perturbation. We will now show that this assumption is crucial: in the presence of a finite reciprocal coupling in the unperturbed field theory the criterion is strongly modified and the addition of non-reciprocity is irrelevant in most physical cases. We consider two fields with a finite reciprocal coupling K_+ and a infinitesimal non-reciprocal one δK_-. They are described by the following dynamical equations:

$$\begin{aligned}\partial_t\phi_1 &= \nabla^2\phi_1 - V'(\phi_1) + \eta_1 + h_1 + (K_+ + \delta K_-)\phi_2\\ \partial_t\phi_2 &= \nabla^2\phi_2 - V'(\phi_2) + \eta_2 + h_2 + (K_+ - \delta K_-)\phi_1\end{aligned} \tag{8.32}$$

For simplicity, we consider a quartic potential $V(\phi) = -\frac{a}{2}\phi^2 + \frac{b}{4}\phi^4$ for the remainder of this section, but we expect our results to hold more generically.

We first review what happens without the non-reciprocal perturbation. Two uncoupled ϕ^4 theory have 4 equivalent minima of the energy: each field can independently have positive or negative magnetization. The introduction of J partially lifts this degeneracy, because the states with same-sign magnetizations are now favored. When lowering the temperature, the system will undergo a phase transition in which one of the two aligned states will be selected. Because the phase transition breaks the $\mathbb{Z}_2$ symmetry between these two favored configurations, we expect it to fall in the Ising universality class. The natural order parameter for this phase transition is the sum of the two fields. We thus define

$$\psi = \frac{\phi_1 + \phi_2}{\sqrt{2}}\ , \qquad\qquad \varphi = \frac{\phi_1 - \phi_2}{\sqrt{2}}\ . \tag{8.33}$$

Rewriting the dynamical equations in terms of ψ and φ yields

$$\partial_t\psi = \nabla^2\psi + \eta_\psi + (a+J)\psi - b\left(\frac{\psi^3}{2} + \frac{3}{2}\psi\varphi^2\right) - \delta K\varphi \tag{8.34}$$

$$\partial_t\varphi = \nabla^2\varphi + \eta_\varphi + (a-J)\varphi - b\left(\frac{\varphi^3}{2} + \frac{3}{2}\varphi\psi^2\right) + \delta K\psi\ , \tag{8.35}$$

where η_ψ and η_φ are Gaussian white noises with the same statistics as η_1 and η_2. When $\delta K = 0$, ψ and φ are only coupled through a cubic term. Neglecting this, we have two uncoupled ϕ^4 theories that only differ for their linear term, leading to two different transition points. ψ has

a larger linear term, therefore it will be the first to undergo the $\mathbb{Z}_2$-symmetry-breaking phase transition, as we expected. The cubic term that couples ψ to φ^2 is irrelevant for the critical properties of the system, since we already know it has to fall in the Ising universality class. To see that, let us separate φ^2 as $\varphi^2 = \varphi_0^2 + \tilde{\varphi}$, where φ_0 is a constant part while $\tilde{\varphi}$ are the fluctuations around φ_0^2. φ_0^2 will simply shift the transition point for ψ. When ψ undergoes the phase transition, φ is still subcritical: as such the fluctuations $\tilde{\varphi}$ do not exhibit long range correlations and therefore will not change the large scale properties of the system.

The new fields ψ and φ are coupled anti-symmetrically by the perturbation, the system thus falls in the category considered in Section 8.4.1. We can therefore use the results of the previous section to conclude that adding a non-reciprocal perturbation on top of finite reciprocal interactions is an irrelevant perturbation.

This prediction is confirmed in numerical simulations of the non-reciprocal Ising Model performed in [291]: the addition of a reciprocal coupling between the two species of spins indeed leads to the re-stabilization of the paramagnetic to ferromagnetic transition (see the phase diagram in Figure 8.3b). We have measured the critical exponents of this phase transition in 3 dimensions[1], and they are very close to the Ising ones, albeit not always within errorbars (Figure 8.4). This is probably due to an underestimation of the errors.

8.4.3 Random perturbations

The dynamical procedure to evaluate the relevance of a non-reciprocal perturbation can be used also for random ones, as we have already done to derive the Harris criterion.

Uncoupled fields case

We now consider as a perturbation a space-dependent random antisymmetric interaction $\delta K_-(\mathbf{x})$, coupling $\phi_1(\mathbf{x})$ and $\phi_2(\mathbf{x})$. $\delta K_-(\mathbf{x})$ is Gaussian distributed with mean zero and delta correlations $\overline{\delta K_-(\mathbf{x})\delta K_-(\mathbf{x}')} = \delta\sigma_K^2\delta(\mathbf{x}-\mathbf{x}')$; the overbar indicates an average over the quenched disorder.

As before, we can use the MSRDJ formalism to expand the correction to the order parameter $\langle\phi_i\rangle$ in powers of the interactions. Because of their randomness, the correction will also be a random quantity. Since the random interactions are centered in 0, the correction at linear order will average to 0. Its variance is given by:

$$\overline{\langle\phi_i(x,t)\rangle^2}_c \sim \epsilon\langle\phi_j\rangle_0^2 \int_{x',t',t''} \langle\frac{\partial\phi_i(x,t)}{\partial h_i(x',t')}\rangle_0 \langle\frac{\partial\phi_i(x,t)}{\partial h_i(x',t'')}\rangle_0 \ .$$

Close to the critical point, the response function scales as [350]:

$$\langle\frac{\partial\phi_i(x,t)}{\partial h_i(x',t')}\rangle_0 = \xi^{-d-z+\frac{\gamma}{\nu}} f\left(\frac{x-x'}{\xi}, \frac{t-t'}{\tau}\right) \ . \tag{8.36}$$

Plugging this form in the integral we find:

$$\overline{\langle\phi_i(x,t)\rangle^2}_c \sim \epsilon(T-T_c)^{2\beta-2\gamma+d\nu} \sim (T-T_c)^{6\beta-\nu d} \ . \tag{8.37}$$

To determine whether the perturbation is relevant, we need to compare the standard deviation of the correction to the unperturbed order parameter. We find that the introduction of random non reciprocal interactions is relevant if:

$$2\beta - \frac{\nu d}{2} > 0 \ . \tag{8.38}$$

[1] The numerical simulations of the non-reciprocal Ising model were performed by Yael Avni.

This inequality is not satisfied by the 3D Ising model, therefore in that case the universality class will not change.

Our computation can be generalized to non antisymmetric interactions, i.e. to the case in which the system is perturbed by two random interactions coefficients $\delta K_{12}(\mathbf{x})$ (for the effect of ϕ_2 on ϕ_1) and $\delta K_{21}(\mathbf{x})$ (for the effect of ϕ_1 on ϕ_2). We find that the scaling of the correction is unchanged, for any value of the correlation coefficient between $\delta K_{12}(\mathbf{x})$ and $\delta K_{21}(\mathbf{x})$. Indeed the result we found is the same that would be obtained from an equilibrium treatment of random symmetric interactions, but our dynamical approach allowed us to generalize it to an out-of-equilibrium case.

Non-reciprocally coupled fields case

We now consider the case of antisymmetric interactions with a finite constant component K_- and a random, inhomogeneous perturbation $\delta K_-(\mathbf{x})$, where $\delta K_-(\mathbf{x})$ is as before a Gaussian quenched variable, δ-correlated in space. In Section 8.3 we showed that, without the randomness, the introduction of the constant non-reciprocal coupling K_- changes the critical behavior with respect to the case $K_- = 0$. In the case of the 3D Ising model, the addition of a nonzero K_- leads to the non-reciprocal Ising Model [291, 304] where the paramagnetic to ferromagnetic transition is replaced by a transition to an oscillating phase, dubbed *swap phase*, that breaks time-translational invariance [291, 292]. The phase diagram from [304] is reproduced in Figure 8.3a. In this swap phase, the fields ϕ_1 and ϕ_2 homogeneously oscillate in time, without exhibiting any decay in synchronization: they form a perfect time-crystal. The order parameter quantifying this transition to oscillations is the momentum $\mathcal{L} = \langle \dot{\phi}_1 \phi_2 - \dot{\phi}_2 \phi_1 \rangle$. The phase transition is believed to fall in the XY universality class. All the critical exponents have been measured and agree with the XY values within uncertainty [291] (see Figure 8.4).

The transition from the disordered to the swap phase can be triggered by lowering the temperature, by increasing the intra-species couplings, or by decreasing the non-reciprocal interactions K_- (see Figure 8.3a). Since the transition can be triggered by a change in K_-, the perturbation $\delta K_-(\mathbf{x})$ locally shifts the distance from the critical point. It does not break chiral symmetry, which is the symmetry that will be broken at the transition. Therefore its relevance can be evaluated with the Harris criterion, thanks to the fact that we have proved its validity also for non-equilibrium systems: it will be relevant if $\frac{\nu d}{2} < 1$. If the system does indeed fall in the XY universality class, in 3 dimensions the perturbation is irrelevant.

8.5 Conclusions

In conclusion, we have developed a series of criteria on the critical exponents of a generic phase transition to determine whether perturbing the system with non-reciprocal interactions can modify its critical behavior. As for the Harris criterion on the relevance of disorder at a phase transitions, our criteria are expressed in terms of the unperturbed critical exponents. The class of systems we considered are bipartite field theories that can be either coupled (reciprocally or non-reciprocally) or uncoupled in the absence of the perturbation. The systems are perturbed by non-reciprocal interactions between the two parts, which can either be homogeneous or random in space. Our results are summarized in the table in Figure 8.1. We find that for homogeneous interactions the result crucially depends on whether the two field theories are reciprocally coupled before the perturbation: in the uncoupled case the perturbation is relevant, if they are reciprocally coupled it is irrelevant. These findings are confirmed by the numerical results reported in [291]. We also considered spatially heterogeneous non-reciprocal interactions. If the fields are uncoupled before the perturbation, this turns out to be relevant if $2\beta - \nu d/2 < 0$.

If they are non-reciprocally coupled we find the same result as in the original Harris criterion: relevance of the random perturbation for $\nu d/2 < 1$.

Chapter 9

Conclusions and perspectives

Biological systems are inherently complex and operate far from equilibrium — features that are crucial to the rich emergent behaviors observed in nature. These systems often also display multiple levels of organization, in which case they can be described as networks of coupled complex systems. This hierarchical structure [8, 15], which may also be relevant outside biological contexts [9], gives rise to both unique theoretical challenges and intriguing emergent phenomena. In this thesis, I have described two classes of systems composed of interacting complex components: diverse ecological meta-communities and pairs of complex systems coupled through non-reciprocal interactions, which I introduced respectively in Chapters 2 and 5.

The main analytical tool throughout the thesis was Dynamical Mean Field Theory, which I described in Chapter 3. DMFT provides an effective description of many-body systems in term of the dynamics of a single degree of freedom, coupled to an additional noise source. When applied to ecological systems, DMFT allows us to bridge the gap between complex ecological models and single species stochastic descriptions, offering insights into why these two perspectives often yield similar results. I leveraged this mapping to derive the species abundance distribution under a number of simplified dynamics. I also proposed an approximate solution scheme for the dynamical phase, which could enable the study of chaotic dynamics in a spatially extended ecosystem. In Chapters 4, 6 and 7, I have generalized DMFT to systems with two levels of organization. Instead of obtaining an effective dynamics for a single degree of freedom, the resulting description involves multiple degrees of freedom: infinitely many in the case of ecological meta-communities, and two in the case of non-reciprocally coupled complex systems.

In Chapter 4, I studied a model that combines ecological dynamics, heterogeneous interactions and spatial structure, uncovering a novel mechanism for the survival of diversity-rich ecosystems in the presence of demographic fluctuations. For a single species, one finds a continuous phase transition between an extinction and a survival state, which falls into the universality class of Directed Percolation. The same is true in the case of many species with constant competitive interactions. The introduction of heterogeneity in the interaction network generates instead a richer behavior, with two distinct regimes in the transition from survival to extinction. In the presence of sufficiently strong demographic noise, the system exhibits behavior akin to the single-species case, undergoing a continuous transition. Conversely, at low demographic noise, the transition becomes discontinuous and the system exhibits novel features, that are a signature of the ecosystem's complexity. The combined effects of the heterogeneity in the interaction network and migration enable the community to thrive even in situations where demographic noise would lead to the extinction of isolated species. This is possible thanks to the spontaneous emergence of mutualistic interactions, due to the exclusion of strongly competing species from the community. The emergence of mutualism induces the development of global bistability, accompanied by sudden tipping points. I proposed a way to predict the catastrophic shift from

high diversity to extinction by probing responses to perturbations as an early warning signal.

In Chapter 6 I studied pairs of complex agents, whose internal dynamics I modeled by a spin-glass, coupled by non-reciprocal interactions. Glassy systems do not reach equilibrium even on very long time scales: their dynamics exhibits instead a dramatic slowdown known as aging. While it was long believed that any amount of non-reciprocity would destroy glassiness in marginal models, I demonstrated that the outcome strongly depends on the structure of the system. Specifically, I considered a bipartite many-body spin-glass system with random symmetric interactions in each part, and fixed antisymmetric interactions between the two parts. I uncovered a finite temperature non-reciprocal spin-glass transition between a static disordered phase and a time-dependent amorphous phase. At low temperature, the system undergoes a "non-reciprocal aging" dynamics, characterized by both slow dynamics and oscillations. The mechanism underpinning the destabilization of the usual spin-glass in favor of the non-reciprocal one is a spectral singularity called exceptional point. The inversion symmetry that is spontaneously broken at long times in the usual spin-glass phase is dynamically restored, and replaced by a spontaneous breaking of chiral symmetry. Asymptotically, the system rotates in the plane of the two lowest energy modes of the uncoupled system. Interestingly, these phenomena are destroyed if the non-reciprocal coupling are randomly sampled from a continuous distribution, whereas they persist if the distribution is restricted to a finite set of discrete values. These two cases correspond indeed to two distinct physical scenarios, with "microscopic" versus "macroscopic" non-reciprocity.

In Chapter 7 I presented some preliminary results and ongoing works on the impact of non-reciprocity on the dynamics of other aging systems. Non-reciprocal aging, combining slow dynamics and oscillations, also occurs in the coarsening dynamics of two non-reciprocally coupled $O(N)$ models. I conjecture that aging is instead always interrupted in the p-spin model, but on a timescale that diverges very strongly at small non-reciprocity. For even p, I find a phase transition between a chaotic phase, in which the system decorrelates from initial conditions and becomes time-translationally invariant, to an oscillating phase, in which it rotates indefinitely in a plane set by the initial conditions. The existence of this oscillating phase requires an even p, as this guarantees the symmetry of the single-system energy landscape under inversion. I also propose how to couple two trap models to study the effect of non-reciprocity on activated dynamics.

In Chapter 8, I studied the effect of non-reciprocal interactions on the critical behavior of pairs of systems undergoing a phase transition. I developed some criteria on the critical exponents of the unperturbed systems to predict whether the critical behavior would be modified by different kinds of infinitesimal non-reciprocal perturbations. For uniform non-reciprocal interactions, the perturbation is relevant whenever the susceptibility diverges at the phase transition, as confirmed by numerical results on the non-reciprocal Ising model. If we consider instead spatially heterogeneous random perturbations, I find a different non-trivial criterion on the critical exponents. The procedure is quite general, and also allows one to generalize the Harris criterion on the relevance of disorder at a phase transition to non-equilibrium systems.

I would like to conclude this thesis by outlining some promising directions for future research. The behavior of spatially-extended diverse ecosystems in the strong heterogeneity regime is still poorly understood. In the symmetric interactions case, a single community performs an aging dynamics in a complex landscape with an exponential number of equilibria. Considering a network of local communities coupled in space by migration could have a strong impact on this aging dynamics. Starting from independent initial conditions, different communities could explore different equilibria, which could then coarsen in competing patches with similar compositions. The possibility for equilibria to propagate in space could lead to an increased relevance of solutions that are very stable but have a small basin of attraction. Beyond its

ecological relevance, such a system would be quite interesting also from the disordered systems perspective: each local community would correspond to a "real replica" of a spin-glass with the same disorder, all coupled in space by the migration.

In the case of non-symmetric interactions, aging is replaced by chaotic dynamics. In a single community, in the presence of finite immigration, the abundances of all species fluctuates over several orders of magnitude. Without immigration, if we consider a finite extinction threshold, the fluctuations lead to the progressive extinction of some fraction of the species, until the diversity decreases enough to allow for a marginally stable (but invadable) equilibrium. In a spatially extended system, unsynchronized fluctuations in different locations could prevent extinctions, allowing the chaotic dynamics to self-sustain. This could be a crucial mechanism for the stabilization of diversity in natural ecosystems, in which chaotic dynamics has been experimentally demonstrated to be widespread. However, strong diffusion could synchronize the system, leading again to global extinctions. The transition between the chaotic and fixed point regimes has never been explored analytically in spatially extended ecosystems. Since the fixed point solution is an absorbing state of the system, there could also be some interesting connection with the Directed Percolation problem, but in a system with an exponential number of absorbing states.

Several research directions remain open also regarding the non-reciprocal coupling of complex agents. In the case of the $O(N)$ model, it would be interesting to perform numerical simulations of the coarsening dynamics for $N > 1$, to compare with our analytical results. For what regards the p-spin, a small non-reciprocity expansion could allow us to confirm whether aging is always destroyed, and to obtain the scaling of the timescale on which it is interrupted. The peculiar transition from chaos to oscillating memory that we find for even p also deserves further investigations. The effect of non-reciprocity on activated dynamics could be analyzed in the trap model that I proposed here, whose study is still at a preliminary stage.

The macroscopic non-reciprocal coupling between complex agents may also have direct applications in a variety of biological, economic, and sociological contexts. In machine learning, pairs of networks with adversarial goals can perform useful tasks. One example is Generative Adversarial Networks [356]. They are composed of a generator network that attempts to produce images resembling those in a training set, and a discriminator network that tries to distinguish between real and generated images. This antagonistic interaction enables the two networks to train each other, but can also introduce instabilities in the learning process. It would be interesting to apply the framework developed in this thesis to gain deeper insight into such systems.

Appendix A

Diverse ecological systems

A.1 Stationary probability distribution in the symmetric case

In the case of symmetric interactions ($\gamma = 1$), in the single equilibrium phase, the system relaxes to equilibrium and it verifies the Fluctuation-Dissipation Theorem (FDT) [158]:

$$R_d(\tau) = -\frac{1}{T}\frac{dC(\tau)}{d\tau} \ . \tag{A.1}$$

We can integrate by parts the term with the memory kernel:

$$\begin{aligned} \int_0^t R_d(t-s)N(s)ds = \frac{1}{T}\int_0^t \frac{dC_d(t-s)}{ds}N(s)ds = \\ = \frac{1}{T}\left(C_d^0 N(t) - C(t)N(0) - \int_0^t C_d(t-s)\dot{N}(s)ds\right) = \\ = \frac{1}{T}\left(\left(C_d^0 - C_d^\infty\right)N(t) - \int_0^t \left(C_d(t-s) - C_d^\infty\right)\dot{N}(s)ds\right) \ . \end{aligned} \tag{A.2}$$

We have obtained an additional quadratic term in $N(t)$, and a friction term. The friction term and the noise ξ describe the coupling of the system to an effective colored bath at temperature T, that replaces the coupling of one species to all the others.

Using Martin-Siggia-Rose-De Dominicis-Janssen (MSRDJ) formalism, we can show that the stationary probability distribution associated with the stochastic differential equation To show that this is the correct equilibrium distribution we need to verify that, with this as an initial condition, time reversal is a symmetry of the associated MSRDJ action. We will do it, following reference [175], for a simplified dynamics, that contains all the crucial ingredients:

$$\dot{N} = N\left(1 - N - \xi(t) - \int_0^t \nu(t,s)\dot{N}(s)ds\right) + \eta(t)\sqrt{N} + \lambda \tag{A.3}$$

$$\langle \xi(t)\xi(s)\rangle = T\nu(t-s) \tag{A.4}$$

$$\langle \eta(t)\eta(s)\rangle = 2T\delta(t-s) \ . \tag{A.5}$$

Its equilibrium distribution is given by:

$$P_{eq}(N) = \frac{e^{-\beta H}}{Z} \tag{A.6}$$

$$H = N^2/2 - N + (T-\lambda)\log N \ , \tag{A.7}$$

where $\beta = 1/T$, the inverse temperature. The white noise should be interpreted according to Ito's discretization. It is convenient to convert it to Stratonovich's discretization, which is left

invariant by time reversal. The multiplicative nature of the noise makes the two discretizations not equivalent: we then need to introduce an additional drift term as follows

$$\eta\sqrt{N} \to \eta\sqrt{N} - \frac{1}{2}\frac{\sqrt{2T}}{2\sqrt{N}}\sqrt{2TN} = \eta\sqrt{N} - \frac{T}{2} \ . \tag{A.8}$$

The MSRDJ action can be written in terms of a deterministic and a dissipative part [175,357]

$$S[N,\hat{N}] = S^{det}[N,\hat{N}] + S^{diss}[N,\hat{N}] \tag{A.9}$$

$$S^{det}[N,\hat{N}] = \log P_{eq}(N(-T)) + \int_{-T}^{T} du \left(i\hat{N}(N(1-N) + \lambda - T/2 - T/2) + N - 1/2 \right) \tag{A.10}$$

$$S^{diss}[N,\hat{N}] = \int_u i\hat{N}_u \int_v (\delta(u-v) + \nu(u-v)\theta(u-v)N_u)(iT\hat{N}_v N_v - \dot{N}_v) \ . \tag{A.11}$$

The time reversal transformation for the two fields is given by:

$$N(t) \longrightarrow N_R(t) = N(-t) \tag{A.12}$$

$$i\hat{N}(t) \longrightarrow i\hat{N}_R(t) = i\hat{N}(-t) + \frac{1}{TN(-t)}\frac{\partial}{\partial t}N(-t) \ . \tag{A.13}$$

The deterministic and dissipative part of the action are independently invariant under this transformation:

$$\begin{aligned}
S^{det}[N_R,\hat{N}_R] &= -\log Z - \beta H(N(T)) + \\
&+ \int_u \left(\left(i\hat{N}_{-u} + \frac{1}{TN_{-u}}\frac{\partial}{\partial u}N_{-u} \right)(N_{-u}(1-N_{-u}) + \lambda - T) + N_{-u} - 1/2 \right) = \\
&= -\log Z - \frac{1}{T}(N_T^2/2 - N_T + (T-\lambda)\ln N_T) + \\
&+ \frac{1}{T}\int_u \frac{\partial}{\partial u}\left(N_u^2/2 - N_u + (T-\lambda)\ln N_u \right) + \int_u \left(i\hat{N}_u(N_u(1-N_u) + \lambda - T) + N_u - 1/2 \right) = \\
&= -\log Z - \beta H(N(-T)) + \int_u \left(i\hat{N}_u(N_u(1-N_u) + \lambda - T) + N_u - 1/2 \right) = S^{det}[N,\hat{N}]
\end{aligned}$$

$$\begin{aligned}
S^{diss}[N_R,\hat{N}_R] &= \int_u \left(i\hat{N}_{-u} + \frac{1}{TN_{-u}}\frac{\partial}{\partial u}N_{-u} \right) \int_v (\delta_{u-v} + \nu_{u-v}\theta_{u-v}N_u) iT\hat{N}_{-v}N_{-v} = \\
&= \int_u \left(iT\hat{N}_u N_u - \dot{N}_u \right) \int_v (\delta_{v-u} + \nu_{v-u}\theta_{v-u}N_v) i\hat{N}_v = S^{diss}[N,\hat{N}] \ .
\end{aligned} \tag{A.14}$$

The action is invariant under the time reversal transformation using P_{eq} as initial and final condition, therefore P_{eq} is the correct equilibrium probability distribution.

A.2 SAD under white demographic and colored environmental noise

The species abundance distribution under a combination of a white demographic noise and a colored environmental one was obtained in Mathematica by integrating the approximate UCNA Fokker-Planck equation. Its logarithm takes the following form:

$$\frac{1}{2}\Bigg(-\frac{n^2\,r^2\,\tau}{k^2\,Te+k\,r\,Td\,\tau}+\frac{2\,n\,r\left(r^2\,Td\,\tau^2+k\,Te\left(-1+r\,\tau\right)\right)}{\left(k\,Te+r\,Td\,\tau\right)^2}+$$

$$\Bigg(2\,k^{3/2}\,Te\left(r^2\,Td^2\,\tau^2\left(Td-2\,\lambda\left(2+r\,\tau\right)\right)+k\,r\,Td\left(-Te\,\lambda\,\tau\left(5+4\,r\,\tau\right)+Td\left(1+r\,\tau+2\,Te\,\tau\right)\right)+$$

$$k^2\,Te\left(Te\,(Td-\lambda)+r\left(Td-2\,Te\,\lambda\,\tau\right)\right)\right)\text{ArcTanh}\Big[\frac{k\left(Td+2\,n\,Te\right)+2\,n\,r\,Td\,\tau}{\sqrt{k}\;\sqrt{Td}\;\sqrt{-4\,r\,Td\,\lambda\,\tau^2+k\left(Td-4\,Te\,\lambda\,\tau\right)}}\Big]\Bigg)\Big/$$

$$\left(\sqrt{Td}\,\left(k\,Te+r\,Td\,\tau\right)^3\,\sqrt{-4\,r\,Td\,\lambda\,\tau^2+k\left(Td-4\,Te\,\lambda\,\tau\right)}\right)-\frac{2\,(Td-\lambda)\,\text{Log}[n]}{Td}+2\,\text{Log}\Big[k\,n+n^2\,r\,\tau+k\,\lambda\,\tau\Big]-$$

$$\frac{1}{Td\left(k\,Te+r\,Td\,\tau\right)^3}\Big(k^3\,Te^2\left(-r\,Td+Te\,(Td+\lambda)\right)+k\,r^2\,Td^2\,Te\left(5\,Td+2\,\lambda\right)\tau^2+2\,r^3\,Td^4\,\tau^3-$$

$$k^2\,r\,Td\,Te\left(Td+r\,Td\,\tau-4\,Td\,Te\,\tau-3\,Te\,\lambda\,\tau\right)\Big)\,\text{Log}\Big[k\,n\,Td+k\,n^2\,Te+n^2\,r\,Td\,\tau+k\,Td\,\lambda\,\tau\Big]\Bigg)$$

`n` is the abundance, `r` the growth rate, `k` the carrying capacity, `Te` the amplitude of the environmental noise, τ its correlation time, `Td` the amplitude of the demographic noise, λ the immigration rate.

A.3 DMFT derivation

Here we outline the derivation, adapted from reference [66], of the Dynamical Mean Field Theory for our system, for generic value of the spatial correlation of the interactions ρ.

We consider S species, indexed by $i = 1, ...S$, and their Lotka-Volterra dynamics,

$$\dot{N}_{i,u} = N_{i,u}\left(1 - N_{i,u} - \sum_j \alpha^u_{ij} N_{j,u} + \zeta_{i,u}\right) + D\left(\frac{1}{c}\sum_{v\in\partial u} N_{i,v} - N_{i,u}\right) + \eta^u_i(t)\sqrt{N_{i,u}} + \lambda_{i,u}$$

to which we have added a perturbation to the carrying capacity $\zeta_{i,u}$ and an external immigration $\lambda_{i,u}$, that will be taken to zero at the end of the computation. These equations (for a given value of the $\eta^u_i(t)$) define the trajectories $N_{i,u}(t)$. We add a new species, $i = 0$, to the system, and we draw its interactions and initial conditions independently from the rest of the system and with the same statistics. At large S, thanks to the scaling of the interactions, the presence of a new species is a small perturbation to the system, so that the trajectories of the other S species will only be slightly modified. We consider their linear response:

$$\delta N_{i,u}(t) = \sum_{v\in\partial u, j}\int_0^t \frac{\delta N_{i,u}(t)}{\delta\zeta_{j,v}(t')}(-\alpha^v_{j0}N_{0,v}(t'))dt' = \sum_{v\in\partial u, i}\int_0^t R^{u,v}_{i,j}(t,t')(-\alpha^v_{j0}N_{0,v}(t'))dt' \quad \text{(A.15)}$$

We have introduced the response function $R^{u,v}_{i,j}(t,t')$ of the abundance of species i in patch u at time t to a variation in the carrying capacity of species j in patch v at time t'.

The dynamics of species 0 will depend on these new trajectories:

$$\dot{N}_{0,u} = N_{0,u}\left(1 - N_{0,u} - \sum_i \alpha^u_{0i}\left(N^0_{i,u} + \delta N_{i,u}\right)\right) + D\left(\frac{1}{c}\sum_{v\in\partial u} N_{0,v} - N_{0,u}\right) + \eta_{0,u}(t)\sqrt{N_{0,u}}\ .$$

Because the correlations between interaction coefficients in any two patches are the same, these Gaussian variables can generically be decomposed into a common random contribution, identical in all patches and proportional to the correlation ρ, and one independent in different patches, proportional to $\sqrt{1-\rho^2}$. We thus introduce the matrix $a_{i,j}$ and $a^u_{i,j}$ such that $\alpha^u_{i,j} = \mu/S + \sigma\left(\rho a_{i,j} + \sqrt{1-\rho^2}a^u_{i,j}\right)$, $\mathbb{E}\left[a_{i,j}\right] = \mathbb{E}\left[a^u_{i,j}\right] = 0$, $\mathbb{E}\left[a^2_{i,j}\right] = \mathbb{E}\left[{a^u_{i,j}}^2\right] = 1/S$, $\mathbb{E}\left[a_{i,j}a_{j,i}\right] = \mathbb{E}\left[a^u_{i,j}a^u_{j,i}\right] = \gamma/S$ and all other correlations are 0. We can rewrite the interaction term as:

$$\begin{aligned}-\sum_i \alpha_{0i}\left(N^0_{i,u} + \delta N_{i,u}\right) = -\sum_i \left(\mu/S + \sigma\left(\rho a_{0i} + \sqrt{1-\rho^2}a^u_{0i}\right)\right) N^0_{i,u} + \\ + \sum_{i,j}\left(\mu/S + \sigma\left(\rho a_{i0} + \sqrt{1-\rho^2}a^u_{i0}\right)\right)\left(\mu/S + \sigma\left(\rho a_{0j} + \sqrt{1-\rho^2}a^u_{0j}\right)\right)\cdot \\ \cdot \sum_{v\in\partial u}\int_0^t R^{u,v}_{i,j}(t,t')N_{0,v}(t')dt' \ .\end{aligned} \tag{A.16}$$

We want to describe its statistical properties in the limit $S \to \infty$. The response function $R^{u,v}_{i,j}(t,t')$ is defined on the unperturbed trajectories, and is therefore uncorrelated from the interactions coefficients with species 0. $R^{u,v}_{i,j}(t,t') \sim 1/\sqrt{S}$ for $i \neq j$ [66], so that the off-diagonal terms can be neglected. Thanks to the central limit theorem, $\sum_j a_{0j}a_{j0}R^{u,v}_{j,j}(t,t')$ will converge to its average:

$$\sum_j a_{0j}a_{j0}R^{u,v}_{j,j}(t,t') \to S\mathbb{E}\left[a_{0j}a_{j0}\right]\mathbb{E}\left[R^{u,v}_{j,j}(t,t')\right] = \gamma\mathbb{E}\left[R^{u,v}_{j,j}(t,t')\right] \ . \tag{A.17}$$

By similarly evaluating all terms in (A.16) we obtain:

$$\begin{aligned}-\sum_j \alpha_{0j}\left(N^0_{j,u} + \delta N_{j,u}\right) \to -\mu\mathbb{E}\left[N^0_{j,u}\right] - \sigma\rho\tilde{\xi}_u(t) - \sigma\sqrt{1-\rho^2}\tilde{\psi}_u(t) + \\ +\sigma^2\rho^2\gamma\sum_{v\in\partial u}\int_0^t \mathbb{E}\left[R^{u,v}_{j,j}(t,t')\right]N_{0,v}(t')dt' + \sigma^2(1-\rho^2)\gamma\int_0^t \mathbb{E}\left[R^{u,u}_{j,j}(t,t')\right]N_{0,u}(t')dt' \ ,\end{aligned} \tag{A.18}$$

where $\tilde{\xi}_u(t)$ and $\tilde{\psi}_u(t)$ are Gaussian fields with zero mean and covariance $\mathbb{E}\left[\tilde{\xi}_u(t)\tilde{\xi}_v(t')\right] = \mathbb{E}\left[N^0_{j,u}(t)N^0_{j,v}(t')\right]$, $\mathbb{E}\left[\tilde{\psi}_u(t)\tilde{\psi}_v(t')\right] = \delta_{uv}\mathbb{E}\left[N^0_{j,u}(t)N^0_{j,u}(t')\right]$. Note that $\tilde{\xi}_u$ and the first integral of A.18 derive from the component of the interactions constant across patches, a_{ij}, as we can see from the ρ-dependent prefactors, and they therefore couple different patches. $\tilde{\psi}_u$ and the second integral of A.18 derive instead from the component of the interactions independent across patches, a^u_{ij}, and therefore represent diagonal correlations and responses. Plugging this expression in the dynamical equation for species 0 we obtain:

$$\begin{aligned}\dot{N}_{0,u} = N_{0,u}\Bigg(1 - N_{0,u} - \mu\mathbb{E}\left[N^0_{j,u}\right] - \sigma\rho\tilde{\xi}_u(t) - \sigma\sqrt{1-\rho^2}\tilde{\psi}_u(t) + \\ +\sigma^2\rho^2\gamma\sum_{v\in\partial u}\int_0^t \mathbb{E}\left[R^{u,v}_{j,j}(t,t')\right]N_{0,v}(t')dt' + \sigma^2(1-\rho^2)\gamma\int_0^t \mathbb{E}\left[R^{u,u}_{j,j}(t,t')\right]N_{0,u}(t')dt'\Bigg) + \\ +D\left(\frac{1}{c}\sum_{v\in\partial u}N_{0,v} - N_{0,u}\right) + \eta_{0,u}(t)\sqrt{N_{0,u}} \ .\end{aligned} \tag{A.19}$$

Species 0 is statistically equivalent to all the others, we can therefore replace the averages over the S original species with averages with respect to this new dynamics for a single species,

obtaining some self-consistent equations:

$$\begin{aligned}\dot{N}_u =& N_u\Bigg(1 - N_u - \mu h_u - \sigma\rho\tilde{\xi}_u(t) - \sigma\sqrt{1-\rho^2}\tilde{\psi}_u(t) + \sigma^2\rho^2\gamma\int_0^t \sum_{v\in\partial u} R_{uv}(t,s)N_v(s)ds + \\ &+ \sigma^2(1-\rho^2)\gamma\int_0^t R_{uu}(t,s)N_u(s)ds\Bigg) + D\left(\frac{1}{c}\sum_{v\in\partial u} N_v - N_u\right) + \eta_u(t)\sqrt{N_u}\end{aligned} \tag{A.20}$$

$$\langle\tilde{\xi}_u(t)\tilde{\xi}_v(s)\rangle = C_{uv}(t-s) = \mathbb{E}[N_u(t)N_v(s)] \tag{A.21}$$

$$\langle\tilde{\psi}_u(t)\tilde{\psi}_v(s)\rangle = \delta_{uv}C_{uu}(t-s) \tag{A.22}$$

$$R_{uv}(t,s) = \mathbb{E}\left[\left.\frac{\delta N_u(t)}{\delta\zeta_v(s)}\right|_{\zeta=0}\right] \tag{A.23}$$

$$h_u = \mathbb{E}[N_u]\ . \tag{A.24}$$

Since species have been effectively decoupled, we can suppress the species index.

In the single equilibrium phase, we expect the process to reach a time translation invariant regime, in which the one-time averages are time-independent and two-times observables only depend on the times difference. This was shown in [12] for a single community with demographic noise and fixed immigration and it is known to be the case for Directed Percolation [89] and in a many-species metacommunity with constant interactions [79]. It is also confirmed by our numerical results that show a quick relaxation of one-time observables to an asymptotic value (see Section 4.5.2), at least away from phase transitions. Since the auto-correlation of the abundance of one species doesn't tend to zero at large times, we can decompose ξ_u and ψ_u into a constant and a fluctuating component:

$$\tilde{\xi}_u(t) = \hat{\xi}_u + \xi_u(t) \tag{A.25}$$

$$\tilde{\psi}_u(t) = \hat{\psi}_u + \psi_u(t)\ , \tag{A.26}$$

where $\hat{\xi}_u$ and $\hat{\psi}_u$ are (time independent) Gaussian variables with zero mean and correlations $\lim_{\tau\to\infty} C_{uv}(t,t+\tau) = C^\infty_{uv}$ and $\delta_{uv}C^\infty_{uu}$ and the auto-correlation of ξ_u and ψ_u go to zero at long times. Averaging over ξ_u, ψ_u and η at fixed $\hat{\xi}_u$ and $\hat{\psi}_u$ corresponds to performing a time-average for one species in one patch, averaging also over $\hat{\psi}_u$ and $\hat{\xi}_u$ corresponds to averaging over patches and species. In this sense $\hat{\xi}_u$ and $\hat{\psi}_u$ play the role of the quenched disorder, that was previously represented by the interaction matrix α^u_{ij}. We will refer to the average over ξ and η at fixed $\hat{\xi}_u$ and $\hat{\psi}_u$ as *thermal average* and indicate it with brackets, and to the average over $\hat{\xi}_u$ and $\hat{\psi}_u$ as *disorder average* and indicate it with an overline.

While the derivation is so far valid for any spatial network, we will now restricted ourselves to a fully connected network, in which the empirical average over neighbors can be replaced by its thermal average. In the large L limit the connected correlation over thermal fluctuations between N_u and N_v is sub-dominant, so that ξ_u and ξ_v become independent. A perturbation in patch v influences the abundance in patch u through the diffusion term, that in a fully connected network is of order $1/L$, therefore R_{uv} for $u \neq v$ scales as $1/L$, whereas R_{uu} is of order 1. Since all patches are equivalent, the elements of the R_{uv} matrix can only take two values:

$$R_{uu} = R_d \tag{A.27}$$

$$R_{uv} = R_0/L,\ u \neq v\ . \tag{A.28}$$

Same thing for C_{uv}:

$$C^{\infty}_{uu} = C^{\infty}_{d} \tag{A.29}$$
$$C^{\infty}_{uv} = C^{\infty}_{0},\ u \neq v\ . \tag{A.30}$$

We separate $\hat{\xi}_u$ in a patch independent and a patch dependent part: $\hat{\xi}_u = z\sqrt{C^{\infty}_0} + w_u\sqrt{C^{\infty}_d - C^{\infty}_0}$. We call patch disorder average the average over w_u and $\hat{\psi}_u$; species disorder average the average over z. $\frac{1}{L}\sum_v N_v$ concentrates around its average over thermal fluctuations and patch disorder N^*, that will be a function of the static Gaussian field z. Substituting in the dynamical equation and using time translational invariance we obtain:

$$\begin{aligned}
\dot{N} = N\left(k - N - \mu h - \sigma\left(\rho\sqrt{C^{\infty}_0}z + \rho\sqrt{C^{\infty}_d - C^{\infty}_0}w + \sqrt{1-\rho^2}\sqrt{C^{\infty}_d}\hat{\psi} + \rho\xi + \sqrt{1-\rho^2}\psi\right)\right) + \\
+N\sigma^2\gamma\left(\rho^2\int_0^t R_d(t-s)N(s)ds + \rho^2\int_0^t R_0(t-s)N^*(s)ds + (1-\rho^2)\int_0^t R_d(t-s)N(s)ds\right) + \\
+D(N^* - N) + \eta(t)\sqrt{N} = \\
= N\left(k - N - \mu h - \sigma\left(\rho\sqrt{C^{\infty}_0}z + \sqrt{C^{\infty}_d - \rho^2 C^{\infty}_0}w + \xi\right)\right) + \\
+N\sigma^2\gamma\left(\int_0^t R_d(t-s)N(s)ds + \rho^2 R^{int}_0 N^*\right) + D(N^* - N) + \eta(t)\sqrt{N}\ ,
\end{aligned}$$

where we have summed the random variables that had the same behaviour of the correlations (w and $\hat{\psi}$, ξ and ψ), and

$$R^{int}_0 = \int_0^{\infty} d\tau R_0(\tau)\ . \tag{A.31}$$

The equations simplify in the extreme cases $\rho = 1$ and $\rho = 0$, because only one of the components of the static part of the disorder is present, either w or z. For $\rho = 1$ $C^{\infty}_d = C^{\infty}_0$. For $\rho = 0$ N^* coincides with h, so that we have one less self-consistent equation, and R_0 is not present; these two facts greatly simplify the numerical solution of the equations.

A.4 Asymmetric interactions

The MSRDJ action with non symmetrical interactions is given by:

$$\begin{aligned}
S[N,\hat{N}] = \int_u i\Bigg(\hat{N}_u\Bigg(N_u\left(k - D\left(1 - \sigma^2\gamma N^* R^{int}_0\right) - \mu h + \sigma\sqrt{C^{\infty}_d}z - N_u\right) + \\
-T + DN^*\Bigg) + N - \frac{1}{2}\Bigg) + \int_u i\hat{N}_u(iT\hat{N}_u N_u - \dot{N}_u) + \\
+\frac{\sigma^2}{2}\int_u i\hat{N}_u N_u\int_v C^c(u-v)i\hat{N}_v N_v + \gamma\sigma^2\int_u i\hat{N}_u N_u\int_v R(u-v)N_v + (\log P(N(0))),
\end{aligned} \tag{A.32}$$

where we have defined $C^c(u-v) = C_d(u-v) - C^{\infty}_d$. If the introduction of a small asymmetry in the interactions ($\epsilon = 1 - \gamma \ll 1$) is a non-singular perturbation, all the self-consistently determined quantities in the action (h, C_d, R^{int}_0 and R_d) will be close to their counterparts for $\gamma = 1$. At first order in ϵ we can neglect their change; therefore R_d and C_d will still respect a Fluctuation-Dissipation Relation. We can separate the action in a part that would respect FDT and a part that breaks it explicitly:

$$\delta S = \frac{\epsilon\sigma^2}{T}\int_{u>v} C^c_{u-v} i\hat{N}_u N_u \dot{N}_v\ . \tag{A.33}$$

An average $\langle f(N_t)\rangle$ can be expanded as:

$$\langle f(N_t)\rangle = \langle f(N_t)\rangle_0 + \langle f(N_t)\delta S\rangle_0 + O(\epsilon^2) \ , \tag{A.34}$$

where $\langle\cdot\rangle_0$ indicates the average with respect to the action neglecting δS.

We want to estimate the scaling of

$$\langle f(N_t)\delta S\rangle_0 = \frac{\epsilon\sigma^2}{T}\int_{u>v} C^c_{u-v} i\langle f(N_t)\hat{N}_u N_u \dot{N}_v\rangle_0 = \frac{\epsilon\sigma^2}{T}\int_{u>v} C^c_{u-v} i\frac{\partial}{\partial v}\frac{\delta}{\delta\zeta_u}\langle f(N_t)N_v\rangle_0 \tag{A.35}$$

to show that it is not singular approaching a phase transition. In the simple equilibrium phase the connected correlation function decays exponentially, with a typical relaxation time τ that could diverge at the phase transitions:

$$C^c(u-v) \sim (\overline{\langle N^2\rangle - \langle N\rangle^2})e^{-|u-v|/\tau} \ . \tag{A.36}$$

The correlation function $\langle f(N_t)N_v\rangle_0$ will contain a v independent part (that we can neglect since we will be taking the derivative in v) and a connected component of order 1 that decays with the same relaxation time τ. Perturbing the system with a field ζ_u this observable will respond as:

$$\frac{\delta}{\delta\zeta_u}\langle f(N_t)N_v\rangle_0 \propto \frac{1}{T\tau}e^{-(t-v)/\tau} \ . \tag{A.37}$$

Inserting these scalings in equation A.35 we obtain:

$$\begin{aligned}\langle f(N_t)\delta S\rangle_0 &\propto \frac{\epsilon\sigma^2}{T}\int_{u>v} e^{-(u-v)/\tau}\frac{\partial}{\partial v}\left(\frac{1}{T\tau}e^{-(t-v)/\tau}\right) = \\ &= \frac{\epsilon\sigma^2}{T^2\tau^2}\int_{-\infty}^{t} dv e^{-(t-v)/\tau}\int_v^t du e^{-(u-v)/\tau} = \\ &= \frac{\epsilon\sigma^2}{T^2\tau}\int_{-\infty}^{t} dv e^{-(t-v)/\tau}\left(1-e^{-(t-v)/\tau}\right) = \frac{\epsilon\sigma^2}{T^2\tau}\left(\tau-\frac{\tau}{2}\right) = \frac{\epsilon\sigma^2}{2T^2} \ .\end{aligned} \tag{A.38}$$

Considering a small asymmetry in the interactions observables are shifted by a correction of order ϵ, where the prefactor is of order 1 and has no divergence at the phase transitions. We thus expected the phase diagram to remain qualitatively unchanged.

A.5 Extinction threshold and diversity (for $\rho = 1$)

The self-consistency condition for N^* reads:

$$N^*(z) = \langle N\rangle_{H_{eff}(N;h,C_d^0,C_d^\infty,R_0^{int},z,N^*)} = \frac{\int_0^\infty dN N e^{-\beta H_{eff}(N;h,C_d^0,C_d^\infty,R_0^{int},z,N^*)}}{\int_0^\infty dN e^{-\beta H_{eff}(N;h,C_d^0,C_d^\infty,R_0^{int},z,N^*)}} \ . \tag{A.39}$$

$N^* = 0$ is always a solution of this equation, we want to find the value of z at which it becomes unstable.

We can separate the effective Hamiltonian into a quadratic and a logarithmic part:

$$H_{eff}(N;h,C_d^0,C_d^\infty,R_0^{int},z,N^*) = H_q(N;h,C_d^0,C_d^\infty,R_0^{int},z,N^*) + (T-DN^*)\ln N \ . \tag{A.40}$$

For $N^* \to 0$ the logarithmic part gives rise to a non-integrable divergence in 0 in the denominator. To improve the numerical stability of our solution at small N^* we performed an integration by parts of the denominator:

$$\int_0^\infty dN e^{-\beta H_{eff}} = \int_0^\infty dN e^{-\beta H_q} N^{-1+\beta D N^*} = \frac{1}{DN^*}\int_0^\infty dN e^{-\beta H_q} N^{\beta D N^*}\frac{dH_q}{dN} \ . \tag{A.41}$$

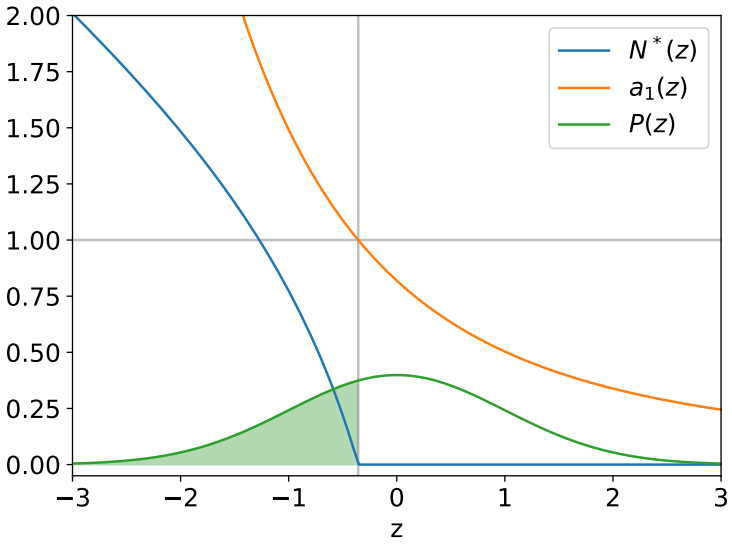

Figure A.1: Self-consistent solution for $N^*(z)$ (blue), coefficient of the first order expansion $c_1(z)$ (orange) and Gaussian probability distribution $P(z)$ (green). The highlighted region corresponds to the non-extinct species, its area is the diversity of the ecosystem. $T = 0.4$, $D = 0.15$, $\mu = 1$, $\sigma = 0.5$.

The integral is now finite for $N^* \to 0$ and we can expand eq. (A.39) in powers of N^*:

$$\begin{aligned} N^*(z) &= DN^*(z)\frac{\int_0^\infty dN e^{-\beta H_q} N^{\beta D N^*(z)}}{\int_0^\infty dN e^{-\beta H_q}\frac{dH_q}{dN} N^{\beta D N^*(z)}} = \\ &= N^*(z) D \frac{\int_0^\infty dN e^{-\beta H_q}}{\int_0^\infty dN e^{-\beta H_q}\frac{dH_q}{dN}} + O((N^*(z))^2) \ . \end{aligned} \tag{A.42}$$

The term of order $N^*(z)^2$ is always negative, therefore the number of solution depends on the coefficient of the $N^*(z)$ term: if $c_1(z) < 1$ the only solution is $N^*(z) = 0$, if $c_1(z) > 1$ the $N^*(z) = 0$ solution is unstable and there is a positive stable one. We define the effective growth rate $r_{eff} = 1 - \sigma^2\beta(C_d^0 - C_d^\infty))$ and the effective growth factor $r_{eff} g_{eff}(z) = k - \mu h - z\sqrt{C_d^\infty}\sigma + D\sigma^2 N^* R_0^{int}$. The extinction threshold z^* (Figure A.1) is given by:

$$1 = D\sqrt{\frac{\beta\pi}{2r_{eff}}} \exp\left(\frac{\beta}{2}\frac{(g_{eff}(z^*)r_{eff} - D)^2}{r_{eff}}\right)\left(1 + \text{erf}\left(\sqrt{\frac{\beta}{2}}\left(\frac{g_{eff}(z^*)r_{eff} - D}{\sqrt{r_{eff}}}\right)\right)\right) \ . \tag{A.43}$$

As noted in reference [79], this is the same condition that would determine the criticality of the Directed Percolation process with corresponding growth rate and growth factor:

$$\dot{N_u} = r_{eff}(N_u^2/2 - g_{eff}N_u) + D\left(\frac{1}{L}\sum_v N_v - N_u\right) + \eta\sqrt{N_u} \tag{A.44}$$

$$\langle \eta(t)\eta(t')\rangle = 2T\delta(t - t') \ . \tag{A.45}$$

The diversity, given by the fraction of non extinct species, can be obtained as:

$$\phi = \int_{z^*}^\infty P(z)dz = \frac{1}{2}\,\text{erfc}\left(\frac{z^*}{\sqrt{2}}\right) \ . \tag{A.46}$$

A.5.1 Continuous transition point

At the continuous transition, all moments of N tend to zero, and we can expand the extinction condition (A.43) in powers of these moments. Keeping only the zeroth order we obtain an equation on the critical value of the diffusion constant:

$$D_0\sqrt{\frac{\beta\pi}{2}}e^{\frac{\beta}{2}(k-D_0)^2}\left(1+\mathrm{erf}\left(\sqrt{\frac{\beta}{2}}\,(k-D_0)\right)\right)=1\ . \tag{A.47}$$

This condition has no dependence on the distribution of the interactions, indeed it is the same that we have derived for a single DP process in Sec. 4.2.1, or that would be obtained with constant competitive interactions [79].

By a careful (and cumbersome) expansion of the self-consistent equations, we can show that approaching the continuous transition $h \propto q_d \propto D - D_0$, $q_0 \propto (D-D_0)^2$, and z^* (and therefore ϕ) has a finite limit.

A.6 Response to a variation of the carrying capacity

Here we study the response of the system to a perturbation of the carrying capacity k in the case of independent interaction coefficients ($\rho = 0$). The response of the order parameters to a variation of k involves some connected moments of N and the derivative of H in k:

$$\begin{aligned}\frac{dh}{dk}=\int\mathcal{D}z\left(\frac{\int dN N e^{-\beta H}(-\beta)dH/dk}{\int dN e^{-\beta H}}-\frac{\int dN N e^{-\beta H}\int dN e^{-\beta H}(-\beta)dH/dk}{\left(\int dN e^{-\beta H}\right)^2}\right)=\\ =-\beta\left(\overline{\langle N\frac{dH}{dk}\rangle}-\overline{\langle N\rangle\langle\frac{dH}{dk}\rangle}\right)\end{aligned} \tag{A.48}$$

$$\frac{dC_d^0}{dk}=-\beta\left(\overline{\langle N^2\frac{dH}{dk}\rangle}-\overline{\langle N^2\rangle\langle\frac{dH}{dk}\rangle}\right) \tag{A.49}$$

$$\frac{dC_d^\infty}{dk}=-2\beta\left(\overline{\langle N\rangle\langle N\frac{dH}{dk}\rangle}-\overline{\langle N\rangle^2\langle\frac{dH}{dk}\rangle}\right)\ . \tag{A.50}$$

Thanks to the fact that $\rho = 0$, H has the simplified form:

$$H=\left(1-\sigma^2\beta\left(C_d^0-C_d^\infty\right)\right)N^2/2+(\mu h-k+D-z\sqrt{C_d^\infty}\sigma)N+(T-Dh)\ln N\ . \tag{A.51}$$

dH/dk depends on the derivative of the order parameters in k:

$$\frac{dH}{dk}=-N+\frac{\partial H}{\partial h}\frac{dh}{dk}+\frac{\partial H}{\partial C_d^0}\frac{dC_d^0}{dk}+\frac{\partial H}{\partial C_d^\infty}\frac{dC_d^\infty}{dk} \tag{A.52}$$

$$\frac{\partial H}{\partial h}=\mu N-D\ln N \tag{A.53}$$

$$\frac{\partial H}{\partial C_d^0}=-\frac{\sigma^2\beta}{2}N^2 \tag{A.54}$$

$$\frac{\partial H}{\partial C_d^\infty}=\frac{\sigma^2\beta}{2}N^2-\frac{1}{2\sqrt{C_d^\infty}}z\sigma N\ . \tag{A.55}$$

Substituting dH/dk in Equations (A.48-A.50) we obtain:

$$\begin{aligned}\frac{dh}{dk} = -\beta\Big\{ &- \left(\overline{\langle N^2\rangle} - \overline{\langle N\rangle^2}\right) + \\ &+ \left[\mu\left(\overline{\langle N^2\rangle} - \overline{\langle N\rangle^2}\right) - D\left(\overline{\langle N\log N\rangle} - \overline{\langle N\rangle\langle\log N\rangle}\right)\right]\frac{dh}{dk} + \\ &- \frac{\sigma^2\beta}{2}\left(\overline{\langle N^3\rangle} - \overline{\langle N\rangle\langle N^2\rangle}\right)\frac{dC_d^0}{dk} + \\ &+ \left[\frac{\sigma^2\beta}{2}\left(\overline{\langle N^3\rangle} - \overline{\langle N\rangle\langle N^2\rangle}\right) - \frac{1}{2\sqrt{C_d^\infty}}\sigma\left(\overline{\langle N^2\rangle z} - \overline{\langle N\rangle^2 z}\right)\right]\frac{dC_d^\infty}{dk}\Big\}\end{aligned} \tag{A.56}$$

$$\begin{aligned}\frac{dC_d^0}{dk} = -\beta\Big\{ &- \left(\overline{\langle N^3\rangle} - \overline{\langle N^2\rangle\langle N\rangle}\right) + \\ &+ \left[\mu\left(\overline{\langle N^3\rangle} - \overline{\langle N^2\rangle\langle N\rangle}\right) - D\left(\overline{\langle N^2\log N\rangle} - \overline{\langle N^2\rangle\langle\log N\rangle}\right)\right]\frac{dh}{dk} + \\ &- \frac{\sigma^2\beta}{2}\left(\overline{\langle N^4\rangle} - \overline{\langle N^2\rangle^2}\right)\frac{dC_d^0}{dk} + \\ &+ \left[\frac{\sigma^2\beta}{2}\left(\overline{\langle N^4\rangle} - \overline{\langle N^2\rangle^2}\right) - \frac{1}{2\sqrt{C_d^\infty}}\sigma\left(\overline{\langle N^3\rangle z} - \overline{\langle N^2\rangle\langle N\rangle z}\right)\right]\frac{dC_d^\infty}{dk}\Big\}\end{aligned} \tag{A.57}$$

$$\begin{aligned}\frac{dC_d^\infty}{dk} = -2\beta\Bigg\{ &- \left(\overline{\langle N\rangle\langle N^2\rangle} - \overline{\langle N\rangle^3}\right) + \\ &+ \left[\mu\left(\overline{\langle N\rangle\langle N^2\rangle} - \overline{\langle N\rangle^3}\right) - D\left(\overline{\langle N\rangle\langle N\log N\rangle} - \overline{\langle N\rangle^2\langle\log N\rangle}\right)\right]\frac{dh}{dk} + \\ &- \frac{\sigma^2\beta}{2}\left(\overline{\langle N\rangle\langle N^3\rangle} - \overline{\langle N\rangle^2\langle N^2\rangle}\right)\frac{dC_d^0}{dk} + \\ &+ \left[\frac{\sigma^2\beta}{2}\left(\overline{\langle N\rangle\langle N^3\rangle} - \overline{\langle N\rangle^2\langle N^2\rangle}\right) - \frac{1}{2\sqrt{C_d^\infty}}\sigma\left(\overline{\langle N\rangle\langle N^2\rangle z} - \overline{\langle N\rangle^3 z}\right)\right]\frac{dC_d^\infty}{dk}\Bigg\}.\end{aligned} \tag{A.58}$$

We collect the three order parameters in a vector $\vec{p} = (h, C_d^0, q_0)^T$. Then $\frac{d\vec{p}}{dk}$ satisfies:

$$\frac{d\vec{p}}{dk} = \hat{J}\frac{d\vec{p}}{dk} + \vec{s}\,, \tag{A.59}$$

where $\hat{J}$ is a 3×3 matrix and s a vector; their elements are the coefficients of Equations (A.56-A.58). The solution is given by:

$$\frac{d\vec{p}}{dk} = -(\hat{J} - \hat{1})^{-1}\vec{s}\,. \tag{A.60}$$

The response to a variation of k diverges if $\hat{J} - \hat{1}$ has a zero eigenvalue, this is found to happen when approaching the discontinuous transition.

We expect the same qualitative behavior of the response to perturbations for generic values of ρ, but for $\rho \neq 0$ we need to take into account also the variations of the function $N^*(z)$, which leads to the study of an infinite dimensional matrix.

A.7 Numerical scheme

The numerical simulation of demographic noise poses some technical challenges. Naively sampling it as a Gaussian variable can result in negative species abundances, an unphysical result that makes the scheme numerically unstable. A clever solution was found in reference [180], and improved in [12, 181]. The idea is to separate the process in a deterministic part:

$$\dot{N}_{i,u} = N_{i,u}\left(1 - N_{i,u} - \sum_j \alpha^u_{ij} N_{j,u}\right) + D\left(\frac{1}{L}\sum_v N_{i,v} - N_{i,u}\right) \tag{A.61}$$

and a stochastic one:

$$\dot{N}_{i,u} = \sqrt{N_{i,u}}\eta_{i,u} \ . \tag{A.62}$$

At each time step we numerically integrate the two in sequence. For the stochastic part an exact solution of the associated Fokker-Planck equation is available for any initial condition, and it can be efficiently sampled using Gamma and Poisson variables:

$$\tilde{N}_{i,u}(t) = \text{Gamma}\left(\text{Poisson}\left(\frac{N_{i,u}(t)}{Tdt}\right)\right) Tdt \ . \tag{A.63}$$

For the deterministic part we rely on Euler method.

$$N_{i,u}(t+dt) = \left(\tilde{N}_{i,u}(t)\left(1 - \tilde{N}_{i,u}(t) - \sum_j \alpha^u_{ij}\tilde{N}_{j,u}(t)\right) + D\left(\frac{1}{L}\sum_v \tilde{N}_{i,v}(t) - \tilde{N}_{i,u}(t)\right)\right) dt \ .$$

Appendix B

Non-reciprocal interactions

B.1 DMFT derivation for two non-reciprocally coupled spherical SK models

Given the noise realizations $\eta_i^a(t)$, Eq. (6.1) deterministically define the trajectories $s_i^a(t)$ for the 2 clones of the N spins, indexed from 1 to N. Let us imagine to now add a new spin, with index 0, to each of the clones, and draw their initial conditions and interactions independently from the rest of the system. Since the interactions with each of the other components are of order $1/\sqrt{N}$, its introduction can be considered a small perturbation, and we can compute the linear response of each of the trajectories to it, $\delta s_i^a(t)$:

$$\delta s_i^a(t) = \sum_{b,j} \int_0^t dt' R_{ij}^{ab}(t,t') J_{j0} s_0^b(t') \ , \tag{B.1}$$

where $R_{ij}^{ab}(t,t') = \frac{\delta s_i^a(t)}{\delta h_j^b(t')}$ is the response of spin i to a perturbation applied on spin i.

The dynamics of spins 0 will depend on the new trajectories of all the others:

$$\dot{s}_0^a = \sum_{j=1}^N J_{0j}(s_j^a + \delta s_j^a) - \ell^a s_0^a + \sum_b \alpha \epsilon_{ab} s_0^b + \eta_0^a + h_0^a \ . \tag{B.2}$$

We now want to describe the statistic of the interaction term $\sum_{j=1}^N J_{0j}(s_j^a + \delta s_j^a)$ in the limit $N \to \infty$. Because it is the sum of many weakly correlated terms, we expect it to be Gaussian, so that we only need to compute its two first moments. The unperturbed trajectories contribute a colored noise $\sum_j J_{0j} s_j^a \sim \xi_a$. Since the s_j^a are by definition uncorrelated from the interactions with spins 0, we can easily compute the statistics of ξ_a:

$$\langle \xi_a(t) \rangle = 0 \ , \tag{B.3}$$

$$\langle \xi_a(t) \xi_b(t') \rangle = \mathbb{E}\left[s_i^a(t) s_i^b(t') \right] = C_{ab}(t,t') \ . \tag{B.4}$$

The perturbations of the trajectories are instead correlated to the interactions with 0. We can use their explicit expression from Eq. (B.1):

$$\sum_i J_{0i} \delta s_i^a = \sum_i J_{0i} \sum_{j,b} J_{j0} \int_0^t dt' R_{ij}^{ab}(t,t') s_0^b(t') \sim$$

$$\sim \sum_b \int_0^t dt' \overline{R_{jj}^{ab}(t,t')} s_0^b(t') = \sum_b \int_0^t dt' R_{ab}(t,t') s_0^b(t') \ .$$

We have approximated the sums over spins with averages, and used the fact that $\overline{J_{0i}J_{j0}} = \delta_{ij}$, where the overline indicates an average over spins. $R_{ab}(t,t')$ is the average response function of a spin to a perturbation of its dynamics. It is possible to show that the off-diagonal terms give subleading contributions [66].

Substituting the results in the dynamics for s_0^a we obtain:

$$\dot{s}_0^a = -\ell^a s_0^a + \sum_b \alpha\epsilon_{ab} s_0^b + \eta_0^a + h_0^a + \xi_a + \sum_b \int_0^t dt' R_{ab}(t,t') s_0(t') \ . \tag{B.5}$$

It is now crucial to note that spins 0 are equivalent to all others, and that when N is large the system composed by N or $N+1$ spins are equivalent. Therefore the response and correlation functions that define the effective dynamics of spins 0 can be self-consistently computed as averages over the effective two spin dynamics.

The resulting equation does not depend on the index, therefore we can drop the index 0 in the following and rewrite the equation in vectorial form as:

$$\dot{\mathbf{s}} = -\Lambda\mathbf{s} + \alpha\epsilon\mathbf{s} + \xi + \int_0^t dt' R(t,t')\mathbf{s}(t') + \mathbf{h} \ , \tag{B.6}$$

where $\mathbf{s} = [s^1, s^2]^T$ is a two-dimensional vector that contains the two spins, $\Lambda = \mathrm{diag}(\ell^1, \ell^2)$ is the diagonal matrix of the Lagrange multipliers, ϵ is the fully anti-symmetric Levi-Civita symbol. The noise vector ξ is Gaussian with zero mean and variance $\langle \xi_a(t)\xi_b(t')\rangle = 2T\delta_{ab}\delta(t-t') + C_{ab}(t,t')$. Finally,

$$C_{ab}(t,t') = \langle s_a(t) s_b(t')\rangle, \qquad R_{ab}(t,t') = \frac{\partial\langle s_a(t)\rangle}{\partial h_b(t')} \ . \tag{B.7}$$

are the average correlation and response matrices, which have to be determined self-consistently.

B.2 DMFT derivation for two non-reciprocally coupled spherical p-spin models

In this appendix, we derive the DMFT equations for two non-reciprocally coupled p-spin models. Since the procedure is analogous to all previously considered cases, we simply sketch the main steps: We start from the dynamics of two pairs of N spins:

$$\dot{s}_i^1 = \frac{1}{(p-1)!}\sum_{i_2,\dots i_p} J_{i,i_2,\dots i_p} s_{i_2}^1 \dots s_{i_p}^1 - l_1 s_i^1 + \alpha s_i^2 + \eta_i^1 + h_i^1 \tag{B.8}$$

$$\dot{s}_i^2 = \frac{1}{(p-1)!}\sum_{i_2,\dots i_p} J_{i,i_2,\dots i_p} s_{i_2}^2 \dots s_{i_p}^2 - l_2 \sigma_i^2 - \alpha s_i^1 + \eta_i^2 + h_i^2 \tag{B.9}$$

We add a new spin, with index 0, to each of the systems, and sample randomly its initial conditions and interaction coefficients. The introduction of spin 0 leads to a small perturbation of the dynamics of all other spins, which at linear order is given by:

$$\begin{aligned}\delta s_i^a(t) &= \sum_{j,b}\int_{-\infty}^t dt' \frac{\delta s_i^a(t)}{\delta h_j^b(t')}\frac{1}{(p-1)!}\sum_{i_3,\dots i_p} J_{j,0,i_3,\dots,i_p} s_0^b(t') s_{i_3}^b(t') \dots s_{i_p}^b(t') = \\ &= \frac{1}{(p-1)!}\sum_{j,b}\int_{-\infty}^t dt' R_{ij}^{ab}(t,t') \sum_{i_3,\dots i_p} J_{j,0,i_3,\dots,i_p} s_0^b(t') s_{i_3}^b(t') \dots s_{i_p}^b(t')\end{aligned} \tag{B.10}$$

The dynamics of spin 0 depends on the perturbed trajectories of all other spins:

$$\dot{s}_0^a = \frac{1}{(p-1)!}\sum_{i_2,\dots i_p} J_{0,i_2,\dots i_p}((s_{i_2}^a)^0+\delta s_{i_2}^a)\dots((s_{i_p}^a)^0+\delta s_{i_p}^a) - l_a s_0^a + \sum_b \alpha\epsilon_{ab}s_0^b + \eta_0^a + h_0^a \quad \text{(B.11)}$$

Since we are interested in the linear order, we only keep terms with a single perturbation of the trajectory, which can be rewritten as:

$$\begin{aligned}
&\sum_{i_2,\dots i_p} J_{0,i,\dots i_p} s_{i_3}^a(t)\dots s_{i_p}^a(t)\delta s_i^a(t) = \\
&= \sum_{i_2,\dots i_p} J_{0,i,\dots i_p} s_{i_3}^a(t)\dots s_{i_p}^a(t)\frac{1}{(p-1)!}\cdot \\
&\cdot \sum_{j,b}\int_{-\infty}^t dt' R_{ij}^{ab}(t,t')\sum_{i_3,\dots i_p} J_{j,0,i_3,\dots,i_p} s_0^b(t')s_{i_3}^b(t')\dots s_{i_p}^b(t') \sim \\
&\sim \frac{p!}{2N^{p-1}}\sum_b \int_{-\infty}^t dt' R_{ab}(t,t')C_{ab}(t,t')^{p-2}s_0^b(t')
\end{aligned} \quad \text{(B.12)}$$

The terms with the unperturbed trajectories can be replaced by a Gaussian noise:

$$\frac{1}{(p-1)!}\sum_{i_2,\dots i_p} J_{0,i_2,\dots i_p}(s_{i_2}^a)^0\dots(s_{i_p}^a)^0 \sim \xi_a \quad \text{(B.13)}$$

The noise has mean 0 and correlations:

$$\langle \xi_a(t)\xi_b(t')\rangle = \frac{p}{2}C_{ab}(t,t')^{p-1} \quad \text{(B.14)}$$

Plugging these contributions in the dynamics for s_0^a we obtain:

$$\dot{s}^a = -l_a s^a + \sum_b \epsilon_{ab}\alpha s^b + \eta_a + \xi_a + \frac{p(p-1)}{2}\int_{-\infty}^t dt' \sum_b R_{ab}(t,t')C_{ab}(t,t')^{p-2}s(t') \quad \text{(B.15)}$$

By multiplying by s^b and averaging or by differentiating by the effective noise we can obtain a set of closed integro-differential equations for R and C:

$$\begin{aligned}
\frac{\partial C(t,t')}{\partial t} &= -\Lambda(t)C(t,t') + \alpha\epsilon C(t,t') + 2TR(t',t) + \\
&+ \frac{1}{2}\int_{-\infty}^{t'} dt'' R(t',t'')\left(D(t,t'') + D(t,t'')^T\right) + \int_{-\infty}^t dt'' \Sigma(t,t'')C(t'',t')
\end{aligned} \quad \text{(B.16)}$$

$$\frac{\partial R(t,t')}{\partial t} = -\Lambda(t)R(t,t') + \alpha\epsilon R(t,t') + \delta(t,t')\mathbb{1} + \int_{t'}^t dt'' \Sigma(t,t'')R(t'',t') \quad \text{(B.17)}$$

where Λ is the diagonal matrix containing the two Lagrange multipliers, which are given by

$$\ell_a(t) = T + \frac{p}{2}\left(p-\frac{1}{2}\right)\sum_b \int_0^t dt'' R_{ab}(t,t'')C_{ab}(t,t'')^{p-1} + \quad \text{(B.18)}$$

$$+ \frac{p}{4}\sum_b \int_0^t dt'' R_{ab}(t,t'')C_{ba}(t,t'')^{p-1}\ , \quad \text{(B.19)}$$

and

$$D(t,t') = \frac{p}{2}\begin{pmatrix} C_{11}(t,t')^{p-1} & C_{12}(t,t')^{p-1} \\ C_{21}(t,t')^{p-1} & C_{22}(t,t')^{p-1}\end{pmatrix} \quad \text{(B.20)}$$

$$\Sigma(t,t') = \frac{p(p-1)}{2}\begin{pmatrix} R_{11}(t,t')C_{11}(t,t')^{p-2} & R_{12}(t,t')C_{12}(t,t')^{p-2} \\ R_{21}(t,t')C_{21}(t,t')^{p-2} & R_{22}(t,t')C_{22}(t,t')^{p-2}\end{pmatrix}\ . \quad \text{(B.21)}$$

My publications

[1] **Giulia Garcia Lorenzana**, Ada Altieri, and Giulio Biroli. Interactions and Migration Rescuing Ecological Diversity. *PRX Life*, 2(1):013014, March 2024.

[2] **Giulia Garcia Lorenzana**, Ada Altieri, Giulio Biroli, Michel Fruchart, and Vincenzo Vitelli. Non-reciprocal spin-glass transition and aging. arXiv:2408.17360, to appear on *Physical Review Letters*, August 2024.

[3] **Giulia Garcia Lorenzana**, Ada Altieri, Giulio Biroli, Michel Fruchart, and Vincenzo Vitelli. Non-reciprocal spin-glasses: Exceptional-points mediated phase transitions and aging. Under review at *Physical Review E*, 2025.

[4] **Giulia Garcia Lorenzana**, David Martin, Yael Avni, Michel Fruchart, Daniel Seara, Giulio Biroli, and Vincenzo Vitelli. When does non-reciprocity change a phase transition? *In preparation*, 2025.

[5] **Giulia Garcia Lorenzana** and Ada Altieri. Well-mixed Lotka-Volterra model with random strongly competitive interactions. *Physical Review E*, 105(2):024307, February 2022.

[6] Matilde Baroni, **Giulia Garcia Lorenzana**, Tommaso Rizzo, and Marco Tarzia. Corrections to the Bethe lattice solution of Anderson localization. *Physical Review B*, 109(17):174216, May 2024.

Bibliography

[1] Giulia Garcia Lorenzana, Ada Altieri, and Giulio Biroli. Interactions and Migration Rescuing Ecological Diversity. *PRX Life*, 2(1):013014, March 2024.

[2] Giulia Garcia Lorenzana, Ada Altieri, Giulio Biroli, Michel Fruchart, and Vincenzo Vitelli. Non-reciprocal spin-glass transition and aging, August 2024.

[3] Giulia Garcia Lorenzana, Ada Altieri, Giulio Biroli, Michel Fruchart, and Vincenzo Vitelli. Non-reciprocal spin-glasses: Exceptional-points mediated phase transitions and aging. *Under review*, 2024.

[4] Giulia Garcia Lorenzana, David Martin, Yael Avni, Michel Fruchart, Daniel Seara, Giulio Biroli, and Vincenzo Vitelli. When does non-reciprocity change a phase transition? *In preparation*, 2025.

[5] Giulia Garcia Lorenzana and Ada Altieri. Well-mixed Lotka-Volterra model with random strongly competitive interactions. *Physical Review E*, 105(2):024307, February 2022.

[6] Matilde Baroni, Giulia Garcia Lorenzana, Tommaso Rizzo, and Marco Tarzia. Corrections to the Bethe lattice solution of Anderson localization. *Physical Review B*, 109(17):174216, May 2024.

[7] Patrick Charbonneau, Enzo Marinari, Giorgio Parisi, Federico Ricci-Tersenghi, Gabriele Sicuro, Francesco Zamponi, and Marc Mezard. *Spin Glass Theory and Far Beyond: Replica Symmetry Breaking after 40 Years*. World Scientific, 2023.

[8] Ferenc Jordan and Sven Erik Jørgensen, editors. *Models of the Ecological Hierarchy: From Molecules to the Ecosphere*. Elsevier, 1st edition edition, December 2012.

[9] Denise Pumain, editor. *Hierarchy in Natural and Social Sciences*. Springer Netherlands, Dordrecht, 2006.

[10] Guy Bunin. Ecological communities with Lotka-Volterra dynamics. *Physical Review E*, 95(4):1–8, 2017.

[11] Giulio Biroli, Guy Bunin, and Chiara Cammarota. Marginally stable equilibria in critical ecosystems. *New Journal of Physics*, 20(8):083051, August 2018.

[12] Ada Altieri, Felix Roy, Chiara Cammarota, and Giulio Biroli. Properties of Equilibria and Glassy Phases of the Random Lotka-Volterra Model with Demographic Noise. *Physical Review Letters*, 126(25):258301, June 2021.

[13] A. Crisanti and H. Sompolinsky. Dynamics of spin systems with randomly asymmetric bonds: Langevin dynamics and a spherical model. *Physical Review A*, 36(10):4922–4939, November 1987.

[14] P. W. Anderson. More Is Different. *Science*, 177(4047):393–396, August 1972.

[15] Alain Pavé. Biological and Ecological Systems Hierarchical Organisation. In Denise Pumain, editor, *Hierarchy in Natural and Social Sciences*, pages 39–70. Springer Netherlands, Dordrecht, 2006.

[16] William B. Ludington and William W. Ja. Drosophila as a model for the gut microbiome. *PLOS Pathogens*, 16(4):e1008398, April 2020.

[17] Walter P. Carson, Stefan A. Schnitzer, and Smithsonian Tropical Research Institute, editors. *Tropical Forest Community Ecology*. Wiley-Blackwell Pub, Chichester ; Malden, MA, 2008.

[18] James H. Brown. *Macroecology*. University of Chicago Press, Chicago, IL, June 1995.

[19] Robert H. Whittaker. *Communities and Ecosystems*. Macmillan USA, New York, 2nd edition edition, January 1975.

[20] Gary G. Mittelbach and Brian J. McGill. *Community Ecology*. Oxford University Press, Oxford, United Kingdom ; New York, NY, 2e édition edition, 2019.

[21] Peter J. Morin. *Community Ecology*. John Wiley & Sons, April 2009.

[22] Charles Darwin and Leonard Kebler. *On the Origin of Species by Means of Natural Selection, or, The Preservation of Favoured Races in the Struggle for Life*. J. Murray, London, 1859.

[23] Stephan C. Schuster. Next-generation sequencing transforms today's biology. *Nature Methods*, 5(1):16–18, January 2008.

[24] Paul D N Hebert, Alina Cywinska, Shelley L Ball, and Jeremy R deWaard. Biological identifications through DNA barcodes. *Proceedings of the Royal Society B: Biological Sciences*, 270(1512):313–321, February 2003.

[25] Ahmed Abdelfattah, Antonino Malacrinò, Michael Wisniewski, Santa O. Cacciola, and Leonardo Schena. Metabarcoding: A powerful tool to investigate microbial communities and shape future plant protection strategies. *Biological Control*, 120:1–10, May 2018.

[26] Antonio M. Martin-Platero, Brian Cleary, Kathryn Kauffman, Sarah P. Preheim, Dennis J. McGillicuddy, Eric J. Alm, and Martin F. Polz. High resolution time series reveals cohesive but short-lived communities in coastal plankton. *Nature Communications*, 9(1):266, January 2018.

[27] Gretchen C. Daily and Pamela A. Matson. Ecosystem services: From theory to implementation. *Proceedings of the National Academy of Sciences*, 105(28):9455–9456, July 2008.

[28] Gian-Reto Walther, Eric Post, Peter Convey, Annette Menzel, Camille Parmesan, Trevor J. C. Beebee, Jean-Marc Fromentin, Ove Hoegh-Guldberg, and Franz Bairlein. Ecological responses to recent climate change. *Nature*, 416(6879):389–395, March 2002.

[29] Julian R. Marchesi, David H. Adams, Francesca Fava, Gerben D. A. Hermes, Gideon M. Hirschfield, Georgina Hold, Mohammed Nabil Quraishi, James Kinross, Hauke Smidt, Kieran M. Tuohy, Linda V. Thomas, Erwin G. Zoetendal, and Ailsa Hart. The gut microbiota and host health: A new clinical frontier. *Gut*, 65(2):330–339, February 2016.

[30] Antti Karkman, Jenni Lehtimäki, and Lasse Ruokolainen. The ecology of human microbiota: Dynamics and diversity in health and disease. *Annals of the New York Academy of Sciences*, 1399(1):78–92, July 2017.

[31] Amir Bashan, Travis E. Gibson, Jonathan Friedman, Vincent J. Carey, Scott T. Weiss, Elizabeth L. Hohmann, and Yang-Yu Liu. Universality of human microbial dynamics. *Nature*, 534(7606):259–262, June 2016.

[32] Joseph Grinnell. Geography and Evolution. *Ecology*, 5(3):225–229, 1924.

[33] Charles S. Elton. *Animal Ecology*. Macmillan Co., New York, 1927.

[34] Aaron M. Olsen. Feeding ecology is the primary driver of beak shape diversification in waterfowl. *Functional Ecology*, 31(10):1985–1995, 2017.

[35] G. Hardin. The Competitive Exclusion Principle. *Science*, 131(3409):1292–1297, April 1960.

[36] G. F. Gause. *The Struggle for Existence*. Courier Dover Publications, October 2019.

[37] G. Evelyn Hutchinson. Concluding Remarks. *Cold Spring Harbor Symposia on Quantitative Biology*, 22:415–427, January 1957.

[38] Robert Mac Arthur. Species packing, and what competition minimizes*†. *Proceedings of the National Academy of Sciences*, 64(4):1369–1371, December 1969.

[39] Peter Chesson. MacArthur's consumer-resource model. *Theoretical Population Biology*, 37(1):26–38, February 1990.

[40] Enrico Ser-Giacomi, Lucie Zinger, Shruti Malviya, Colomban De Vargas, Eric Karsenti, Chris Bowler, and Silvia De Monte. Ubiquitous abundance distribution of non-dominant plankton across the global ocean. *Nature Ecology & Evolution*, 2(8):1243–1249, August 2018.

[41] Colomban de Vargas, Stéphane Audic, Nicolas Henry, Johan Decelle, Frédéric Mahé, Ramiro Logares, Enrique Lara, Cédric Berney, Noan Le Bescot, Ian Probert, Margaux Carmichael, Julie Poulain, Sarah Romac, Sébastien Colin, Jean-Marc Aury, Lucie Bittner, Samuel Chaffron, Micah Dunthorn, Stefan Engelen, Olga Flegontova, Lionel Guidi, Aleš Horák, Olivier Jaillon, Gipsi Lima-Mendez, Julius Lukeš, Shruti Malviya, Raphael Morard, Matthieu Mulot, Eleonora Scalco, Raffaele Siano, Flora Vincent, Adriana Zingone, Céline Dimier, Marc Picheral, Sarah Searson, Stefanie Kandels-Lewis, Tara Oceans Coordinators, Silvia G. Acinas, Peer Bork, Chris Bowler, Gabriel Gorsky, Nigel Grimsley, Pascal Hingamp, Daniele Iudicone, Fabrice Not, Hiroyuki Ogata, Stephane Pesant, Jeroen Raes, Michael E. Sieracki, Sabrina Speich, Lars Stemmann, Shinichi Sunagawa, Jean Weissenbach, Patrick Wincker, Eric Karsenti, Emmanuel Boss, Michael Follows, Lee Karp-Boss, Uros Krzic, Emmanuel G. Reynaud, Christian Sardet, Matthew B. Sullivan, and Didier Velayoudon. Eukaryotic plankton diversity in the sunlit ocean. *Science*, 348(6237):1261605, May 2015.

[42] G. E. Hutchinson. The Paradox of the Plankton. *The American Naturalist*, 95(882):137–145, 1961.

[43] Stephen P. Hubbell. *The Unified Neutral Theory of Biodiversity and Biogeography (MPB-32)*. Princeton University Press, June 2011.

[44] Stephen P. Hubbell. Neutral theory in community ecology and the hypothesis of functional equivalence. *Functional Ecology*, 19(1):166–172, 2005.

[45] James Rosindell and Stephen J. Cornell. Species-area relationships from a spatially explicit neutral model in an infinite landscape. *Ecology Letters*, 10(7):586–595, July 2007.

[46] Igor Volkov, Jayanth R. Banavar, Stephen P. Hubbell, and Amos Maritan. Neutral theory and relative species abundance in ecology. *Nature*, 424(6952):1035–1037, August 2003.

[47] Jonas Denk, Stephen Martis, and Oskar Hallatschek. Chaos may lurk under a cloak of neutrality. *Proceedings of the National Academy of Sciences*, 117(28):16104–16106, July 2020.

[48] Robert E. Ricklefs. The Unified Neutral Theory of Biodiversity: Do the Numbers Add Up? *Ecology*, 87(6):1424–1431, 2006.

[49] Ryan A. Chisholm and James P. O'Dwyer. Species ages in neutral biodiversity models. *Theoretical Population Biology*, 93:85–94, May 2014.

[50] Thomas Jones and Gary Montz. Population increase and associated effects of zebra mussels Dreissena polymorpha in Lake Mille Lacs, Minnesota, U.S.A. *BioInvasions Records*, 9(4):772–792, 2020.

[51] Michael E. Gilpin and Francisco J. Ayala. Global Models of Growth and Competition. *Proceedings of the National Academy of Sciences*, 70(12):3590–3593, December 1973.

[52] Jacques Monod. THE GROWTH OF BACTERIAL CULTURES. *Annual Review of Microbiology*, 3(Volume 3, 1949):371–394, October 1949.

[53] R.M. Nisbet and William Gurney. *Modelling Fluctuating Populations*. John Wiley & Sons, Chichester, 1982.

[54] J. M. Halley and Y. Iwasa. Extinction rate of a population under both demographic and environmental stochasticity. *Theoretical Population Biology*, 53(1):1–15, February 1998.

[55] HIROSHI Hakoyama and YOH Iwasa. Extinction Risk of a Density-dependent Population Estimated from a Time Series of Population Size. *Journal of Theoretical Biology*, 204(3):337–359, June 2000.

[56] Russell Lande. Risks of Population Extinction from Demographic and Environmental Stochasticity and Random Catastrophes. *The American Naturalist*, 142(6):911–927, 1993.

[57] Alex Kamenev, Baruch Meerson, and Boris Shklovskii. How Colored Environmental Noise Affects Population Extinction. *Physical Review Letters*, 101(26):268103, December 2008.

[58] O. L. Petchey, A. Gonzalez, and H. B. Wilson. Effects on population persistence: The interaction between environmental noise colour, intraspecific competition and space. *Proceedings of the Royal Society B: Biological Sciences*, 264(1389):1841–1847, December 1997.

[59] Eric De Giuli and Camille Scalliet. Dynamical mean-field theory: From ecosystems to reaction networks. *Journal of Physics A: Mathematical and Theoretical*, 55(47):474002, November 2022.

[60] Ferran Larroya and Tobias Galla. Demographic noise in complex ecological communities. *Journal of Physics: Complexity*, 2023.

[61] Lev R. Ginzburg, Lawrence B. Slobodkin, Keith Johnson, and Andrew G. Bindman. Quasiextinction Probabilities as a Measure of Impact on Population Growth. *Risk Analysis*, 2(3):171–181, 1982.

[62] M Mangel and C Tier. A simple direct method for finding persistence times of populations and application to conservation problems. *Proceedings of the National Academy of Sciences*, 90(3):1083–1086, February 1993.

[63] Ricard Solé, Victor Maull, Daniel R. Amor, Jordi Pla Mauri, and Conde-Pueyo Núria. Synthetic Ecosystems: From the Test Tube to the Biosphere. *ACS Synthetic Biology*, 13(12):3812–3826, December 2024.

[64] Robert H. MacArthur and Edward O. Wilson. *The Theory of Island Biogeography*. Princeton University Press, 1967.

[65] David A Kessler and Nadav M Shnerb. Generalized model of island biodiversity. *Physical Review E*, 91(4):042705, April 2015.

[66] F Roy, G Biroli, G Bunin, and C Cammarota. Numerical implementation of dynamical mean field theory for disordered systems: Application to the Lotka–Volterra model of ecosystems. *Journal of Physics A: Mathematical and Theoretical*, 52(48):484001, November 2019.

[67] Carlos A. Serván, José A. Capitán, Jacopo Grilli, Kent E. Morrison, and Stefano Allesina. Coexistence of many species in random ecosystems. *Nature Ecology & Evolution*, 2(8):1237–1242, August 2018.

[68] Daniel S. Simberloff and Edward O. Wilson. Experimental Zoogeography of Islands. A Two-Year Record of Colonization. *Ecology*, 51(5):934–937, 1970.

[69] M. A. Leibold, M. Holyoak, N. Mouquet, P. Amarasekare, J. M. Chase, M. F. Hoopes, R. D. Holt, J. B. Shurin, R. Law, D. Tilman, M. Loreau, and A. Gonzalez. The metacommunity concept: A framework for multi-scale community ecology. *Ecology Letters*, 7(7):601–613, 2004.

[70] Michel Loreau, Nicolas Mouquet, and Robert D. Holt. Meta-ecosystems: A theoretical framework for a spatial ecosystem ecology. *Ecology Letters*, 6(8):673–679, 2003.

[71] Peter Chesson. General Theory of Competitive Coexistence in Spatially-Varying Environments. *Theoretical Population Biology*, 58(3):211–237, November 2000.

[72] Michel Loreau, Nicolas Mouquet, and Andrew Gonzalez. Biodiversity as spatial insurance in heterogeneous landscapes. *Proceedings of the National Academy of Sciences*, 100(22):12765–12770, October 2003.

[73] Renato Casagrandi and Marino Gatto. A Persistence Criterion for Metapopulations. *Theoretical Population Biology*, 61(2):115–125, March 2002.

[74] Gösta Nachman. Effects of demographic parameters on metapopulation size and persistence: An analytical stochastic model. *Oikos*, 91(1):51–65, 2000.

[75] A. Eriksson, F. Elías-Wolff, and B. Mehlig. Metapopulation dynamics on the brink of extinction. *Theoretical Population Biology*, 83:101–122, February 2013.

[76] Rodrigo Crespo-Miguel, Javier Jarillo, and Francisco J. Cao-García. Dispersal-induced resilience to stochastic environmental fluctuations in populations with Allee effect. *Physical Review E*, 105(1):014413, January 2022.

[77] Jennifer G. Howeth and Mathew A. Leibold. Species dispersal rates alter diversity and ecosystem stability in pond metacommunities. *Ecology*, 91(9):2727–2741, 2010.

[78] P. A. Venail, R. C. MacLean, T. Bouvier, M. A. Brockhurst, M. E. Hochberg, and N. Mouquet. Diversity and productivity peak at intermediate dispersal rate in evolving metacommunities. *Nature*, 452(7184):210–214, March 2008.

[79] Jonas Denk and Oskar Hallatschek. Self-consistent dispersal puts tight constraints on the spatiotemporal organization of species-rich metacommunities. *Proceedings of the National Academy of Sciences*, 119(26):e2200390119, June 2022.

[80] Ankit Vikrant, Susanne Pettersson, and Martin Nilsson Jacobi. Spatial coherence and the persistence of high diversity in spatially heterogeneous landscapes. *Ecology and Evolution*, 12(6):e9004, 2022.

[81] Dominique Gravel, Frédéric Guichard, Michel Loreau, and Nicolas Mouquet. Source and sink dynamics in meta-ecosystems. *Ecology*, 91(7):2172–2184, 2010.

[82] Dominique Gravel, François Massol, and Mathew A. Leibold. Stability and complexity in model meta-ecosystems. *Nature Communications*, 7(1):12457, November 2016.

[83] Simon A. Levin. Dispersion and Population Interactions. *The American Naturalist*, 108(960):207–228, 1974.

[84] Nicolas Mouquet and Michel Loreau. Community patterns in source-sink metacommunities. *The American Naturalist*, 162(5):544–557, November 2003.

[85] Mason R. Stothart, Ruth J. Greuel, Stefan Gavriliuc, Astrid Henry, Alastair J. Wilson, Philip D. McLoughlin, and Jocelyn Poissant. Bacterial dispersal and drift drive microbiome diversity patterns within a population of feral hindgut fermenters. *Molecular Ecology*, 30(2):555–571, 2021.

[86] Guim Aguadé-Gorgorió, Alexander R. A. Anderson, and Ricard Solé. Modeling tumors as complex ecosystems. *iScience*, 27(9), September 2024.

[87] Sergei Petrovskii, Kohkichi Kawasaki, Fugo Takasu, and Nanako Shigesada. Diffusive waves, dynamical stabilization and spatio-temporal chaos in a community of three competitive species. *Japan Journal of Industrial and Applied Mathematics*, 18(2):459–481, June 2001.

[88] A. Cangiani, E. H. Georgoulis, A. Yu Morozov, and O. J. Sutton. Revealing new dynamical patterns in a reaction-diffusion model with cyclic competition via a novel computational framework. *Proceedings of the Royal Society A: Mathematical, Physical and Engineering Sciences*, 474(2213), 2018.

[89] Haye Hinrichsen. Non-equilibrium critical phenomena and phase transitions into absorbing states. *Advances in Physics*, 49(7):815–958, November 2000.

[90] S. R. Broadbent and J. M. Hammersley. Percolation processes: I. Crystals and mazes. *Mathematical Proceedings of the Cambridge Philosophical Society*, 53(3):629–641, July 1957.

[91] J L Cardy and R L Sugar. Directed percolation and Reggeon field theory. *Journal of Physics A: Mathematical and General*, 13(12):L423–L427, December 1980.

[92] Mauro Mobilia, Ivan T Georgiev, and Uwe C Täuber. Phase Transitions and Spatio-Temporal Fluctuations in Stochastic Lattice Lotka–Volterra Models. *Journal of Statistical Physics*, 128(1-2):447–483, June 2007.

[93] Ulrich Dobramysl, Mauro Mobilia, Michel Pleimling, and Uwe C. Tauber. Stochastic population dynamics in spatially extended predator-prey systems. *Journal of Physics A: Mathematical and Theoretical*, 51(6), 2018.

[94] José Moran and Jean-Philippe Bouchaud. May's instability in large economies. *Physical Review E*, 100(3):032307, September 2019.

[95] Richard M. Goodwin. *Chaotic Economic Dynamics*. Oxford University Press, November 1990.

[96] Ulrich Behn, J. Leo van Hemmen, and Bernhard Sulzer. Memory B Cells Stabilize Cycles in a Repressive Network. In *Theoretical and Experimental Insights into Immunology*, pages 249–260. Springer Berlin Heidelberg, Berlin, Heidelberg, 1992.

[97] Immanuel M. Bomze. Lotka-Volterra equation and replicator dynamics: New issues in classification. *Biological Cybernetics*, 72(5):447–453, 1995.

[98] Alfred J. Lotka. Analytical Note on Certain Rhythmic Relations in Organic Systems. *Proceedings of the National Academy of Sciences*, 6(7):410–415, July 1920.

[99] V Volterra. Variazioni e fluttuazioni del numero d'individui in specie animali conviventi. *Memoria della regia accademia nazionale del lincei ser.*, 62:31–113, 1926.

[100] Jacob D. Davis, Daniel V. Olivença, Sam P. Brown, and Eberhard O. Voit. Methods of quantifying interactions among populations using Lotka-Volterra models. In *Frontiers in Systems Biology*, volume 2, page 1021897, October 2022.

[101] Eugene P. Wigner. On the statistical distribution of the widths and spacings of nuclear resonance levels. *Mathematical Proceedings of the Cambridge Philosophical Society*, 47(4):790–798, October 1951.

[102] Eugene P. Wigner. Random Matrices in Physics. *SIAM Review*, 9(1):23, January 1967.

[103] Eugene P. Wigner. On the Distribution of the Roots of Certain Symmetric Matrices. *Annals of Mathematics*, 67(2):325–327, 1958.

[104] Freeman J. Dyson. Statistical Theory of the Energy Levels of Complex Systems. I. *Journal of Mathematical Physics*, 3(1):140–156, January 1962.

[105] M Mezard, G Parisi, and M Virasoro. *Spin Glass Theory and Beyond: An Introduction to the Replica Method and Its Applications*, volume 9 of *World Scientific Lecture Notes in Physics*. WORLD SCIENTIFIC, November 1986.

[106] Robert M. May. Will a Large Complex System be Stable? *Nature*, 238(5364):413–414, August 1972.

[107] Jean Ginibre. Statistical Ensembles of Complex, Quaternion, and Real Matrices. *Journal of Mathematical Physics*, 6(3):440–449, March 1965.

[108] Charles C. Elton. *The Ecology of Invasions by Animals and Plants*. Springer Netherlands, Dordrecht, 1977.

[109] Robert MacArthur. Fluctuations of Animal Populations and a Measure of Community Stability. *Ecological Society of America*, 36(3):533–536, 1955.

[110] Stefano Allesina and Si Tang. Stability criteria for complex ecosystems. *Nature*, 483(7388):205–208, March 2012.

[111] Jacopo Grilli, Tim Rogers, and Stefano Allesina. Modularity and stability in ecological communities. *Nature Communications*, 7(1):12031, June 2016.

[112] Shai Pilosof, Mason A. Porter, Mercedes Pascual, and Sonia Kéfi. The multilayer nature of ecological networks. *Nature Ecology & Evolution*, 1(4):1–9, March 2017.

[113] Matthew C. Hutchinson, Bernat Bramon Mora, Shai Pilosof, Allison K. Barner, Sonia Kéfi, Elisa Thébault, Pedro Jordano, and Daniel B. Stouffer. Seeing the forest for the trees: Putting multilayer networks to work for community ecology. *Functional Ecology*, 33(2):206–217, 2019.

[114] Joseph W. Baron and Tobias Galla. Dispersal-induced instability in complex ecosystems. *Nature Communications*, 11(1):6032, November 2020.

[115] H. Rieger. Solvable model of a complex ecosystem with randomly interacting species. *Journal of Physics A: Mathematical and General*, 22(17):3447–3460, 1989.

[116] S. Diederich and M. Opper. Replicators with random interactions: A solvable model. *Physical Review A*, 39(8):4333–4336, 1989.

[117] Manfred Opper and Sigurd Diederich. Phase transition and $1/f$ noise in a game dynamical model. *Physical Review Letters*, 69(10):1616–1619, September 1992.

[118] Manfred Opper and Sigurd Diederich. Replicator dynamics. *Computer Physics Communications*, 121–122:141–144, September 1999.

[119] Tobias Galla. Random replicators with asymmetric couplings. *Journal of Physics A: Mathematical and General*, 39(15):3853–3869, April 2006.

[120] Mikhail Tikhonov and Remi Monasson. Collective Phase in Resource Competition in a Highly Diverse Ecosystem. *Physical Review Letters*, 118(4):1–5, 2017.

[121] A. Townsend Peterson. *Ecological Niches and Geographic Distributions (MPB-49)*. Princeton University Press, November 2011.

[122] Pietro Valigi, Izaak Neri, and Chiara Cammarota. Local sign stability and its implications for spectra of sparse random graphs and stability of ecosystems, March 2023.

[123] Stav Marcus, Ari M. Turner, and Guy Bunin. Local and collective transitions in sparsely-interacting ecological communities. *PLOS Computational Biology*, 18(7):e1010274, July 2022.

[124] Stav Marcus, Ari M. Turner, and Guy Bunin. Local and extensive fluctuations in sparsely-interacting ecological communities, August 2023.

[125] Stav Marcus, Ari M. Turner, and Guy Bunin. Extinctions as a vestige of instability: The geometry of stability and feasibility, May 2024.

[126] Tommaso Tonolo, Maria Chiara Angelini, Sandro Azaele, Amos Maritan, and Giacomo Gradenigo. Generalized Lotka-Volterra model with sparse interactions: Non-Gaussian effects and topological multiple-equilibria phase, March 2025.

[127] Lyle Poley, Tobias Galla, and Joseph W. Baron. Interaction networks in persistent Lotka-Volterra communities. *Physical Review E*, 111(1):014318, January 2025.

[128] Fabián Aguirre-López. Heterogeneous mean-field analysis of the generalized Lotka–Volterra model on a network. *Journal of Physics A: Mathematical and Theoretical*, 57(34):345002, September 2024.

[129] Jong Il Park, Deok-Sun Lee, Sang Hoon Lee, and Hye Jin Park. Incorporating Heterogeneous Interactions for Ecological Biodiversity. *Physical Review Letters*, 133(19):198402, November 2024.

[130] Juan Giral Martínez, Silvia de Monte, and Matthieu Barbier. Stabilization of macroscopic dynamics by fine-grained disorder in many-species ecosystems, March 2025.

[131] Lyle Poley, Joseph W. Baron, and Tobias Galla. Generalized Lotka-Volterra model with hierarchical interactions. *Physical Review E*, 107(2):024313, February 2023.

[132] Samir Suweis, Francesco Ferraro, Sandro Azaele, and Amos Maritan. Generalized Lotka-Volterra Systems with Time Correlated Stochastic Interactions, July 2023.

[133] Ada Altieri and Giulio Biroli. Effects of intraspecific cooperative interactions in large ecosystems. *SciPost Physics*, 12(1):013, January 2022.

[134] Ian A. Hatton, Onofrio Mazzarisi, Ada Altieri, and Matteo Smerlak. Diversity begets stability: Sublinear growth and competitive coexistence across ecosystems. *Science*, 383(6688):eadg8488, March 2024.

[135] Tobias Galla. Dynamically evolved community size and stability of random Lotka-Volterra ecosystems(a). *Epl*, 123(4):1–13, 2018.

[136] Joseph W. Baron, Thomas Jun Jewell, Christopher Ryder, and Tobias Galla. Breakdown of Random-Matrix Universality in Persistent Lotka-Volterra Communities. *Physical Review Letters*, 130(13):137401, March 2023.

[137] Tobias Galla. Generating-functional analysis of random Lotka-Volterra systems: A step-by-step guide, May 2024.

[138] Jean-Philippe Bouchaud, Leticia F. Cugliandolo, Jorge Kurchan, and Marc Mézard. Out of equilibrium dynamics in spin-glasses and other glassy systems. In *Spin Glasses and Random Fields*, volume Volume 12 of *Series on Directions in Condensed Matter Physics*, pages 161–223. WORLD SCIENTIFIC, December 1997.

[139] Giulio Biroli. A crash course on ageing. *Journal of Statistical Mechanics: Theory and Experiment*, 2005(05):P05014, May 2005.

[140] L. F. Cugliandolo. Course 7: Dynamics of Glassy Systems. In Jean-Louis Barrat, Mikhail Feigelman, Jorge Kurchan, and Jean Dalibard, editors, *Slow Relaxations and Nonequilibrium Dynamics in Condensed Matter*, pages 367–521, Berlin, Heidelberg, 2003. Springer.

[141] Thibaut Arnoulx de Pirey and Guy Bunin. Aging by Near-Extinctions in Many-Variable Interacting Populations. *Physical Review Letters*, 130(9):098401, February 2023.

[142] Thibaut Arnoulx De Pirey and Guy Bunin. Many-Species Ecological Fluctuations as a Jump Process from the Brink of Extinction. *Physical Review X*, 14(1):011037, March 2024.

[143] Thibaut Arnoulx De Pirey and Guy Bunin. Critical behavior of a phase transition in the dynamics of interacting populations. *SciPost Physics*, 18(2):051, February 2025.

[144] Francesco d'Ovidio, Silvia De Monte, Séverine Alvain, Yves Dandonneau, and Marina Lévy. Fluid dynamical niches of phytoplankton types. *Proceedings of the National Academy of Sciences of the United States of America*, 107(43):18366–18370, October 2010.

[145] Ashley Shade, Stuart E. Jones, J. Gregory Caporaso, Jo Handelsman, Rob Knight, Noah Fierer, and Jack A. Gilbert. Conditionally Rare Taxa Disproportionately Contribute to Temporal Changes in Microbial Diversity. *mBio*, 5(4):10.1128/mbio.01371–14, July 2014.

[146] Kevin J. Flynn, Aditee Mitra, William H. Wilson, Susan A. Kimmance, Darren R. Clark, Angela Pelusi, and Luca Polimene. 'Boom-and-busted' dynamics of phytoplankton–virus interactions explain the paradox of the plankton. *New Phytologist*, 234(3):990–1002, 2022.

[147] Alan Hastings, Carole L. Hom, Stephen Ellner, Peter Turchin, and H. Charles J. Godfray. Chaos in Ecology: Is Mother Nature a Strange Attractor? *Annual Review of Ecology and Systematics*, 24:1–33, 1993.

[148] Elisa Benincá, Jef Huisman, Reinhard Heerkloss, Klaus D. Jöhnk, Pedro Branco, Egbert H. Van Nes, Marten Scheffer, and Stephen P. Ellner. Chaos in a long-term experiment with a plankton community. *Nature*, 451(7180):822–825, 2008.

[149] Stephan B. Munch, Tanya L. Rogers, Bethany J. Johnson, Uttam Bhat, and Cheng-Han Tsai. Rethinking the Prevalence and Relevance of Chaos in Ecology. *Annual Review of Ecology, Evolution, and Systematics*, 53(1):227–249, 2022.

[150] Tanya L. Rogers, Bethany J. Johnson, and Stephan B. Munch. Chaos is not rare in natural ecosystems. *Nature Ecology & Evolution*, 6(8):1105–1111, August 2022.

[151] Tanya L. Rogers, Stephan B. Munch, Shin-ichiro S. Matsuzaki, and Celia C. Symons. Intermittent instability is widespread in plankton communities. *Ecology Letters*, 26(3):470–481, 2023.

[152] Jef Huisman and Franz J. Weissing. Biodiversity of plankton by species oscillations and chaos. *Nature*, 402(6760):407–410, November 1999.

[153] J. C. Allen, W. M. Schaffer, and D. Rosko. Chaos reduces species extinction by amplifying local population noise. *Nature*, 364(6434):229–232, July 1993.

[154] Graeme D. Ruxton. Low levels of immigration between chaotic populations can reduce system extinctions by inducing asynchronous regular cycles. *Proceedings of the Royal Society of London. Series B: Biological Sciences*, 256(1346):189–193, January 1997.

[155] Michael T. Pearce, Atish Agarwala, and Daniel S. Fisher. Stabilization of extensive fine-scale diversity by ecologically driven spatiotemporal chaos. *Proceedings of the National Academy of Sciences*, 117(25):14572–14583, June 2020.

[156] Felix Roy, Matthieu Barbier, Giulio Biroli, and Guy Bunin. Complex interactions can create persistent fluctuations in high-diversity ecosystems. *PLoS Computational Biology*, 16(5):1–14, 2020.

[157] H. Sompolinsky and Annette Zippelius. Relaxational dynamics of the Edwards-Anderson model and the mean-field theory of spin-glasses. *Physical Review B*, 25(11):6860–6875, June 1982.

[158] Ada Altieri, Giulio Biroli, and Chiara Cammarota. Dynamical mean-field theory and aging dynamics. *Journal of Physics A: Mathematical and Theoretical*, 53(37):375006, September 2020.

[159] Leticia F. Cugliandolo. Recent Applications of Dynamical Mean-Field Methods. *Annual Review of Condensed Matter Physics*, 15(1):177–213, March 2024.

[160] L. F. Cugliandolo and J. Kurchan. Analytical solution of the off-equilibrium dynamics of a long-range spin-glass model. *Physical Review Letters*, 71(1):173–176, July 1993.

[161] L. F. Cugliandolo, J. Kurchan, and F. Ritort. Evidence of aging in spin-glass mean-field models. *Physical Review B*, 49(9):6331–6334, March 1994.

[162] Silvio Franz and Marc Mézard. On mean field glassy dynamics out of equilibrium. *Physica A: Statistical Mechanics and its Applications*, 210(1):48–72, September 1994.

[163] Leticia F. Cugliandolo and Pierre Le Doussal. Large time nonequilibrium dynamics of a particle in a random potential. *Physical Review E*, 53(2):1525–1552, February 1996.

[164] Antoine Georges, Gabriel Kotliar, Werner Krauth, and Marcelo J. Rozenberg. Dynamical mean-field theory of strongly correlated fermion systems and the limit of infinite dimensions. *Reviews of Modern Physics*, 68(1):13–125, January 1996.

[165] Robert Zwanzig. *Nonequilibrium Statistical Mechanics*. Oxford Univ. Press, Oxford, 2001.

[166] R. Kubo. The fluctuation-dissipation theorem. *Reports on Progress in Physics*, 29(1):255, January 1966.

[167] Gérard Ben Arous, Amir Dembo, and Alice Guionnet. Cugliandolo-Kurchan equations for dynamics of Spin-Glasses. *Probability Theory and Related Fields*, 136(4):619–660, December 2006.

[168] Fabrizio Olmeda and Steffen Rulands. Long-range interactions and disorder facilitate pattern formation in spatial complex systems, March 2023.

[169] Alessandro Salvatore, Fabián Aguirre-López, and Ruben Zakine. Patterns robust to Disorder in spatially-interacting Generalized Lotka-Volterra Ecosystems, January 2025.

[170] Jacopo Grilli. Macroecological laws describe variation and diversity in microbial communities. *Nature Communications*, 11(1):4743, December 2020.

[171] R. A. Fisher, A. Steven Corbet, and C. B. Williams. The Relation Between the Number of Species and the Number of Individuals in a Random Sample of an Animal Population. *Journal of Animal Ecology*, 12(1):42–58, 1943.

[172] Werner Ulrich, Marcin Ollik, and Karl Inne Ugland. A meta-analysis of species—abundance distributions. *Oikos*, 119(7):1149–1155, 2010.

[173] William R. Shoemaker, Kenneth J. Locey, and Jay T. Lennon. A macroecological theory of microbial biodiversity. *Nature Ecology & Evolution*, 1(5):107, April 2017.

[174] Elita Baldridge, David J. Harris, Xiao Xiao, and Ethan P. White. An extensive comparison of species-abundance distribution models. *PeerJ*, 4:e2823, December 2016.

[175] Camille Aron, Giulio Biroli, and Leticia F. Cugliandolo. Symmetries of generating functionals of Langevin processes with colored multiplicative noise. *Journal of Statistical Mechanics: Theory and Experiment*, 2010(11):P11018, November 2010.

[176] P. C. Martin, E. D. Siggia, and H. A. Rose. Statistical Dynamics of Classical Systems. *Physical Review A*, 8(1):423–437, July 1973.

[177] Hans-Karl Janssen. On a Lagrangean for classical field dynamics and renormalization group calculations of dynamical critical properties. *Zeitschrift für Physik B Condensed Matter*, 23(4):377–380, December 1976.

[178] C. De Dominicis. Dynamics as a substitute for replicas in systems with quenched random impurities. *Physical Review B*, 18(9):4913–4919, November 1978.

[179] William Feller. Two Singular Diffusion Problems. *Annals of Mathematics*, 54(1):173–182, 1951.

[180] Ivan Dornic, Hugues Chaté, and Miguel A. Muñoz. Integration of Langevin Equations with Multiplicative Noise and the Viability of Field Theories for Absorbing Phase Transitions. *Physical Review Letters*, 94(10):100601, March 2005.

[181] Haim Weissmann, Nadav M. Shnerb, and David A. Kessler. Simulation of spatial systems with demographic noise. *Physical Review E*, 98(2):022131, August 2018.

[182] Peter E. Kloeden and Eckhard Platen. *Numerical Solution of Stochastic Differential Equations*. Springer, Berlin, Heidelberg, 1992.

[183] A. E. Magurran. Species abundance distributions: Pattern or process? *Functional Ecology*, 19(1):177–181, 2005.

[184] Peter Jung and Peter Hänggi. Dynamical systems: A unified colored-noise approximation. *Physical Review A*, 35(10):4464–4466, May 1987.

[185] Ronald Forrest Fox. Uniform convergence to an effective Fokker-Planck equation for weakly colored noise. *Physical Review A*, 34(5):4525–4527, November 1986.

[186] G. E. Uhlenbeck and L. S. Ornstein. On the Theory of the Brownian Motion. *Physical Review*, 36(5):823–841, September 1930.

[187] Catherine A. Lozupone, Jesse I. Stombaugh, Jeffrey I. Gordon, Janet K. Jansson, and Rob Knight. Diversity, stability and resilience of the human gut microbiota. *Nature*, 489(7415):220–230, September 2012.

[188] Thilo Gross, Wolfgang Ebenhöh, and Ulrike Feudel. Long food chains are in general chaotic. *Oikos*, 109(1):135–144, 2005.

[189] Michael P. Hassell, Hugh N. Comins, and Robert M. Mayt. Spatial structure and chaos in insect population dynamics. *Nature*, 353(6341):255–258, September 1991.

[190] Ingrid A. van de Leemput, Egbert H. van Nes, and Marten Scheffer. Resilience of Alternative States in Spatially Extended Ecosystems. *PLOS ONE*, 10(2):e0116859, February 2015.

[191] Robert M. May. *Stability and Complexity in Model Ecosystems*, volume 1. Princeton University Press, 1974.

[192] Sandro Azaele, Samir Suweis, Jacopo Grilli, Igor Volkov, Jayanth R. Banavar, and Amos Maritan. Statistical mechanics of ecological systems: Neutral theory and beyond. *Reviews of Modern Physics*, 88(3):035003, July 2016.

[193] David A. Vasseur and Peter Yodzis. The Color of Environmental Noise. *Ecology*, 85(4):1146–1152, 2004.

[194] John Realpe-Gomez, Mara Baudena, Tobias Galla, Alan J. McKane, and Max Rietkerk. Demographic noise and resilience in a semi-arid ecosystem model. *Ecological Complexity*, 15:97–108, September 2013.

[195] Graham Bell and Associate Editor: Dolph Schluter. The Distribution of Abundance in Neutral Communities. *The American Naturalist*, 155(5):606–617, 2000.

[196] Lauren G. Shoemaker, Lauren L. Sullivan, Ian Donohue, Juliano S. Cabral, Ryan J. Williams, Margaret M. Mayfield, Jonathan M. Chase, Chengjin Chu, W. Stanley Harpole, Andreas Huth, Janneke HilleRisLambers, Aubrie R. M. James, Nathan J. B. Kraft, Felix May, Ranjan Muthukrishnan, Sean Satterlee, Franziska Taubert, Xugao Wang, Thorsten Wiegand, Qiang Yang, and Karen C. Abbott. Integrating the underlying structure of stochasticity into community ecology. *Ecology*, 101(2):e02922, 2020.

[197] Fabio Peruzzo, Mauro Mobilia, and Sandro Azaele. Spatial Patterns Emerging from a Stochastic Process Near Criticality. *Physical Review X*, 10(1):011032, February 2020.

[198] Jiliang Hu, Daniel R. Amor, Matthieu Barbier, Guy Bunin, and Jeff Gore. Emergent phases of ecological diversity and dynamics mapped in microcosms. *Science*, 378(6615):85–89, October 2022.

[199] Susanne Pettersson and Martin Nilsson Jacobi. Spatial heterogeneity enhance robustness of large multi-species ecosystems. *PLOS Computational Biology*, 17(10):e1008899, October 2021.

[200] Aditya Mahadevan, Michael T Pearce, and Daniel S Fisher. Spatiotemporal ecological chaos enables gradual evolutionary diversification without niches or tradeoffs. *eLife*, 12:e82734, April 2023.

[201] H. K. Janssen. Spontaneous Symmetry Breaking in Directed Percolation with Many Colors: Differentiation of Species in the Gribov Process. *Physical Review Letters*, 78(15):2890–2893, April 1997.

[202] Marten Scheffer, Steve Carpenter, Jonathan A. Foley, Carl Folke, and Brian Walker. Catastrophic shifts in ecosystems. *Nature*, 413(6856):591–596, October 2001.

[203] Sonia Kéfi, Max Rietkerk, Minus van Baalen, and Michel Loreau. Local facilitation, bistability and transitions in arid ecosystems. *Theoretical Population Biology*, 71(3):367–379, May 2007.

[204] Timothy M. Lenton, Hermann Held, Elmar Kriegler, Jim W. Hall, Wolfgang Lucht, Stefan Rahmstorf, and Hans Joachim Schellnhuber. Tipping elements in the Earth's climate system. *Proceedings of the National Academy of Sciences*, 105(6):1786–1793, February 2008.

[205] Jean-Philippe Bouchaud. Crises and Collective Socio-Economic Phenomena: Simple Models and Challenges. *Journal of Statistical Physics*, 151(3):567–606, May 2013.

[206] Jonas Denk and Oskar Hallatschek. Tipping points emerge from weak mutualism in metacommunities. Preprint, Ecology, February 2023.

[207] Charles K. Fisher and Pankaj Mehta. The transition between the niche and neutral regimes in ecology. *Proceedings of the National Academy of Sciences of the United States of America*, 111(36):13111–13116, 2014.

[208] Emanuele Pigani, Damiano Sgarbossa, Samir Suweis, Amos Maritan, and Sandro Azaele. Delay effects on the stability of large ecosystems. *Proceedings of the National Academy of Sciences*, 119(45):e2211449119, November 2022.

[209] Matthieu Barbier, Jean François Arnoldi, Guy Bunin, and Michel Loreau. Generic assembly patterns in complex ecological communities. *Proceedings of the National Academy of Sciences of the United States of America*, 115(9):2156–2161, 2018.

[210] G. Ben Arous and A. Guionnet. Symmetric Langevin spin glass dynamics. *The Annals of Probability*, 25(3):1367–1422, July 1997.

[211] Sheng Chen and Uwe C. Täuber. Non-equilibrium relaxation in a stochastic lattice Lotka–Volterra model. *Physical Biology*, 13(2):025005, April 2016.

[212] Jim Wu, Pankaj Mehta, and David Schwab. Understanding Species Abundance Distributions in Complex Ecosystems of Interacting Species, March 2021.

[213] Timothy M. Lenton. Environmental Tipping Points. *Annual Review of Environment and Resources*, 38(Volume 38, 2013):1–29, October 2013.

[214] Marten Scheffer, Stephen R. Carpenter, Timothy M. Lenton, Jordi Bascompte, William Brock, Vasilis Dakos, Johan van de Koppel, Ingrid A. van de Leemput, Simon A. Levin, Egbert H. van Nes, Mercedes Pascual, and John Vandermeer. Anticipating Critical Transitions. *Science*, 338(6105):344–348, October 2012.

[215] Vasilis Dakos, Chris A. Boulton, Josh E. Buxton, Jesse F. Abrams, David I. Armstrong McKay, Sebastian Bathiany, Lana Blaschke, Niklas Boers, Daniel Dylewsky, Carlos López-Martínez, Isobel Parry, Paul Ritchie, Bregje van der Bolt, Larissa van der Laan, Els Weinans, and Sonia Kéfi. Tipping Point Detection and Early-Warnings in climate, ecological, and human systems. *EGUsphere*, pages 1–35, August 2023.

[216] F. P. Kelly. *Reversibility and Stochastic Networks*. Cambridge University Press, revised ed. edition edition, August 2011.

[217] Jean-Louis Barrat, Mikhail Feigelman, Jorge Kurchan, and Jean Dalibard, editors. *Slow Relaxations and Nonequilibrium Dynamics in Condensed Matter: Les Houches Session LXXVII, 1-26 July, 2002*. Springer, Berlin, Heidelberg, 2003.

[218] Giorgio Parisi. Order Parameter for Spin-Glasses. *Physical Review Letters*, 50(24):1946–1948, June 1983.

[219] S. F. Edwards and P. W. Anderson. Theory of spin glasses. *Journal of Physics F: Metal Physics*, 5(5):965, May 1975.

[220] Massimo Bernaschi, Alain Billoire, Andrea Maiorano, Giorgio Parisi, and Federico Ricci-Tersenghi. Strong ergodicity breaking in aging of mean-field spin glasses. *Proceedings of the National Academy of Sciences*, 117(30):17522–17527, July 2020.

[221] Giampaolo Folena, Silvio Franz, and Federico Ricci-Tersenghi. Rethinking Mean-Field Glassy Dynamics and Its Relation with the Energy Landscape: The Surprising Case of the Spherical Mixed p-Spin Model. *Physical Review X*, 10(3):031045, August 2020.

[222] J. P. Bouchaud. Weak ergodicity breaking and aging in disordered systems. *Journal de Physique I*, 2(9):1705–1713, September 1992.

[223] L. F. Cugliandolo and J. Kurchan. Weak ergodicity breaking in mean-field spin-glass models. *Philosophical Magazine B*, 71(4):501–514, April 1995.

[224] L. F. Cugliandolo and J. Kurchan. On the out-of-equilibrium relaxation of the Sherrington-Kirkpatrick model. *Journal of Physics A: Mathematical and General*, 27(17):5749, September 1994.

[225] Leticia F. Cugliandolo, David S. Dean, and Jorge Kurchan. Fluctuation-Dissipation Theorems and Entropy Production in Relaxational Systems. *Physical Review Letters*, 79(12):2168–2171, September 1997.

[226] Andrea Cavagna. Supercooled liquids for pedestrians. *Physics Reports*, 476(4):51–124, June 2009.

[227] Walter Kob and Hans C. Andersen. Testing mode-coupling theory for a supercooled binary Lennard-Jones mixture. II. Intermediate scattering function and dynamic susceptibility. *Physical Review E*, 52(4):4134–4153, October 1995.

[228] P. Lunkenheimer, R. Wehn, U. Schneider, and A. Loidl. Glassy Aging Dynamics. *Physical Review Letters*, 95(5):055702, July 2005.

[229] L. C. E. Struik. Physical aging in plastics and other glassy materials. *Polymer Engineering & Science*, 17(3):165–173, 1977.

[230] K. H. Fischer and J. A. Hertz. *Spin Glasses*. Cambridge Studies in Magnetism. Cambridge University Press, Cambridge, 1991.

[231] Eric Vincent, Jacques Hammann, Miguel Ocio, Jean-Philippe Bouchaud, and Leticia F. Cugliandolo. Slow dynamics and aging in spin glasses. In Miguel Rubí and Conrado Pérez-Vicente, editors, *Complex Behaviour of Glassy Systems*, pages 184–219, Berlin, Heidelberg, 1997. Springer.

[232] Ralph V. Chamberlin. Time decay of the thermoremanent magnetization in spin-glasses as a function of the time spent in the field-cooled state. *Physical Review B*, 30(9):5393–5395, November 1984.

[233] M. Ocio, M. Alba, and J. Hammann. Time scaling of the ageing process in spin-glasses : A study in CsNiFeF 6. *Journal de Physique Lettres*, 46(23):1101–1107, December 1985.

[234] E. Vincent, J. P. Bouchaud, J. Hammann, and F. Lefloch. Contrasting effects of field and temperature variations on ageing in spin glasses. *Philosophical Magazine B*, 71(4):489–500, April 1995.

[235] J.-P. Bouchaud and D. S. Dean. Aging on Parisi's Tree. *Journal de Physique I*, 5(3):265–286, March 1995.

[236] A.J. Bray. Theory of phase-ordering kinetics. *Advances in Physics*, 43(3):357–459, June 1994.

[237] S. Kirkpatrick, C. D. Gelatt, and M. P. Vecchi. Optimization by Simulated Annealing. *Science*, 220(4598):671–680, May 1983.

[238] David Gamarnik, Cristopher Moore, and Lenka Zdeborová. Disordered systems insights on computational hardness. *Journal of Statistical Mechanics: Theory and Experiment*, 2022(11):114015, November 2022.

[239] Giuseppe Carleo, Ignacio Cirac, Kyle Cranmer, Laurent Daudet, Maria Schuld, Naftali Tishby, Leslie Vogt-Maranto, and Lenka Zdeborová. Machine learning and the physical sciences. *Reviews of Modern Physics*, 91(4):045002, December 2019.

[240] Marylou Gabrié, Surya Ganguli, Carlo Lucibello, and Riccardo Zecchina. Neural Networks: From the Perceptron to Deep Nets. In *Spin Glass Theory and Far Beyond*, pages 477–497. WORLD SCIENTIFIC, February 2023.

[241] Giulio Biroli and Marc Mézard. Generative diffusion in very large dimensions. *Journal of Statistical Mechanics: Theory and Experiment*, 2023(9):093402, September 2023.

[242] Giulio Biroli, Tony Bonnaire, Valentin de Bortoli, and Marc Mézard. Dynamical regimes of diffusion models, 2024.

[243] Marco Baity-Jesi, Levent Sagun, Mario Geiger, Stefano Spigler, Gerard Ben Arous, Chiara Cammarota, Yann LeCun, Matthieu Wyart, and Giulio Biroli. Comparing dynamics: Deep neural networks versus glassy systems. In Jennifer Dy and Andreas Krause, editors, *Proceedings of the 35th International Conference on Machine Learning*, volume 80 of *Proceedings of Machine Learning Research*, pages 314–323. PMLR, 2018-07-10/2018-07-15.

[244] Thomas E. Angelini, Edouard Hannezo, Xavier Trepat, Manuel Marquez, Jeffrey J. Fredberg, and David A. Weitz. Glass-like dynamics of collective cell migration. *Proceedings of the National Academy of Sciences*, 108(12):4714–4719, March 2011.

[245] Simon Garcia, Edouard Hannezo, Jens Elgeti, Jean-François Joanny, Pascal Silberzan, and Nir S. Gov. Physics of active jamming during collective cellular motion in a monolayer. *Proceedings of the National Academy of Sciences*, 112(50):15314–15319, December 2015.

[246] Liesbeth M. C. Janssen. Active glasses. *Journal of Physics: Condensed Matter*, 31(50):503002, September 2019.

[247] Ludovic Berthier and Jorge Kurchan. Non-equilibrium glass transitions in driven and active matter. *Nature Physics*, 9(5):310–314, May 2013.

[248] Ludovic Berthier, Elijah Flenner, and Grzegorz Szamel. Glassy dynamics in dense systems of active particles. *The Journal of Chemical Physics*, 150(20):200901, May 2019.

[249] Yann-Edwin Keta, Robert L. Jack, and Ludovic Berthier. Disordered Collective Motion in Dense Assemblies of Persistent Particles. *Physical Review Letters*, 129(4):048002, July 2022.

[250] Rituparno Mandal and Peter Sollich. Multiple types of aging in active glasses. *Physical Review Letters*, 125(21):218001, November 2020.

[251] Guy Bunin. Directionality and community-level selection. *Oikos*, 130(4):489–500, 2021.

[252] Carles Martorell, Rubén Calvo, Alessia Annibale, and Miguel A. Muñoz. Dynamically selected steady states and criticality in non-reciprocal networks, December 2023.

[253] J. M. Luck and A. Mehta. Slow synaptic dynamics in a network: From exponential to power-law forgetting. *Physical Review E*, 90(3):032709, September 2014.

[254] Daniel J Amit, Hanoch Gutfreund, and H Sompolinsky. Statistical mechanics of neural networks near saturation. *Annals of Physics*, 173(1):30–67, January 1987.

[255] J J Hopfield. Neural networks and physical systems with emergent collective computational abilities. *Proceedings of the National Academy of Sciences*, 79(8):2554–2558, April 1982.

[256] Daniel Martí, Nicolas Brunel, and Srdjan Ostojic. Correlations between synapses in pairs of neurons slow down dynamics in randomly connected neural networks. *Physical Review E*, 97(6):062314, June 2018.

[257] David Dahmen, Sonja Grün, Markus Diesmann, and Moritz Helias. Second type of criticality in the brain uncovers rich multiple-neuron dynamics. *Proceedings of the National Academy of Sciences*, 116(26):13051–13060, June 2019.

[258] S. Reich, S. Maoz, Y. Kaplan, H. Rappeport, N. Q. Balaban, and O. Agam. Slow relaxation and aging in the model of randomly connected cycles network. *Physical Review Research*, 4(3):033127, August 2022.

[259] Silvio Franz and John Hertz. Glassy Transition and Aging in a Model Without Disorder. *Physical Review Letters*, 74(11):2114–2117, March 1995.

[260] A. Barrat and M. Mézard. Phase Space Diffusion and Low Temperature Aging. *Journal de Physique I*, 5(8):941–947, August 1995.

[261] Cécile Monthus and Jean-Philippe Bouchaud. Models of traps and glass phenomenology. *Journal of Physics A: Mathematical and General*, 29(14):3847, July 1996.

[262] Felix Ritort. Glassiness in a Model without Energy Barriers. *Physical Review Letters*, 75(6):1190–1193, August 1995.

[263] David Sherrington and Scott Kirkpatrick. Solvable model of a spin-glass. *Physical Review Letters*, 35(26):1792–1796, December 1975.

[264] G. Parisi. Infinite number of order parameters for spin-glasses. *Physical Review Letters*, 43(23):1754–1756, December 1979.

[265] L F Cugliandolo and D S Dean. On the dynamics of a spherical spin-glass in a magnetic field. *Journal of Physics A: Mathematical and General*, 28(17):L453–L459, September 1995.

[266] J. M. Kosterlitz, D. J. Thouless, and Raymund C. Jones. Spherical Model of a Spin-Glass. *Physical Review Letters*, 36(20):1217–1220, May 1976.

[267] Cirano De Dominicis and Irene Giardina. *Random Fields and Spin Glasses*. Cambridge University Press, Cambridge, September 2006.

[268] Jacopo Niedda, Tommaso Tonolo, and Giacomo Gradenigo. Probing marginal stability in the spherical p = 2 model. *Journal of Statistical Mechanics: Theory and Experiment*, 2024(11):113301, November 2024.

[269] Marc Potters and Jean-Philippe Bouchaud. *A First Course in Random Matrix Theory: For Physicists, Engineers and Data Scientists*. Cambridge University Press, Cambridge, 2020.

[270] G. J. Rodgers and M. A. Moore. Distribution of barrier heights in infinite-range spin glass models. *Journal of Physics A: Mathematical and General*, 22(8):1085, April 1989.

[271] Damien Barbier, Pedro H De Freitas Pimenta, Leticia F Cugliandolo, and Daniel A Stariolo. Finite size effects and loss of self-averageness in the relaxational dynamics of the spherical Sherrington–Kirkpatrick model. *Journal of Statistical Mechanics: Theory and Experiment*, 2021(7):073301, July 2021.

[272] Isaac Newton, N. W. Life of Sir Isaac Newton Chittenden, Daniel Adee, Andrew Motte, and Theodore Preston Early American mathematics books CU-BANC Hill. *Newton's Principia : The Mathematical Principles of Natural Philosophy*. New-York : Published by Daniel Adee, 1846.

[273] Alberto Dinelli, Jérémy O'Byrne, Agnese Curatolo, Yongfeng Zhao, Peter Sollich, and Julien Tailleur. Non-reciprocity across scales in active mixtures. *Nature Communications*, 14(1):7035, November 2023.

[274] Alberto Dinelli. *Scalar Active Matter across Scales*. PhD thesis, Université Paris Cité, July 2024.

[275] Naomichi Hatano and David R. Nelson. Localization Transitions in Non-Hermitian Quantum Mechanics. *Physical Review Letters*, 77(3):570–573, July 1996.

[276] Jung-Wan Ryu, Jae-Ho Han, Chang-Hwan Yi, Moon Jip Park, and Hee Chul Park. Exceptional classifications of non-Hermitian systems. *Communications Physics*, 7(1):1–7, March 2024.

[277] Yuto Ashida, Zongping Gong, and Masahito Ueda. Non-Hermitian physics. *Advances in Physics*, 69(3):249–435, July 2020.

[278] Laura Guislain and Eric Bertin. Hidden collective oscillations in a disordered mean-field spin model with non-reciprocal interactions, June 2024.

[279] Laura Guislain and Eric Bertin. Collective oscillations in a three-dimensional spin model with non-reciprocal interactions, May 2024.

[280] Laura Guislain and Eric Bertin. Nonequilibrium Phase Transition to Temporal Oscillations in Mean-Field Spin Models. *Physical Review Letters*, 130(20):207102, May 2023.

[281] David Martin, Daniel Seara, Yael Avni, Michel Fruchart, and Vincenzo Vitelli. An exact model for the transition to collective motion in nonreciprocal active matter, July 2023.

[282] Suropriya Saha, Jaime Agudo-Canalejo, and Ramin Golestanian. Scalar Active Mixtures: The Nonreciprocal Cahn-Hilliard Model. *Physical Review X*, 10(4):041009, October 2020.

[283] Zhihong You, Aparna Baskaran, and M. Cristina Marchetti. Nonreciprocity as a generic route to traveling states. *Proceedings of the National Academy of Sciences*, 117(33):19767–19772, August 2020.

[284] Sarah A. M. Loos, Sabine H. L. Klapp, and Thomas Martynec. Long-range order and directional defect propagation in the nonreciprocal XY model with vision cone interactions. *Physical Review Letters*, 130(19):198301, May 2023.

[285] H. Sompolinsky, A. Crisanti, and H. J. Sommers. Chaos in Random Neural Networks. *Physical Review Letters*, 61(3):259–262, July 1988.

[286] Ruben Zakine, Jérôme Garnier-Brun, Antoine-Cyrus Becharat, and Michael Benzaquen. Socioeconomic agents as active matter in nonequilibrium Sakoda-Schelling models. *Physical Review E*, 109(4):044310, April 2024.

[287] G. Parisi. Asymmetric neural networks and the process of learning. *Journal of Physics A: Mathematical and General*, 19(11):L675, August 1986.

[288] J. A. Hertz, G. Grinstein, and S. A. Solla. Memory networks with asymmetric bonds. In *AIP Conference Proceedings*. AIP, 1986.

[289] B Derrida, E Gardner, and A Zippelius. An Exactly Solvable Asymmetric Neural Network Model. *Europhysics Letters (EPL)*, 4(2):167–173, July 1987.

[290] David G. Clark and L. F. Abbott. Theory of coupled neuronal-synaptic dynamics. *Physical Review X*, 14(2):021001, April 2024.

[291] Yael Avni, Michel Fruchart, David Martin, Daniel Seara, and Vincenzo Vitelli. The nonreciprocal Ising model, November 2023.

[292] Michel Fruchart, Ryo Hanai, Peter B. Littlewood, and Vincenzo Vitelli. Non-reciprocal phase transitions. *Nature*, 592(7854):363–369, April 2021.

[293] Ryo Hanai. Nonreciprocal frustration: Time crystalline order-by-disorder phenomenon and a spin-glass-like state. *Physical Review X*, 14(1):011029, February 2024.

[294] Romain Daviet, Carl Philipp Zelle, Achim Rosch, and Sebastian Diehl. Nonequilibrium Criticality at the Onset of Time-Crystalline Order. *Physical Review Letters*, 132(16):167102, April 2024.

[295] Carl Philipp Zelle, Romain Daviet, Achim Rosch, and Sebastian Diehl. Universal phenomenology at critical exceptional points of nonequilibrium O(N) models. *Physical Review X*, 14(2):021052, June 2024.

[296] Bertrand Ottino-Löffler and Steven H. Strogatz. Volcano Transition in a Solvable Model of Frustrated Oscillators. *Physical Review Letters*, 120(26):264102, June 2018.

[297] Axel Prüser, Sebastian Rosmej, and Andreas Engel. Nature of the Volcano Transition in the Fully Disordered Kuramoto Model. *Physical Review Letters*, 132(18):187201, April 2024.

[298] Axel Prüser and Andreas Engel. Role of Coupling Asymmetry in the Fully Disordered Kuramoto Model, August 2024.

[299] Hiroaki Daido. Quasientrainment and slow relaxation in a population of oscillators with random and frustrated interactions. *Physical Review Letters*, 68(7):1073–1076, February 1992.

[300] H. Daido. Population dynamics of randomly interacting self-oscillators. I: Tractable models without frustration. *Progress of Theoretical Physics*, 77(3):622–634, March 1987.

[301] Adrià Garcés and Demian Levis. Phase Transitions in single species Ising Models with Non-Reciprocal couplings, November 2024.

[302] Colin Scheibner, Anton Souslov, Debarghya Banerjee, Piotr Surówka, William T. M. Irvine, and Vincenzo Vitelli. Odd elasticity. *Nature Physics*, 16(4):475–480, April 2020.

[303] Michel Fruchart, Colin Scheibner, and Vincenzo Vitelli. Odd Viscosity and Odd Elasticity. *Annual Review of Condensed Matter Physics*, 14(Volume 14, 2023):471–510, March 2023.

[304] Yael Avni, Michel Fruchart, David Martin, Daniel Seara, and Vincenzo Vitelli. Dynamical phase transitions in the nonreciprocal Ising model, February 2025.

[305] Laura Guislain and Eric Bertin. Discontinuous phase transition from ferromagnetic to oscillating states in a nonequilibrium mean-field spin model. *Physical Review E*, 109(3):034131, March 2024.

[306] Mohammad-Ali Miri and Andrea Alù. Exceptional points in optics and photonics. *Science*, 363(6422), January 2019.

[307] Emil J. Bergholtz, Jan Carl Budich, and Flore K. Kunst. Exceptional topology of non-Hermitian systems. *Reviews of Modern Physics*, 93(1):015005, February 2021.

[308] Laura Guislain and Eric Bertin. Far-from-equilibrium complex landscapes, May 2024.

[309] D.C. Mattis. Solvable spin systems with random interactions. *Physics Letters A*, 56(5):421–422, April 1976.

[310] G Toulouse et al. Theory of the frustration effect in spin glasses: I. *Spin Glass Theory and Beyond: An Introduction to the Replica Method and Its Applications*, 9:99, 1987.

[311] A. Crisanti and H. Sompolinsky. Dynamics of spin systems with randomly asymmetric bonds: Ising spins and Glauber dynamics. *Physical Review A*, 37(12):4865–4874, June 1988.

[312] Heinz Horner. Drift, creep and pinning of a particle in a correlated random potential. *Zeitschrift für Physik B Condensed Matter*, 100(2):243–257, March 1996.

[313] Leticia F. Cugliandolo, Jorge Kurchan, Pierre Le Doussal, and Luca Peliti. Glassy behaviour in disordered systems with nonrelaxational dynamics. *Physical Review Letters*, 78(2):350–353, January 1997.

[314] Jean-Louis Barrat and Ludovic Berthier. Fluctuation-dissipation relation in a sheared fluid. *Physical Review E*, 63(1):012503, December 2000.

[315] Ludovic Berthier, Jean-Louis Barrat, and Jorge Kurchan. A two-time-scale, two-temperature scenario for nonlinear rheology. *Physical Review E*, 61(5):5464–5472, May 2000.

[316] L. Berthier, L. F. Cugliandolo, and J. L. Iguain. Glassy systems under time-dependent driving forces: Application to slow granular rheology. *Physical Review E*, 63(5):051302, April 2001.

[317] Yan V. Fyodorov, Ewa Gudowska-Nowak, Maciej A. Nowak, and Wojciech Tarnowski. Fluctuation-dissipation relation for non-Hermitian Langevin dynamics, October 2023.

[318] Ludovic Berthier and Jean-Louis Barrat. Nonequilibrium dynamics and fluctuation-dissipation relation in a sheared fluid. *The Journal of Chemical Physics*, 116(14):6228–6242, April 2002.

[319] Kunimasa Miyazaki, David R. Reichman, and Ryoichi Yamamoto. Supercooled liquids under shear: Theory and simulation. *Physical Review E*, 70(1):011501, July 2004.

[320] Natsuda Klongvessa, Félix Ginot, Christophe Ybert, Cécile Cottin-Bizonne, and Mathieu Leocmach. Active Glass: Ergodicity Breaking Dramatically Affects Response to Self-Propulsion. *Physical Review Letters*, 123(24):248004, December 2019.

[321] G. Iori and E. Marinari. On the stability of the mean-field spin glass broken phase under non-Hamiltonian perturbations. *Journal of Physics A: Mathematical and General*, 30(13):4489, July 1997.

[322] Jérôme Garnier-Brun, Michael Benzaquen, and Jean-Philippe Bouchaud. Unlearnable Games and "Satisficing" Decisions: A Simple Model for a Complex World. *Physical Review X*, 14(2):021039, June 2024.

[323] Nathan C. Keim, Joseph D. Paulsen, Zorana Zeravcic, Srikanth Sastry, and Sidney R. Nagel. Memory formation in matter. *Reviews of Modern Physics*, 91(3):035002, July 2019.

[324] Francesco Arceri, François P. Landes, Ludovic Berthier, and Giulio Biroli. A statistical mechanics perspective on glasses and aging. In *Encyclopedia of Complexity and Systems Science*, pages 1–68. Springer Berlin Heidelberg, 2021.

[325] Ludovic Berthier and Giulio Biroli. Theoretical perspective on the glass transition and amorphous materials. *Reviews of modern physics*, 83(2):587–645, 2011.

[326] Federico Ghimenti, Ludovic Berthier, and Frédéric van Wijland. Irreversible Monte Carlo Algorithms for Hard Disk Glasses: From Event-Chain to Collective Swaps. *Physical Review Letters*, 133(2):028202, July 2024.

[327] Federico Ghimenti, Ludovic Berthier, Grzegorz Szamel, and Frédéric van Wijland. Sampling efficiency of transverse forces in dense liquids. *Physical Review Letters*, 131(25):257101, December 2023.

[328] Giorgio Parisi. THE OVERLAP IN GLASSY SYSTEMS. In David Sherrington, Paul Goldbart, and Nigel Goldenfeld, editors, *Stealing the Gold: A Celebration of the Pioneering Physics of Sam Edwards*, pages 192–211. Oxford University Press, December 2004.

[329] Tosio Kato. *Perturbation Theory for Linear Operators*. Springer, 2nd corr. print. of the 2nd ed. edition, 1984.

[330] Lloyd N. Trefethen and Mark Embree. *Spectra and Pseudospectra: The Behavior of Nonnormal Matrices and Operators*. Princeton University Press, Princeton, N.J, 2005.

[331] Elsen Tjhung and Ludovic Berthier. Discontinuous fluidization transition in time-correlated assemblies of actively deforming particles. *Physical Review E*, 96(5):050601, November 2017.

[332] A. Barrat, R. Burioni, and M. Mézard. Ageing classification in glassy dynamics. *Journal of Physics A: Mathematical and General*, 29(7):1311, April 1996.

[333] H. E. Stanley. Dependence of Critical Properties on Dimensionality of Spins. *Physical Review Letters*, 20(12):589–592, March 1968.

[334] A. Crisanti and H. J. Sommers. The sphericalp-spin interaction spin glass model: The statics. *Zeitschrift für Physik B Condensed Matter*, 87(3):341–354, October 1992.

[335] Daniel A. Stariolo and Leticia F. Cugliandolo. Activated dynamics of the Ising p-spin disordered model with finite number of variables. *Europhysics Letters*, 127(1):16002, August 2019.

[336] B. Derrida. Random-Energy Model: Limit of a Family of Disordered Models. *Physical Review Letters*, 45(2):79–82, July 1980.

[337] Bernard Derrida. Random-energy model: An exactly solvable model of disordered systems. *Physical Review B*, 24(5):2613–2626, September 1981.

[338] M. Baity-Jesi, G. Biroli, and C. Cammarota. Activated aging dynamics and effective trap model description in the random energy model. *Journal of Statistical Mechanics: Theory and Experiment*, 2018(1):013301, January 2018.

[339] Jiří Černý and Tobias Wassmer. Aging of the Metropolis dynamics on the random energy model. *Probability Theory and Related Fields*, 167(1):253–303, February 2017.

[340] M. A. Tsyganov, J. Brindley, A. V. Holden, and V. N. Biktashev. Quasisoliton Interaction of Pursuit-Evasion Waves in a Predator-Prey System. *Physical Review Letters*, 91(21):218102, November 2003.

[341] Ernest Montbrió and Diego Pazó. Kuramoto Model for Excitation-Inhibition-Based Oscillations. *Physical Review Letters*, 120(24):244101, June 2018.

[342] H. Sompolinsky and I. Kanter. Temporal association in asymmetric neural networks. *Physical Review Letters*, 57(22):2861–2864, December 1986.

[343] Gideon Lee, Tony Jin, Yu-Xin Wang, Alexander McDonald, and Aashish Clerk. Entanglement Phase Transition Due to Reciprocity Breaking without Measurement or Postselection. *PRX Quantum*, 5(1):010313, January 2024.

[344] João Ferreira, Tony Jin, Jochen Mannhart, Thierry Giamarchi, and Michele Filippone. Transport and Nonreciprocity in Monitored Quantum Devices: An Exact Study. *PHYSICAL REVIEW LETTERS*, 2024.

[345] Daniel S. Seara, Jonathan Colen, Michel Fruchart, Yael Avni, David Martin, and Vincenzo Vitelli. Sociohydrodynamics: Data-driven modelling of social behavior, January 2024.

[346] Lara Braverman, Colin Scheibner, Bryan VanSaders, and Vincenzo Vitelli. Topological Defects in Solids with Odd Elasticity. *Physical Review Letters*, 127(26):268001, December 2021.

[347] A. B. Harris. Effect of random defects on the critical behaviour of Ising models. *Journal of Physics C: Solid State Physics*, 7(9):1671, May 1974.

[348] Harris A Brooks. The 'Harris criterion' lives on. *Journal of Physics: Condensed Matter*, 28(42):421006, October 2016.

[349] Thomas Vojta and Ronald Dickman. Spatiotemporal generalization of the Harris criterion and its application to diffusive disorder. *Physical Review E*, 93(3):032143, March 2016.

[350] John Cardy. *Scaling and Renormalization in Statistical Physics*. Cambridge Lecture Notes in Physics. Cambridge University Press, Cambridge, 1996.

[351] P. C. Hohenberg and B. I. Halperin. Theory of dynamic critical phenomena. *Reviews of Modern Physics*, 49(3):435–479, July 1977.

[352] S. Elitzur, R. B. Pearson, and J. Shigemitsu. Phase structure of discrete Abelian spin and gauge systems. *Physical Review D*, 19(12):3698–3714, June 1979.

[353] Cintia M. Lapilli, Peter Pfeifer, and Carlos Wexler. Universality Away from Critical Points in Two-Dimensional Phase Transitions. *Physical Review Letters*, 96(14):140603, April 2006.

[354] Kei-ichi Tainaka. Stationary pattern of vortices or strings in biological systems: Lattice version of the Lotka-Volterra model. *Physical Review Letters*, 63(24):2688–2691, December 1989.

[355] L. Frachebourg, P. L. Krapivsky, and E. Ben-Naim. Spatial organization in cyclic Lotka-Volterra systems. *Physical Review E*, 54(6):6186–6200, December 1996.

[356] Ian Goodfellow, Jean Pouget-Abadie, Mehdi Mirza, Bing Xu, David Warde-Farley, Sherjil Ozair, Aaron Courville, and Yoshua Bengio. Generative Adversarial Nets. In *Advances in Neural Information Processing Systems*, volume 27. Curran Associates, Inc., 2014.

[357] Camille Aron, Daniel G. Barci, Leticia F. Cugliandolo, Zochil González Arenas, and Gustavo S. Lozano. Dynamical symmetries of Markov processes with multiplicative white noise. *Journal of Statistical Mechanics: Theory and Experiment*, 2016(5):053207, May 2016.

RÉSUMÉ

De nombreux systèmes complexes — des communautés écologiques aux réseaux neuronaux, et des grandes économies aux verres de spin — sont composés d'un grand nombre d'éléments simples interagissant de manière hétérogène. Ces systèmes peuvent présenter des comportements émergents surprenants qui peuvent être étudiés à l'aide des outils de la physique statistique. Pourtant, on en sait encore peu sur ce qui se produit lorsque deux ou plus de ces systèmes complexes sont couplés, une situation générale qui peut se produire dès qu'il existe plusieurs niveaux d'organisation. Dans cette thèse, j'étudie deux cas pour lesquels un tel cadre est pertinent.

Le premier est une méta-communauté écologique, un réseau de communautés écologiques locales (chacune composée de nombreuses espèces), interconnectées par la migration des individus. Alors que dans une communauté isolée, les fluctuations conduiraient à l'extinction progressive de toutes les espèces, le réseau spatial permet de compenser ces extinctions locales par des recolonisations. J'ai montré que la présence d'interactions hétérogènes permet de stabiliser l'écosystème bien au-delà de ce qui serait possible sans elles. Cela est dû à l'émergence spontanée d'interactions mutuellement bénéfiques. Toutefois, ce même mécanisme induit un point de bascule : au-delà d'un seuil critique, l'écosystème s'effondre, passant d'une grande diversité à une extinction totale. J'ai identifié des signaux permettant d'anticiper ce basculement avant qu'il ne survienne.

Dans la deuxième partie de la thèse, je décris l'effet des interactions non réciproques sur des paires de systèmes complexes. Certains systèmes complexes peuvent subir une transition de phase, après laquelle ils présentent un phénomène appelé vieillissement : plus le système est ancien, plus il évolue lentement. Il avait été suggéré que toute non-réciprocité détruirait ce phénomène, menant à la place à une dynamique chaotique. J'ai montré au contraire que le sort de cette phase ralentie dépend de la manière dont cette non-réciprocité est introduite. J'ai découvert une transition d'une phase désordonnée statique à une phase amorphe oscillante, caractérisée par un vieillissement non réciproque avec une dynamique lente et des oscillations. J'ai également développé une série de critères pour déterminer si l'ajout de interactions non réciproques infinitésimales à un système subissant une transition de phase modifierait son comportement critique.

MOTS CLÉS

Physique statistique, Ecologie théorique, désordre, dynamique hors-equilibre, interactions non-réciproques

ABSTRACT

Many complex systems — from ecological communities to neural networks, and from large economies to spin-glasses — are composed of many simple components interacting in a heterogeneous way. These systems can exhibit surprising emergent behavior which can be studied with the tools of statistical physics. However, little is known about what happens when two — or many — of such complex systems are coupled together, a general situation that can arise whenever there are multiple levels of organization. In this thesis, I study two cases for which such a framework is relevant.

The first is a diverse ecological meta-community, a network of local ecological communities (each composed of many interacting species), interconnected by migration of individuals. While in an isolated community fluctuations would lead to the progressive extinctions of all species, the spatial network enables the compensation of local extinctions by recolonizations. I have shown that the presence of heterogeneous interactions stabilizes the ecosystem in conditions in which an isolated species would go extinct. This is possible thanks to the spontaneous emergence of mutualistic interactions. However, this same mechanism induces a tipping point, beyond which the ecosystem collapses, shifting from high diversity to extinction of all species. I have identified probes that enable to predict this tipping point before it occurs.

In the second part of the thesis, I describe the effect of non-reciprocal interactions on pairs of complex systems. Disordered systems can undergo a glass transition, after which they exhibit aging: the older the system is, the slower it evolves. Previous studies have long suggested that non-reciprocity tends to destroy glassiness, generating instead chaotic dynamics. Studying a bipartite spherical Sherrington-Kirkpatrick model I was able to show that this is not always the case. I uncovered an exceptional-point mediated transition from a static disordered phase to an oscillating amorphous one, characterized by non-reciprocal aging with slow dynamics and oscillations. I have also developed a series of criteria to determine whether adding small non-reciprocal interactions to a system undergoing a phase transition would change its critical behavior.

KEYWORDS

Statistical physics, theoretical ecology, disorder, non-equilibrium dynamics, non-reciprocal interactions